UNIVERSITY OF CAPE TOWN
IYUNIVESITHI YASEKAPA • UNIVERSITEIT VAN KAAPSTAD

INVESTIGATION OF PARTICULATE HIV-1 ENV VACCINE CANDIDATES USING ZERA® AND SPYTAG/SPYCATCHER TECHNOLOGIES

Phindile Thobeka Ximba

A Thesis Presented for the Degree of DOCTOR OF PHILOSOPHY (PhD) in the Faculty of Health Sciences, Division of Medical Virology, Department of Pathology, Faculty of Health Sciences, University of Cape Town

August 2021

Supervisor: Professor Ed Rybicki
Co-supervisors: Professor Anna-Lise Williamson
Dr Ros Chapman and Dr Ann Meyers

GENERAL TABLE OF CONTENTS

ACKNOWLEDGEMENTS

My sincere appreciation goes to the following people and institutions for their contributions toward the completion of this project.

- My supervisors, Prof Ed Rybicki, Prof Anna-Lise Williamson, Dr Ros Chapman and Dr Ann Meyers, for their intellectual guidance and excellent mentorship throughout this project. I have benefitted greatly from your wealth of knowledge!
- Special thanks to Ros and Ann, who patiently and meticulously read many revisions of this thesis.
- Dr Michiel van Diepen, for your genuine belief in my capabilities, unwavering support, intellectual guidance, and training me on several techniques.
- Dr Emmanuel Margolin, for your intellectual input in this project, editing Zera® and SpyTag manuscripts and training me on plant expression experiments.
- Miss Susan Lanfear for assisting with admin-related matters
- The Strategic Health Innovation Partnerships (SHIP)- a partnership between the SAMRC and the Department of Science and Innovation) for funding this project.
- Mrs Susan Cooper at UCT Confocal And Light Microscope Imaging Facility for assistance with confocal microscopy work
- Dr Brandon Weber, Miss Kaylene Baron and Mr Phillip Venter (Centre for Imaging & Analysis) for assisting with size exclusion chromatography
- Mr Mohamed Jaffer at UCT Electron Microscope Unit for assistance with electron microscopy experiments
- Noel Markgraaff (University of Stellenbosch) and Rodney Lucas (Research Animal Facility, UCT) for their assistance with rabbit experiments and ensuring the welfare of these animals
- Our collaborators at NICD: Lynn Morris, Penny Moore, Tandile Hermanus, Carol Growther and Nigel Makoah for conducting neutralisation assays on serum samples from rabbits.
- Frances Lees (Afrigen Biologics & Vaccines) for assistance with dynamic light scattering
- Staff and students at Prof Anna-Lise Williamson's Group and the Biopharming Research Unit for their support.
- Special thanks to my officemates for making the workplace a little brighter and a whole lot of fun!
- My brother (Sandile) and sister(Nokwethemba) for offering much needed moral support
- Most importantly kuBazalibami- MaSotobe no Mlaba, isandla sidlula ikhanda, Ngiyabonga! Thank you so much for being so supportive and valuing my wellbeing more than this degree!
    - "I couldn't ask for better parents. I keep that at the forefront of whatever I do, and every time I feel like I can't take another step, I see their faces, and that drives me"- Tiger Shroff.

DECLARATIONS

The work described in this thesis was conducted in the Institute of Infectious Diseases and Molecular Medicine and the Biopharming Research Unit in the Department of Molecular and Cell Biology, University of Cape Town. Research was conducted under the supervision of Professor Ed Rybicki, Professor Anna-Lise Williamson, Dr Ros Chapman and Dr Ann Meyers

I, Phindile Thobeka Ximba, hereby declare that the work outlined in this thesis is my original work (except where acknowledgements indicate otherwise) and that neither the whole work nor any part of it has been or is being submitted for another degree in this or any other university. All assistance provided by other people has been acknowledged. All citations in this manuscript are reflected using the style of the Journal of Virology as the convention. Furthermore, I authorise the university to reproduce for the purpose of research either the whole or any portion of the contents in any manner whatsoever.

Phindile Thobeka Ximba

ABBREVIATIONS

%	Percentage
˚C	degrees Celsius
µg	microgram
µl	microlitre
α	anti
aa	amino acid
Ad5	adenovirus type-5
ADCC	antibody-dependent cellular cytotoxicity
ADCP	antibody-dependent cellular phagocytosis
ADCVI	antibody-dependent cellular-mediated virus inhibition
AEC	animal ethics committee
Amp(R)	ampicillin resistance
ATPS	aqueous two-phase system
BCR	B-cell receptor
BN PAGE	Blue native polyacrylamide gel electrophoresis
bNAbs	broadly neutralising antibodies
bp	base pairs
BSA	bovine serum albumin
C(1-5)	HIV constant domains
CA	capsid protein
CCR5	C-C chemokine receptor type 5
CD4	cluster of differentiation 4
CDR-H3	complementary determining region loop three
CE	cellulose ester
CHO	Chinese hamster ovary
Cos1	monkey kidney cells
CPMV	cowpea mosaic virus
CT	cytoplasmic tail
Cy3	Cyanine dye 3
DMEM	Dulbecco's Modified Eagle's Medium
DMSO	Dimethyl sulfoxide
DNA	Deoxyribonucleic acid
DSL	dynamic light scattering
DTT	Dithiothreitol
E.coli	*Escherichia coli*
ECFP	enhanced cyan fluorescence protein
EDTA	Ethylenediaminetetraacetic acid
eGFP	enhance green fluorescent protein
ELISA	enzyme-linked immunosorbent assay
ELP	Elastin-like polypeptides
EM	electron microscopy
Env	envelope
ERAD	ER-associated degradation
ESCRT	endosomal complexes required for transport
FACS	Fluorescence-activated cell sorting
FCS	Foetal Calf Serum
FP	fusion peptide
FT	bacteriophage T4 fibritin
g	gravitational force
g	gram
Gag	group specific antigen
GNL	*Galanthus nivalis* lectin
HBV	hepatitis B virus
HEK	human embryonic kidney cells
HEK293T	human embryonic kidney cells with SV40 large T antigen
HeLa	Henrietta Lacks' cervical epithelial cells
HEV	hepatitis E virus
HFBI	hydrophobin-I
HIV	human immunodeficiency virus
HPV	human papillomavirus
HR1 & HR2	heptad-repeats 1&2
HRP	Horseradish peroxidase
HT	hypertranslatable
HVTN	The HIV Vaccine Trials Network
IgG	Immunoglobulin G
INF-ɣ	interferon gamma
IPTG	Isopropylthiogalactose
IRES-Neo	internal ribosome entry site and neomycin resistance
kDa	kilodalton
KDEL	endoplasmic reticulum retention signal
l	litre
LB	left border

LB	Luria Bertani
LPH	murine mAb24 heavy chain signal peptide
LRT	Long terminal repeat
LS	lumazine synthase
MA	matrix protein
mAb	monoclonal antibody
MHC	major histocompatibility complex
MLV	murine leukaemia virus
MMP	methyl αD-manno-pyranoside
MPER	membrane-proximal external region
MRC	Medical Research Counsel
NC	nucleocapsid
nef	negative effector
NFL	native flexible linker
ng	nanogram
NHP	non-human primate
NS-EM	negative stain electron microscopy
NTA	nitrilotriacetic acid
OD	optical density
PBs	Protein bodies
PBS	Phosphate buffered saline
PBST	Phosphate buffered saline with 0.1% tween 20
PCR	Polymerase chain reaction
PCV	porcine circovirus
PDH	pyruvate dehydrogenase
PDI	polydispersity index
PEG	Polyethylene glycol
PEI	polyethylenimine-branched
PFU	plaque forming units
PI	primary infection
pMExT	plasmid for Mammalian Expression with TPA leader
PNGase F	peptide-N-glycosidase F
PVDF	Polyvinylidene fluoride
RBD	receptor-binding domain
RER	(rough) endoplasmic reticulum
rev	regulator of viral gene expression
rpm	revolutions per minute
RSV	respiratory syncytial virus
RT	room temperature
SBTI	soy-bean trypsin inhibitor
SC	SpyCatcher
SDS-PAGE	Sodium dodecyl-sulfate polyacrylamide gel electrophoresis
SEC	Size Exclusion Chromatography
SHIP	The Strategic Health Innovation Partnerships
SIV	simian immunodeficiency virus
SOSIP	Modifications to HIV-1 Env: SOS, a disulfide between residues 501 and 605; IP, I559P mutation
SP	signal peptide
ST	SpyTag
tat	transcriptional transactivator
tat	transcriptional transactivator
TBSV	tomato bushy virus
TGN	trans-Golgi network
TGX	Tris-Glycine eXtended
TLR	toll-like receptors
TMD	transmembrane domain
TPA	tissue plasminogen activator
TSP	total soluble protein
UNIAIDS	Joint United Nations Programme on HIV/AIDS
UTR	untranslated region
V(1-5)	gp120 variable regions 1-5
VH	variable heavy chain
vif	viral infectivity factor
VLP	virus-like particles
vpr	viral protein r
vpu	viral protein u
WFI	water for injection
Zera	γ-zein ER-accumulating domain

ABSTRACT

The HIV-1 envelope glycoprotein (Env) is the primary focus of prophylactic HIV vaccine development. However, the unusually low density of Env spikes on the virion (≈14 spikes/virion) is unfavourable for eliciting high titre, long-lasting antibody responses. It is possible that increasing the Env spike density of particulate vaccine candidates generated by protein body formation or via the display of Env on nanoparticles could improve the induction of long-lasting neutralising antibodies (NAbs). For this thesis, two different nanoparticle approaches were therefore investigated. The HIV-1 Env sequence used for both approaches was derived from the superinfecting subtype C CAP256 virus. This was truncated to remove the transmembrane domain, and engineered to contain a flexible linker (FL) in place of the furin cleavage site and an I559P mutation to generate soluble, stable and cleavage-independent gp140 proteins.

The first approach investigated the impact of genetically fusing a 27 kDa proline-cysteine-rich domain of the ɣ-zein maize seed storage protein - Zera® - to either the N- or C-terminus of CAP256 gp140. Fusion of Zera® to a protein of interest can promote the self-assembly of large protein bodies (PBs) containing the protein of interest, thereby improving yields of the recombinant protein and enabling easy isolation using gradient ultracentrifugation. The purification of Zera-induced Env PBs from infiltrated *Nicotiana benthamiana* plants was not optimal. Consequently, the generation of Zera®-induced gp140 protein bodies was evaluated in a mammalian expression system. Stable HEK293 cell lines expressing Zera®-gp140 or gp140-Zera® were generated. A mixture of small PB-like structures was observed in cells expressing gp140-Zera®. However, no PB-like structures were seen in cells expressing Zera®-gp140. The immunogenicity of Zera®-gp140 and gp140-Zera® was evaluated by in rabbits. Binding and Tier 1A neutralising serum titres were higher for gp140-Zera® than for Zera®-gp140. Neither gp140-Zera® nor Zera®-gp140-specific sera neutralised a Tier 1B pseudovirus or the autologous Tier 2 CAP256SU pseudovirus, suggesting that Zera® might have compromised the structure of the Zera®-tagged gp140 proteins.

The second approach investigated the two-component SpyCatcher/SpyTag technology. The stable HEK293 cell line expressing CAP256 gp140-SpyTag (gp140-ST) was generated, and trimers were purified to homogeneity using gel filtration. SpyCatcher (SC)-AP205 VLPs were produced in *E. coli* and purified by ultracentrifugation. The gp140-ST trimers and the SC-AP205 VLPs were mixed in varying molar ratios to generate VLPs displaying the glycoprotein (AP205-gp140-ST particles). SDS-PAGE, dynamic light scattering and negative stain electron microscopy indicated that gp140-ST was successfully bound to the VLPs, although not all potential binding sites were occupied. The immunogenicity of the coupled VLPs was evaluated in a pilot study in rabbits. One group was injected four times with coupled VLPs. The second group was primed with DNA vaccines expressing Env and a mosaic Gag, followed by modified vaccinia Ankara expressing the same antigens and then boosted twice with coupled VLPs. Encouragingly, gp140-ST displayed on SC-AP205 VLPs was an effective boost to heterologously primed rabbits, leading to induction of autologous Tier 2 neutralising antibodies in 2/5 rabbits. These results demonstrate that careful selection of a geometrically-suitable nanoparticle scaffold to achieve a high-density display of HIV-1 envelope trimers is an important consideration and that this could improve the effect of nanoparticle-displayed gp140.

CHAPTER 1: LITERATURE REVIEW

1.1 Introduction

Since the identification of human immunodeficiency virus type 1 (HIV-1) as a causative agent of the acquired immunodeficiency syndrome (AIDS) epidemic (Gottlieb *et al.* 1981; Barré-Sinoussi *et al.* 1983), 75.7 million infections and 32.7 million deaths due to AIDS-related illnesses (UNAIDS 2020. The global roll-out of antiretroviral therapy (ART) tremendously reduced HIV transmissions and HIV/AIDS-related mortalities (Cohen *et al.* 2011; Fauci & Marston. 2014). However, owing to limitations such as the emergence of drug-resistant strains and poor adherence to ART, an effective vaccine remains essential to end the HIV pandemic (Fauci. 2017). To this end, only seven phase 2b/3 efficacy trials have tested candidate HIV-1 vaccines with the hope of eliciting either humoral or cellular immune responses. These are VAX004, VAX003, Step, Phambili, RV144, HVTN505 (Lema *et al.* 2014; Sheets *et al.* 2016) and a recently terminated HVTN702 trial that was conducted in South Africa (Cohen. 2020; Slomski. 2020). Of these trials, the RV144 Thailand trial based on a heterologous prime-boost regimen is the only HIV-1 vaccine trial ever to demonstrate moderate (31%) but significant efficacy in preventing HIV-1 acquisition (Vaccari *et al.* 2010). This overall lack of efficacy motivates the continued efforts in the search for an effective vaccine.

1.2 HIV origin, distributions and classification

Two independent zoonotic transmissions of simian immunodeficiency viruses (SIVs) from non-human primates to humans generated two HIV lineages: these are HIV-1 and HIV-2. Sooty mangabey monkeys (*Cercocebys atys*) are natural reservoirs of lentiviruses that are related to HIV-2 (Hirsch *et al.* 1989; Gao *et al.* 1992) while chimpanzees (subspecies *Pan troglodyte troglodytes*) and gorillas (*Gorilla gorilla*) are natural reservoirs of HIV-1-type viruses (Gao *et al.* 1999; D'arc *et al.* 2015). While HIV-2 is confined to West African nations, it is less transmissible thus leading to slower progression to AIDS. HIV-1 is prevalent worldwide, readily transmissible and progresses at a faster rate to AIDS (Nyamweya *et al.* 2013). HIV-1 is classified into four groups according to different zoonotic transmission events: these are M (major), O (outlier), N (non-M and non-O) and P (Simon *et al.* 1998; Sharp. 2002; Plantier *et al.* 2009; Sharp & Hahn. 2011; Vallari *et al.* 2011; Hemelaar. 2012). Group M is the most common circulating HIV-1 group. Phylogenetic analysis of Group M sequences led to further classification into nine subtypes or clades: A, B, C, D, F, G, H, J and K, as well as unique and circulating recombinant forms (URFs or CRFs) as a result of recombination events having taken place in dually infected individuals (Figure 1.1) (Hemelaar *et al.* 2006). HIV-1 group M subtypes are distributed unevenly across the globe. For instance, subtype C is the most prevalent, accounting for more than 50% of the global AIDS pandemic, and accounts for the majority of HIV-1 infections in Southern Africa (Hemelaar. 2012; Bbosa *et al.* 2019).

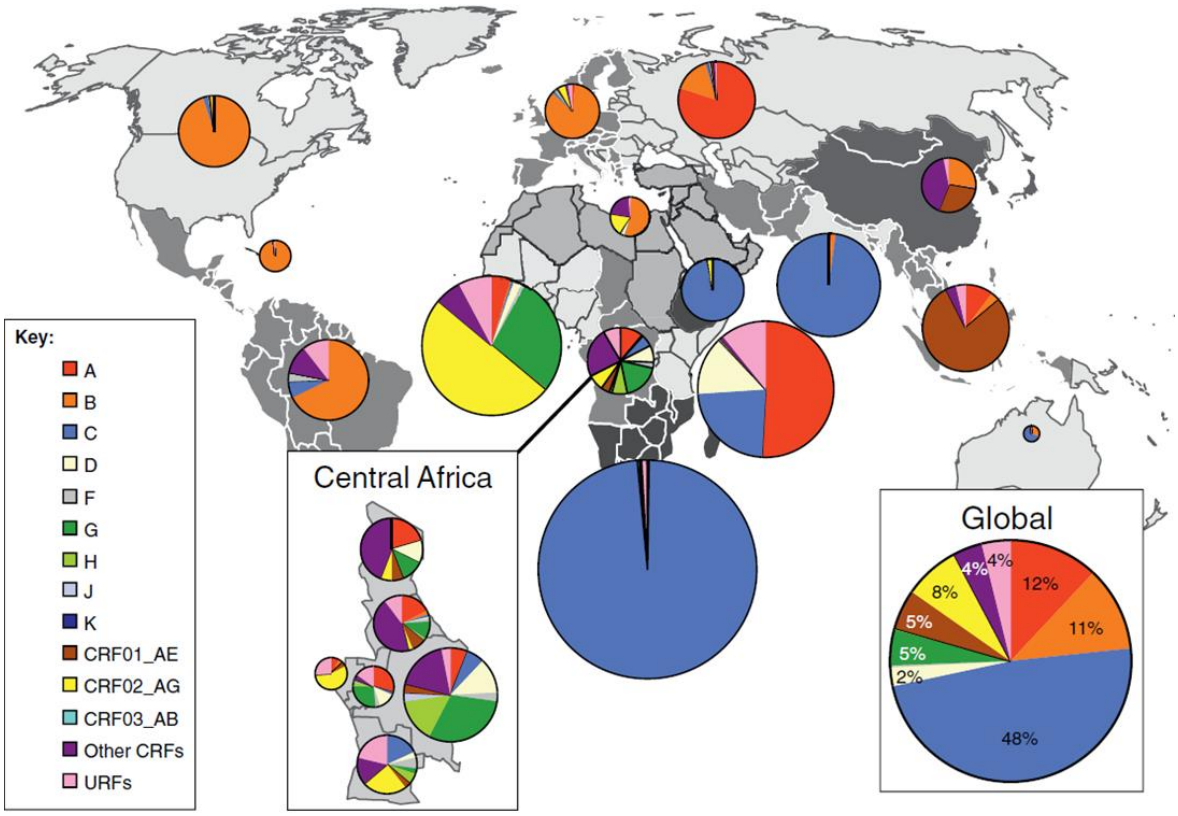

Figure 1.1: Global distribution of HIV-1 group M subtypes and recombinant forms. Pie charts were superimposed on different regions to illustrate the proportion of subtypes in each region as well as the global proportion of the subtypes. The diagram was taken from Hemelaar (2012) with permission provided by Elsevier.

1.3 HIV-1 genome and an overview of the functions of structural proteins encoded by nine genes of HIV

HIV-1 and HIV-2 belong to the *Lentivirus* genus of the *Retroviridae* family. The HIV-1 genome contains two copies of single-stranded RNA packaged within the spherical, enveloped viral particle (≈100 nm) (Ganser-Pornillos *et al.* 2012)(Figure 2 A and B). After binding and fusion of the virion with the host cell, reverse transcription in the core particle converts the single-stranded RNA to a double-stranded viral DNA, which can integrate into the host genome (Rajarapu. 2013). The HIV-1 genome contains nine genes; namely, *gag*, *pol*, *env*, *tat*, *rev*, *nef*, *vif*, *vpr* and *vpu* (Figure 1.2) (Mushahwar. 2006; Watts *et al.* 2009). These genes encode 19 proteins, which play specific roles during the HIV-1 assembly and replication. Integrated HIV-1 genomes are flanked by long terminal repeat (LTR) sequences at both ends (5' LTR and 3' LTR). The *gag*, *pol* and *env* genes encode the structural proteins of the virus (Engelman & Cherepanov. 2012; Freed. 2015). The *gag* gene is translated into the Gag polyprotein precursor (Pr55Gag) by cytosolic ribosomes, and is then trafficked to the plasma membrane (Göttlinger. 2001; Murakami. 2012; Mailler *et al.* 2016).

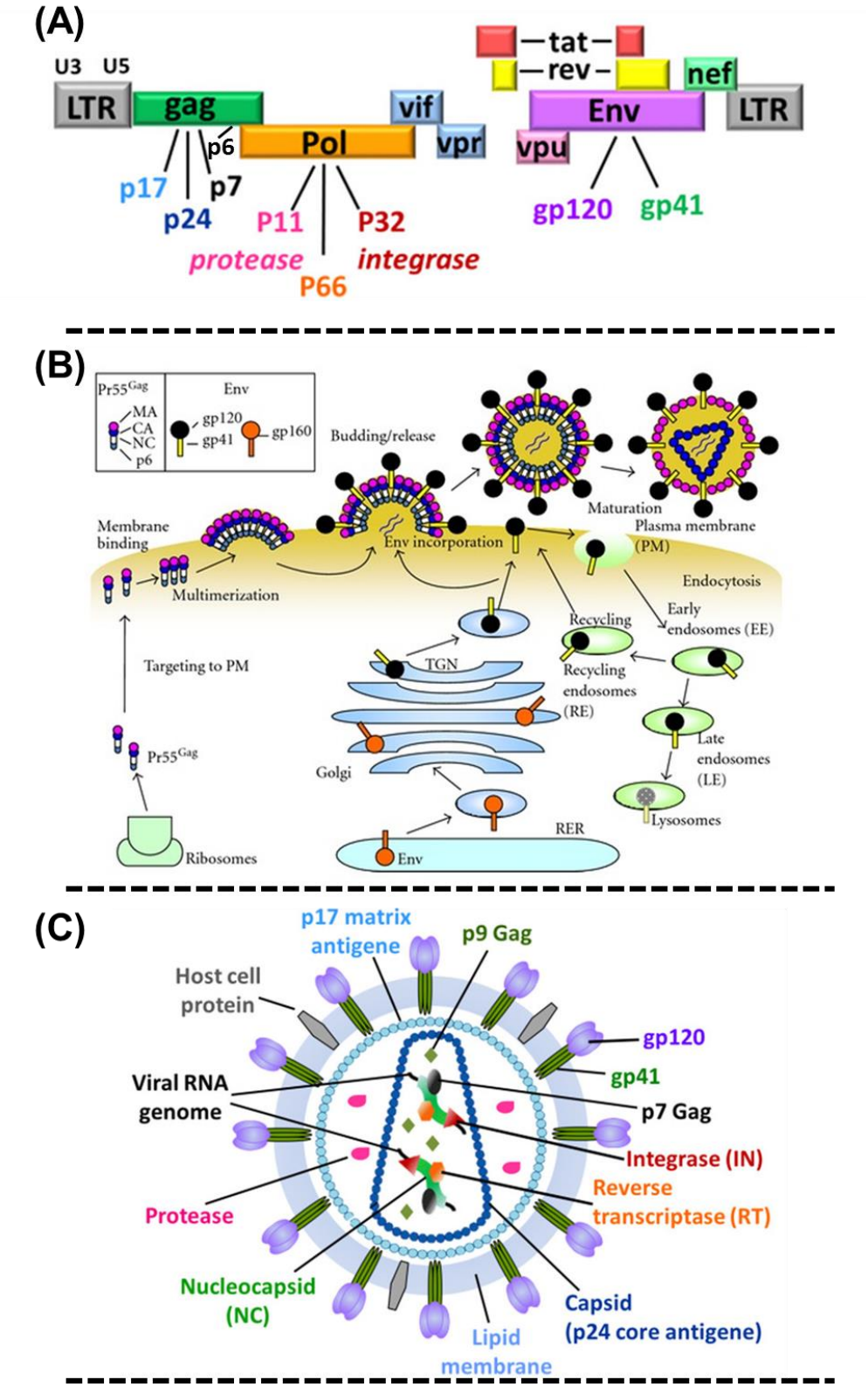

Figure 1.2: Genomic organisation, synthesis and the structure of mature HIV-1 virion. (**A**) Schematic showing the arrangement of HIV-1 structural genes (*gag*, *pol* and *env*), accessory genes (*nef, vif, vpr* and *vpu*) and regulatory genes (*tat* and *rev*) flanked by long terminal repeat (5'-LTR and 3'-LTR) sequences. Lines indicate the viral proteins expressed following the translation of these genes. **(B)** Synthesis, trafficking, assembly, budding and maturation of HIV-1 virion. **(C)** Structure of the mature HIV-1 virus showing different proteins expressed. Figure 2 **(A)** & **(C)** were both adapted from Musumeci

et al. (2015), while Figure 2 **(B)** was taken from Murakami (2012) following the guidelines of the Creative Commons copyright License.

The Gag precursor contains the core structural proteins: these include the matrix (MA or p17), capsid (CA or p24), nucleocapsid (NC or p7), as well as a smaller stabilising protein (p6) and two “spacer” regions (p1 and p2). Co-translational modification of the Gag precursor adds an N-terminal myristoyl group to the MA, which, together with the highly basic N-terminal residues of the matrix domain, promotes the association of the precursor with the phospholipid components of the host plasma membranes (Saad *et al.* 2006; Dalton *et al.* 2007). The accumulation and multimerisation of Gag precursors in the vicinity of a plasma membrane result in the formation of a semi-spherical viral particle that fuses or anchors with a host membrane (Saad *et al.* 2006). The p6 domain interacts with cellular machinery called endosomal complexes required for transport (ESCRT) to promote budding of immature viral particles (Votteler & Sundquist. 2013; Lippincott-Schwartz *et al.* 2017). The immature viral particle eventually buds off, acquiring its membrane from the cellular plasma membrane, and is deposited into the extracellular space. The viral protease (part of the RT-Pro polyprotein) then processes the immature virus to generate mature, infectious virions (Mattei *et al.* 2014; Kleinpeter & Freed. 2020). The Gag capsid domain promotes the interaction between Gag molecules and forms an outer shell of the mature viral core. The nucleocapsid is responsible for the packaging of two copies of single-stranded RNAs into assembling viral particles (Göttlinger *et al.* 1989; Göttlinger. 2001; Checkley *et al.* 2011; Freed. 2015).

The *pol* gene encodes the protease (viral protease (p11PR)), reverse transcriptase (p51RT), RNase H (p15) and integrase (p32)) enzymes that together with single-stranded RNAs are encapsulated into a mature virion to mediate viral replication, synthesis and integration into a host genome (Sundquist & Kräusslich. 2012; Konvalinka *et al.* 2015; Pornillos & Ganser-Pornillos. 2019). The *env* gene encodes gp160 Env precursor (prGp160) that is synthesized in the ER, glycosylated and proteolytically cleaved in the Golgi aparatus to generate non-covalently associated surface gp120 (SU) and transmembrane gp41 (TM) glycoproteins. The membrane-bound gp120-gp41 complex is translocated to the plasma membrane, incorporated into a virion particle by MA-mediated mechanisms, and mediates viral attachment and fusion into a target cell (Checkley *et al.* 2011; Freed. 2015; Murphy & Saad. 2020). The HIV-1 genome also contains genes that encode four accessory proteins: *nef* (negative effector), *vif* (viral infectivity factor), *vpr* (viral protein r) and *vpu* (viral protein u) and two regulatory proteins: *tat* (transcriptional transactivator) and *rev* (regulator of viral gene expression) (Seelamgari *et al.* 2004; Mushahwar. 2006; Zotova *et al.* 2019).

1.4 Synthesis and trafficking of Env

The HIV-1 envelope (Env) glycoprotein is synthesised in the rough endoplasmic reticulum (RER) as a polyprotein precursor, gp160 (Figure 2B above) (Checkley *et al.* 2011; Beitari *et al.* 2019). This precursor is directed to the RER by the ER signal peptide present upstream of the gp160 precursor coding sequence. The signal peptide is co-translationally cleaved by cellular proteases in the ER. The N- and O-glycans are also co-translationally added during gp160 synthesis in the ER. The gp160 precursor subunits oligomerise into predominantly trimeric Env species that translocate into the cis-Golgi network, and the high-mannose glycans acquire complex modifications in the trans-Golgi network (TGN) (Murphy & Saad. 2020). In the Golgi, the gp160 precursor is proteolytically cleaved at a conserved motif (K/R-X-K/R) by cellular furin protease to produce non-covalently associated surface (SU) gp120 and the transmembrane (TM) gp41 mature glycoproteins (Checkley *et al.* 2011; Pornillos & Ganser-Pornillos. 2019). Furin proteolysis is critical for Env to assume the quaternary configuration capable of mediating viral fusion to the cell membranes during HIV-1 infecting events (Chen. 2019). The gp120-gp41 complexes produce heterotrimeric Env spikes that traffic to the plasma membrane where approximately 14 Env spikes incorporate into each budding virion (Yuste *et al.* 2004; Zhu *et al.* 2006; Checkley *et al.* 2011; Schiller & Chackerian. 2014).

1.5 Structural organisation and functions of domains of gp120 and gp41 glycoproteins

Gp120 is a receptor (CD4)-binding domain that is made up of five hypervariable loops (V1-V5) that alternate with five relatively conserved domains (C1-C5) (Starcich *et al.* 1986) (Figure 1.3 A). While the conserved domains are directly involved in the CD4 binding, the variable loops are not essential for CD4 binding (Olshevsky *et al.* 1990; Pollard *et al.* 1992; Wyatt *et al.* 1993). V1V2 loops, which appears at the tip of the trimer, show considerable heterogeneity in length, sequences and number of glycosylation sites between different strains, and this is implicated in the viral escape from neutralising antibodies (Curlin *et al.* 2010; Zolla-Pazner & Cardozo. 2010). The V3 loop is hidden under the V1V2 loops, and this position is almost the centre of the trimer. Following CD4-binding induced conformational changes, the V3 loop is then exposed to interact with the chemokine receptors CCR4 or CXCR4 (Speck *et al.* 1997; Tamamis & Floudas. 2014; Shaik *et al.* 2019; Murphy & Saad. 2020). The V4-V5 loops project outward of the trimer. The deletion of any of the V1-V5 loops hinders viral entry (Wyatt *et al.* 1993; Yuan *et al.* 2013).

The gp41 transmembrane glycoprotein is more highly conserved than gp120 and plays a key role in the fusion of the virus with host membranes (Checkley *et al.* 2011). Gp41 comprises three domains: these are an N-terminal ectodomain, a transmembrane domain (TMD) and a C-terminal cytoplasmic tail (CT) (Figure 1.3 A). The ectodomain, which is critical for Env

trimerisation, is organised into a hydrophobic fusion peptide (FP), disulphide-linked N- and C-terminal heptad-repeats (HR1 and HR2, respectively), and a membrane-proximal external region (MPER). Pre-viral fusion, the ectodomain is buried within the gp120-gp41 trimer complex and is only exposed as a result of CD4-binding induced conformational changes. The exposed fusion peptide interacts with the cell membranes and forms a pre-hairpin conformation with the MPER domain to bridge the viral and cell membranes (Figure 1.3 B) (Gallo *et al.* 2003; Cai *et al.* 2011). Three molecules of HR1 and three molecules of HR2 fold over to form a coiled-coiled six-helix bundle that enhances the affinity of viral and cell membranes for fusion to occur (Weissenhorn *et al.* 1997; Melikyan *et al.* 2000; Chen. 2019). The TMD is highly conserved, anchors Env into the lipid bilayer and plays essential roles in viral conformational changes and fusion (Shang *et al.* 2008; Kondo *et al.* 2010; Chen. 2019). The CT domain contains lentivirus lytic peptides which are implicated in Env fusion, incorporation into a virus, as well as the stability and oligomerisation of Env (Lee *et al.* 2000; Piller *et al.* 2000; Bültmann *et al.* 2001; Lee *et al.* 2002; Kalia *et al.* 2003; Tedbury & Freed. 2015; Chen. 2019).

Furthermore, the Env glycoprotein contains 18 conserved cysteine residues and is also heavily glycosylated (there are 20-35 N-glycosylation sites in gp120 and 3-5 N-glycosylation sites in gp41 subunits) (Allan *et al.* 1985; Leonard *et al.* 1990). Cysteine residues form approximately nine disulphide bonds that stabilise the Env tertiary structure (Leonard *et al.* 1990). Glycans determine Env conformation, viral entry and infectivity (Li *et al.* 2008; Raska & Novak. 2010). HIV-1 uses these glycans as an immune evasion mechanism to mask epitopes capable of eliciting antibody-mediated neutralisation (Montefiori *et al.* 1988; Leonard *et al.* 1990; Wei *et al.* 2003; Kumar *et al.* 2011; Huang *et al.* 2012).

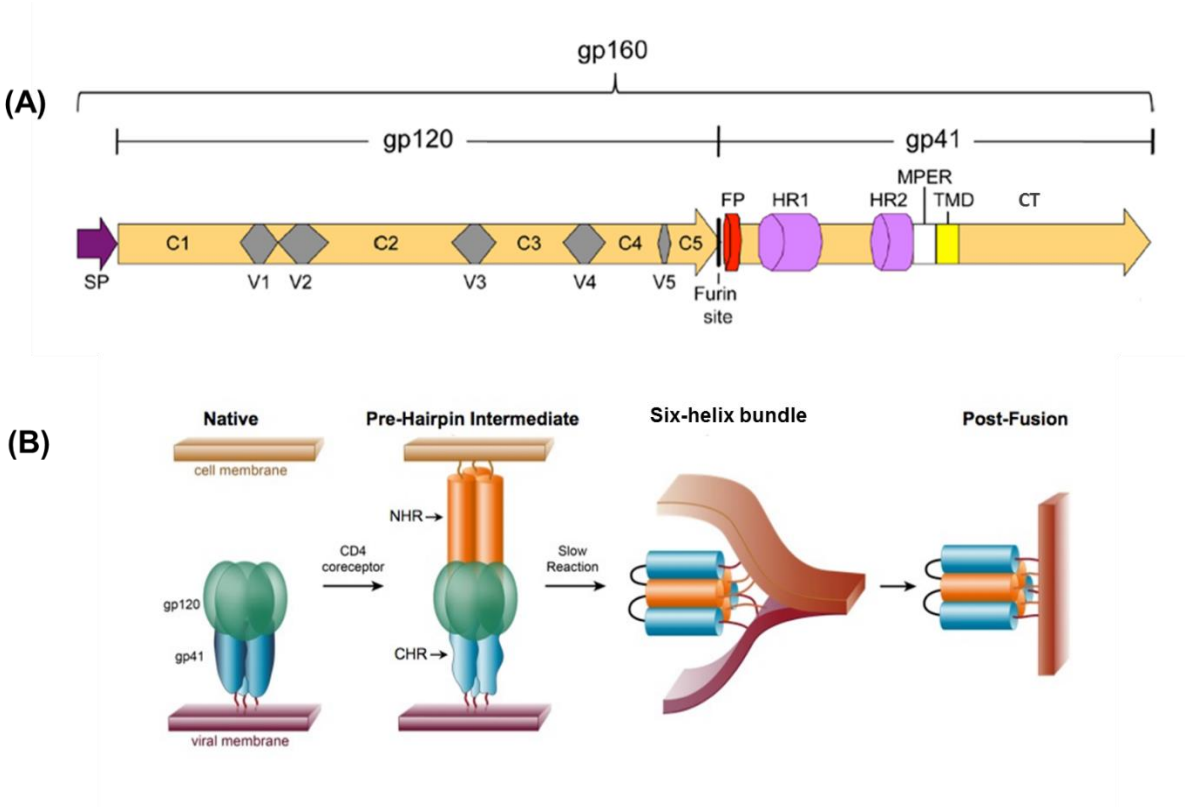

Figure 1.3: Linear organisation of HIV-1 Env and its fusion with the host cell membranes. **(A)** Gp160 precursor contains the signal peptide (SP) that is cleaved by proteases in the endoplasmic reticulum. In the Golgi complex, the precursor is proteolytically cleaved to generate non-covalently linked gp120 and gp41 subunits. Gp120 contains five conserved domains (C1-C5) interspersed with five hypervariable loops (V1-V5). Gp41 contains an ectodomain comprising the fusion peptide (FP), heptad-repeats (HR1 and HR2) and the membrane-proximal external region (MPER), a transmembrane domain (TMD), and a cytoplasmic tail (CT). **(B)** The binding of gp120 to CD4 and coreceptor results in conformational changes that allow the fusion peptide of the gp41 to interact with cellular membranes and form a pre-hairpin structure. The second conformational changes involving HR1 (NHR) and HR2 (CHR) form a six-helix bundle that facilitates the fusion of viral and cell membranes. In the post-fusion state, the viral and cell membranes are merged. Figure 3 **(A)** was adapted from Checkley *et al.* (2011) with permission provided by Elsevier while Figure 3 **(B)** was retrieved (29/03/20) from peterkimlab.stanford.edu/home and edited accordingly.

1.6 Conformational flexibility and Tier classification of HIV-1 Env spikes

HIV-1 Env spikes exist in various conformations (Figure 1.4). On a membrane of a functional HIV-1 virion, mature Env predominantly exists in a “closed” pre-fusion conformation that conceals conserved functional epitopes to evade neutralising antibody responses (Cai *et al.* 2011; Munro *et al.* 2014; Guttman *et al.* 2015). The pre-fusion state rearranges to an intermediate open conformation to allow the binding of Env to the host CD4 and CCR5/CXCR4 coreceptor (Munro *et al.* 2014; Herschhorn *et al.* 2016). Upon the fusion of the viral membrane with the host plasma membrane, Env adopts an “open” post-fusion conformation which exposes non-functional Env epitopes (Munro *et al.* 2014; Guttman *et al.* 2015). In contrast to

an “open” conformation where epitopes are exposed, the V1/V2 loops are intact, and the V3 is hidden in a “closed” conformation (Guttman *et al.* 2015).

Based on the conformation that a trimer frequently adopts and the sensitivity to neutralisation, HIV-1 isolates (standardised panel of molecularly cloned Env-pseudotyped viruses, (Mascola *et al.* 2005)) are classified into Tier 1A (open conformation, most sensitive), Tier 1B (intermediate conformation, next most sensitive) and Tier 2 and 3 (closed conformation, moderate and least sensitive, respectively) phenotypes (Seaman *et al.* 2010; Montefiori *et al.* 2018). Tier 2 viruses represent most of the circulating viruses, suggesting that an effective vaccine should elicit antibody responses against Env that largely adopts the “closed” conformation.

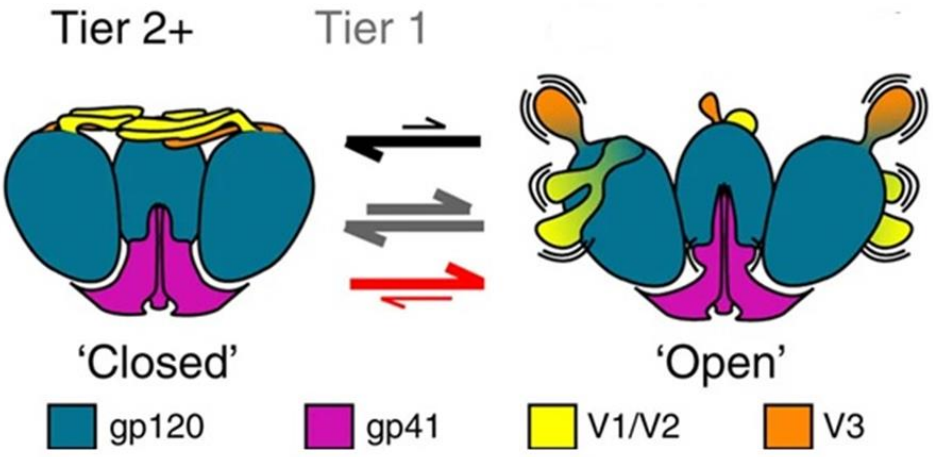

Figure 1.4: Conformational states adopted by HIV-1 Env trimers. The trimer oscillates between closed, intermediate and open conformations. The conserved epitopes, such as V3, are exposed as the trimer opens up. Based on susceptibility to the neutralisation, HIV-1 isolates are classified into Tier 1 (most sensitive) and Tier 2 (moderate sensitivity) viruses. The diagram was adapted from Guttman *et al.* (2015) with permission provided by Springer Nature.

1.7 Development of neutralising antibodies during natural infection and other antibody functions

Upon infection with HIV-1, an immune response is generated against different viral antigens. However, only antibodies directed to Env glycoprotein spikes can neutralise the virion. Within two months post-infection, most HIV-1-infected people develop potent yet limited autologous (strain-specific) neutralising antibody responses that target the variable regions of Env (Figure 1.5) (Richman *et al.* 2003; Wei *et al.* 2003; Li *et al.* 2006; Gray *et al.* 2007; Landais & Moore. 2018). The virus readily escapes the immune pressure exerted by strain-specific antibodies;

thus, most circulating escape viruses are resistant to pre-existing neutralising antibodies directed to a precedent virus (Arendrup *et al.* 1992; Wei *et al.* 2003; Frost *et al.* 2005). Following the emergence of limited cross-neutralising antibodies 1-year post-infection, 10-25% of chronically infected individuals develop heterologous neutralising antibodies over 2-3 years post-infection (Doria-Rose *et al.* 2009; Stamatatos *et al.* 2009; Gray *et al.* 2011b; Hraber *et al.* 2014). A small subset, 1%, of HIV-infected individuals are elite neutralisers, which refers to individuals that elicit broadly neutralising antibodies (bNAbs) that can potently neutralise viruses within a clade group and across at least four clades (Simek *et al.* 2009). Vaccine development strategies focus on designing immunogens that can elicit bNAbs to prevent viral entry or kill HIV-1 infected cells (Landais & Moore. 2018; Liu *et al.* 2020).

In addition to virus neutralisation, different isotypes of HIV-specific antibodies in elite controllers often exhibit strong polyfunctional effector functions, which are mediated by the binding of their fragment crystallisable region (Fc) to the receptors on target cells (e.g. natural killer cells) to induce killing of infected cells (Chung *et al.* 2011; Ackerman *et al.* 2016; Tay *et al.* 2016; Madhavi *et al.* 2017). These antibody effector functions include antibody-dependent cellular cytotoxicity (ADCC), antibody-dependent cellular phagocytosis (ADCP), and complement-dependent cytotoxicity (CDC), and contribute to the control of HIV-1 during natural infection (Ackerman *et al.* 2016; Chen *et al.* 2018; Moris *et al.* 2019).

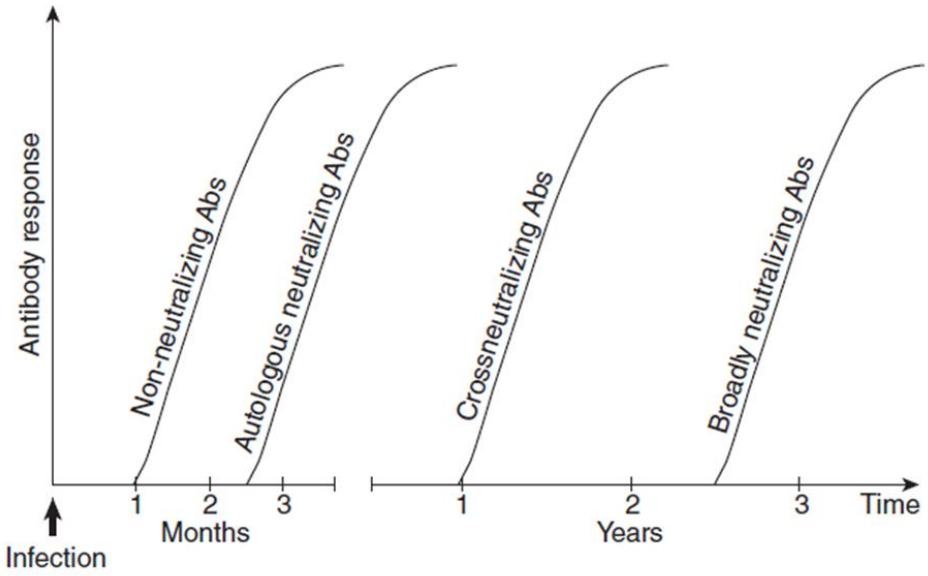

Figure 1.5: Development of antibody types over time to HIV during infection. The diagram was taken from Geiß and Dietrich (2015).

1.8 Regions targeted by bNAbs

The identification of the elite neutralisers offered an opportunity to map HIV-1 Env epitopes targeted by bNAbs and enabled the isolation of human monoclonal antibodies (mAbs), which recapitulate the neutralisation breadth observed in donor's sera. Significant enthusiasm is focusing on evaluating the protective efficacy of these bNAbs. Varying degrees of protection following passive immunisation with bNAbs have been demonstrated in non-human primates challenged with chimaeric SHIV viruses (viruses that express HIV-1 Env in the backbone of the simian immunodeficiency virus (SIV) (Moldt *et al.* 2012; Pegu *et al.* 2014; Gautam *et al.* 2016; Moldt *et al.* 2016; Gruell & Klein. 2018; Garber *et al.* 2020; Liu *et al.* 2020). Screening techniques involving single B-cell sorting and next-generation sequencing, among others, identified a great deal of new potent and highly glycan dependent mAbs that target sites of vulnerability on the native Env spike. These sites include the V2 site, N332 supersite, the CD4-binding site, the gp120-gp41 interface, and the MPER (Wibmer *et al.* 2015; McCoy. 2018). The common characteristics among these bNAbs, which renders them hard to elicit by vaccination due to the complicated maturation processes required, are their propensity to undergo extensive somatic mutations and that a large proportion of these antibodies bear an extraordinary long heavy chain complementary determining region loop three (CDR-H3) (Wibmer *et al.* 2015; McCoy. 2018). Potent and broadly neutralising mAbs isolated against these vulnerability sites are shown in Figure 1.6, and some are discussed in Sections 1.8.1-1.8.5.

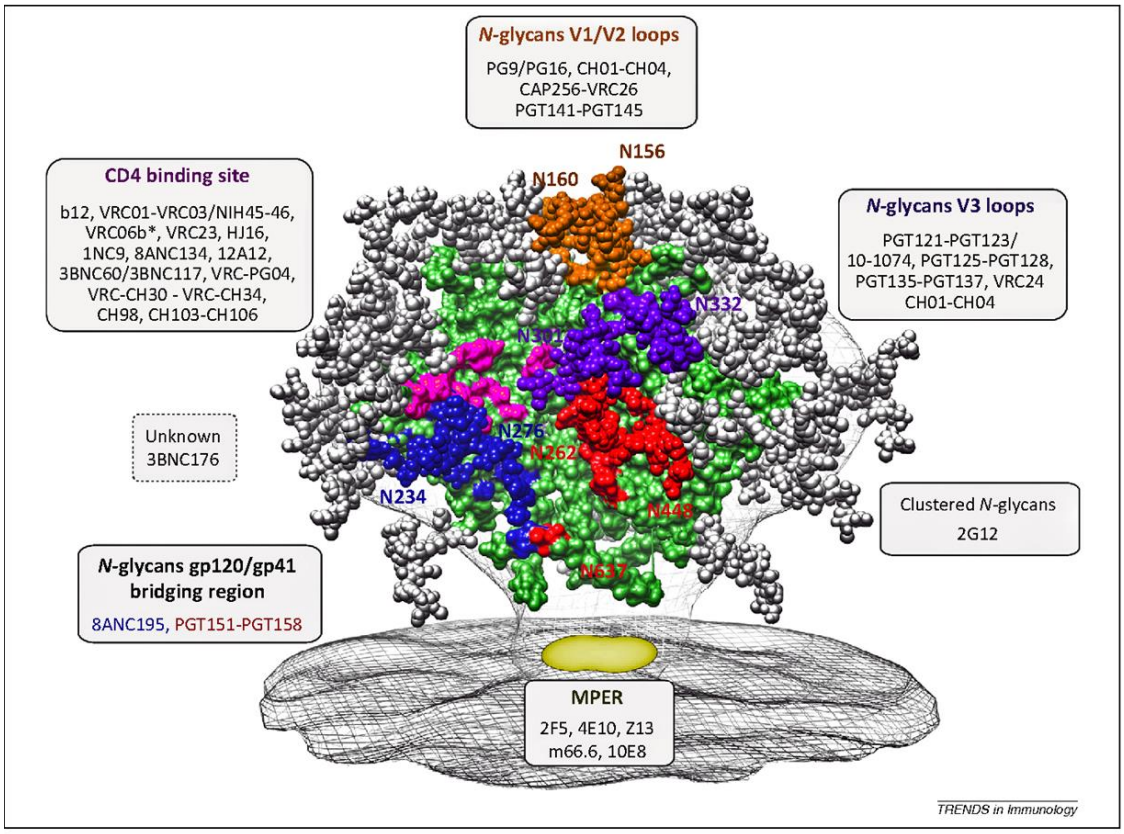

Figure 1.6: The sites of bNAb vulnerability outlined in the crystal structure of the native-like HIV-1 Env trimer. Neutralising mAbs recognising the glycan-dependent epitopes in the V1V2 loops (orange), V3 loop (purple), gp120-gp41 interface (blue and red) and CD4-binding site (pink) in gp120, as well as the MPER (yellow)-specific mAbs, are indicated in boxes near each site of vulnerability. The diagram was taken from Mouquet (2014) with permission provided by Elsevier.

1.8.1 V2 site/V1V2 apex

The prototypes of V2 apex-specific mAbs include PG9/PG16, PGT145, CH01 and CAP256.VRC26.09. The shared characteristics between these mAbs include recognition of the N160 glycan and a four-residue, lysine-rich strand C (KKQR) of the V2 domain (Walker *et al.* 2009; McLellan *et al.* 2011; Walker *et al.* 2011; Pancera *et al.* 2013; Doria-Rose *et al.* 2014; Andrabi *et al.* 2015; Lee *et al.* 2017). These antibodies contain long (> 24 amino acid), anionic, and tyrosine-sulphated CDR-H3 loops that either adopt a hammerhead or ß-hairpin conformation to penetrate the glycan shield and access epitopes on the trimer (McLellan *et al.* 2011; Julien *et al.* 2013; Andrabi *et al.* 2015). PG9 and PG16 mAbs are two somatic variants that were isolated from a clade A-infected African donor and demonstrated differences in neutralisation potency and breadth against the viruses that were assessed (Walker *et al.* 2009). In addition to interaction with N160 glycan, the N156 and N173 glycans are important for the specificity of PG9 and PG16 (Walker *et al.* 2009; McLellan *et al.* 2011). PGT145 mAb shares binding specificity with PG9 and PG16 (Walker *et al.* 2011; Lee *et al.* 2017). The

longitudinal study (59-206 weeks post-infection) to determine virus and bNAb co-evolution in HIV-1 subtype C superinfected CAP256 donor, resulted in a CAP256-VRC26.25 lineage comprising 33 (CAP256.01-CAP256.33) somatically related V2-specific mAbs (Doria-Rose *et al.* 2014; Bhiman *et al.* 2015; Doria-Rose *et al.* 2016). These mAbs differ in neutralisation potency and breadth, and CAP256-VRC26.25 mAb demonstrated 10-fold higher potency and broadest neutralisation breadth than the rest of the members of this lineage (Doria-Rose *et al.* 2014). The CAP256-VRC26 antibodies are characterised by very long (35-37 amino acid) CDR-H3 loops and partial dependency to N160 glycan (Doria-Rose *et al.* 2014; Andrabi *et al.* 2015; Doria-Rose *et al.* 2016). Some of the members of CAP256-VRC26.25 lineage evolved an ability to engage the sialic acid-bearing glycans on the Env trimer (Andrabi *et al.* 2017). The sialic acid-binding serves as an anchor that enhances bNAb maturation by minimising virus escape (Andrabi *et al.* 2017; McCoy. 2018). BG1 is a novel apex-specific bNAb that differs from PG9, PG16 and PGT145 in that instead of one antigen-binding fragment (Fab) per trimer stoichiometry, two BG1 Fabs engages with the V1V2 epitope of each Env trimer and it does not contain a long protruding CDR-H3 (Wang *et al.* 2017). The N90-VRC38 lineage is another V1V2-directed mAbs that does not feature a long protruding loop (Cale *et al.* 2017).

1.8.2 CD4 binding site (CD4bs)

CD4 binding site (CD4bs) play a crucial role in viral entry by binding to the host cell CD4 receptor, and the majority of its features are functionally conserved across multiple HIV isolates; thus, it is classified as one of the supersites of vulnerability for vaccine design (Kwong *et al.* 1998). Studies have reported that CD4bs bNAbs take longer than other bNAbs to develop and have the highest level of somatic mutation, indicating a barrier to elicit these responses (Kwong & Mascola. 2012; Lynch *et al.* 2012; Wu *et al.* 2015). Antibody b12 was the first CD4bs-specific mAb that was derived from a Clade B-infected donor (Burton *et al.* 1994). VRC01 and its somatic variant VRC02 were the second CD4bs-directed mAb found on functional Env trimers and neutralised 90% of circulating HIV-1 strains as compared to 40% neutralised by b12 (Wu *et al.* 2010). Based on B cell ontogenies (class) and the structural mode of antibody recognition (type), a series of CD4bs mAbs from different donors have been isolated and are classified into VRC01-class and non-VRC01 loop-dependent CD4bs mAb (Kwong & Mascola. 2012; Zhou *et al.* 2015). The distinguishing features of VRC01-like mAbs include the use of VH1-2 genes and the light chain genes encoding a relatively small 5-residue CDR-L3 (Scheid *et al.* 2011; West *et al.* 2012; Zhou *et al.* 2015). Another VRC01-class mAb, PCIN63, with relatively less somatic mutation and rapid affinity maturation compared to the prototype VRC01, has been isolated recently from a subtype C-infected donor, an observation that may guide vaccine design (Umotoy *et al.* 2019). N6 and N49P7 are examples of VRC01-

class mAbs with the remarkable breadth that potently neutralised more than 89-100% of the tested global panel of HIV-1 pseudoviruses (Huang *et al.* 2016; Sajadi *et al.* 2018).

1.8.3 Asn332 (N332) glycan-dependent supersite

The N332 supersite is found between the overlapping glycan-dependent epitopes such as the V3 and V2 epitopes that exist near each other at a trimer apex (Julien *et al.* 2013; Kong *et al.* 2013). PGT21 and PGT128 potently neutralise the majority of circulating viruses from all clades, including clade C viruses (Walker *et al.* 2011). They are both V3-specific mAb that highly depends on glycans at positions N301 and N332 to recognise their 8-residue epitope through a glycan-penetrating long CDR-H3 loop (Pejchal *et al.* 2011). PGT135 is another N332-dependent mAb that uses a long 18-residue CDR-H3 and an extended CDR-H1 loop to penetrate the glycan shield and access the V4 loop in contrast to the V3 loop targeted by PGT21 and PGT128. In addition to the recognition of N332 glycan, PGT135 interacts with three glycans at positions N295, N368 and N392 (Kong *et al.* 2013). A clade B-neutralising mAb 2G12 represents the N332 supersite antibody which does not penetrate the glycan shield. Instead, 2G12 utilises a unique variable heavy (VH) chain domain swap structure to recognise the outermost mannose sugars of the four glycans at positions N295, N332, N339 and N392 of gp120 (Calarese *et al.* 2003).

1.8.4 gp120-gp41 epitope

Human mAb 8ANC195, PGT151, and 35O22 are prototypes representing the mAbs with epitopes that span both the gp120 and gp41 regions on the Env spike (Wibmer *et al.* 2015). 8ANC195 requires the glycans at positions N234 and N276 of gp120 and the presence of a non-glycan penetrating 22-residue long CDR-H3 to induce neutralisation. The CDR-H3 of this antibody rearranges to interact with the light chain, thus forming a paratope that comes into contact with an inner region of gp120 that interacts with gp41 (Scharf *et al.* 2014). The 35O22 mAb interacts with an epitope near the N234 glycan recognised by 8ANC195 mAb (Huang *et al.* 2014; Pancera *et al.* 2014). PGT151 is another mAb that interacts with a gp120-gp41 epitope lying between the 8ANC195 and 35O22 epitopes, and 2 Fabs of this antibody bind specifically to cleaved trimers (Blattner *et al.* 2014; Falkowska *et al.* 2014). Thus, PGT151 is often used in antigenicity assays to evaluate the conformation of soluble native-like trimers. Both 35O22 and PGT151 monoclonal antibodies recognise the glycan-dependent antigenic sites. 35O22 neutralisation depends on the glycans at position N88, N230 and N241 of gp120 while PGT151 depends on the glycans at position N611 and N637 of gp41 (Falkowska *et al.* 2014; Huang *et al.* 2014).

1.8.5 MPER supersite

The highly conserved membrane-proximal external region (MPER) in gp41 is a relevant epitope for bNAb responses to HIV-1 (Caillat *et al.* 2020). Three mAbs (2F5, Z13e1 and 4E10) were first isolated targeting the linear epitopes in the MPER (Muster *et al.* 1993; Zwick *et al.* 2001; Nelson *et al.* 2007). Even though these antibodies were identified as broad neutralisers, they had limited potency and were highly autoreactive. The latter is due to the proximity of MPER to the viral membrane, which promotes the interaction of their long CDR-H3 loops with viral lipid membranes (Haynes *et al.* 2005; Alam *et al.* 2009; Irimia *et al.* 2016). The 10E8 mAb is a relatively more potent and broad MPER-specific mAb that lacks the limiting characteristics observed for 2F5 and 4E10 (Huang *et al.* 2012). The crystal structure indicated that the potency and breadth of 10E8 are derived from a unique conformation that this antibody adopts when interacting with conserved epitopes within the MPER (Huang *et al.* 2012; Irimia *et al.* 2016). The recently isolated MPER-specific antibody DH511 (Williams *et al.* 2017), VRC42 (Krebs *et al.* 2019), LN01 (Pinto *et al.* 2019) and PGZL1 (Zhang *et al.* 2019) target the linear helical epitopes adjacent to the transmembrane domain (Caillat *et al.* 2020).

1.9 Features of HIV-1 Env spikes that challenge the design of immunogens for eliciting bNAbs

The conformational flexibility of Env trimers attributes to features that the HIV-1 Env evolved to evade neutralising antibodies and causes Env to be a complex antigen that challenges vaccine design (Klasse *et al.* 2020). The presence of open, non-functional Env trimers on the surface of an infecting virion or immunisation with Env immunogens adopting an “open” rather than a “closed” conformation, elicit antibodies that are unable to neutralise the circulating viruses because they cannot access their epitopes on a native spike (Munro *et al.* 2014; Guttman *et al.* 2015). Other features of HIV-1 Env that contribute to immune evasion strategies are illustrated (Figure 1.7). These features include rapid escape mutation resulting in the high diversity of the circulating viruses (Richman *et al.* 2003; Wei *et al.* 2003), glycan shield (Binley *et al.* 2010; Watanabe *et al.* 2020), conformational masking of the CD4 binding site (Kwong *et al.* 2002), steric hindrance which limits the access of antibodies to gp120 epitopes (Labrijn *et al.* 2003), transient exposure of gp41 MPER epitopes (Frey *et al.* 2008), non-functional immunological Env decoys such as gp120/gp41 monomers, gp41 stumps and unprocessed gp160 (Poignard *et al.* 2003; Moore *et al.* 2006) and unusual incorporation of sparse, widely spaced Env spikes (≈ 14 spikes per virion) (Zhu *et al.* 2006; Klein & Bjorkman. 2010; Schiller & Chackerian. 2014). The implications of the low spike density on the immunogenicity of HIV-1 Env immunogens are further explained in Section 1.13.

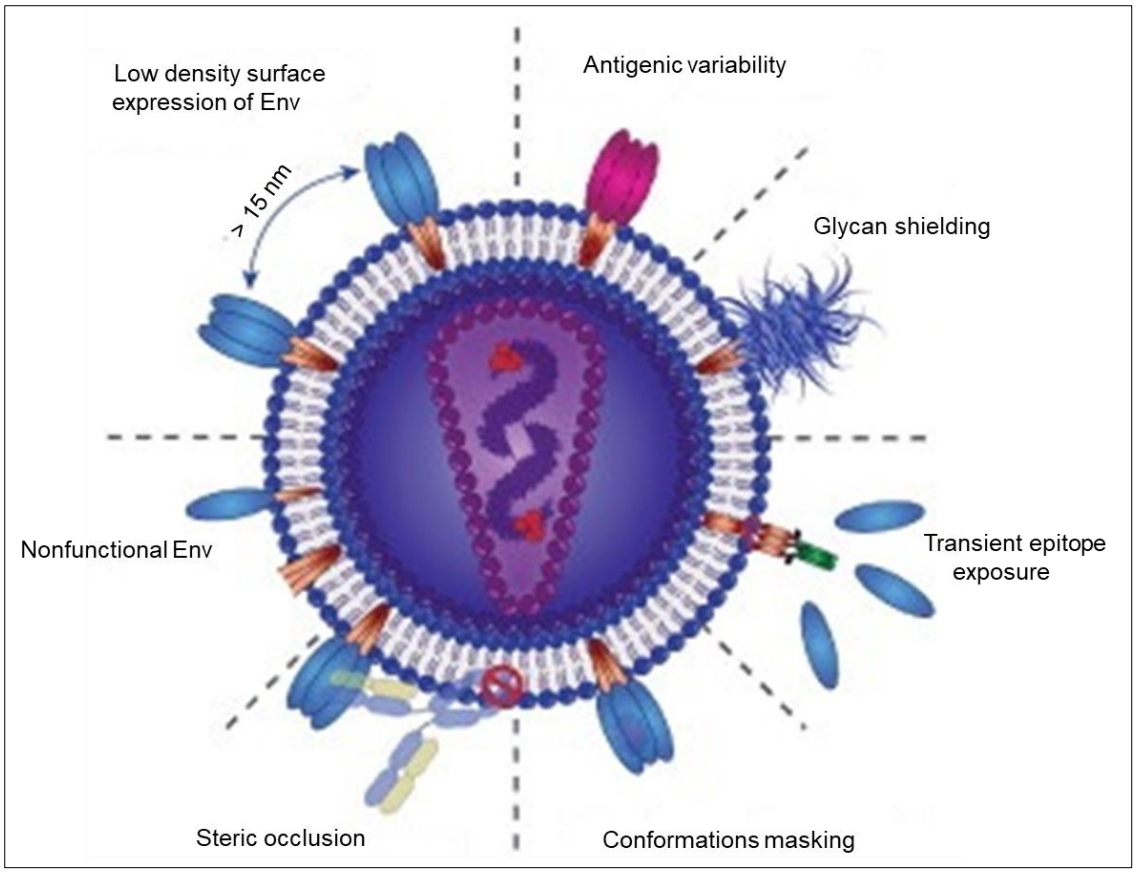

Figure 1.7: Schematic showing the antigenic features that HIV-1 Env evolved to evade neutralising antibody responses. The diagram was taken from Mouquet (2014) with permission provided by Elsevier.

1.10 Overview of vaccine efficacy trials

This section provides an outline of the seven efficacy trials that have tested candidate HIV-1 vaccine regimens in phase 2b/3. Of the seven candidate vaccine regimens, the RV144 regimen remains the only one that demonstrated modest yet controversial efficacy against HIV-1 acquisition (Rerks-Ngarm *et al.* 2009; Desrosiers. 2017; Tomaras & Plotkin. 2017). The candidate vaccine regimens that progressed to a phase 2b/3 efficacy trial in humans have had been tested in non-human primate challenge models during preclinical evaluations (Sheets *et al.* 2016). The inconsistencies in efficacy observed in NHP challenge models vs efficacy trials in humans using similar candidate vaccine regimens demonstrated that the immunogenicity in NHP does not always translate/ predict vaccine responses in humans, suggesting that the preclinical animal models can be limiting (Morgan *et al.* 2008; Watkins *et al.* 2008; McChesney & Miller. 2013; Rahman & Robert-Guroff. 2019).

1.10.1 VAX004 and VAX003: Recombinant gp120 subunit vaccine

Two early phase 3 trials, VAX004 and VAX003, enrolled different risk populations and tested a protein-only vaccine regimen consisting of bivalent gp120 glycoproteins (AIDSVAX B/B or

AIDSVAX B/E) (Flynn *et al.* 2005; Pitisuttithum *et al.* 2006). Even though non-neutralising gp120 antibodies and antibody-dependent cell-mediated virus inhibition (ADCVI) responses were observed in vaccinees, no efficacy was observed since these vaccines did not prevent HIV-1 infection or slow HIV-1 disease progression (Flynn *et al.* 2005; Pitisuttithum *et al.* 2006; Forthal *et al.* 2007). The lack of efficacy was attributed to the inability of sera from vaccinees to neutralise diverse HIV-1 isolates (Gilbert *et al.* 2005; Montefiori *et al.* 2012). Despite the lack of efficacy in VAX004 and VAX003, these trials indicated for the first time that conducting a phase 3 HIV-1 efficacy trial was feasible (Flynn *et al.* 2005; Sheets *et al.* 2016).

1.10.2 STEP and Phambili: Adenovirus serotype 5-vectored vaccine

Two subsequent phased 2b 'test-of-concept' trials, the STEP and Phambili, were initiated in the USA and South Africa, respectively. These trials tested a replication-incompetent adenovirus serotype 5 (Ad5) trivalent vaccine (MRKAd5/HIV-1 Gag/Pol/Nef) designed to induce CD8+ cellular responses instead of humoral responses (Buchbinder *et al.* 2008; McElrath *et al.* 2008; Priddy *et al.* 2008; Gray *et al.* 2011b). Despite eliciting HIV-1-specific interferon-gamma (INF-ɣ)-secreting CD8+ T cells in vaccinees, these vaccines showed no efficacy since they failed to lower the rate of HIV-1 acquisition (Buchbinder *et al.* 2008; McElrath *et al.* 2008; Gray *et al.* 2011b). In fact, the exploratory multivariate analysis of the STEP data indicated an increased risk of HIV-1 acquisition in vaccinees with pre-existing Ad5 antibodies and/or uncircumcised compared to placebo recipients (Buchbinder *et al.* 2008; Duerr *et al.* 2012). The Phambili trial was discontinued and unblinded (reveal to participants whether they had received the vaccine or the placebo) due to the interim STEP trial analysis (Gray *et al.* 2011b; Gray *et al.* 2014). From these two trials, it was evident that the candidate vaccines that only elicit T cell responses are not likely to prevent HIV-1 acquisition (Sheets *et al.* 2016). This observation suggested that an effective vaccine regimen would need to elicit both cellular and humoral responses (Haynes & Shattock. 2008).

1.10.3 RV144: Canarypox vector prime-Env (subtype B/E) protein boost

The fifth trial, RV144 (Thailand), tested a prime-boost vaccine regimen that was designed to elicit both cellular and humoral responses to the HIV-1 envelope (Rerks-Ngarm *et al.* 2009). This regimen consisted of a replication-defective defective canarypox vector (ALVAC-HIV; encoding HIV-1 Gag and protease proteins of subtype B as well as CRF01-AE gp120 linked to the transmembrane domain of subtype B gp41) prime and a bivalent gp120 (AIDSVAX® clade B/E) boost (Rerks-Ngarm *et al.* 2009). Encouragingly, for the first time, a moderate but significant 31% efficacy against HIV-1 infection was reported in this trial; and this demonstrated that a vaccine regimen could elicit protective cellular and humoral immune responses against HIV-1 (Rerks-Ngarm *et al.* 2009; Haynes *et al.* 2012; Corey *et al.* 2015).

This efficacy was unexpected as neither the ALVAC-HIV nor AIDSVAX B/E was effective when used alone (Nitayaphan *et al.* 2004; Pitisuttithum *et al.* 2006; Forthal *et al.* 2007).

Multiple (six) immune responses that correlated with moderate protection in the RV144 trials were identified using seventeen different humoral and cellular immune assays (Haynes *et al.* 2012). These vaccine-induced immune responses included binding antibodies (plasma Env IgA, Env IgG avidity, V1V2 IgG), neutralising antibodies and cellular immunity (Env-specific CD4+ T cells) as reviewed by Tomaras and Plotkin (2017) and Pitisuttithum and Marovich (2020). Non-neutralising IgG binding antibodies directed to the V1V2 region of Env primarily corresponded with a reduced risk of HIV-1 infection while the plasma IgA binding to Env directly correlated with an increase in HIV-1 acquisition (Haynes *et al.* 2012; Tomaras *et al.* 2013; Yates *et al.* 2014). In addition, the secondary immune correlates analysis showed that a combination of low Env IgA titres and high titres of ADCC-mediating antibodies (targeting the conformational C1 epitope of HIV-1 Env) inversely correlated with HIV-1 acquisition (Bonsignori *et al.* 2012; Haynes *et al.* 2012). The genetic sieve analysis also demonstrated that the vaccine efficacy was improved against viruses that matched the vaccine strain at residue 169 (lysine) of the V2 region of Env (Rolland *et al.* 2012; Liao *et al.* 2013). The V2 residue K169-specific monoclonal antibodies (CH58 and CH59) isolated from the vaccinees demonstrated the antibody effector function that mediated the killing of HIV-1-infected CD4+ cells (Liao *et al.* 2013). However, the RV144 regimen failed to elicit Tier 2 bNAbs (Montefiori *et al.* 2012). The identification of the functional Fc-mediated polyfunctional antibodies in the RV144 vaccinees suggested that vaccine regimens that fail to elicit sufficient neutralising antibodies could potentially offer protective immune responses through polyfunctional responses (Rerks-Ngarm *et al.* 2009; Haynes *et al.* 2012; Barouch *et al.* 2015; Alter & Barouch. 2018). The RV144 trial provided valuable insights for the subsequent vaccine regimens that were/are tested in phase 1 or 2 clinical trials in continued efforts to develop the improved HIV-1 vaccination regimens (Easterhoff *et al.* 2020; Pitisuttithum & Marovich. 2020).

1.10.4 HVTN505: Multigene-multiclade DNA vectored prime- Adenoviral vectored boost

The sixth efficacy trial, HVTN (HIV Vaccine Trials Network) 505, tested a multigene, multiclade DNA-prime-recombinant adenovirus serotype 5 boost (DNA/rAd5) vaccine regimen in participants (Ad5 seronegative and circumcised) at high risk of HIV-1 infection in the United States (Hammer *et al.* 2013). This prime-boost regimen was designed to elicit both humoral and cellular responses. However, this vaccine regimen was not efficacious in reducing HIV-1 acquisition or viral load in vaccinees that eventually got infected. Low titres of V1V2 binding antibodies were observed in the HVTN505 vaccinees compared to RV144 vaccinees, giving a possible indication of the lack of efficacy in the HVTN505 trial (Hammer *et al.* 2013). This

regimen also induced CD8+ T cell responses with a limited breadth of HIV-1 inhibition (Hayes *et al.* 2016). A follow-up study indicated that the vaccine recipients that had low levels of Env-specific CD8+ T cells and high titres of binding IgG Env antibodies showed a reduced risk of HIV-1 acquisition, suggesting high titres of binding antibodies could correlate with reduced risk of HIV acquisition in the absence of cellular responses (Fong *et al.* 2018). However, the presence of high Env-specific CD8+ T cells correlated with reduced risk regardless of the levels of binding Env responses (Fong *et al.* 2018).

1.10.5 HVTN702/Uhambo: Canarypox vector prime-Env (subtype C) protein boost

Building on the knowledge from the RV144 trial that reported moderate protection against HIV-1 acquisition, the HVTN 702 trial was established in South Africa and used the RV144 regimen that was adjusted to express HIV-1 antigens that matched the circulating subtype C strains in South Africa (Bekker *et al.* 2018). This vaccine regimen consisted of the ALVAC-HIV (vCP2438) prime followed by boosting with bivalent subtype C gp120 formulated in an oil-in-water MF59 adjuvant. The safety and immunogenicity profile of this regimen was first evaluated in a phase 1/2 clinical trial (HVTN 100) that recruited South African participants (Bekker *et al.* 2018; Laher *et al.* 2020a; Laher *et al.* 2020b) before the HVTN 702 2b/3 vaccine efficacy trial was initiated (Bekker *et al.* 2018). In comparison to the RV144 trial, the HVTN702 vaccinees received a 12-month booster immunisation in an effort to improve the longevity of the immune responses (Bekker *et al.* 2018; Easterhoff *et al.* 2020; Laher *et al.* 2020a). The HVTN 702 trial was stopped due to the lack of efficacy that was indicated by 129 vaccinees that became HIV infected compared to 123 placebo recipients (Cohen. 2020; Slomski. 2020). Studies are underway to determine the immunological responses elicited by this regimen.

Table 1: Overview of the candidate HIV-1 vaccine regimens that have been tested in phase 2b/3 efficacy trials. This table was modified from Tomaras and Plotkin (2017) and Pitisuttithum and Marovich (2020).

Trial name, trial duration, period, trial site	participants age, HIV status/ risk status, other	Phase	vaccine regimen	Observed immune responses	Major immune correlates of decreased HIV acquisition	Immune correlates that reduced vaccine efficacy	immune correlates that reduced viral load after infection	Overall vaccine efficacy
Vax004 1998-2003 North America, Netherlands	18-62 years old, HIV-1 negative MSM and high-risk heterosexual women	3	AIDSVAX B/B: Contained bivalent subtype B/B (MN and GNE8 isolates) gp120 antigens in alum adjuvant.	Non-neutralising anti-gp120 binding antibodies, ADCVI, tier 1 nAbs	anti-gp120 binding antibodies, tier 1 nAbs, ADCVI	No	n.d	no efficacy
VAX003 1999-2000 Thailand	20-59 years old, HIV-1 negative injection drug users (IDUs)	3	AIDSVAX B/E: Contained recombinant gp120 from subtype B (MN) and subtype RF01-AE (A244) formulated in alum adjuvant.	non-neutralising anti-gp120 antibodies	No	No	No	no efficacy
STEP (HVTN 502, Merck 023) 2004-2007 North America, South America, Caribean	18-45 years old, HIV-1 negative people at high risk of HIV-1 acquisition, including MSM	2b	MRKAD5 HIV-1: trivalent replication-incompetent Adenovirus serotype 5 (Ad5) vectors encoding HIV-1 subtype B gag or pol or nef genes.	IFN-ɣ ELISPOT responses, Gag-specific T cells	No	n.d	CD8+ T cell breadth	No efficacy, increased risk of HIV-1 infection in uncircumcised vaccinees and/or vaccinees with Ad5 pre-

								existing immunity
Phambili (HVTN 503) 2007-2007 South Africa	18-35 years old, HIV-1 negative heterosexual men and women with pre-existing Ad5 responses	2b	MRKAD5HIV-1 gag/pol/nef (subtype B) vaccine used in STEP trial.	IFN-ɣ secreting T cell responses to clade B and C antigens	n.d	n.d	n.d	No efficacy, the study was discontinued and unblinded due to interim STEP trial analysis.
RV144 2003-2005 Thailand	18-30 years old, HIV-1 negative heterosexual adults	3	Primed with a replication-defective canarypox vector vaccine (ALVAC-HIV [vCP1521]) expressing Gag, Pol and Env antigens and boosted with AIDSVAX B/E bivalent gp120 vaccine used in VAX003 trial.	Env-V1V2 IgG binding antibodies, ADCC-mediating antibodies, IG3 Fc-mediated effector functions, Tier 1A, Env IgA	Env-V1V2 IgG binding antibodies, ADCC, Fc-mediated effector functions	Yes, plasma Env IgA	n.d	60% and **31.2% efficacy** at 12 and 42 months after the final vaccination.
HVTN 505 2009-2017 United States	18-50 years old, HIV-1 negative men or men who have sex with transgender women, circumcised and with no pre-existing Ad5 neutralizing antibodies	2b	Multiclade DNA/rAd5 vaccine: Participants were primed with 6 plasmids DNA encoding Clade B Gag, Pol and Nef and Env proteins from Clades A, B and C. This was followed by boosting with four rAd5 vectors expressing Clade B Gag-Pol fusion	HIV-1-specific CD4+ and CD8+ T cells; poor tier 1 neutralising antibodies	Env-specific CD8+ T cells, high levels of binding Env responses when CD8+ T cells were low	No	n.d	No efficacy

			proteins and Env from Clades A, B and C.					
HVTN 702/ Uhambo 2016-2020 South Africa	18-35 years of age, HIV-negative, sexually active men and women	2b/3	Primed with ALVAC-HIV (vCP2438) and boosted with subtype C gp120 (bivalent) formulated in MF59 adjuvant.	n.d	n.d	n.d	n.d	No efficacy

(ADCVI =antibody-dependent cellmediated viral inhibition, ADCC = antibody-dependent cellular cytotoxity, IFN-ɣ = interferon gamma, rAd5 = replication-incompetent adenovirus serotype 5, n.d = not determined).

1.11 Justification for designing improved next-generation Env immunogens for eliciting bNAbs

An effective HIV-1 antibody-based vaccine that targets the vulnerable sites of Env (discussed in Section 1.8) is expected to meet two main criteria: these are to elicit polyfunctional, non-neutralising antibodies that drive clearance of the virus and/or broadly neutralising antibodies capable of blocking infection of multiple circulating viral strains; and to be scalable for large production using suitable recombinant protein expression systems. None of the immunogens tested so far has been able to evoke substantial levels of heterologous Tier 2 neutralising antibody responses (Das *et al.* 2020). Considering how bNAbs evolve in natural infections, even though the autologous Tier 2 NAb responses are not sufficient for an effective vaccine, an immunogen that can consistently induce high titres of autologous Tier 2 NAbs, will indicate substantial advances in vaccine designs (Klein *et al.* 2013; Liao *et al.* 2013; Derdeyn *et al.* 2014; Wibmer *et al.* 2015).

The passive transfer of monoclonal bNAbs, even at low titres, has consistently demonstrated that bNAbs offer protection against SHIV infections in non-human primate challenge models (Veazey *et al.* 2005; Hessell *et al.* 2009; Shingai *et al.* 2014; Gautam *et al.* 2016; Julg *et al.* 2017; Xu *et al.* 2017; Gautam *et al.* 2018; Felber *et al.* 2020; Garber *et al.* 2020). However, in the RV144 trial, the non-neutralising antibodies, instead of bNAbs, conferred protection against HIV-1 acquisition by mediating ADCC effector functions (Bonsignori *et al.* 2012; Haynes *et al.* 2012). These results suggested that when neutralisation antibody titres and CD8+ T cell responses are minimal, the Fc-mediated antibody effector functions, particularly ADCC-mediating Env antibodies, need to be appreciated as they may mediate alternative protective immunity against HIV-1 or control disease progression and transmission (Lewis. 2014; Kim *et al.* 2015; Alter & Barouch. 2018; Su *et al.* 2019).

Due to the overall failure of immunogens used in the aforementioned efficacy trials (Section 1.10) to elicit bNAbs, the immunogenicity and safety of several next-generation candidate HIV-1 vaccines and vaccination regimens designed to elicit bNAbs have been or are currently being evaluated in phase 1 or 2 clinical trials (Baden *et al.* 2016; Easterhoff *et al.* 2017; Kratochvil *et al.* 2017; Bekker *et al.* 2018; Pantaleo *et al.* 2019; Moodie *et al.* 2020; Pitisuttithum & Marovich. 2020). However, none of these immunogens has advanced to efficacy trials – hence substantial efforts are focusing on designing improved immunogens to elicit bNAbs.

1.12 Design of soluble Env trimers and their immunogenicity

Initial immunogen designs utilised laboratory-adapted viruses to produce monomeric gp120 immunogens. However, gp120 monomers administered on their own did not elicit Tier 2 neutralising antibodies (VanCott *et al.* 1995a; Pitisuttithum *et al.* 2006; Gilbert *et al.* 2010). It is possible that to elicit Tier 2 neutralising antibodies, immunisation with gp140 trimers rather than monomeric gp120 might be the only relevant immunogen to elicit bNAbs (Kim *et al.* 2005; Kovacs *et al.* 2012).

The transmembrane domain and the cytoplasmic tail were removed from the Env sequence to produce predominantly non-membrane associated, glycosylated and secreted/soluble gp140 trimers suitable for optimal production using relevant recombinant protein expression systems (Earl *et al.* 1991). Simply, the soluble gp140 trimers consist of gp120 and the ectodomain of gp41. To further increase the expression of the soluble gp140, the native signal sequence of gp140 was replaced with a signal sequence derived from a human tissue plasminogen activator (TPA) (Chapman *et al.* 1991; Jeffs *et al.* 1996). However, the soluble Env trimers were unstable in solution, forming varying proportions of different Env species, including gp120-gp41 monomers, dimers, trimers and higher molecular weight aggregates (VanCott *et al.* 1995b; Yang *et al.* 2000b; Jeffs *et al.* 2004). Due to noncovalent interaction between gp120 and gp41, even after purification of the trimers from other Env species, the trimeric fraction still dissociated into monomeric species (Jeffs *et al.* 2004). Consequently, interventional approaches were devised to stabilise the soluble Env trimer mimetics. These strategies are described in Sections 1.12.1-1.12.3 and include the “uncleaved” gp140, cleavage-dependent trimers and cleavage-independent trimers.

1.12.1 Soluble “uncleaved” gp140 trimers

The first attempt in stabilising the soluble Env gp140 trimers involved the inactivation of the cleavage site (REKR sequence was changed to SEKS, which is not recognised by furin proteases) between the gp120 and gp41 (ectodomain) subunits to form “uncleaved” soluble gp140 proteins (Figure 1.8) (Earl *et al.* 1991; Yang *et al.* 2000b). Instead of the noncovalently associated trimers in the native virus, these mutations resulted in a covalent interaction of the gp120-gp41 subunits of these soluble gp140 proteins. However, it was apparent that the yields of the trimeric Env species in these “uncleaved” soluble gp140 preparations were low (Yang *et al.* 2000b; Jeffs *et al.* 2004). To improve folding and yields of the “uncleaved” gp140 trimers, a trimerisation motif such as the isoleucine zipper (derived from GCN4 transcription activator of *Saccharomyces cerevisiae*) or the foldon (FT) (derived from bacteriophage T4 fibritin trimeric protein), was inserted directly downstream of gp41 ectodomain sequence (Figure 9) (Harbury *et al.* 1994; Yang *et al.* 2000a; Yang *et al.* 2000b; Yang *et al.* 2002; Güthe *et al.* 2004;

Du *et al.* 2009). However, these uncleaved gp140 trimers with or without the trimerisation motifs rarely induced detectable levels of Tier 2 neutralising antibodies (Yang *et al.* 2001; Du *et al.* 2009; Nkolola *et al.* 2010). Since the "uncleaved" gp140 trimers failed to induce neutralising antibodies, their trimeric forms are referred to as pseudotrimers (Sanders & Moore. 2017).

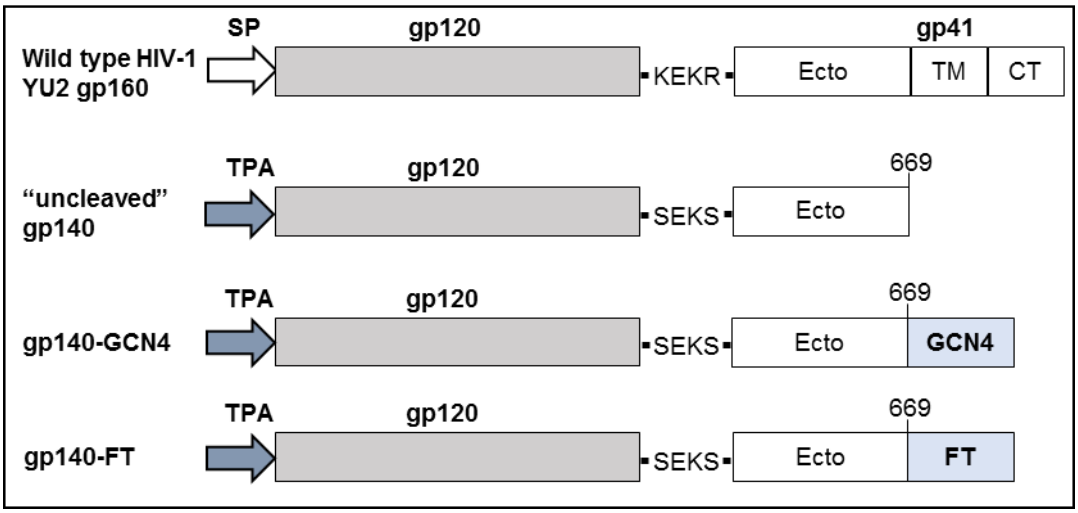

Figure 1.8: Design of the "uncleaved" gp140 trimers from the Env sequence derived from YU2 HIV-1 isolate. Schematic representation of wild-type gp160 (YU2 isolate) showing the native HIV-1 signal peptide (SP), the gp120 subunit, the furin cleavage motif (KEKR), the gp41 ectodomain (Ecto), the transmembrane domain (TM) and the cytoplasmic domain (CT). The soluble "uncleaved" gp140 sequence was generated by replacing the native SP sequence with the human tissue plasminogen activator leader sequence (TPA), the furin cleavage motif, KEKR, was replaced with an uncleavable SEKS motif and the gp160 sequence was truncated at amino acid residue 669. The trimerisation motif, isoleucine zipper (GCN4), or bacteriophage T4 fibritin (FT), was inserted downstream of the "uncleaved" gp140 coding sequence to generate gp140-GCN4 or gp140-FT, respectively.

1.12.2 Cleavage-dependent SOSIP trimers

Instead of eliminating the cleavage of the soluble gp140, an alternative strategy was to retain the natural cleavage requirement which seemed essential in the natural processing of gp160 and rationally introduce changes to enhance the stability of the cleaved gp140 (Binley *et al.* 2000). In addition to noncovalent interactions between gp120 and the ectodomain of gp41, it was apparent that the proteolytic processing of gp140 by host furin was not optimal (Binley *et al.* 2000). Insufficient proteolysis indicated that the host proteases were saturated with highly expressed gp140 and could not optimally process the excessively expressed gp140 proteins. Proteolytic processing was then enhanced by co-transfecting the gp140-encoding plasmid with a furin encoding plasmid (Binley *et al.* 2000). However, co-transfection reduced gp140 yields, probably as a result of the competition between the translation of the soluble gp140 and furin, or the accumulation of gp140-furin complexes that were not secreted (Binley *et al.* 2000; Binley *et al.* 2002). Later on, the proteolytic cleavage by furin was further enhanced by

replacing the native REKR cleavage site between gp120 and g41 ectodomain of SOS gp140 (discussed below) with a polyarginine (RRRRRR; R6) furin-sensitive cleavage site. Of note, the presence of the RRRRRR site did not reduce the yields of the SOS gp140 trimers (Binley *et al.* 2002).

A disulphide bond was introduced to stabilise the interaction between gp120 and the gp41 ectodomain (characterised by shedding of gp120) of the cleaved gp140 trimers produced in the presence of co-expressed furin (Binley *et al.* 2000). This stabilising mutation was achieved by amino acid substitution with double cysteines (SOS) in the A501C position of gp120 and T605C position of gp41 ectodomain of the Env sequence derived from the JR-FL isolate (subtype B). The soluble proteins stabilised by the addition of the disulphide were referred to as cleavage-dependent SOS gp140 trimers. Encouragingly, the SOS gp140 was more antigenically similar to the native Env trimers than the uncleaved pseudotrimers that demonstrated unfavourable antigenic profiles. However, sucrose velocity gradients indicated that SOS gp140 still contained a considerable amount of gp120 monomers; thus, it's strong binding with mAbs was not expected. The observed strong reactivity of SOS gp140 with mAb suggested that this protein adopted a conformation that mainly exposed the native-like epitopes while occluding the non-neutralising epitopes (Binley *et al.* 2000; Schülke *et al.* 2002). Schülke *et al.* (2002) further evaluated the oligomeric state of SOS gp140 using mass spectrophotometer, ultracentrifugation, size exclusion chromatography (SEC) as well as Blue Native polyacrylamide gel electrophoresis (BN-PAGE), and confirmed that SOS gp140 was indeed mostly monomeric. This necessitated further modification of the SOS gp140 to attain better antigenic mimics of the native gp140 trimers (Schülke *et al.* 2002).

To further stabilise the SOS gp140 in its trimeric state, Sanders *et al.* (2002) introduced an isoleucine-to-proline at position 559 (I559P) in the heptad repeat region of gp41, a six-helix bundle destabiliser that limited the conformation of gp41 to a prefusion state instead of a postfusion state (Sanders *et al.* 2002). Gp140 SOS protein with the I559P modification, designated SOSIP gp140, was proteolytically cleaved, largely trimeric, and its antigenic features were native-like (Sanders *et al.* 2002). To further improve the solubility, homogeneity and stability of SOSIP gp140 trimers in the absence of detergents, the gp41 ectodomain coding sequence was truncated at residue 664 of the MPER region to generate SOSIP.664 gp140 trimers (the MPER sequence was truncated at position 681 for the predecessor SOSIP gp140) (Klasse *et al.* 2013).

The next generation of cleaved SOSIP.664 gp140 involved identifying sequences from the elite neutralisers that could yield better trimers and introducing other modifications to expand their bNAb epitopes. This screening led to the identification of HIV-1 BG505, a subtype A

transmitted-founder (T/F) virus that was isolated from a 6-week old Kenyan infant enrolled in a mother-child cohort (Wu *et al.* 2006; Goo *et al.* 2014). Modifications in the BG505 Env sequence such as SOS, I559P, truncation of MPER at position 664, and T332N substitution to form epitopes that depended on this glycan generated the prototypic native-like trimers referred to as BG505.SOSIP.664 gp140 (Figure 1.9) (Sanders *et al.* 2013). The SOSIP.664 modifications have been successfully applied to Env sequences from various genotypes and new SOSIP.664 variants that contain further stabilising mutations have been reported (de Taeye *et al.* 2015; Julien *et al.* 2015; Sanders *et al.* 2015; Klasse *et al.* 2016; Torrents *et al.* 2018; Sliepen *et al.* 2019).

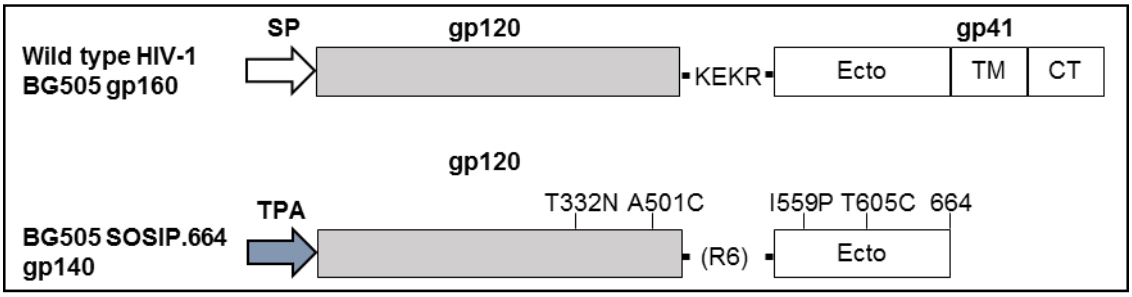

Figure 1.9: Design of cleavage-dependent SOSIP.664 gp140 trimers from the Env sequence derived from BG505 HIV-1 isolate. Schematic representation of the wild-type BG505 gp160 showing the native HIV-1 signal peptide (SP), the gp120 subunit, the furin cleavage motif (KEKR), the gp41 ectodomain (Ecto), the transmembrane (TM) and the cytoplasmic domain (CT). The designed SOSIP.664 gp140 sequence contained the following modifications: the native signal peptide (SP) sequence was replaced with the human tissue plasminogen activator leader sequence (TPA), the T332N substitution was included in gp120 sequence, the double cysteines (SOS) substitution in A501C position of gp120 and T605C position of gp41 ectodomain were included, the furin cleavage motif, KEKR, was replaced with polyarginine (RRRRRR; R6) furin-sensitive cleavage site, the I559P substitution was added, and the gp160 sequence was truncated at amino acid residue 664.

1.12.3 Cleavage-independent NFL trimers

Although the cleaved SOSIP.664 gp140 generated native-like trimers (excellent antigenic profile and uniform three-lobed, propeller-like structures), efficient proteolytic cleavage between the gp120-gp41 ectodomain junction to assume a closed conformation required furin co-expression (Sanders *et al.* 2013). However, the dependence on furin co-expression could compromise the formation of cleaved native-like SOSIP.664 trimers when furin is limited. Furin shortages could occur in nanoparticle-based Env preparations where the furin cleavage site might be obstructed or in DNA or viral vector vaccines where the cleavage only relies on endogenous furin (Capucci *et al.* 2017; Brinkkemper & Sliepen. 2019; Brouwer & Sanders. 2019).

An alternative to the cleavage-dependent design was the establishment of cleavage-independent approaches that bypass the need for furin but still generate trimers that

antigenically and structurally mimic the prototypic BG505.SOSIP.668 gp140 trimers. Georgiev *et al.* (2015) replaced the furin cleavage site in BG505.SOSIP.664 with the flexible linkers (1-4 repeats of GGSGG) to generate single-chain gp140 trimers (sc-gp140) (Figure 11). Antigenic analysis with conformational monoclonal antibodies indicated that the longer linker (15 residues) formed better trimers than shorter linkers. Additionally, even though the majority of the antigenic properties of the sc-gp140 trimers were similar to BG505.SOSIP.664, sc-gp140 trimers reacted noticeably with the F105 mAb that recognises non-native trimers. The presence of F105-specific Env species required a further purification step, ; hence the F105 negative selection was conducted to remove misfolded trimers recognised by the F105 antibody (Georgiev *et al.* 2015). As an alternative to sc-gp140, Sharma *et al.* (2015) replaced the furin cleavage site with a ten residue flexible linker (2x GGSGG) in JRFL and BG505 gp140 sequences to generate covalently linked trimers called native flexibly linked (NFL) trimers (Figure 1.10) (Sharma *et al.* 2015). Of particular note, the formation of well-ordered trimers using the NFL approach required the presence of an I559P substitution present in the SOSIP.664 design. Antigenic profiling and negative stain electron microscopy indicated that the uncleaved BG505 gp140 NFL was largely trimeric after SEC purification and did not require further purification by negative selection (Sharma *et al.* 2015). Our group have successfully used the NFL strategy to generate HIV-1 subtype C CAP256 gp140 NFL immunogens (van Diepen *et al.* 2018; Margolin *et al.* 2019; van Diepen *et al.* 2019; Chapman *et al.* 2020).

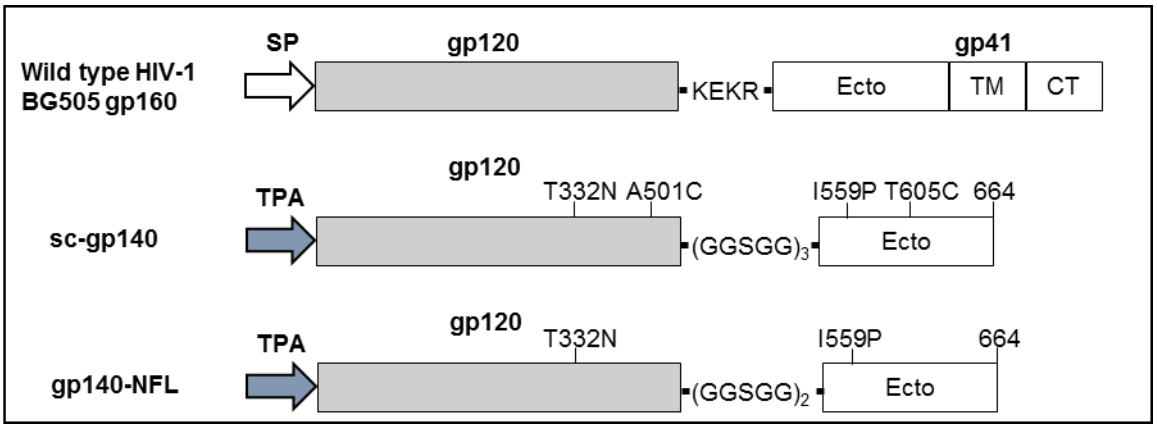

Figure 1.10: Design of the cleavage-independent single-chain (sc) and native flexibly linked (NFL) gp140 sequence from the Env sequence derived from the BG505 HIV-1 isolate. The schematic representation of the wild-type gp160 showing the native HIV-1 signal peptide (SP), the gp120 subunit, the furin cleavage motif (KEKR), the gp41 ectodomain (Ecto), the transmembrane (TM) and the cytoplasmic domain (CT). In the soluble sc-gp140 sequence, the native SP sequence was replaced with the human tissue plasminogen activator leader sequence (TPA), the T332N substitution was added in gp120 sequence, the double cysteines (SOS) substitutions (A501C-T605C) were included, the furin cleavage motif, KEKR, was replaced with a flexible linker (GGSGG x 3), the I559P substitution was included, and the gp160 sequence was truncated at amino acid residue 664. The

gp140-NFL design is similar to the sc-gp140 design except that the SOS substitution was not included, and a 10-amino acid flexible linker (GGSGG x 2) was used instead of a 15-amino acid flexible linker.

High titres of autologous Tier 2 and heterologous Tier 1 nAb responses have been observed in sera from rabbits or guinea pigs intramuscularly (IM) inoculated with SOSIP.664 or NFL immunogens formulated in ISCOMATRIX™, squalene emulsion or AlhydroGel® adjuvants (Sanders *et al.* 2015; Cheng *et al.* 2016; Feng *et al.* 2016; Klasse *et al.* 2016; van Diepen *et al.* 2019). These autologous responses have been observed in various vaccination regimens that incorporate the SOSIP- or NFL designs. Such regimens include sequential immunisation with a combination of trimers from different clades to mimic natural infection (Klasse *et al.* 2016; Torrents *et al.* 2018), immunisation with trimers stabilised by cross-linking with glutaraldehyde (Feng *et al.* 2016), immunisation with trimers complexed with structure-specific mAb (Cheng *et al.* 2016) and immunisation with trimers derived from a consensus sequence of M isolates (conM) (Sliepen *et al.* 2019). Autologous responses are also often observed in heterologous prime-boost regimens. These regimens involve priming with Env/Gag immunogens delivered by non-replicating simian adenovirus or non-replicating poxvirus modified vaccinia virus Ankara (MVA) vectors alone, or in combination with DNA primes, followed by boosting with soluble Env trimers formulated in adjuvants (Capucci *et al.* 2017; van Diepen *et al.* 2019). Of note, the autologous Tier 2 NAb titres are often very low in rhesus macaques inoculated with BG505 SOSIP.664 trimers, raising concerns as to whether such responses will be effectively induced in humans (Sanders *et al.* 2015). The constant challenge to elicit potent bNAbs highlights the need for improved immunogens and vaccination regimens. Recent efforts have focused on optimising immunogens and vaccination regimens that incorporate the multimerisation or high-density display of Env on nanoparticles (Brinkkemper & Sliepen. 2019; Brouwer & Sanders. 2019). These nanoparticle approaches are discussed below.

1.13 Nanoparticle vaccines

The success of virus-like particle (VLP)-based vaccines for other pathogens suggests that particulate presentation of HIV-1 native-like trimers by nanoparticles could be a useful strategy to elicit durable and effective neutralising antibodies. The licenced human prophylactic vaccines against hepatitis B virus (HBV), human papillomavirus (HPV) and hepatitis E virus (HEV), induce durable neutralising responses because of the particulate presentation of relevant viral antigens on VLPs (Zhao *et al.* 2013). Specifically, RECOMBIVAX is the HBV vaccine that uses the surface antigen (HBsAg) which self-assembles into ≈20nm lipid-containing octahedral VLPs. Gardasil is the HPV vaccine that is derived from L1 major capsid protein which self-assembles into ≈55nm isometric protein-only VLPs. Hecolin is the HEV

vaccine that is based on a p239 capsid protein which self-assembles into 20-30nm protein-only VLPs (Zhao *et al.* 2013).

Nanoparticles in vaccinology describe a broad spectrum of biologically-derived nanoscale structures (20-200nm) such as VLPs, liposomes, virosomes, self-assembling protein nanoparticles and rationally designed self-assembling synthetic nanoparticles. Nanoparticles share similar features such as the size range, repetitive surfaces and can be manipulated either for high surface display or encapsulation of the antigen of interest (Bachmann & Jennings. 2010; Karch & Burkhard. 2016; Gomes *et al.* 2017). The majority of the features of nanoparticles resemble those of many viral pathogens, which the immune system has evolved to perceive as "foreign" and thus elicit robust immune responses to clear them. Likewise, these features render nanoparticles more immunogenic compared to soluble (<10nm) immunogens.

From the peripheral site of injection, the size (20-100nm) of nanoparticles allows them to readily drain into the lymph nodes and interact with B cells (Bachmann & Jennings. 2010). Alternatively, nanoparticles are efficiently taken up by antigen-presenting cells (APCs, such as macrophages, B cells and dendritic cells) and processed for presentation to the major histocompatibility complex (MHC) class II (Bachmann & Zinkernagel. 1996). Unlike soluble proteins, the repetitive surface of nanoparticles facilitates the cross-linking of B cell receptors (BCRs, the membrane-bound monomeric configurations of IgD and IgM isotypes). This cross-linking activates B cells even without a need for T helper cells (no need for presentation of antigen via the MHC class II to T helper cells to activate B cells), and induces robust and durable humoral responses. The repetitive surfaces of nanoparticles also enhance the interactions with follicular dendritic cells, leading to better presentation of nanoparticles to the lymph nodes. Unlike the soluble proteins, nanoparticles can also be cross-presented via MHC class I to induce T cell responses. Many VLPs encapsulate non-infectious nucleic acids, which upon release, can activate toll-like receptors (TLR) that possess adjuvant properties that can stimulate strong immune responses (Jennings & Bachmann. 2008; Bachmann & Jennings. 2010; Bárcena & Blanco. 2013; Zabel *et al.* 2013; Gomes *et al.* 2017; Schiller & Lowy. 2018).

Subunit vaccines derived from a wide range of viruses are generally less immunogenic than the live-attenuated viruses; moreover, HIV-1 has evolved immune evasion strategies that make Env-based immunogens even less immunogenic than other viral antigens. The details of the evasion strategies (mentioned in Section 1.9) that are relevant for nanoparticle vaccine designs are expanded here. That is, the unusual low Env spike density (14 spikes per virion) and their spacing (trimers are 230 Å apart) on the HIV-1 viral particle are distinct features that allow HIV-1 to evade neutralising responses (Zhu *et al.* 2006; Klein & Bjorkman. 2010; Schiller & Chackerian. 2014). Hence, developments of HIV-1 nanoparticle vaccines are focusing on

counteracting these features in an attempt to elicit potent neutralising antibodies. Repetitive antigen display and dense spacing (50-100 Å) on pathogens are major determinants that quickly signal the immune system of the introduction of foreign pathogens, thus triggering BCR cross-linking of viral antigens to elicit strong antibody responses (Bachmann & Zinkernagel. 1996).

Structural analysis of enveloped viruses such as influenza, hepatitis B and dengue viruses (Figure 1.11), whose glycoproteins have been shown to elicit potent neutralising antibodies, generally have a high surface spike density and these spikes are tightly packed (Klein & Bjorkman. 2010; Schiller & Chackerian. 2014). For instance, influenza type A virions contain about 450 spikes spaced at ≤100 Å per virion (Yamaguchi *et al.* 2008). Simian immunodeficiency virus (SIV) is a virus closely related to HIV, but unlike HIV, it is also densely decorated with ≈ 70 spikes per virion (Zhu *et al.* 2006). Robust immune responses ascribed to nanoparticles are exemplified by the non-enveloped HPV VLPs that efficiently induced potent neutralising antibodies even in the absence of adjuvants (Zhang *et al.* 2000). This highly immunogenic profile of HPV VLPs is thought to be due to the repetitive display and close packing of L1 major capsid protein that promotes BCR cross-linking leading to potent and durable antibody responses (Schiller & Lowy. 2018). Thus, an effective vaccine will likely require a repetitive display and close packing of spikes to elicit high avidity antibodies in contrast to the sparsely decorated HIV-1 Env, which likely induce monovalent antibodies, thus resulting in low titres of neutralising antibodies (Klein & Bjorkman. 2010; Schiller & Chackerian. 2014). Nanoparticles are now attractive targets for HIV-1 vaccines because they can be manipulated to display dense arrays of Env spikes, hopefully improving their immunogenicity.

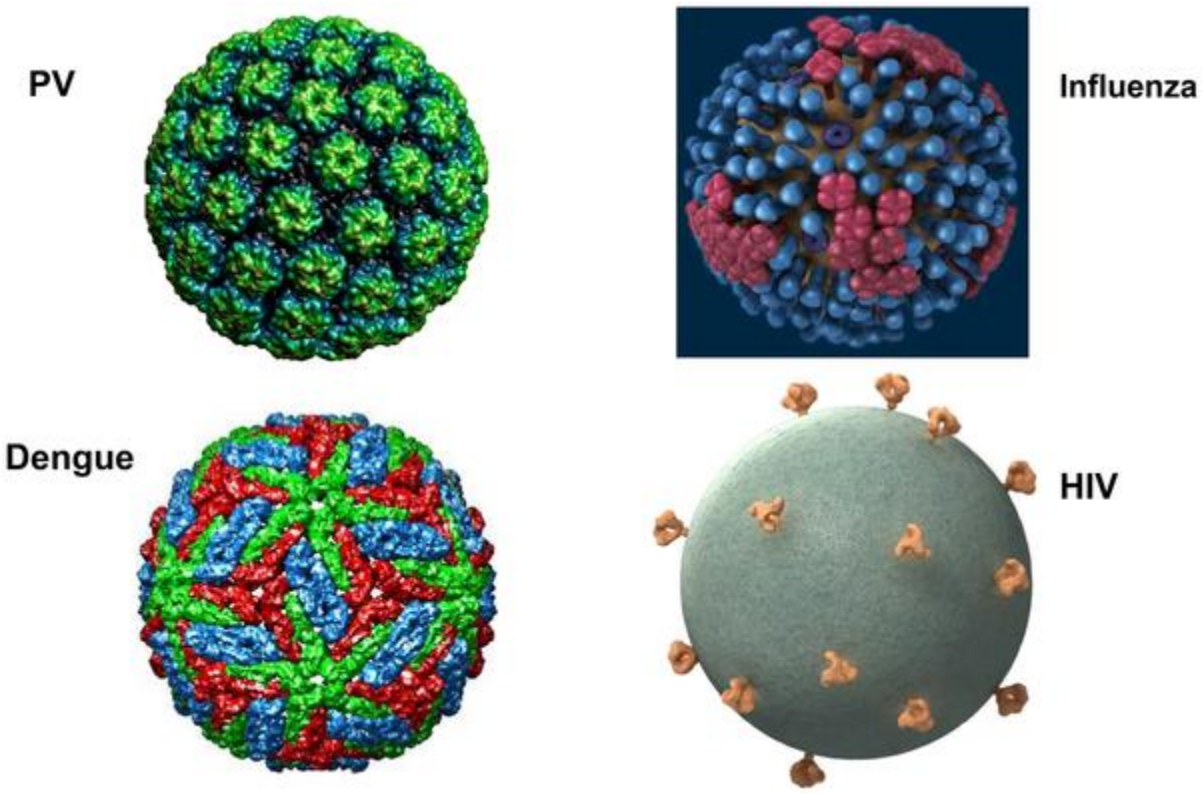

Figure 1.11: Comparison of the density and spacing of HIV-1 envelope spikes to glycoprotein density and spacing observed on bovine papillomavirus (PV), influenza, and dengue virus particles. The diagram was taken from Schiller and Chackerian (2014) following the specific guidelines of the Commons copyright licence.

1.14 Nanoparticle platforms that have been explored for HIV-1 Env trimers

1.14.1 HIV-1 Gag VLPs

Recombinant expression of HIV-1 Gag protein in the absence of other HIV-1 viral proteins is sufficient for assembly into plasma membrane-bound VLPs and their subsequent budding and release into the extracellular medium (Gheysen *et al.* 1989; Karacostas *et al.* 1989; Murakami. 2008; Freed. 2015). In addition, HIV-1 VLPs bearing Env trimers (i.e. Env-VLPs) can be produced by co-expressing Gag and Env proteins and purification by centrifugation (Moore *et al.* 2006; Crooks *et al.* 2007; Chapman *et al.* 2020). An HIV-1 vaccine should present Env trimers in a native-like conformation to increase the chances of eliciting neutralising antibodies. In theory, VLPs are attractive nanoparticles to achieve this because they are non-infectious structures that can present epitopes in their natural membrane context, resulting in native-like trimers without the need for stabilising mutations (Tong *et al.* 2012). However, the size of HIV-1 Gag VLPs (≈110nm) and the incorporation of few Env spikes per virion (≈14), are not favourable characteristics for inducing durable immune responses (Klein & Bjorkman. 2010; Schiller & Chackerian. 2014). Furthermore, a high proportion of the 14 spikes per virion are non-functional Env forms, including uncleaved gp160, gp120/gp41 monomers or gp41 stumps

following the shedding of gp120, and this limits the stimulation of functional neutralising antibodies by VLPs (Poignard *et al.* 2003; Moore *et al.* 2006; Crooks *et al.* 2007).

The non-functional forms of Env on Gag-Env VLP preparations were to some extent addressed by introducing the SOS mutation between gp120 and gp41 or NFL to avoid gp120 shedding, or non-native forms were depleted by digestion with a glycosidase-protease cocktail, leaving the intact native-like trimers called “trimer VLPs” (Crooks *et al.* 2007; Crooks *et al.* 2011; Tong *et al.* 2012). Weak heterologous Tier 2 neutralising antibodies were observed in rabbits immunised with “trimer VLPs” (Crooks *et al.* 2015; Crooks *et al.* 2017). Notably, “trimer VLPs” are generally produced at lower yields in mammalian cells (Crooks *et al.* 2017). To increase the Env spike density on HIV Gag VLPs, Stano *et al.* (2017) used fluorescence-activated cell sorting (FACS) to screen for bNAb-specific producer cells. Following numerous screens, high-Env VLPs displaying on average >127 spikes per virion were identified; however, their immunogenicity is yet to be evaluated (Stano *et al.* 2017). Despite some advances in HIV-1 VLPs, their application as nanoparticles for the presentation of Env trimers is still challenged by the incorporation of few Env spikes as well as the lower yields of these VLPs in mammalian cells (Klein & Bjorkman. 2010; Schiller & Chackerian. 2014; Crooks *et al.* 2017).

1.14.2 Liposomes

Liposomes are spherical vesicles that spontaneously form when lipids are hydrated, resulting in the formation of an aqueous compartment surrounded by one (unilamellar) or more (multilamellar) lipid bilayers (Sharma & Sharma. 1997). Liposomes contain biodegradable phospholipids such as cholesterol, phosphatidylcholine and phosphatidylserine (Kersten & Crommelin. 1995; Sharma & Sharma. 1997). The ability of liposomes to improve antibody responses against HIV-1 Env immunogens was first demonstrated when monomeric gp120 formulated in liposomes elicited higher antibody titres than gp120 formulated in alum adjuvant (Bui *et al.* 1994). As a mucosal vaccine candidate, Bomsel *et al.* (2011) used the commercial virosomes (Moser *et al.* 2007; Herzog *et al.* 2009) to present gp41-derived antigens including the P1 peptide (extended gp41 MPER containing the galactosyl ceramide-binding site, the 2F5 and the 4E10 epitopes) (Alfsen & Bomsel. 2002). These virosome-bound gp41 antigens protected the Chinese rhesus monkeys against repeated SHIV-SK162P3 vaginal. The gp41-specific cervicovaginal IgAs, transcytosis-blocking and ADCC activities were colerates of protection. Interestingly, no neutralising IgG activity was detected in the sera of protected animals (Bomsel *et al.* 2011). Pejawar-Gaddy *et al.* (2014) displayed polyhistidine (His)-tagged gp140 trimers on nitrilotriacetic acid (NTA)-bearing interbilayer-cross-linked multilamellar vesicles (Ni-NTA-ICMVs, ≈27nm). The resulting gp140T-ICMVs liposomes (160

trimers per liposome with the spacing of 330 Å between trimers) were formulated in the toll-like receptor-4 MPLA adjuvant, and their immunogenicity was evaluated in mice. The gp140T-ICMVs elicited higher antibody titres and avidity against the conserved linear peptide epitopes (V2, MPER) compared to soluble gp140 trimers formulated in a potent oil-in-water adjuvant (Pejawar-Gaddy *et al.* 2014).

Advancement in the use of liposomal nanoparticles was reported where well-ordered native-like trimers (JRFL NFL-His-tag, or JRFL SOSIP-His-tag) were displayed on the unilamellar Nickel (Ni^{2+})-chelated liposomes (Ingale *et al.* 2016). This conjugation resulted in trimer-conjugated liposomes (75-250nm in diameter) displaying about 300-500 Env spikes with a spacing of 120-150 Å between trimers (Figure 1.12). Encouragingly, the trimer-conjugated liposomes retained the quaternary-specific Env epitopes, were very stable, highly activated B cells *ex vivo* and elicited modest autologous Tier 2 neutralising antibodies compared to the weak response observed for unconjugated trimers in rabbits (Ingale *et al.* 2016). Autologous Tier 2 neutralising antibodies were also induced in non-human primates vaccinated with liposome-arrayed NFL trimers via the Ni^{2+}-His-tag non-covalent interactions (Martinez-Murillo *et al.* 2017).

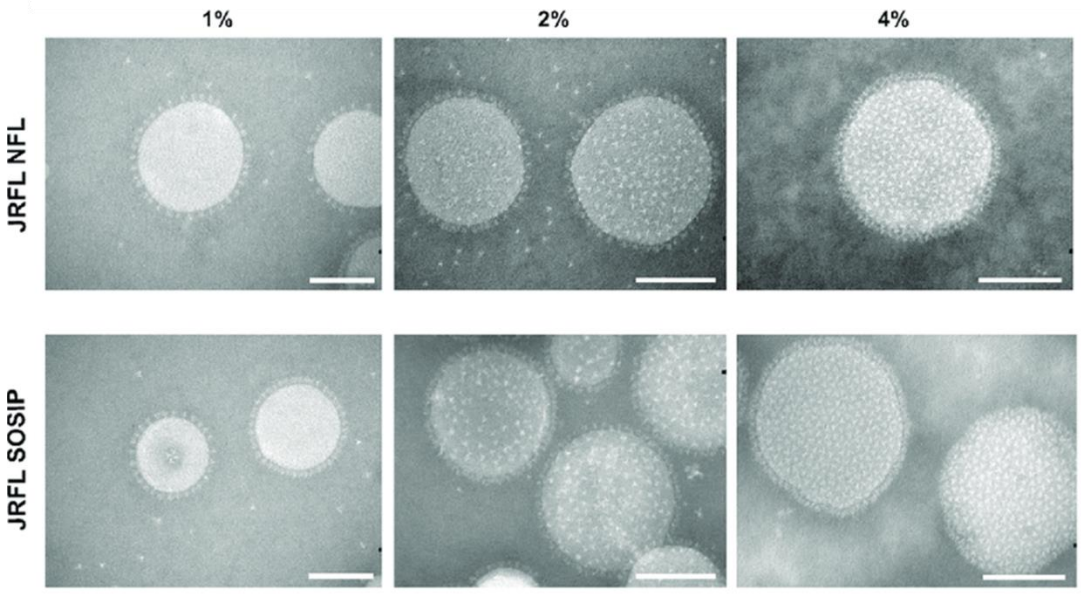

Figure 1.12: Negative-stain EM of liposomes displaying an array of SOSIP or NFL native-like trimers. Nickel-chelated liposomes were generated by incorporating 1-4% of 1,2-dio-leoyl-*sn*-glycero-3-((N-(5-amino-1-carboxypentyl)iminodiacetic acid)succinyl) (nickel salt) (DGS-NTA(Ni)) into a lipid components for generating liposomes. His-tagged JRFL NFL or JRFL SOSIP trimers were displayed on these liposomes by non-covalent Ni^{2+}-His interaction. These electron micrographs were taken from Ingale *et al.* (2016).

To ensure that the trimers did not dissociate before reaching the lymph nodes and B cells due to non-covalent coupling to liposomes, a second-generation of covalently linked liposomes

were generated (Bale *et al.* 2017). Thus, BG505 NFL-Cys trimers were attached to Cys-linked liposomes by maleimide-thiol covalent coupling, resulting in more stable display than the non-covalent conjugations used for the first-generation liposomes. Trimers conjugated to liposomes via covalent interactions elicited higher Env binding antibodies in mice than the soluble trimers or trimers non-covalently displayed on liposomes (Bale *et al.* 2017). However, no autologous Tier 2 neutralising antibodies were elicited, consistent with previous observations that mice BCRs are not efficient in eliciting neutralising antibodies against BG505 trimers (Hu *et al.* 2015; Bale *et al.* 2017). A heterologous prime (with glycan-modified cleavage independent NFL trimers) - boost (with liposomes densely arrayed with heterologous NFL trimers) regimen elicited Tier 2 cross-neutralising antibodies in rabbits. These results indicated a potential of a combination regimen (priming with optimised Env trimers and boosting with a heterologous (to priming trimer) trimers displayed on particulate liposomes) in inducing cross-neutralising antibodies against hard-to-neutralise clinically relevant Tier 2 viruses (Dubrovskaya *et al.* 2019). Even though further optimisations are required to improve the conjugation efficiency, consistent size and quality production of liposomes, they are promising nanoparticles for the presentation of Env trimers (Brinkkemper & Sliepen. 2019).

1.14.3 *In vivo* self-assembling protein nanoparticles

Some naturally occurring proteins can spontaneously self-assemble into nanostructures (10-150nm in diameter) with regular shapes (López-Sagaseta *et al.* 2016). Alternatively, computational designs are used to generate rationally designed proteins that are capable of self-assembling into synthetic nanoparticles (King & Lai. 2013). The symmetry and particulate nature of the self-assembling protein nanoparticles make them attractive scaffolds for dense arrays or encapsulation of vaccine antigens. Antigen display on protein nanoparticles is often achieved by genetically fusing the sequence coding the antigen of interest downstream or upstream of the nanoparticle coding sequence to generate a chimaeric construct, which upon recombinant protein expression, generates nanoparticles displaying the antigen of interest on its surface. Ferritin, E2p, I3-01 and lumazine synthase are protein nanoparticles that have been explored for the presentation of HIV-1 Env immunogens.

1.14.3.1 24-meric Ferritin

Ferritin is a protein produced by almost all living organisms, and its function is to form a shell for iron storage and is crucial in iron homeostasis (López-Sagaseta *et al.* 2016). Each ferritin of the Gram-negative bacterium *Helicobacter pylori* is assembled from 24 identical subunits. Each subunit folds into a four-helix-bundle, which subsequently merges to form a nanoparticle (24-meric, 12.2nm) with an octahedral symmetry (Cho *et al.* 2009). Unlike the bacterial ferritins, each mammalian ferritin results from two non-identical subunits; the light and heavy

chains combining at equal or variable molar ratios to form a 24-meric nanoparticle with tetrahedral symmetry (Lawson *et al.* 1991; Hamburger *et al.* 2005). Due to their chemical stability, thermal stability, as well as their 3-fold axis symmetry, ferritins are suitable scaffolds for trimeric glycoproteins. Ferritins have been used for the presentation of hemagglutinin (HA) from influenza virus (Kanekiyo *et al.* 2013), soluble E2 of Hepatitis C virus (Yan *et al.* 2020), gp350 of Epstein-Barr virus (Kanekiyo *et al.* 2015) and monomeric and trimeric forms of HIV-1 Env (Sliepen *et al.* 2015; He *et al.* 2016; Georgiev *et al.* 2018).

Specifically, *Helicobacter pylori* ferritin displaying BG505 SOSIP.664 gp140 trimers (SOSIP.664-ferritin) elicited higher but nonsignificant autologous Tier 2 NAbs compared to the soluble SOSIP.664 trimers in rabbits (Sliepen *et al.* 2015). The uncleaved prefusion-optimised BG505 ectodomain-swapped trimers (UFO-BG) arrayed on ferritin nanoparticles elicited higher autologous Tier 2 NAbs in mice and rabbits compared to animals vaccinated with the soluble trimers (He *et al.* 2018). The V1V2-ferritin, gp120-ferritin and gp140-ferritin fusions generated homogenous nanoparticles, respectively displaying V1V2, gp120 and gp140 epitopes in their native-like trimeric conformations. Notably, high yields of gp140-ferritin nanoparticles were produced in an ExpiCHO transient expression system, and these ferritin-displayed trimers effectively activated B cells compared to soluble trimers (He *et al.* 2016; He *et al.* 2018). Ferritin nanoparticles displaying the SOSIP conM trimers elicited significantly higher autologous Tier 1A (conM) and appreciable Tier 1B (conS is more resistant than conM) neutralising antibodies compared to their soluble counterparts in rabbits and macaques (Sliepen *et al.* 2019)

Mammalian ferritins allow for a multi-component display of antigens. For instance, ferritin derived from insect *Trichoplusia ni* assembles into 24-meric nanoparticles made up of 12 identical subunits of the light chain and 12 identical subunits of the heavy chain (Hamburger *et al.* 2005). This mammalian ferritin led to the development of two-component ferritin displaying 2x4 HIV-1 Env trimers from two isolates, and another dual ferritin displaying 4x HIV-1 trimers plus 4x influenza HA trimers. In guinea pigs, these two-component ferritin nanoparticles elicited sporadic autologous NAbs against Tier 2 HIV-1 viruses but strong autologous NAbs against autologous influenza virus, indicating that this system was more favourable for influenza than HIV-1 Env trimers (Georgiev *et al.* 2018). The limitations of using ferritin nanoparticles include low (only 8) density display of trimers which could still limit B cell cross-linking and the presence of contaminating monomeric, dimeric, and uncleaved (due to limited access of SOSIP trimers by furin) Env species that cannot be eliminated once the nanoparticles are assembled.

1.14.3.2 60-meric protein nanoparticles: dihydrolipoyl acetyltransferase (E2p), I3-01 and lumazine synthase

E2p protein is a component of a pyruvate dehydrogenase (PDH) multienzyme complex found in *Geobacillus stearothermophilus*. Sixty E2p subunits assemble into a 60-meric heat-stable particle (23nm) with icosahedral symmetry. Due to the natural ability of E2p to non-covalently associate with 60 copies of E1 or E3 components of the PDH, E2p can be used as a scaffold for surface display of foreign antigens without impacting E2p assembly (Izard *et al.* 1999; Domingo & Perham. 2001). He *et al.* (2016) demonstrated that gp120-E2p and gp140-E2p chimaeric fusions generated homogenous E2p particles (37.6nm and 41.5nm in diameter, respectively) displaying gp120 and gp140 in their native-like trimeric conformations. The gp120-E2p and gp140-E2p nanoparticles substantially activated B cells *in vitro* compared to their soluble counterparts (He *et al.* 2016). The immunogenicity of E2p-displayed trimers still needs to be assessed *in vivo*.

I3-01 is a computationally designed, hyperstable nanoparticle made up of trimeric protein building blocks that self-assemble into 60-meric icosahedral particles (25nm) (Hsia *et al.* 2016). A fusion construct containing gp140, T cell epitope (PADRE) and the I3-01 (gp140-PADRE-I3-01) generated hyperstable nanoparticles displaying gp140 trimers with desirable antigenic features. The gp140-PADRE-I3-01 nanoparticles induced modest autologous Tier 2 NAbs in rabbits (He *et al.* 2018).

Lumazine synthase (LS) is an enzyme from the hyperthermophilic bacterium *Aquifex aeolicus* and is capable of self-assembling into 60-meric nanoparticles (14.8nm) with icosahedral symmetry (Zhang *et al.* 2001; Zhang *et al.* 2006). When a computationally designed germline-targeting gp120 outer domain [the outer domain refers to gp120 where the tip of the V3 loop (amino acid residues 303-319) was removed] (eOD-GT6) was multimerised on lumazine synthase and assayed *in vitro*, germline and mature B cells were activated at higher magnitude compared to monomeric and soluble eOD-GT6 gp120 forms (Jardine *et al.* 2013). These LS-eOD-GT6 nanoparticles induced strong immune responses in a knock-in mouse model expressing germline-reverted VRC01 heavy chains (Jardine *et al.* 2015). However, LS fused to the full-length gp120 or gp140, failed to assemble into nanoparticles, possibly due to non-optimal spacing of trimers that possibly overcrowded the surface of the nanoparticle, thus resulting in particle disassembly (He *et al.* 2016).

1.14.4 *In vivo* assembling protein body-inducing fusion tags

In recent years, there has been an increasing enthusiasm in using protein body-inducing fusions as a strategy to improve recombinant protein stability, accumulation, recovery,

purification and immunogenicity simultaneously, especially of plant-produced candidate vaccine antigens (Conley *et al.* 2011; Khan *et al.* 2012; Schmidt. 2013; Schwestka & Stoger. 2021). Protein bodies (PBs) are endoplasmic reticulum (ER)-derived organelles that form in the majority of seeds and function as protein storage compartments. Cereal seed storage proteins (predominantly prolamins) of maize, wheat and rice naturally form PBs (Shewry & Halford. 2002). The best characterised naturally occurring ER-derived PBs are zeins, the seed prolamin storage protein synthesised during endosperm development in maize kernels (Lending & Larkins. 1989). Zeins are synthesised in the membrane-associated polyribosomes and trafficked into the ER where they self-assemble into 1-2µm spherical-shaped PB structures. These PBs are enclosed by ER membranes and remain attached to the ER or bud into the cytosol (Lending & Larkins. 1989; Herman & Larkins. 1999; Chrispeels & Herman. 2000; Galili. 2004; Saberianfar & Menassa. 2017). Fusing zein-derived fusion tags to some recombinant proteins has been shown to induce the formation of PBs encapsulating large amounts of the protein of interest (Llop *et al.* 2006; Torrent *et al.* 2009a; Torrent *et al.* 2009b; Conley *et al.* 2011; Whitehead *et al.* 2014; Mbewana *et al.* 2015; Hofbauer *et al.* 2016). The formation of novel PBs is not restricted to zein fusion; PBs can be induced when recombinant proteins are fused to fungal hydrophobin-I (HFBI) and elastin-like polypeptide (ELP) proteins (Conley *et al.* 2011; Schmidt. 2013).

1.14.4.1 Zera®

Depending on the position and amino acid composition of PBs across the developing endosperm of maize seed, as well as the actual size of PBs, zeins are classified into α-, ß-, δ- and γ-zein (Lending & Larkins. 1989). Gamma-zein (27 kDa) contains proline-cysteine rich regions, and only solubilises in the presence of reducing agents. The proline-rich N-terminal domain of γ-zein is sufficient for ER retention, and to induce the formation of PBs when fused to other proteins (Geli *et al.* 1994; Llop-Tous *et al.* 2010). The N-terminal domain was renamed γ-zein ER-accumulating domain (Zera®, which is essentially a truncated γ-zein) by ERA Biotech – now Zip Solutions - (Barcelona, Spain) (Figure 1.13) (Ludevid *et al.* 2005). Zera® (116 amino acid) domain comprises the CGC motif downstream of the signal peptide, a central proline-rich domain containing a hexapeptide repeat $(PPPVHL)_8$, as well as a C-terminal Pro-X domain with four cysteine residues (Geli *et al.* 1994). The mechanisms by which γ-zeins drive self-assembly into PBs in the ER are not well understood because the sequence contains the N-terminal secretory signal and does not contain an obvious ER-retention signal (H/KDEL), yet PBs are retained intracellularly. It is believed that the hydrophobic interactions between the amphipathic $(PPPVHL)_8$ repeats, the formation of disulphide bonds between Zera® molecules, as well as the high ionic strength and oxidising ER environment, are

characteristic features that allow for self-assembly into PBs (Geli *et al.* 1994; Kogan *et al.* 2001; Llop-Tous *et al.* 2010).

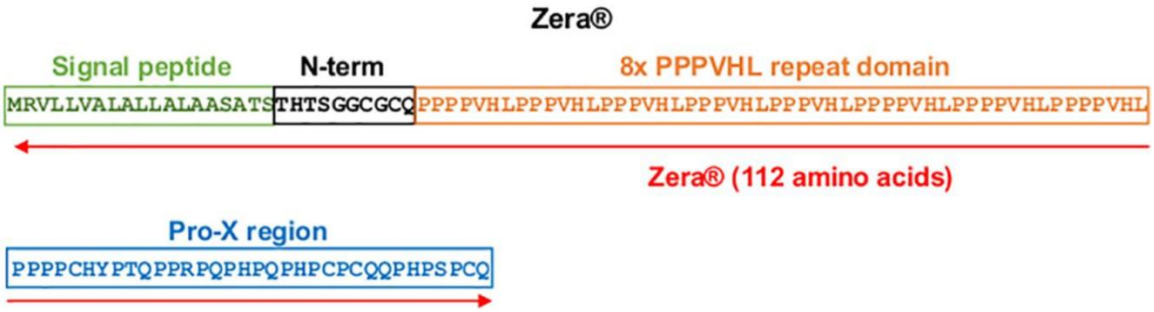

Figure 1.13: Amino acid sequence and domains of Zera®. Zera® is composed of the γ-Zein signal peptide (green), the non-proline N-terminal region with a CGC motif (black), the repeating domain with eight units of the PPPVHL hexapeptide (orange) and the Pro-X C-terminal domain with four cysteine residues (blue).

Protein body induction is not restricted to seeds; they were shown to form when zein was fused to various proteins which were produced in a wide range of non-seed expression hosts including plant, fungal, insect and mammalian cells (Llop *et al.* 2006; Torrent *et al.* 2009a; Torrent *et al.* 2009b; Conley *et al.* 2011; Schmidt. 2013; Whitehead *et al.* 2014; Mbewana *et al.* 2015; Hofbauer *et al.* 2016). An example of the characterisation of protein bodies in plants and mammalian cells is shown in Figure 1.14. The benefits of packaging the protein of interest in Zera®-induced PBs include the retention of protein in the ER (thus providing insulation against proteolysis in the cytoplasm), ease of purification as electron-dense PBs usually allow for simple protein recovery using gradient centrifugation, and the adjuvant effect of the particulate PBs (Torrent *et al.* 2009a; Schmidt. 2013; Whitehead *et al.* 2014). Encouragingly, the ectodomain of influenza HA fused to zein (H5-zein) formed protein bodies in tobacco leaves which were significantly more immunogenic in mice than the soluble H5 HA (Hofbauer *et al.* 2016). The adjuvant effect of H5-zein PBs was similar to the response elicited when the soluble H5 was co-administered with a commercial adjuvant. Moreover, when H5-zein was co-administered with a commercial adjuvant, the H5-zein immune responses could not be enhanced, suggesting that the particulate nature of zein PBs was sufficient to mediate an adjuvant effect (Hofbauer *et al.* 2016).

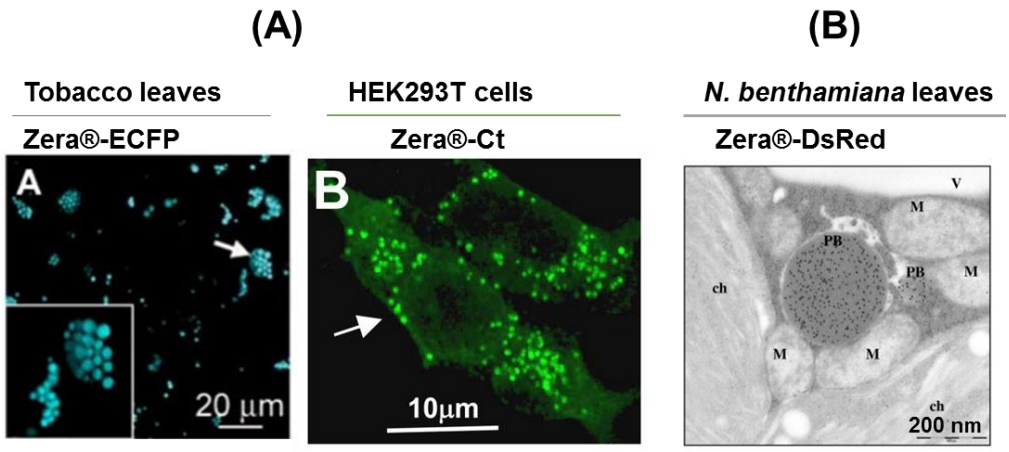

Figure 1.14: Characterisation of Zera®-induced PBs in plant leaves and mammalian cells. (A) Confocal micrographs of PBs in tobacco leaves expressing Zera®-tagged enhanced cyan fluorescence protein (Zera-ECFP), and human embryonic kidney (HEK293T) cells expressing Zera®-calcitonin (Zera®-Ct). **(B)** Immunoelectron micrograph of *N. benthamiana* leaves (thin sections) expressing Zera®-red fluorescent protein (DsRed). Protein body (PB), chloroplast (ch), mitochondria (M) and vacuole (V) are indicated. Scale bars are indicated in each micrograph. **Figure 15 (A)** was adapted from Torrent *et al.* (2009b) while **Figure 15 (B)** was adapted from Joseph *et al.* (2012) with both permissions provided by Springer Nature.

1.14.4.2 Hydrophobin-I (HFBI)

Hydrophobins are small (≈ 10kDa) surface-active (surfactant) globular proteins found solely in fungi. Hydrophobins are characterised by the presence of conserved eight cysteine residues, which form four intramolecular disulphide bonds that confer stability to the amphipathic tertiary structure resulting from self-assembly at hydrophilic-hydrophobic interfaces (Sunde *et al.* 2008; Berger & Sallada. 2019). The surfactant and self-assembly features of hydrophobins are attractive for nanotechnology applications (Conley *et al.* 2011). The fusion of hydrophobin plus ER-retention signal (KDEL) to the protein of interest (green fluorescent protein (GFP) or enzyme glucose oxidase) resulted in the formation of novel PBs encapsulating large amounts of proteins that were effectively purified using an aqueous two-phase system (ATPS) (Joensuu *et al.* 2010). The fusion of hydrophobin I to the hemagglutinin ectodomain of influenza virus (H5-HFBI or H1-HBFI) also resulted in the formation of novel PBs in plant leaves (Jacquet *et al.* 2014; Phan *et al.* 2014). Encouragingly, H1-HBFI PBs (purified by ATPS followed by ammonium sulfate precipitation) elicited neutralising antibodies in mice (Jacquet *et al.* 2014).

1.14.4.3 Elastin-like polypeptides (ELPs)

Elastin-like polypeptides (ELPs) are mammalian elastin-like synthetic pentapolypeptides containing a repeating ‘VPGXG’ sequence where X can be any residue beside proline (Urry. 1988). When heated above their transition temperature, a reversible reaction occurs where the soluble ELPs transition to insoluble, hydrophobic ß-spiral structures (Urry. 1997). The

fusion of ELPs to any recombinant protein of interest allows for simple, cheap and scalable non-chromatographic purification of proteins using temperature-salt dependent or filter-based purification techniques, respectively called centrifugation-based inverse transition cycling (cITC) or membrane-based ITC (mITC) (Meyer & Chilkoti. 1999; Phan & Conrad. 2011). Just like hydrophobin, the fusion of ELPs plus the ER-retention signal to GFP or H5, improved protein accumulation and also resulted in the formation of ER-derived PBs in plants (Conley *et al.* 2009; Phan *et al.* 2014). Interestingly, the plant-produced monomeric HA fused to ELP (H5-ELP) failed to elicit neutralising antibodies in mice. However, autologous and heterologous NAbs were elicited when H5-ELP was stabilised into trimers by including the GCN4-pII isoleucine-zipper trimerisation sequence directly downstream of the H5 ectodomain (Phan *et al.* 2013).

1.14.5 *In vitro*-assembling nanoparticles

Even though the *in vivo*-assembling protein nanoparticles (Gag-Env VLPs and genetically fused ferritin, E2p, I3-01, lumazine and PB-inducing Zera®) are generally novel nanotechnology concepts, they may not be optimal for HIV-1 Env trimers. Besides the possibility of compromising the nanoparticle assembly due to the complex nature of Env, once these nanoparticles assemble intracellularly to display or encapsulate HIV-1 Env, it is impossible to eliminate the misfolded, non-native Env species from the nanoparticles. These non-native Env species may serve as immunological decoys limiting the induction of relevant neutralising antibody responses (Brinkkemper & Sliepen. 2019; Brouwer & Sanders. 2019). For these reasons, recent efforts are focusing on optimising two-component nanoparticles that allow for *in vitro* co-assembly of the two components of the nanoparticle. *In vitro*-assembling nanoparticles allow for the independent production of the protein components and better quality control of both Env trimers and nanoparticles as they can be purified separately, then combined to generate nanoparticles displaying a majority of well-folded Env trimers (Brinkkemper & Sliepen. 2019; Brouwer & Sanders. 2019). The promising *in vitro*-assembling nanoparticles for HIV-1 Env trimers include I53-50 nanoparticles and pre-assembled SpyCatcher-AP205 VLPs for covalently displaying Env-SpyTag proteins (Brinkkemper & Sliepen. 2019; Brouwer & Sanders. 2019).

1.14.5.1 I53-50 nanoparticles

The I53-50 nanoparticle is a computationally designed 60-meric, two-component icosahedral particle (20-40 nm in diameter) generated by combining 20 naturally trimeric “A” (I53-50A) and 12 pentameric “B” (I53-50B) subunits (Bale *et al.* 2016). The application of I53-50 nanoparticle was first observed when the prefusion-stabilised F glycoprotein (DS-Cav1) from the respiratory syncytial virus (RSV) was genetically fused to I53-50A to generate Ds-Cav1-I53-

50A scaffold trimers that were complementary to I53-50B pentamers (Marcandalli *et al.* 2019). Mixing the HEK293-produced Cav1-I53-50A trimers with bacterial-produced I53-50B pentamers *in vitro* resulted in Ds-Ca1-I53-50 nanoparticles displaying ≈20 well folded-trimers spaced at about 150 Å apart. The nanoparticle-arrayed Ds-Ca1 trimers elicited 10-fold higher neutralising antibodies than the soluble trimers in mice and macaques, supporting the notion that high-density antigen display improves B-cell cross-linking (Marcandalli *et al.* 2019). Encouragingly, after a single vaccination in rabbits, HIV-1 Env ConM SOSIP-I53-50 nanoparticles elicited 40-and 10-fold higher autologous NAbs compared to the soluble trimers or ferritin-arrayed trimers, respectively (Brouwer *et al.* 2019; Brouwer & Sanders. 2019).

Recently, a 5-library consisting of tetrahedral, octahedral and icosahedral nanoparticles were tailor-made for the presentation of trimeric viral glycoproteins such as HIV-1 Env trimers (Ueda *et al.* 2020), and their concepts mirror that of the I53-50 nanoparticles. When the ConM-SOSIP-T33_dn2A component (antigen-bearing component) was reacted with the corresponding T33_dn2B component (nanoparticle assembly component), tetrahedral nanoparticles presenting only four trimers per particle were observed (Antanasijevic *et al.* 2020). Interestingly, the ConM-SOSIP-T33_dn2 nanoparticles elicited higher neutralising titres against the autologous conM virus when compared to their soluble ConM-SOSIP.v7 trimers. Additionally, even though the T33_dn2 nanoparticles presents trimers at a lower valency (4 trimers per particle), their immunogenicity was comparable to the trimers presented on the higher valency ferritin (8 trimers per particle) and I53-50 (20 trimers per particle) nanoparticles (Antanasijevic *et al.* 2020).

The I53-50 nanoparticles have also been used as a scaffold for the presentation of SARS-CoV-2 vaccine candidates (Walls *et al.* 2020; Brouwer *et al.* 2021b; Kang *et al.* 2021). Notably, macaques that were vaccinated with I53-50 nanoparticles displaying SARS-CoV-2 spike protein before they were challenged with a high dose of SARS-CoV-2; showed a lower viral load when compared to unvaccinated animals (Brouwer *et al.* 2021b).

1.14.5.2 SpyCatcher-SpyTag-tagged nanoparticles

The discovery that the surface proteins of Gram-positive bacteria such as *Streptococcus pyogenes*, *Streptococcus pneumoniae*, *Staphylococcus aureus*, and *Corynebacterium diphtheria* form spontaneous intramolecular isopeptide bonds, opened attractive protein stabilising alternatives. Naturally forming isopeptide bonds afford alternative protein-stabilising strategies instead of cross-linking with disulphide bonds which are reversible and restricted to specific subcellular compartments (Kang & Baker. 2011). Specifically, the second immunoglobulin-like collagen adhesion domain (CnaB2) in the fibronectin-binding protein of *Streptococcus pyogenes,* is stabilised by the formation of an isopeptide bond that optimally

forms in a wide range of temperature and pH conditions (Kang *et al.* 2007; Hagan *et al.* 2010; Kang & Baker. 2011). Zakeri *et al.* (2012) and Li *et al.* (2014) split the CnaB2 domain of ***S****treptococcus* ***py****ogenes* (Spy) into rationally engineered SpyTag peptide (13 amino acid) and SpyCatcher protein (138 or 116 amino acid) reactive partners. Mixing of the SpyTag and SpyCatcher led to the formation of a rapid, irreversible covalent isopeptide bond. This isopeptide bond formed between the reactive carbonyl carbon of Asp^{117} in the SpyTag and the reactive amine of Lys^{31} in the SpyCatcher. This reaction requires the catalytic activity of Glu^{77} in the SpyCatcher (Figure 1.15).

The SpyTag-SpyCatcher reaction occurred optimally over a wide range of conditions: temperature (4-37°), pH (5-8), buffers (phosphate-buffered saline (PBS), Hepes, Tris) and non-anionic reagents. Since the reaction between the SpyTag and SpyCatcher occurs through the side chains of the amino acids involved, the SpyTag and SpyCatcher can be fused at any position (N-terminally or internally or C-terminally) to the protein of interest (Zakeri *et al.* 2012; Reddington & Howarth. 2015). As a result, the SpyTag and SpyCatcher have been used as a novel bio-conjugation tool in a wide range of applications, including vaccine nanoparticle scaffolds and for stabilisation of enzymes as reviewed elsewhere (Reddington & Howarth. 2015; Brune & Howarth. 2018; Hatlem *et al.* 2019; Keeble & Howarth. 2020). Several variants of Catcher/Spy systems have also been developed: the second-generation systems with faster reacting SpyTag and SpyCatcherΔN1 (N-terminally truncated SpyCatcher from 116 to 84 amino acids) (Li *et al.* 2014) or SpyTag002 and SpyCatcher002 (addition of a positively charged lysine at the C-terminus of the SpyTag and using a phage display library for selection of clones with faster isopeptide bond formation) (Keeble *et al.* 2017) or SpyTag003 and SpyCatcher003 (included additional positively charged residues at the N terminus of the SpyTag002 and the mutations that reduced the loop flexibility while increasing the surface polarity of the SpyCatcher) (Keeble *et al.* 2019), the system that uses SnoopTag and SnoopCatcher derived from an adhesin domain of *Streptococcus pheumoniae* (Izoré *et al.* 2010; Veggiani *et al.* 2016), the tripeptide systems so that the reactive amino acids are located on separate peptides (SpyLigase + SpyTag + KTag or the improved version, SnoopLigase + SnoopTag + DogTag) (Fierer *et al.* 2014; Veggiani *et al.* 2016; Buldun *et al.* 2018) and SpyDock to facilitate the purification of SpyTag-proteins using the Spy&Go system (Anuar *et al.* 2019).

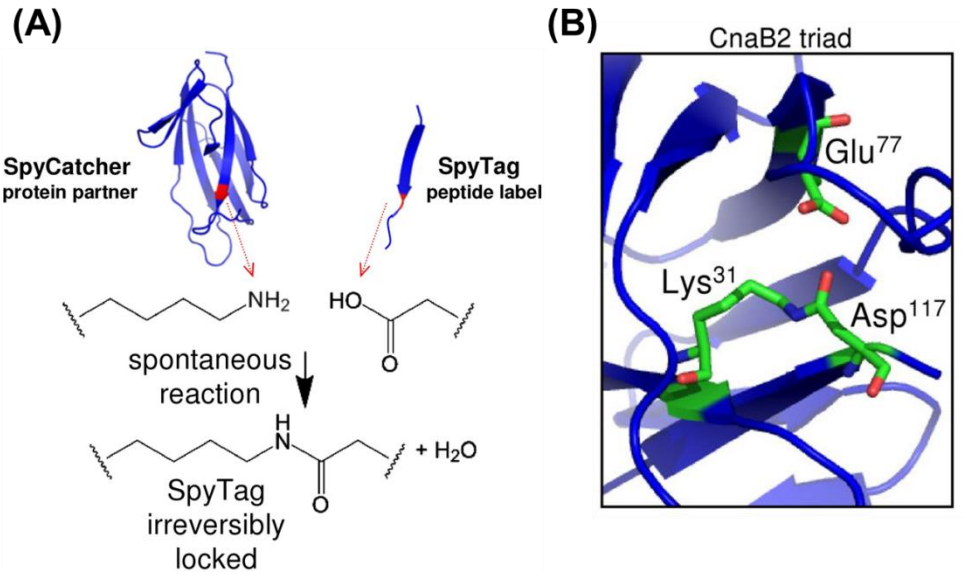

Figure 1.15: Split and engineered *Streptococcus pyogenes*-derived CnaB2 domain into reactive fragments. (A) The CnaB2 was split into SpyCatcher and SpyTag complementary partners, that upon mixing, they spontaneously form an irreversible isopeptide bond. **(B)** Stick model showing three key amino acids (Lys^{31}, Aps^{117} and Glu^{77}) of CnaB2 that are involved in the formation of the isopeptide bond. The diagram was adapted from Zakeri *et al.* (2012).

As an alternative to the conventional conjugation methods (such as chemical cross-linking, affinity approaches using His-Ni^{2+} or biotin-avidin, the addition of unnatural amino acids for click chemistry, sortase, just to mention a few), the Catcher/Tag split-protein technology is a promising strategy for *in vitro* decoration of pre-assembled nanoparticles with complex vaccine antigens (Brune & Howarth. 2018). Brune *et al.* (2016) and Thrane *et al.* (2016) independently constructed the bacterial expression plasmids encoding the SpyCatcher or SpyTag coding sequences genetically fused to the 5' end of the sequence coding the viral coat protein (CP3) of the RNA bacteriophage AP205 that infects the Gram-negative *Acinetobacter* bacteria. These constructs expressed versatile Spy-VLPs (SpyTag-AP205 or SpyCatcher-AP205) that could be covalently decorated with a wide range of Spy-tagged antigens for vaccine purposes (Figure 1.16) (Brune *et al.* 2016; Thrane *et al.* 2016). Each AP205 VLP assembled from 180 coat protein subunits (spaced at about 100 Å) that self-assembled to generate particles (≈ 29nm in diameter) with icosahedral symmetry. AP205 VLPs are attractive scaffolds for vaccines because the C- and N-termini of the coat protein are surface exposed, tolerate fusion of heterologous proteins at both termini without compromising particle assembly, can be produced at high yields in bacteria and encapsulate host-specific RNAs (25-30µg per 100µg coat protein) that can offer adjuvant properties (Klovins *et al.* 2002; van den Worm *et al.* 2006; Spohn *et al.* 2010; Tissot *et al.* 2010; Aves *et al.* 2020).

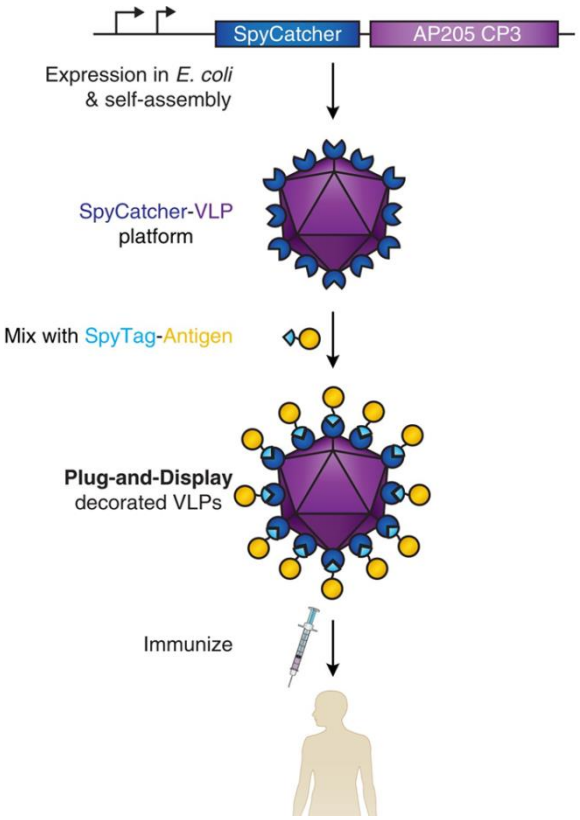

Figure 1.16: The design of the SpyCatcher-AP205 VLPs for the high-density display of the immunological relevant SpyTagged-antigens for vaccine developments. The diagram was adapted from Brune *et al.* (2016) following the copyright guidelines specified by the Creative Commons license**.**

The versatility of the SpyCatcher-AP205 VLPs in vaccine development was initially confirmed by the ability to display a diverse range and size of antigens. These antigens included malarial proteins, *Mycobacterium tuberculosis* and cancer or allergy self-associated proteins ranging between 14.5-118 kDa (Brune *et al.* 2016; Thrane *et al.* 2016). The coupling efficiency (% of VLP occupied) and antigen display capacity (number of antigens per VLP) inversely correlated with an increase in the size of antigens, suggesting that the display of larger proteins on Spy-VLP platforms could be limited by steric hindrance (Thrane *et al.* 2016). Encouragingly, the malarial antigens (Pfs25, VAR2SCA, CIDR, CSP) and self-antigens (CTLA-4, HER2, PD-L1, and HER2) displayed on AP205 VLPs (via SpyTag-SpyCatcher interaction) and sometimes formulated without adjuvants, generally elicited higher antibody responses in mice than the soluble antigens. The Spy-VLP-displayed antigens generally showed one or more features that indicated improved immunological profiles compared to otherwise weakly immunogenic soluble antigens: improved antibody titres, longevity, avidity, quality and functionality (antibodies against malarial vaccines were able to block parasite establishment in mosquitoes, self-associated antigens effectively broke B cell self-tolerance, and anti-HER2 antibodies reduced the growth of mammary carcinomas) (Brune *et al.* 2016; Janitzek *et al.* 2016; Thrane

et al. 2016; Leneghan *et al.* 2017; Palladini *et al.* 2018). When the attractive vaccine targets (heat-stable toxins, ≈ 4.3kDa peptides) against Enterotoxigenic *Escherichia coli* were displayed on AP205 VLPs via the SpyTag-SpyCatcher interaction, robust, cross-neutralising antibodies were elicited in mice in the absence of adjuvants (Govasli *et al.* 2019).

The Spy-VLP system is not only suitable for peptide and monomeric proteins, but it is also a versatile scaffold for displaying multimeric and complex antigens. The presentation of trimeric HIV-1 Env glycoprotein on VLPs via the SpyTag-SpyCatcher has been reported recently. The SpyTagged RC1-4fill native-like trimers (SOSIP.668-stabilised plus 4 additional glycans to block off-target epitopes) was multimerised on Spy-AP205 VLPs. The resulting AP205-RC1-4fill VLPs were able to engage the B cells that expressed the V3-glycan patch-specific bNAb precursors in rhesus macaques (Escolano *et al.* 2019). The SpyTag/ SpyCatcher technology has also enabled the use of protein nanoparticles such as lumazine synthase (LuS) and ferritin as in vitro-assembling nanoparticle platforms for the presentation of trimeric glycoproteins (Zhang *et al.* 2020; Ding *et al.* 2021). Specifically, LuS-SpyTag and ferritin-SpyTag nanoparticles were generated, and their expression, solubility and assembly were improved by the addition of 1-2 potential N-linked glycosylation sites. These nanoparticles efficiently presented the SpyCatcher-tagged trimeric glycoproteins from the respiratory syncytial virus fusion, human parainfluenza virus type 3 fusion glycoprotein and the SARS-CoV-2 spike protein (Zhang *et al.* 2020). Immunogenicity studies in mice indicated that the low-dose SARS-CoV-2 spike-LuS nanoparticles induced 25-fold higher neutralising antibodies compared to the soluble spike trimer (even when used at a higher dose than the nanoparticle-displayed spike) (Zhang *et al.* 2020). Ding *et al.* (2021) used the SpyCatcher-ferritin nanoparticles to display the cleavage-independent SOSIP.664 gp140-SpyTag trimers. A sequential vaccination regimen [priming with DNA encoding gp145 followed by boosting with recombinant China Tiantan vaccinia virus (also encoding gp145) and SOSIP.664 gp140-ferritin nanoparticle] tested in rhesus macaques indicated that the nanoparticle boost increased the binding antibodies titres by 10-fold. This prime-boost regimen also induced neutralising antibodies against autologous and heterologous Tier 2 viruses, and these neutralising responses were protective against a heterologous SHIV challenge. These results indicated that in sequential prime-boost immunisation modalities, an increase in density/capacity of presentation of gp140 trimers could improve the elicitation of neutralising antibody responses against Tier 2 viruses (Ding *et al.* 2021).

Besides the AP205 VLPs, hepatitis B VLPs (Marini *et al.* 2019; Hartzell *et al.* 2020), norovirus-like VLPs (Lampinen *et al.* 2021), and protein nanoparticles, the Tag/Catcher conjugation approach has been applied to other synthetic vaccine scaffolds. A modular plug-and-display technology using orthogonal groups enabled the multimerisation of two malarial antigens,

Pfs25-SpyTag and Pfs28-SnoopTag, on the surface of a synthetic SpyCatcher-IMX-SnoopCatcher scaffold, and elicited more robust antibody responses compared to the soluble Pfs25-SpyTag and Pfs28-SnoopTag (Brune *et al.* 2017). Bruun *et al.* (2018) rationally designed the 2-keto-3-deoxy-phosphogluconate aldolase of the thermophilic *Thermotoga maritima* to generate proteins that self-assemble to form i301 (60-meric) nanoparticles with dodecahedral symmetry. Further deletion of the surface-exposed cysteine residues of the i301 generated stable and homogenous mi3 nanoparticles (26 nm in diameter). In comparison to SpyCatcher-AP205 VLPs, the SpyCatcher-mi3 particles were produced at 10-fold higher yields and showed improved stability and homogeneity. The SpyCatcher-mi3 nanoparticles efficiently displayed various SpyTag-tagged malarial antigens (CIDR, Pfs25 and CyRPA). The mi3-displayed CyRPA elicited higher antibody titres than the soluble CyRPA antigen in mice (Bruun *et al.* 2018).

Recently, the SpyCatcher-AP205 VLPs and SpyCatcher-mi3 nanoparticles were both used for homotypic and heterotypic co-display of HA trimers from different influenza strains (Cohen *et al.* 2021b). Heterotypic nanoparticles refer to nanoparticles where up to 8 trimers were mixed in a single reaction to allow random (since all trimers carried the SpyTag) co-display on a single nanoparticle (mosaic-2, -4 or -8 nanoparticles). Homotypic nanoparticles refer to the mixing of 2-8 nanoparticles pre-conjugated with specific trimers (admix-2, -4 and -8 nanoparticles). The cryo-electron tomography indicated that about 81-144 HA trimers were displayed per AP205 VLP at a spacing of 70-100 Å between trimers. About 18-24 trimers were displayed per mi3 nanoparticle at a spacing of 120-150 Å between trimers. However, the mosaic and admix nanoparticles demonstrated equivalent binding and neutralising antibodies in mice, suggesting that further modifications or different regimens are necessary to develop an effective influenza vaccine (Cohen *et al.* 2020). The hemagglutinin-conjugated SpyCatcher-mi3 nanoparticles were also reported to be a versatile diagnostic tool for serological surveillance of influenza A virus in domestic cats and dogs (Zhao *et al.* 2020). Overall, these studies demonstrate the novel applications of the Catcher/Tag technology in the vaccine or diagnostic assay developments.

The rapid application of the SpyTag/SpyCatcher technology has been demonstrated during the current dire search for an effective vaccine against the ongoing SARS-Cov-2 pandemic (Ma *et al.* 2020; Okba *et al.* 2020; Tan *et al.* 2020; Zhang *et al.* 2020; Cohen *et al.* 2021a; Kang *et al.* 2021; Rahikainen *et al.* 2021). These studies used the SpyTag/SpyCatcher technology to display SARS-Cov-2 vaccine candidates on various nanoparticles, including lumazine synthase, I3-01, E2p, ferritin, I53-50 and mi3. In the Tan *et al.* (2020) study, the SpyTag/SpyCatcher technology was used to densely display the receptor-binding domain (RBD) of the spike subunit of SARS-Cov-2 on the mi3 nanoparticles (referred to as SpyVLP

in that study). RDB displayed on SpyVLPs retained the conformation-specific antigenic features, and these RDB-SpyVLPs were stable (thermostable, not prone to degradation after several rounds of freeze-thaw cycles or lyophilisation) in a wide range of storage conditions. Furthermore, the RDB-SpyVLPs induced higher neutralising antibody titres against the live or pseudotyped SARS-Cov-2 viruses in both mice and pigs compared to the soluble RDB protein (Tan *et al.* 2020). Cohen *et al.* (2021a) used the SpyTag/SpyCatcher for homotypic (presenting RDB from SARS-CoV-2 alone) and mosaic (co-displaying RDB from SARS-CoV-2 and various clades of RDBs from bat SARS-like betacoronaviruses) display on mi3 nanoparticles, and this presentation induced cross-binding and neutralising antibodies in mice. In the He *et al.* (2021) study, the stabilised SARS-CoV-2 spike trimers conjugated on ferritin nanoparticles via the SpyTag/SpyCatcher technology; elicited 7-fold higher neutralising antibody titres in mice compared to their soluble counterparts. When displayed on E2p and I3-01 nanoparticles, the stabilised SARS-CoV-2 spike trimers elicited up to 10-fold neutralising antibody titres in mice when compared to their soluble trimers. Interestingly, when the spike was displayed on I3-01 nanoparticles, a strong T helper and other T cell responses were observed, indicating that these nanoparticles elicited both humoral and cellular responses (He *et al.* 2021).

1.15 Project rationale and objectives

An effective HIV-1 vaccine could work by eliciting potent and broadly neutralising antibodies against the circulating Tier-2 viruses. The development of the soluble native-like Env trimers such as SOSIP- and NFL-stabilised trimers was a major breakthrough in the research field seeking to develop bNAb-based vaccines. In animal studies, these native-like trimers have been shown to consistently elicit high but short-lived titres of autologous Tier 2 neutralising antibodies. In addition, some of these trimers sporadically and weakly induced neutralising antibodies against the heterologous Tier 2 viruses. Even though autologous Tier 2 neutralising antibodies are induced by these native-like trimers, they are short-lived, indicating that these immunogens or vaccination regimens are not yet optimal to elicit durable and potently neutralising antibodies. Particulate presentation of soluble antigens is a promising strategy to improve the immunogenicity of otherwise weakly immunogenic subunit antigens. Therefore, the overall aim of this study was to use Zera®-induced protein bodies and SpyCatcher-AP205 VLPs to improve the immunogenicity of the HIV-1 subtype C CAP256 gp140 protein. This work had three main objectives:

Objective 1: To evaluate the formation of gp140-Zera® and Zera®-gp140 protein bodies in a plant expression system.

Objective 2: To evaluate the formation of gp140-Zera® and Zera®-gp140 protein bodies in a mammalian expression system, and their immunogenicity in rabbits.

Objective 3: To evaluate the display of gp140 trimers on AP205 VLPs via the SpyTag-SpyCatcher interaction, and their immunogenicity when displayed on nanoparticles.

CHAPTER 2: TRANSIENT EXPRESSION AND PARTIAL CHARACTERISATION OF HIV-1 ENVELOPE G140 ZERA®-TAGGED ANTIGENS IN PLANTS

2.1 Introduction

An effective prophylactic vaccine remains an urgent priority to combat the HIV-1 pandemic. Theoretically, a preventative vaccine could work by inducing high titres of antibodies against the HIV-1 envelope glycoprotein (Env) with the capacity to neutralise the circulating viruses and/or mediate effector functions to kill infected cells (Rerks-Ngarm *et al.* 2009; McCoy & Weiss. 2013; Burton & Hangartner. 2016; Alter & Barouch. 2018).

Initial efforts to design vaccines that could potentially elicit neutralising antibodies (NAbs) focused on generating soluble and stable recombinant Env trimers that antigenically and structurally recapitulate the native trimers present on a viral surface. The cleavage-dependent SOSIP and cleavage-independent native flexibly linked (NFL) designs are Env modifications that generate predominantly trimeric Env forms from sequences derived from different HIV-1 isolates (Sanders *et al.* 2013; Sharma *et al.* 2015). Careful selection of Env sequences before the implementation of the SOSIP or NFL modifications is essential to maximise the chances of eliciting NAbs. The HIV-1 Env sequence used in this study was derived from a participant, CAP256, who was initially infected with HIV-1 subtype C virus and subsequently superinfected with another unrelated second subtype C virus (van Loggerenberg *et al.* 2008). Superinfection in CAP256 established potent cross-neutralising antibodies (Gray *et al.* 2011a; Moore *et al.* 2013; Doria-Rose *et al.* 2014; Bhiman *et al.* 2015) in agreement with previous cohorts that indicated that HIV-1 superinfection correlated with improved neutralising breadth and potency (Powell *et al.* 2010; Cortez *et al.* 2012). However, in a follow-up study, it was discovered that CAP256 NAbs did not cross-react with epitopes conserved in both the primary infecting and superinfecting CAP256 viruses, suggesting that there is no evidence that superinfection was essential for broadening of NAb responses (Sheward *et al.* 2018). The sensitivity of CAP256 Env-pseudotyped viruses, including the primary infecting (PI) and the superinfecting (SU) viruses, to broadly neutralising monoclonal antibodies targeting different Env epitopes (Moore *et al.* 2013) and the ability of CAP256 viral variants (referred to as bNAb-initiating Envs) to efficiently engage the V1V2 bNAb precursors (Bhiman *et al.* 2015) still suggest that CAP256-based Env immunogens could elicit potent and broader NAb responses.

Even though the stabilised Env immunogens have been shown to elicit moderate to high titres of binding and autologous neutralising antibodies in animal studies, these titres wane quickly, even when formulated in adjuvants or used in heterologous prime-boost regimens (Sanders *et al.* 2015; Klasse *et al.* 2016; Brouwer *et al.* 2019; Sliepen *et al.* 2019; van Diepen *et al.* 2019). Particulate presentation of soluble antigens through self-assembling nanoparticle platforms is a novel strategy to improve the immunogenicity of subunit antigens (Bachmann &

Jennings. 2010; Zhao *et al.* 2013; Brinkkemper & Sliepen. 2019; Brouwer & Sanders. 2019; Karch *et al.* 2021).

Genetically fusing antigens to protein body (PB)-producing fusion tags such as the maize storage protein zein, is a strategy that can potentially improve the immunogenicity of soluble proteins while also improving their accumulation and recovery (Conley *et al.* 2011; Schwestka & Stoger. 2021). Zein-derived tags such as Zera®, an N-terminal domain of γ-zein, have been shown to successfully induce electron-dense endoplasmic reticulum (ER)-derived PBs when genetically fused to various antigens. These PB-forming chimaeric proteins include the fusion of zein/Zera® to the HIV Nef (de Virgilio *et al.* 2008), HPV type 16 E7 protein (Whitehead *et al.* 2014), an influenza virus A matrix 2 protein ectodomain (M2e) (Mbewana *et al.* 2015), the ectodomain of influenza A haemagglutinin (HA) subtype 5 (Hofbauer *et al.* 2016), bluetongue virus VP2 serotype-specific antigen (van Zyl *et al.* 2017), among others. The benefits of packaging the protein of interest in Zera®-induced PBs include the retention of protein in the ER (thus providing insulation against proteolysis in the cytoplasm), ease of purification as electron-dense PBs allow for simple protein recovery using gradient centrifugation, and the adjuvant effect of the particulate PBs (Torrent *et al.* 2009a; Schmidt. 2013; Whitehead *et al.* 2014; Hofbauer *et al.* 2016).

Plant expression systems have recently gained attention as a cost-effective, safe and scalable alternative to mammalian systems for recombinant production of immunogens, particularly of viral glycoproteins (Rybicki. 2014; Margolin *et al.* 2018; Schoberer & Strasser. 2018). Contrary to time-consuming and low-protein yielding transgenic plants, the advances in plant virus-derived expression vectors such as a hypertranslatable (HT) pEAQ-HT vector derived from a Cowpea mosaic virus; have facilitated the development of a rapid and high-expressing transient system suitable for the production of glycoproteins (Sainsbury *et al.* 2009; Sainsbury *et al.* 2010; Hefferon. 2012; Yamamoto *et al.* 2018). The use of the pEAQ-HT expression vector in combination with an efficient heterologous signal peptide such as the murine monoclonal-derived LPH signal peptide, as well as co-expression with appropriate chaperones to improve glycan occupancy, can achieve appreciable folding and post-translational modifications of glycoproteins along the secretory pathway in plants (Margolin *et al.* 2018; Margolin *et al.* 2019). The majority of zein/Zera®-induced PBs have been recombinantly produced in leaf-based transient expression systems (de Virgilio *et al.* 2008; Torrent *et al.* 2009b; Llop-Tous *et al.* 2010; Conley *et al.* 2011; Joseph *et al.* 2012; Whitehead *et al.* 2014; Mbewana *et al.* 2015; Saberianfar *et al.* 2015; Hofbauer *et al.* 2016). Our group previously reported the successful agroinfiltration-based transient expression and purification of the NFL-stabilised soluble CAP256 gp140 immunogen in *Nicotiana benthamiana* leaves (Margolin *et al.* 2019).

In a continuing effort to identify suitable nanoparticles for the particulate presentation of HIV-1 Env, in this study, experimental antigens consisting of HIV-1 CAP256 gp140 with Zera® fused to either the C-terminus (gp140-Zera®) or N-terminus (Zera®-gp140) were generated, and the formation of PBs evaluated in plant leaves.

2.2 Materials and Methods

2.2.1 Selection and modification of Env sequence

This study formed part of a project funded by the Medical Research Council (MRC) Strategic Health Innovation Partnership (SHIP) to develop and test South African subtype C candidate HIV-1 immunogens that could induce high-titre antibody responses to HIV-1 envelope glycoprotein (Env). In this project, the envelope sequence used was from a superinfecting virus from patient CAP256 (clone CAP256.206sp.032.CA, GenBank accession number: KF241776.1) (Moore *et al.* 2013), and the sequence was kindly provided by Dr Penny Moore (Senior Medical Scientist, Centre for HIV and STIs, National Institute for Communicable Diseases, Johannesburg).

The design of soluble Env antigens was based on the native flexibly linked (NFL) invention by Sharma *et al.* (2015), which results in soluble, cleavage-independent Env trimeric mimics by covalently linking Env heterodimeric gp120 and gp41 using a flexible linker. The CAP256 Env sequence was modified as follows: the furin-sensitive cleavage site between gp120 and gp41 subunits was replaced with a glycine-serine $(G_4S)_2$ flexible linker (FL), which retains conformational mobility closely mimicking the native Env trimers (Kovacs *et al.* 2014; Sharma *et al.* 2015). An I548P (IP) point mutation, equivalent to the I559P present in the SOSIP trimers, was introduced in the N-terminal heptad repeat of gp41 to enhance trimerisation by re-enforcing the interaction between gp41 subunits (Sanders *et al.* 2002). The sequence coding for the full-length CAP256 Env (gp160) was truncated before the transmembrane region by introducing a stop codon after amino acid 653 to generate soluble CAP256 gp140 coding sequence. To ensure the entry into the hosts' secretory pathway, the native leader sequence was either replaced with a heterologous signal sequence from the murine mAb24 heavy chain-derived signal peptide (LPH) for expression in plants or from the human tissue plasminogen activator leader (TPA) for expression in mammalian cells. The genes were human-codon optimised and synthesised by GenScript.

2.2.2 Generation of plant vectors encoding gp140-Zera® or Zera®-gp140

For transient expression of gp140 in plants, Emmanuel Margolin (Senior Scientific Officer, Department of Pathology, University of Cape Town), inserted the murine mAb24 heavy chain-derived LPH signal peptide and the gp140 envelope sequence into a binary pEAQ-HT cowpea

mosaic virus-derived plant expression vector designed by Sainsbury *et al.* (2009) to form plasmid pEAQ-HT: SU gp140 (Margolin *et al.* 2019). The generation of vectors expressing gp140 with Zera® fused to the 3' end for expression in plants is illustrated in Figure 2.1. Briefly, using NotI and XhoI restriction enzymes, Zera® was inserted into pUC57 gp140 to form pUC57 gp140-Zera®. BshTI and XhoI were then used to insert gp140-Zera® into the pEAQ-HT vector to form pEAQ-HT: gp140-Zera®.

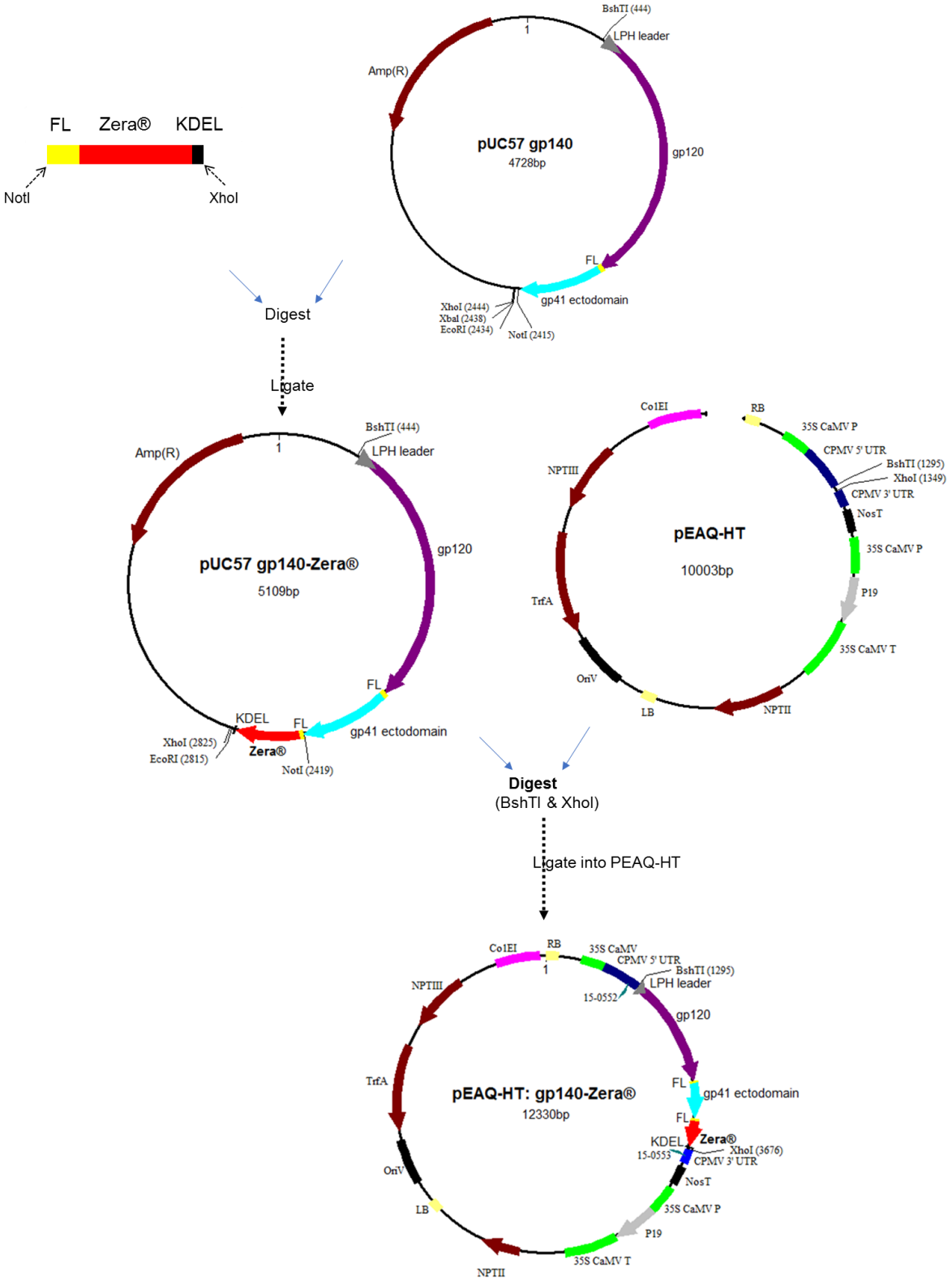

Figure 2.1: Annotated plasmid maps showing the subcloning of gp140-Zera® from pUC57 into the pEAQ-HT plant expression vector. The major features qualifying the pEAQ-HT as a binary vector for protein expression in plants include: 35S CaMV P: 35S promoter from cauliflower mosaic virus; T-DNA right (RB) and left borders (LB); 5' untranslated region (UTR) and 3' UTR from modified cowpea mosaic virus (CPMV) RNA-2; P19: suppressor of gene silencing from tomato bushy virus (TBSV); 35S CaMV T: terminator from CaMV; NosT: nopaline synthase terminator; OriV: *R. radiobacter* origin of

replication; CoIEI: *E. coli* origin of replication; NPTIII: neomycin phosphotransferase conferring the kanamycin resistance; and TrfA: replication essential locus (Sainsbury *et al.* 2009). Amp(R) = ampicillin resistance; FL = flexible linker; LPH = murine mAB24 heavy chain-derived signal peptide; KDEL= endoplasmic reticulum retention signal.

To generate a plasmid encoding HIV-1 gp140 with Zera® tag on its 5' end, the sequence coding for Zera® was inserted into plasmid pEAQ-HT: SU gp140 using BshTI and Kpn2I restriction enzymes to form pEAQ-HT: Zera®-gp140 (Figure 2.2).

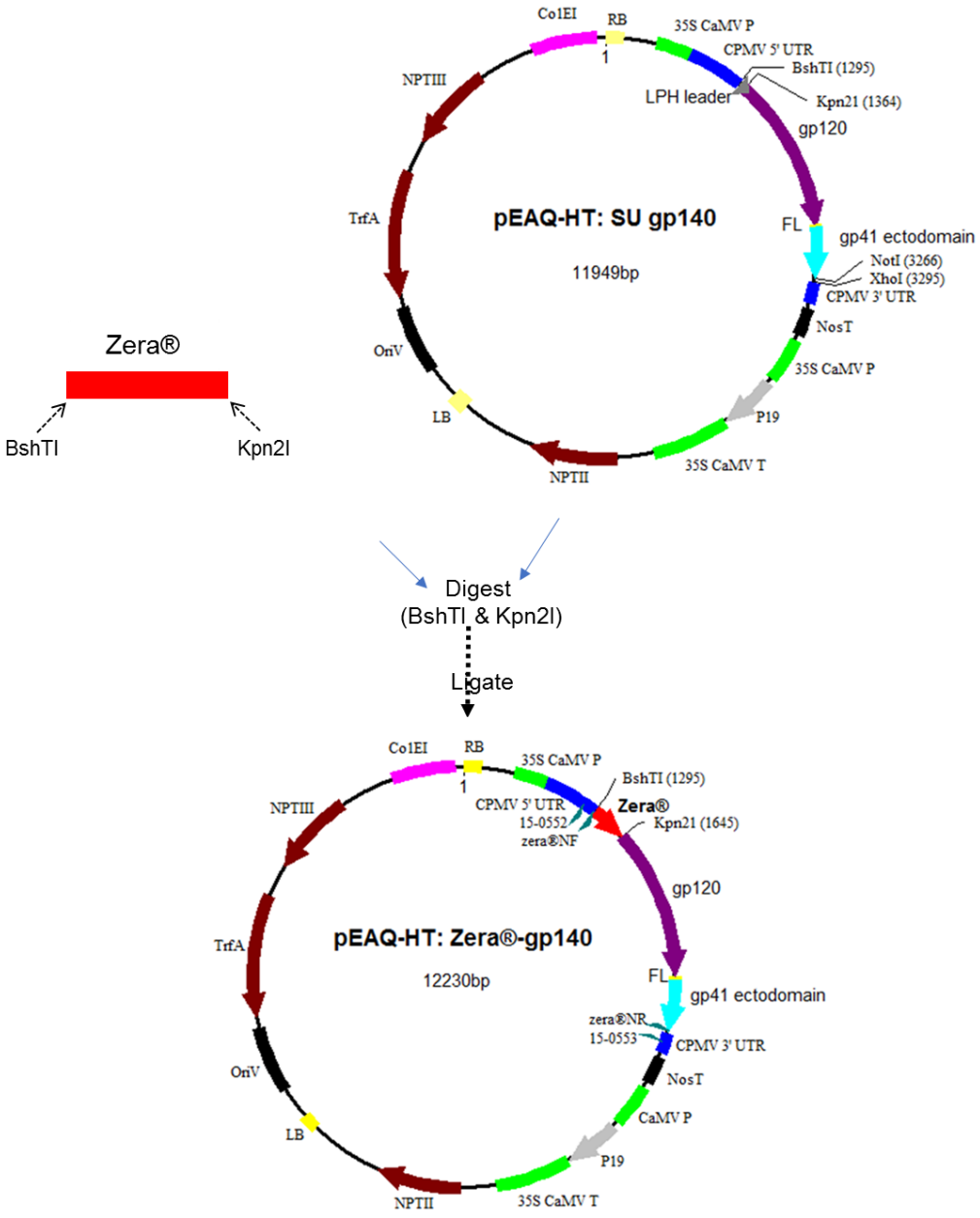

Figure 2.2: Annotated plasmid maps showing the construction of a plant vector encoding Zera®-gp140. pEAQ-HT contained: 35S CaMV P = promoter from cauliflower mosaic virus; RB = right; LB = left border; UTR = untranslated region from modified cowpea mosaic virus (CPMV); LPH = murine mAB24 heavy chain-derived signal peptide; P19 = suppressor of gene silencing; 35S CaMV P and 35S CaMV T= promoter and terminator from Cauliflower mosaic virus; NosT: nopaline synthase terminator; OriV = *R. radiobacter* origin of replication; CoIEI: *E. coli* origin of replication; NPTIII: neomycin

phosphotransferase conferring the kanamycin resistance; and TrfA =: replication essential locus.

2.2.3 Transformation of electrocompetent *Rhizobium radiobacter* AGL1 cells

R. radiobacter (formerly called *Agrobacterium tumefaciens*) AGL cells (ATCC BAA-101) were made electrocompetent using a method described by Shen and Forde (1989). In 0.1 cm electroporation cuvettes (Molecular Bioproducts), 100µl aliquots of these cells were mixed with 400ng of pEAQ-HT: gp140-Zera® or pEAQ-HT: Zera®-gp140 and electroporated according to a method described by Maclean *et al.* (2007). Recombinant *R. radiobacter* were selected by plating on Luria-Bertani (LB) agar plates containing 50µg/ml carbenicillin (Sigma-Aldrich) and 30 µg/ml kanamycin (Sigma-Aldrich). Recombinants were verified by colony PCR using pEAQ-HT-specific primers (15-0552: 5' TTCTTCTTCTTGCTGATTGG 3' and 15-0553: 5' CACAGAAAACCGCTCACC 3') in the presence of the ImmoMix™ Red (Bioline), or OneTaq® 2X Master Mix (Bioline) used according to manufacturer's instructions. The recombinants were propagated in LB broth and stored at -80°C in 1ml aliquots as 25% glycerol stocks.

2.2.4 Transient infiltration of *N. benthamiana* with recombinant *R. radiobacter*

Glycerol stocks of recombinant *R. radiobacter* were added to 10ml LB broth supplemented with 50µg/ml carbenicillin and 30µg/ml kanamycin and incubated at 27°C overnight with shaking. These starter cultures were sequentially expanded in 100ml LB supplemented with appropriate antibiotics and incubated at 27°C overnight with shaking. Before infiltration, cultures were expanded in 1L of LB supplemented with the appropriate antibiotics and 20µM acetosyringone (Sigma-Aldrich) to increase transformation efficiency by activating the virulence (*vir*) gene which enhances the transfer of T-DNA into plants. On the day of infiltration, cultures were adjusted to an OD_{600} of 1 in fresh resuspension medium (10mM MES, 1M $MgCl_2$, pH to 5.6; supplemented with 200µm acetosyringone). Six-week-old *N. benthamiana* plants were placed upside down on the desiccator plate, submerged in a beaker containing the infiltration culture, and placed inside a vacuum chamber. The chamber was tightly closed, and the vacuum was allowed to reach -80 kilopascal, then brought back to 0 kilopascals. Three rounds of vacuum infiltration were applied to ensure complete infiltration of all the leaves. The infiltrated plants were cultivated further at 24°C with a 12h: 8h light: dark cycle until the biomass was harvested.

2.2.5 Small scale extraction of protein from leaves infiltrated with recombinant *R. radiobacter*

On the day of biomass harvest after infiltration, six-leaf clippings (1 leaf per plant, 2 clippings per leaf) were collected per construct using the lid and the brim of an Eppendorf tube. The

collected clippings were crushed into powder in liquid nitrogen using a mortar and pestle, and equivalent amounts were resuspended in 300µl of four different buffers: 1x PBS, pH7.2 (Gibco™) or Zera® buffer PBP3 (100 mM Tris pH8, 50 mM KCl, 6 mM $MgCl_2$, 10 mM EDTA, 0.4 M NaCl) or PBP3 supplemented with 5% Triton X-100 or reducing buffer (100 mM Tris-HCl buffer, pH 7.5, containing 100 mM NaCl, 0.5% SDS, and 200mM DTT). All buffers were supplemented with a 1x cOmplete™ EDTA-free protease inhibitor (Roche). The resultant plant slurries were incubated for 1 hour with shaking at 4°C and then centrifuged at 15 300 x *g* for 15 minutes. The supernatants and pellets were kept at -20°C until ready for analysis. Supernatants were combined with sample loading buffer [(4x SAB):4ml of 100% glycerol, 1.6ml of 1.5M Tris-HCl pH 6.8, 0.8g SDS, 4mg bromophenol blue, 0.5ml 2-beta mercaptoethanol and 3.9ml dH_2O] (adjusted to 1x final concentration), and the pellets were resuspended in 150µl of 1x SAB. These samples were boiled for 10min, and equal volumes were analysed on an 8% reducing SDS-polyacrylamide gel (Appendix A, Section 2.1 and transferred for western blotting (Appendix A, Section 2.2).

2.2.6 Whole-mount immunofluorescence staining of *N. benthamiana* leaves

Immunofluorescence staining of plant-produced Env was achieved using a method adapted from Pasternak *et al.* (2015). Instead of manual sectioning of plant tissues, this is a simple method where the whole-mount tissue is treated to allow for intracellular immunostaining using antibodies targeted to the protein of interest. Plants were infiltrated with recombinant *R. radiobacter,* as described in Section 2.2.4. Five days post-infiltration, leaf discs were harvested as described in Section 2.2.5. The cellular components of the leaves were fixed by incubating the leaf discs in 1.5ml of 100% methanol for 20 minutes at 37°C. Methanol was replaced with another 0.8ml of 100% methanol, and leaf discs were further incubated at 60°C for 3 minutes. Water was added gradually until ~20% methanol concentration was reached (i.e., 3.2 ml water). After 2x washes with water, tweezers were used to carefully transfer each leaf disc into a well of a Nunc™ Lab-Tek® 8-well Chamber Slide™ (ThermoFisher) containing 500µl water. In all cases, leaf discs were kept as flat and unfolded as possible. Cell walls were partially digested at 37°C for 40 minutes by incubation with 0.2% driselase (Sigma-Aldrich) diluted in PBS. Following 4x washes with microtubule-stabilising buffer (MTSB: 100mM PIPES, 10mM EDTA instead of EGTA, 2mM $MgSO_4.7H_2O$, dissolved by the addition of 3M NaOH to pH 6.8), leaf discs were incubated at 37°C for 20 minutes with 500µl of the membrane permeabilisation buffer [3% IGEPAL® (Sigma-Aldrich), 10% DMSO (Sigma-Aldrich) in MTSB]. Following 4x washes with MTSB, leaf discs were blocked with 2% BSA-MTSB for 1 hour at RT. Leaf disks were stained overnight at room temperature with goat anti-HIV-1 gp120 in 2% BSA-PBS. Following washes with PBS, leaf discs were incubated in the dark for 1.5 hours with 1:500 donkey anti-goat-Alexa488 secondary antibody diluted in 2% BSA-PBS. Following

washes in PBS, leaf disks were incubated for 10min with 1:5000 Hoechst nuclei stain diluted in PBS. The plant tissues were transferred onto glass slides and imaged with a confocal microscope (Carl Zeiss 880 LSM confocal with Fast Airyscan technology and the Elyra S1 super-resolution microscope).

2.2.7 Partial purification of Zera®-gp140 from infiltrated leaves

Twenty-six *N. benthamiana* plants were infiltrated with recombinant *R. radiobacter* cells encoding pEAQ-HT: Zera®-gp140 at an OD_{600} of 1. Leaves were harvested (113 g) at 5 days post-infiltration (dpi). Leaves were homogenised with a Waring-type blender at 1:3.5 plant tissue to PBP3 buffer (w/v) supplemented with 10% sucrose and 1x cOmplete™ EDTA-free protease inhibitor. The plant homogenates were incubated at 4°C for 1 hour with gentle agitation and clarified through four layers of Miracloth (Merck). Plant homogenates were further clarified by centrifugation at 1500 x *g* for 10 min at 4°C. The clarified homogenates were underlaid with 5ml of 30% sucrose in PBP3 buffer followed by ultracentrifugation (SW 32 Ti rotor at 79 000 x *g* for 2 hrs at 4°C). The protein pellet from each tube was resuspended in a final volume of 3.5ml PBP3, and the resuspension was filtered through 1 layer of Miracloth to remove co-pelleted large plant debris. The volume of the clarified sample was adjusted accordingly and loaded on a 10-50% (30ml) OptiPrep™ continuous gradient prepared in 38ml Ultra-Clear™ centrifuge tubes (Beckman Coulter) using a dual pump gradient maker (TRIS™, ISCO, Lincoln, USA). Gradients were separated by isopycnic ultracentrifugation (SW32Ti, 175000 x *g*, 16 hours, 4°C). Following ultracentrifugation, gradients were manually fractionated by punching a hole in the bottom of the tube and slowly collecting 1ml fractions. Fractions were analysed on a western blot probed with an antibody to Env.

2.3 Results

2.3.1 Confirmation of recombinant vectors encoding gp140-Zera® and Zera®-gp140

Previous studies from the literature indicated that Zera® PBs could be induced in various expression hosts (Torrent *et al.* 2009a; Whitehead *et al.* 2014; Mbewana *et al.* 2015). We first evaluated the expression and induction of Zera®-induced gp140 PBs in plants. Plant expression vectors containing gp140-Zera® (pEAQ-HT: gp140-Zera®) and Zera®-gp140 (pEAQ-HT: Zera®-gp140) gene fusions were constructed using the pEAQ-HT plasmid. The pEAQ-HT: gp140-Zera® contained the LPH leader sequence, which was not present in the pEAQ-HT: Zera®-gp140 plasmid. The integrity of pEAQ-HT: gp140-Zera® and pEAQ-HT: Zera®-gp140 was confirmed by restriction enzyme mapping (Figure 2.3 A & B) and sequencing.

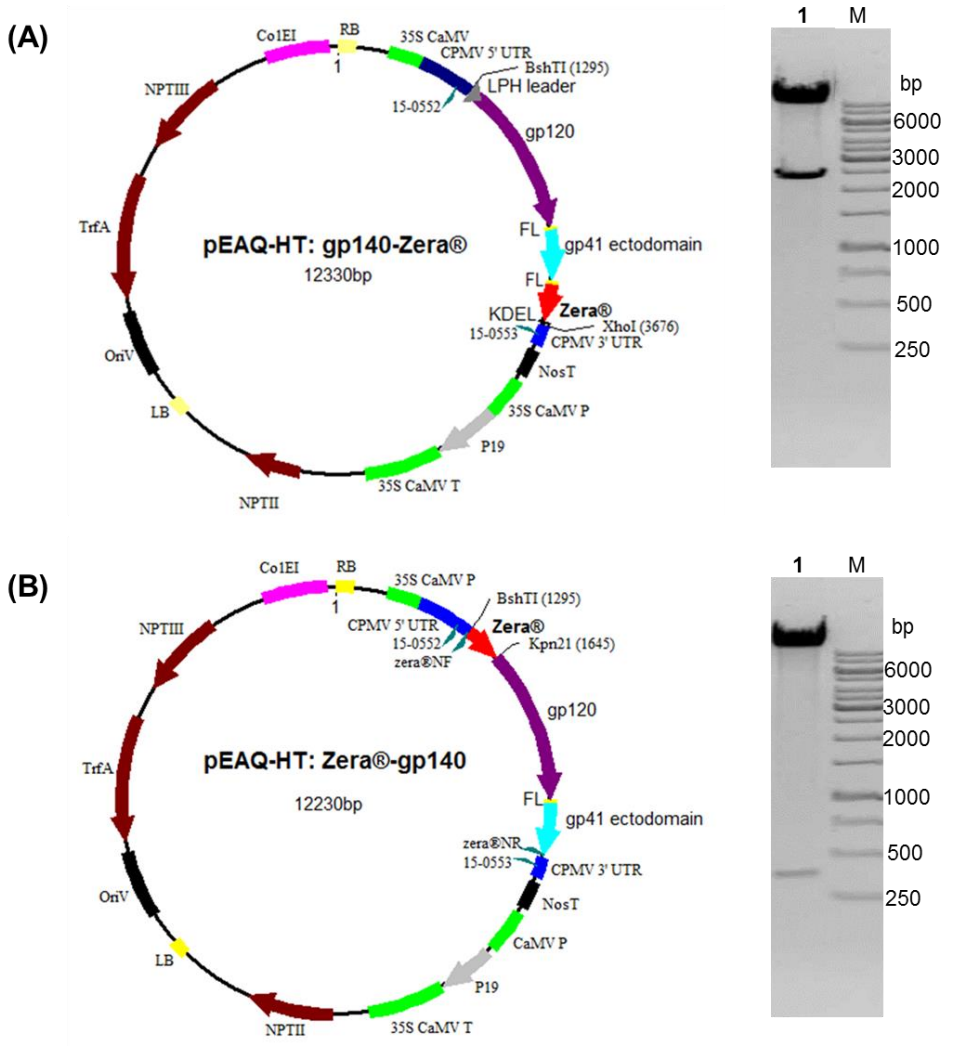

Figure 2.3: Confirmation of the integrity of plant expression vectors encoding gp140-Zera® and Zera®-gp140. (A) Plasmid map of pEAQ-HT: gp140-Zera® and restriction analysis using BshTI and XhoI. **(B)** Plasmid map of pEAQ-HT: Zera®-gp140 and restriction analysis using BshTI and Kpn21**.**

2.3.2 Confirmation of the transformation of gp140-Zera® or Zera®-gp140 encoding plasmids into *R. radiobacter* AGL1 cells

Following the transformation of plasmids into competent *R. radiobacter* AGL1 cells, putative transformants were verified by a colony PCR using pEAQ-HT-specific primers (15-0552 and 15-0553), which bind on either side of the multiple cloning site. *E. coli* recombinants containing pEAQ-HT: gp140-Zera® and pEAQ-HT: Zera®-gp140 were used as positive controls. Colony PCR of *R. radiobacter* cells transformed with pEAQ-HT: gp140-Zera® and pEAQ-HT: Zera®-gp140 indicated that 3/4 and 2/4 respectively of the colonies screened contained the pEAQ-HT plasmid with correct sized inserts (Figure 2.4).

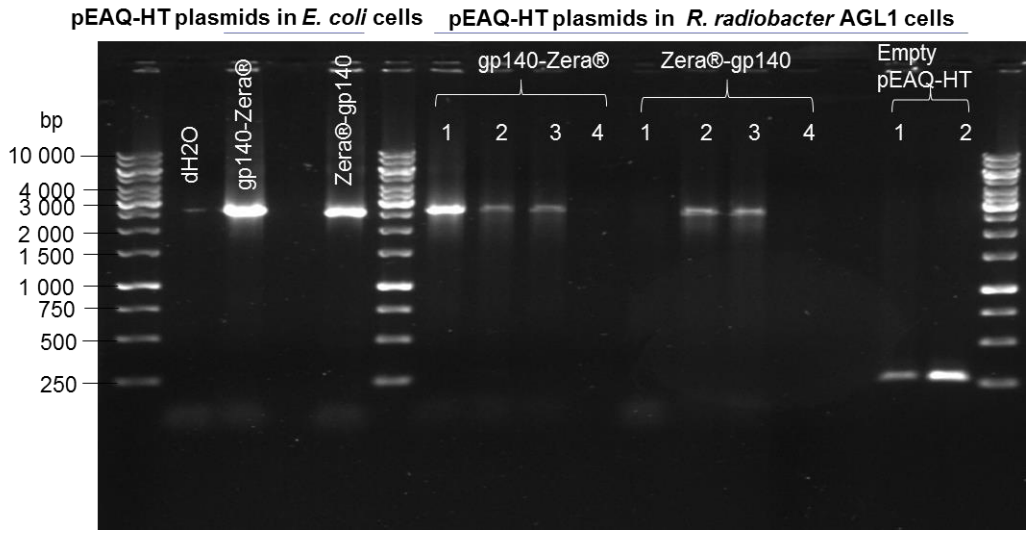

Figure 2.4: Confirmation of the transformation of plant expression vectors into *E. coli* and *R. radiobacter* AGL1 competent cells. Colony PCR using the pEAQ-HT-specific 15-0552 and 15-0553 primers was used to confirm the presence of pEAQ-HT plasmids encoding gp140-Zera® or Zera®-gp140 in *E. coli* and *R. radiobacter* AGL1 cells.

2.3.3 Confirmation of expression of gp140-Zera® or Zera®-gp140 in a small-scale infiltration

The expression of Zera®-tagged gp140 proteins in plants was evaluated by vacuum infiltration of *N. benthamiana* leaves with recombinant *R. radiobacter* cells encoding gp140-Zera® and Zera®-gp140 at an OD of 1. Five- and three-days post infiltration, leaves were sampled and homogenised in the presence of PBP3 buffer. The homogenate was clarified into supernatant (S) and pellet (P) fractions and analysed on a western blot probed with an antibody to Env (Figure 2.5). Western blot analysis indicated that Zera®-gp140 (≈140 kDa band, indicated by an arrow) appeared to accumulate both in the pellet and supernatant. There were no qualitative differences in the accumulation of gp140 between samples harvested early (3 days) vs samples harvested late (5 days) based on protein band density. Surprisingly, there was no expression of gp140 in samples harvested from leaves infiltrated with *R. radiobacter* encoding gp140-Zera®. The expression of gp140 (expected ≈140 kDa band for gp140 positive control, also indicated by an arrow) was observed in both the pellet and the supernatant extracted 5 days post-infiltration. Higher molecular weight (>245 kDa) Env-specific proteins were detected in plants expressing gp140 and Zera®-gp140. These higher molecular weight Env-specific products were presumed to be aggregates that were not fully resolved by SDS-PAGE. As expected, no gp140 signal was detected in the homogenates derived from plants infiltrated with recombinant *R. radiobacter* that was transformed with the empty pEAQ-HT vector (indicated by the asterisks). It is important to note that the differences in gp140 expression were only assessed qualitatively (samples were treated the same, and the same volumes were loaded) by western blotting.

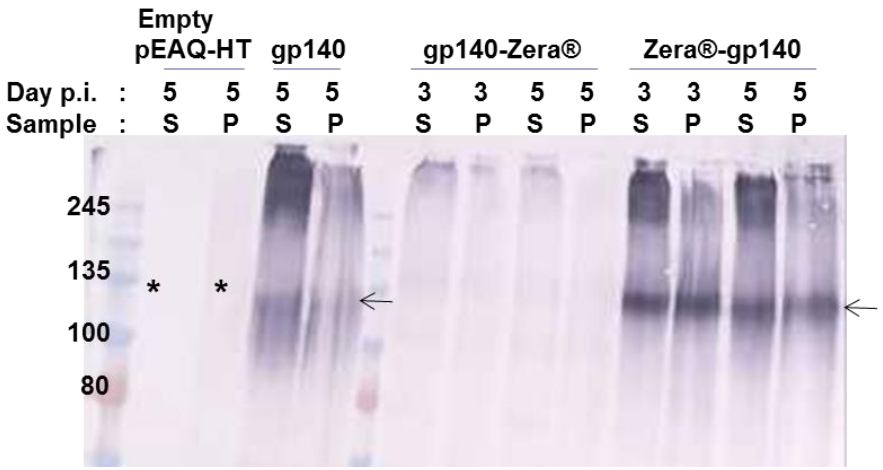

Figure 2.5 Transient expression of gp140 in plants infiltrated with recombinant *R. radiobacter* that had been transformed with pEAQ-HT encoding gp140, gp140-Zera® and Zera®-gp140. Recombinant cultures were adjusted to an OD_{600} of 1 and vacuum infiltrated into *N. benthamiana* leaves. Three- and five-days post infiltration (p.i.), leaf homogenates in PBS buffer were clarified into supernatant (S) and pellet (P) fractions, treated the same, and the same volumes were analysed on a western blot probed with an antibody to Env (arrows indicate the expected 140 kDa Env band). Negative control samples were extracted from leaves infiltrated with recombinant *R. radiobacter* AGL1 cells that had been transformed with an empty pEAQ-HT vector (asterisks).

Since the time point at which protein is harvested post-infiltration, as well as the buffer used for protein extraction, can influence protein recovery, the small-scale infiltrations were repeated to compare extraction of Zera®-gp140 and gp140-Zera® using four different buffers at 3 and 5 dpi. In addition to a routinely used PBP3 buffer for extraction of Zera®-tagged proteins, Tris-HCl buffer supplemented with SDS and DTT or β-mercaptoethanol was tested as it has been used successfully by others for recovery of Zera®-tagged antigens (Alvarez *et al.* 2010; Llop-Tous *et al.* 2010; Whitehead *et al.* 2014). Extraction was also done with PBS as it has been used in our lab to efficiently recover Env from plant tissues (Margolin *et al.* 2019).

Protein samples harvested using different buffers over a 5-day experiment were analysed on a western blot probed with an antibody to Env (Figure 2.6). Zera®-gp140 was predominantly detected in the plant pellet (P) regardless of the buffer used for protein extraction (Figure 2.6 A). Expression of Zera®-gp140 peaked at 5 days post-infiltration, and better protein extraction was achieved using the PBP3 buffer as suggested by the darker intensity of the ≈140kDa band. As seen in Figure 2.5, the higher molecular weight Env-specific products were observed, and presumed to be aggregates that were not fully resolved by SDS-PAGE. The addition of Triton-X100 did not improve the yields of Zera®-gp140. Poor extraction of Zera®-gp140 was observed when Tris-HCl buffer supplemented with DTT and SDS was used instead of PBP3. Regardless of the buffer used for extraction and the time point at which samples were harvested, no expression of gp140-Zera® was observed (Figure 2.6 B). These results indicated that the expression of Zera®-tagged gp140 in plants worked when the Zera®

sequence was fused to the N-terminus of gp140 (Zera®-gp140) than to the C-terminus (gp140-Zera®). Since PBP3 buffer is mostly used for the isolation of Zera® PBs in the literature and does not contain any denaturing detergents which could potentially solubilise PBs, for all subsequent extractions, this buffer was used for protein extraction at 5-days post-infiltration. Due to no expression of gp140-Zera® in plants, Zera®-gp140 was used for all further optimisations.

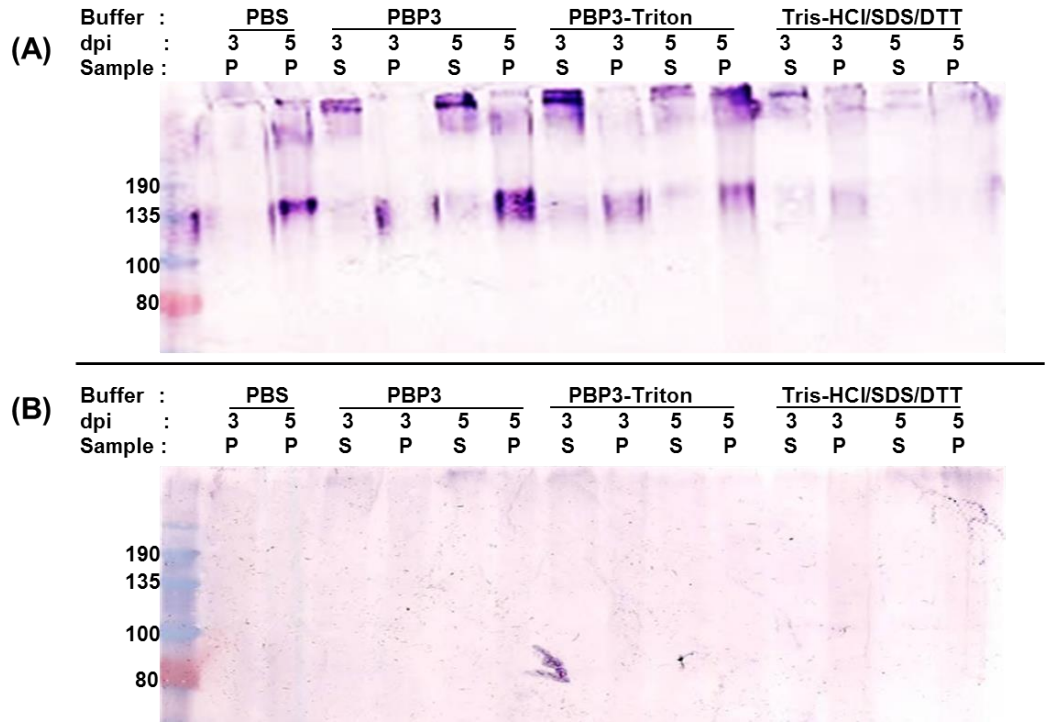

Figure 2.6: Transient expression of g140-Zera® and Zera®-gp140 in plants. Cultures of recombinant *R. radiobacte*r AGL1 cells encoding Zera®-gp140 **(A)** and gp140-Zera® **(B)** were vacuum-infiltrated into *N. benthamiana* leaves. Three- and five-days post infiltration (dpi), leaves were homogenised with different buffers and clarified into protein supernatants (S) and pellets (P) followed by analysis on an anti-Env western blot.

The physical appearance of infiltrated plants was monitored throughout expression to evaluate any pathological effect associated with recombinant protein expression (Figure 2.7). In comparison to the image taken just after infiltration, chlorosis of the apical leaves of all plants was generally observed 3 days (images not shown) post-infiltration. Five days post-infiltration, the pathology of plants expressing Zera®-gp140 progressed from chlorosis to necrosis. However, the apical leaves of plants expressing gp140-Zera® or an empty pEAQ-HT vector remained chlorotic. The pathology observed in plants expressing Zera®-gp140 corresponded with an increase in protein accumulation while the failure of plants expressing gp140-Zera® to progress into necrosis tied in with no Env expression as shown in western blots (Figure 2.6). These observations indicated that the observed pathology in plants was in response to expression of Zera®-gp140 and not as a result of infiltration with *R. radiobacter* since no

obvious pathology was evident in plants infiltrated with an empty *R. radiobacter* (pEAQ-HT) control.

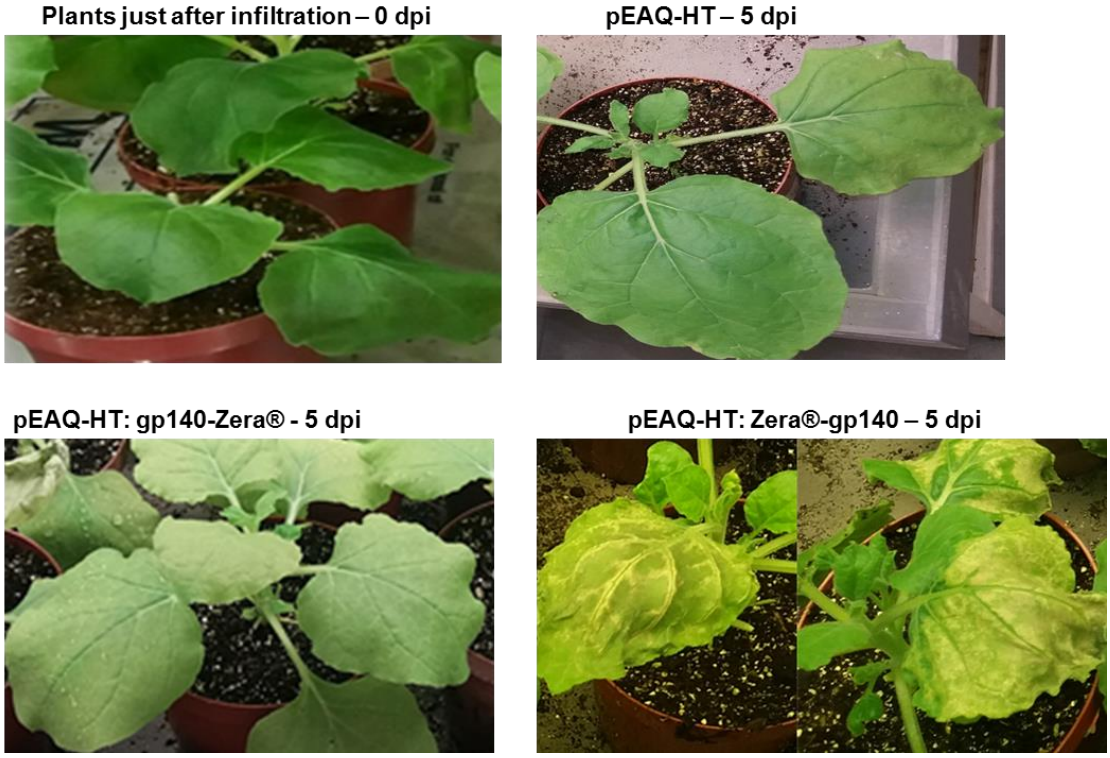

Figure 2.7 Phenotype of representative leaves (0 and 5 days post infiltration (dpi)) showing the pathological effects of expression of gp140-Zera® or Zera®-gp140.

2.3.4 Whole-mount immunofluorescent staining of the protoplasts expressing gp140 and Zera®-gp140

Immunofluorescent staining of protoplasts from infiltrated leaves was conducted to detect Zera®-gp140 PBs. The formation of gp140-Zera® PBs was not evaluated by immunofluorescent staining because no protein expression was observed in western blot analysis (Figure 2.5 and 2.6). Five days post-infiltration, protoplasts from infiltrated leaves were stained with an antibody to HIV-1 Env, detected with an Alexa-488-labelled secondary antibody and imaged with a confocal microscope (Figure 2.8). Protoplasts from un-infiltrated leaf clippings were included as a negative control. Interestingly, small PB-like fluorescent structures lining the edges of epidermal cells (epidermal cells are indicated by white arrows) were observed in the protoplast prepared from leaves expressing Zera®-gp140 (see on the zoom-in image). However, instead of PB-like structures, gp140 appeared as a diffused fluorescence in the cytoplasm or apoplastic space of epidermal cells. Notably, epidermal cells assumed a typical jigsaw puzzle pattern expected for *N. benthamiana* leaves.

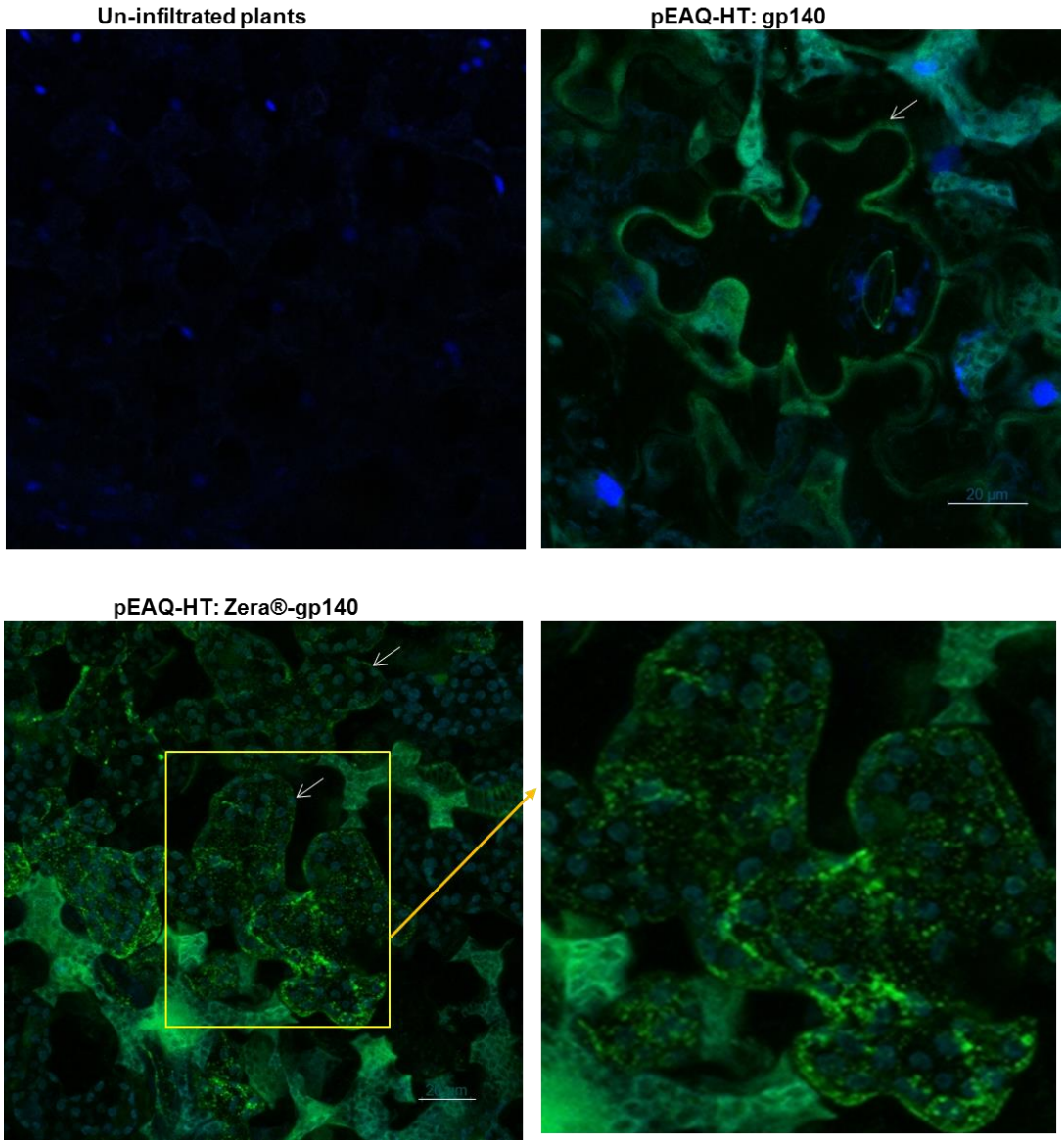

Figure 2.8: Immunofluorescent staining of Zera®-gp140 produced in plants. Protoplasts from un-infiltrated leaf clippings, or leaves expressing gp140 or leaves expressing Zera®-gp140, were prepared. Protoplasts expressing gp140 and Zera®-gp140 were then probed with an antibody to Env and anti-Alexa 488-labelled secondary antibody before imaging with a confocal microscope. The inset (yellow rectangle) is an enlargement (indicated by a yellow arrow) of typical spherical, PB-like structures in leaves expressing Zera®-gp140. Nuclei were detected with a Hoechst stain (blue), and white arrows indicate the epidermal cells. Scale bars represent 20µM.

2.3.5 Scale-up and purification of Zera®-gp140 from plants

Extracts from leaves infiltrated with Zera®-gp140 were subjected to different centrifugation methods in an attempt to purify PBs. It is important to note that in theory, if Zera®-tagged gp140 passes through a gradient and is pelleted following rate zonal ultracentrifugation, it would suggest that PBs were formed, whereas if Zera®-tagged gp140 remained in the gradient supernatant, that would indicate that gp140 was soluble and not encapsulated in PBs. Five days post-infiltration, leaf homogenate (116g) was clarified by filtration through Miracloth

followed by low-speed centrifugation. The clarified supernatant was passed through a 30% sucrose cushion using ultracentrifugation. Collected fractions were analysed on a western blot probed with an antibody to Env (Figure 2.9). After ultracentrifugation, Zera®-gp140 was mainly concentrated in the protein pellet compared to the supernatant (Figure 2.9 A). The presence of a Zera® tag in the final protein pellet was confirmed by detection of an expected ≈140kDa protein band on a western blot probed with Zera®-specific antiserum (Figure 2.9 B). The final protein pellet was very green and contained big lumps of plant debris (Figure 2.9 C), and this resulted in poor resolution of the Zera®-gp140 on the western blot. The poor quality of the sample after centrifugation through a sucrose cushion suggested that cushion-based ultracentrifugation could only be used for concentrating the homogenates containing Zera®-gp140, but not as a sole purification method.

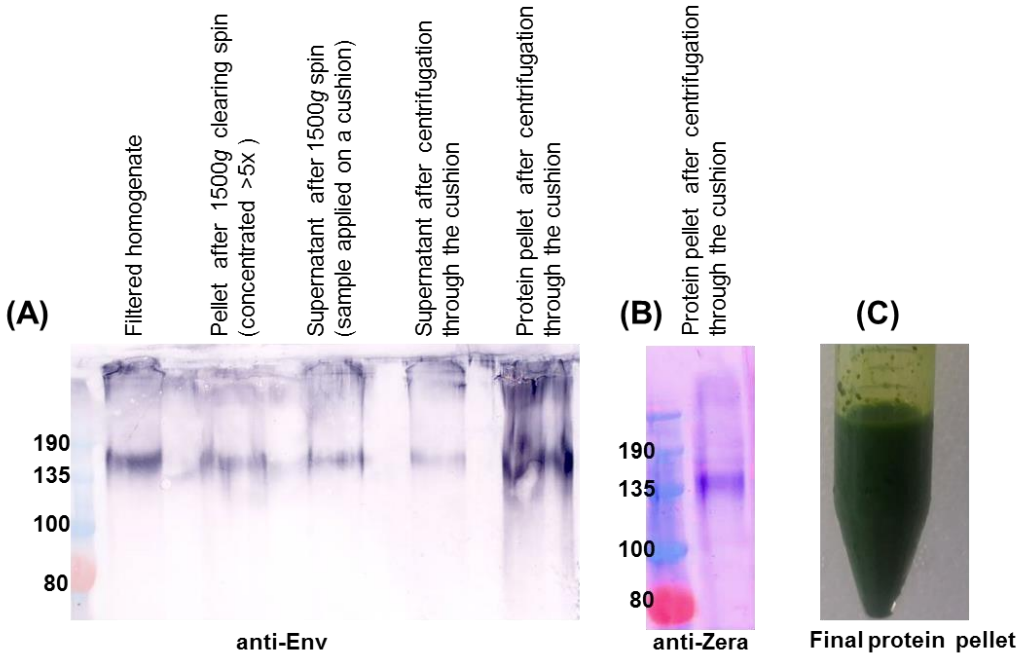

Figure 2.9: Concentration of homogenates from *N. benthamiana* leaves expressing Zera®-gp140. Plant homogenates were clarified by filtration through Miracloth and low-speed centrifugation. The clarified homogenate was passed through a 30% sucrose cushion by ultracentrifugation. The final protein pellet was resuspended in PBS. Sampled fractions were analysed on a western blot probed with anti-Env **(A)** or anti-Zera® **(B)** antibodies. **(C)** The appearance of the final protein pellet is presented.

To further optimise the purification of Zera®-gp140 from plants, Zera®-gp140 concentrated in Figure 2.9 was subsequently fractionated through a 10-50% continuous OptiPrep™ gradient by isopycnic ultracentrifugation. Following isopycnic ultracentrifugation, the OptiPrep™ gradient resulted in separation into different phases (Figure 2.10 A). These included a transparent layer at the bottom of the tube, a cloudy layer, a very green layer containing visible plant debris, as well as a light green layer without plant granules. Gradients were manually fractionated by punching a hole in the bottom of the tube and slowly collecting 1ml fractions.

These fractions were analysed on a western blot probed with an antibody to Env (Figure 2.10 B). Zera®-gp140 was predominantly detected in fractions (#18-25). However, it was noted that Zera®-gp140 was still co-sedimenting with a lot of plant debris, suggesting that additional clarifying steps should be carried out on the fractions in an effort to minimise the inclusion of insoluble plant protein contaminants in the pellet after ultracentrifugation.

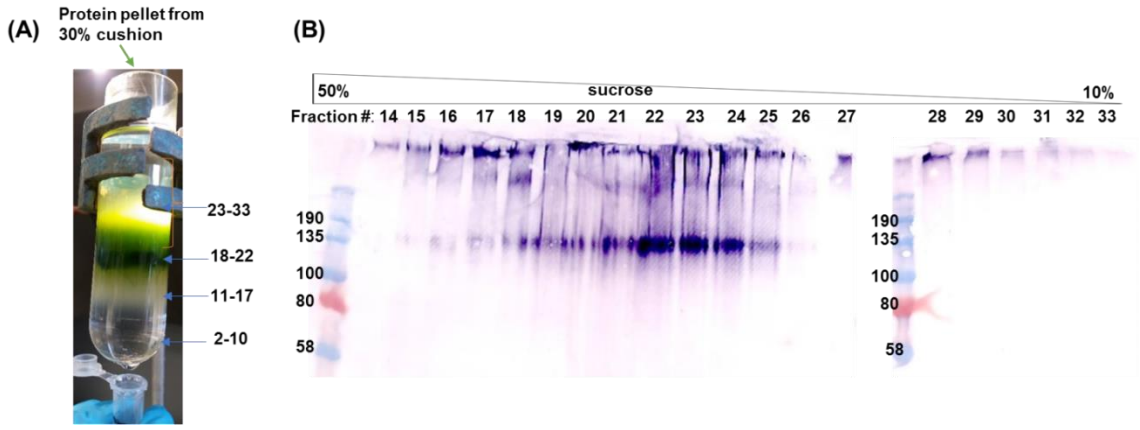

Figure 2.10: Isopycnic ultracentrifugation of plant homogenate containing Zera®-gp140. (A) Zera®-gp140 (concentrated through a 30% sucrose cushion) was fractionated through a 10-50% continuous OptiPrep™ gradient by isopycnic ultracentrifugation. **(B)** Fractions were analysed on western blots probed with antibodies to Env.

Several approaches were carried out to minimise molecular interactions between the protein of interest and the insoluble plant material. The first approach included pooling Env-containing fractions after ultracentrifugation and filtering the pooled sample through the Miracloth to separate the plant debris from Env. This approach was unsuccessful because the small volume of protein sample was absorbed by the Miracloth, thus requiring additional buffer to elute the sample, which increased the chances of sample contamination.

The second approach was to carry out more extreme pre-treatment conditions with the hope of separating native plant proteins from recombinant Env proteins more effectively. These pre-treatment conditions included lowering the pH and increasing the temperature of homogenised plant extracts. These pH/heat shifts, i.e., the adjustment of the plant extract pH from 6 to 4, followed by heating at 42°C, was adapted from (D'Aoust *et al*. 2008). Following filtration through three layers of Miracloth, the homogenate was split equally and subjected to 1) no pH/heat shift, 2) pH 5.5 and heating at 42°C, and 3) pH 4 and heating at 42°C. Precipitation of plant debris during pH and heat treatment was monitored. When compared to the untreated sample, no discernible precipitation of plant debris was observed at pH values between 6 and 5.5. However, the precipitation of plant debris was visibly apparent at pH 4. Processed homogenates were then clarified by low-speed centrifugation, and the resultant supernatants were concentrated through a 30% sucrose cushion. Collected fractions during this procedure

were analysed on a western blot probed with an antibody to Env (Figure 2.11). Low levels of Env were detected in the initial filtered homogenate, and no Env loss was observed after the initial clarification by centrifugation. When comparing the bands' intensities corresponding to Zera®-gp140 in the final protein pellets after ultracentrifugation, the recovery of Zera®-gp140 from the homogenates subjected to pH adjustments and heating was reduced compared to that of the untreated sample. As much as the pH/heat shift treatment was able to precipitate plant debris, however, protein losses and the effect of pH/heat treatment on gp140 trimers or PBs were major concerns for this approach. Thus, this approach was not pursued further.

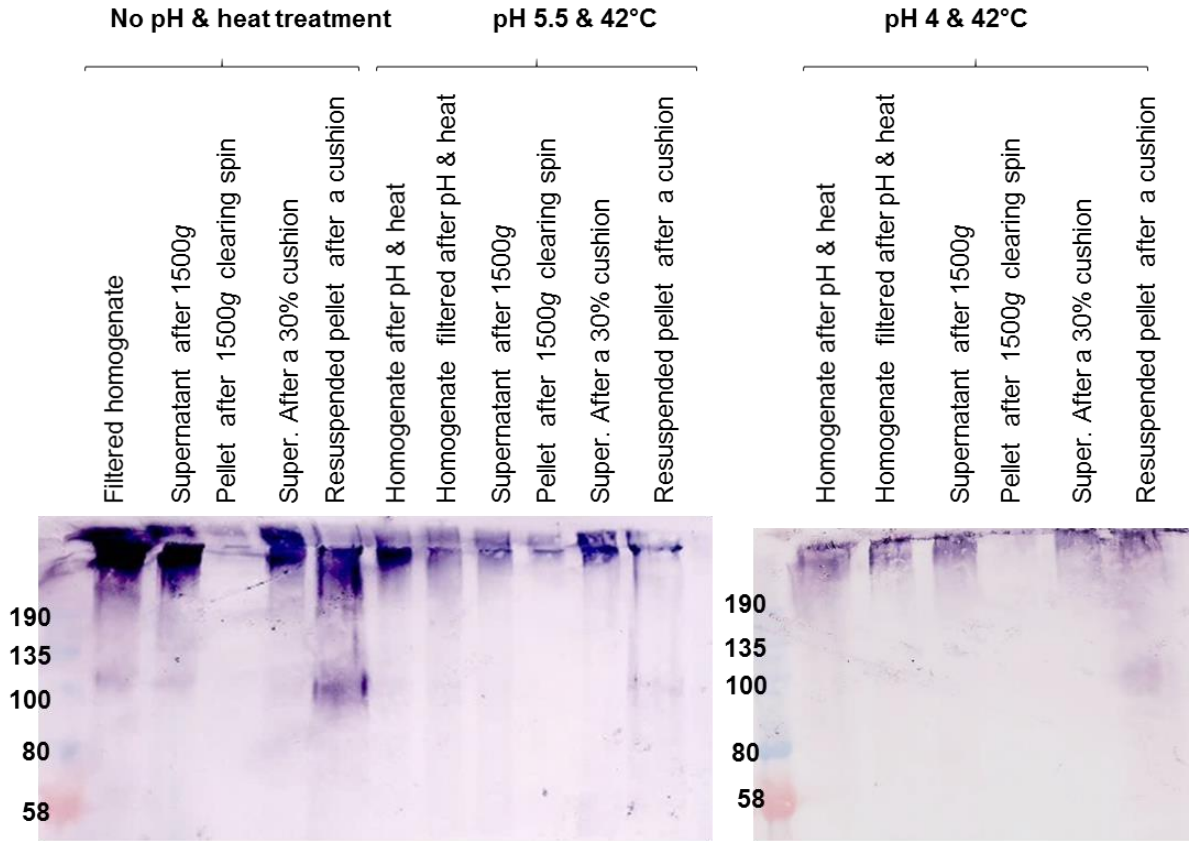

Figure 2.11: Pre-clarification by pH and heat adjustment of the plant homogenates containing Zera®-gp140 before concentration on a sucrose cushion. Filtered plant homogenates were subjected to pH & heat shifts before a low-speed clarification step and concentration through a 30% sucrose cushion. Samples were analysed on a western blot probed with an antibody to Env.

2.4 Discussion

We previously developed a scalable transient expression system for the production of the HIV-1 CAP256 gp140 (FL-stabilised) vaccine candidate in *Nicotiana benthamiana* plants (Margolin *et al.* 2019). This transient expression system involves cloning the expression cassette containing the Env gene into the pEAQ-HT expression vector, the transformation of the

plasmid into *Rhizobium radiobacter* AGL1 cells and vacuum infiltration of the resulting recombinant bacterium suspensions into *N. benthamiana* leaves.

Given the potential advantages associated with the nanoparticle presentation of subunit vaccines, in this study, we evaluated the feasibility of encapsulating Env in Zera®-induced protein bodies. We also evaluated the feasibility of using the relatively cheap, non-chromatographic purification techniques for the recovery of Zera®-tagged Env from the plant tissues.

We designed two Zera®-tagged gp140 constructs by fusing the sequence encoding Zera® to either the C- or N-terminus of HIV-1 CAP256 gp140 to generate gp140-Zera® or Zera®-gp140, respectively. While Zera®-gp140 yielded decent levels of Env expression in crude plant homogenates, the expression of gp140-Zera® (≈140 kDa) was not detected by western blot analysis. The immunofluorescent staining of protoplasts showed that in comparison to untagged gp140 that appeared as a diffused fluorescence in the apoplastic space of epidermal leaf cells, Zera®-gp140 appeared as small spherical structures. The spherical structures observed for Zera®-gp140 were smaller than ER-localised 1-2µm PBs previously reported for the plant-produced Zera®-ECFP (Torrent *et al.* 2009a; Llop-Tous *et al.* 2010) and Zera®-DsRed (Joseph *et al.* 2012; Hofbauer *et al.* 2014). The inability to induce larger PBs for Zera®-gp140 may be due to the complexity of and size extent of HIV Env that is hindering the optimal formation of Zera®-induced PBs. To our knowledge, the largest Zera®-fusion protein that has been shown to form protein bodies is the ±75 kDa influenza H5 (Hofbauer *et al.* 2016). It is possible that the fusion of the 140 kDa-sized Env is beyond the capability of protein body formation due to the hindrance of PB assembly by its large size.

Previous studies have shown that zein-derived domains induce the formation of electron-dense PBs that allow for simple protein recovery using rate zonal or isopycnic density ultracentrifugation (Torrent *et al.* 2009a; Mainieri *et al.* 2014). However, in this study, it was observed that both rate-zonal and isopycnic ultracentrifugation did not efficiently separate Zera®-gp140 from the plant debris. It is possible that the suboptimal subcellular fractionation of Zera®-gp140 from plant debris was not only due to the low concentration/numbers of gp140 PBs but might have also been due to an ongoing challenge in downstream processing or primary recovery of recombinant proteins from the plant homogenates (Nikolov & Woodard. 2004; Wilken & Nikolov. 2012; Buyel *et al.* 2015). The clarification of homogenates by heat/pH treatment was able to separate the plant debris by precipitation but at the expense of Env yields. Although this may be an appropriate clarification step, the treatment with heat or decrease in pH could potentially influence the functionality of Env immunogens as a result of these causing improper protein folding.

In conclusion, Zera®-gp140 was produced in plants and formed small PB-like structures, whereas gp140-Zera® was not expressed at all. The ultracentrifugation-based purifications of Zera®-gp140 from the plant homogenates were not optimal for the generation of immunogens at a good quality for assessing the immunogenicity of Zera®-tagged gp140 in animal models. Thus, in Chapter 3, the induction of PBs in mammalian cells was evaluated.

CHAPTER 3: CHARACTERISATION AND IMMUNOGENICITY OF MAMMALIAN-PRODUCED HIV-1 ENVELOPE GP140 ZERA®-TAGGED ANTIGENS

3.1 Introduction

Although the majority of zein/Zera®-tagged fusions have been produced in plants (Llop-Tous *et al.* 2010; Llop-Tous *et al.* 2011; Joseph *et al.* 2012; Hofbauer *et al.* 2014; Mainieri *et al.* 2014; Whitehead *et al.* 2014; Mbewana *et al.* 2015; Saberianfar *et al.* 2015; Hofbauer *et al.* 2016; Saberianfar *et al.* 2016; van Zyl *et al.* 2017), the successful induction of Zera-Ct (calcitonin), Zera-hGH (human growth hormone) and Zera-EGF (epidermal growth factor) PBs either in the human embryonic kidney (HEK293T) or Chinese hamster ovary (CHO) or monkey kidney (Cos1) cells serve as a proof of concept for induction of Zera®-tagged PBs in mammalian-based expression systems (Torrent *et al.* 2009a). In addition, even though the plant expression systems generally offer economical (infrastructure-wise) and scalability advantages over the mammalian expression systems, the post-translational machinery (including glycosylation, folding and proteolytic maturation) of mammalian cells are considerably more suitable than plants for the production of functional native-like glycoproteins, including HIV Env that derives its glycans from the expression host (Strasser *et al.* 2008; Margolin *et al.* 2018). In contrast to mammalian expression systems, the downstream processing of plant-produced proteins to remove plant debris or compounds before upstream purification steps remains a significant challenge for plant-produced vaccines (Buyel & Fischer. 2014; Chen & Davis. 2016).

In the previous Chapter, it was observed that gp140-Zera® was not expressed in plants. In addition, purification of Zera®-gp140 from contaminating proteins in plant homogenates using density gradient ultracentrifugation was difficult. As the plant-produced Zera®-tagged gp140 PBs could not be purified using ultracentrifugation, it was decided they were unsuitable for use as a vaccine in animals. The expression of Zera®-tagged gp140 PBs was therefore tested in mammalian cells. This Chapter reports their expression, characterisation and purification and subsequent use as immunogens in rabbits.

3.2 Material and methods

3.2.1 Construction of mammalian vectors encoding gp140-Zera® or gp120-Zera®

For expression of gp140 in mammalian cells, plasmid pMExT gp140-FL-IP as described (van Diepen *et al.* 2018) was used. The pMExT vector is derived from pTHpCapR backbone that contains a porcine circovirus type I (PCV-1) enhancer element (PcapR) that drives increased recombinant protein expression, upstream of a cytomegalovirus (CMV) promoter (Tanzer *et al.* 2011). To generate mammalian plasmids expressing HIV-1 CAP256 gp120 or gp140 with a C-terminal Zera® tag, the sequence coding for Zera® (ZIP Solutions, Spain) appended with a flexible-linker (FL) on its 5' end and the KDEL endoplasmic reticulum (ER) retention signal

on its 3' end was inserted between the BamHI and EcoRI sites of pMExT gp140-FL-IP to generate pMExT gp120-Zera® or between the NotI and EcoRI sites to generate pMExT gp140-Zera® (Figure 3.1). A plasmid expressing gp140-Zera® without the TPA leader and KDEL sequence was generated to evaluate how the absence of a signal peptide and the KDEL sequence influenced recombinant expression and induction of protein bodies. This plasmid was constructed by PCR amplification of gp140-Zera® using zera®CF (5' CGAAGCTTCCACCATGGGGCTGTGGGTCACTGTC 3', HindIII site underlined) and zera®CR1 (5' GAGAATTCTCATGTCTGACAAGGGCTTGG 3', EcoRI site underlined) primers. The PCR product was digested with HindIII and EcoRI and inserted into the pMEx vector to form pMEx gp140-Zera®ΔTK (Figure 3.1).

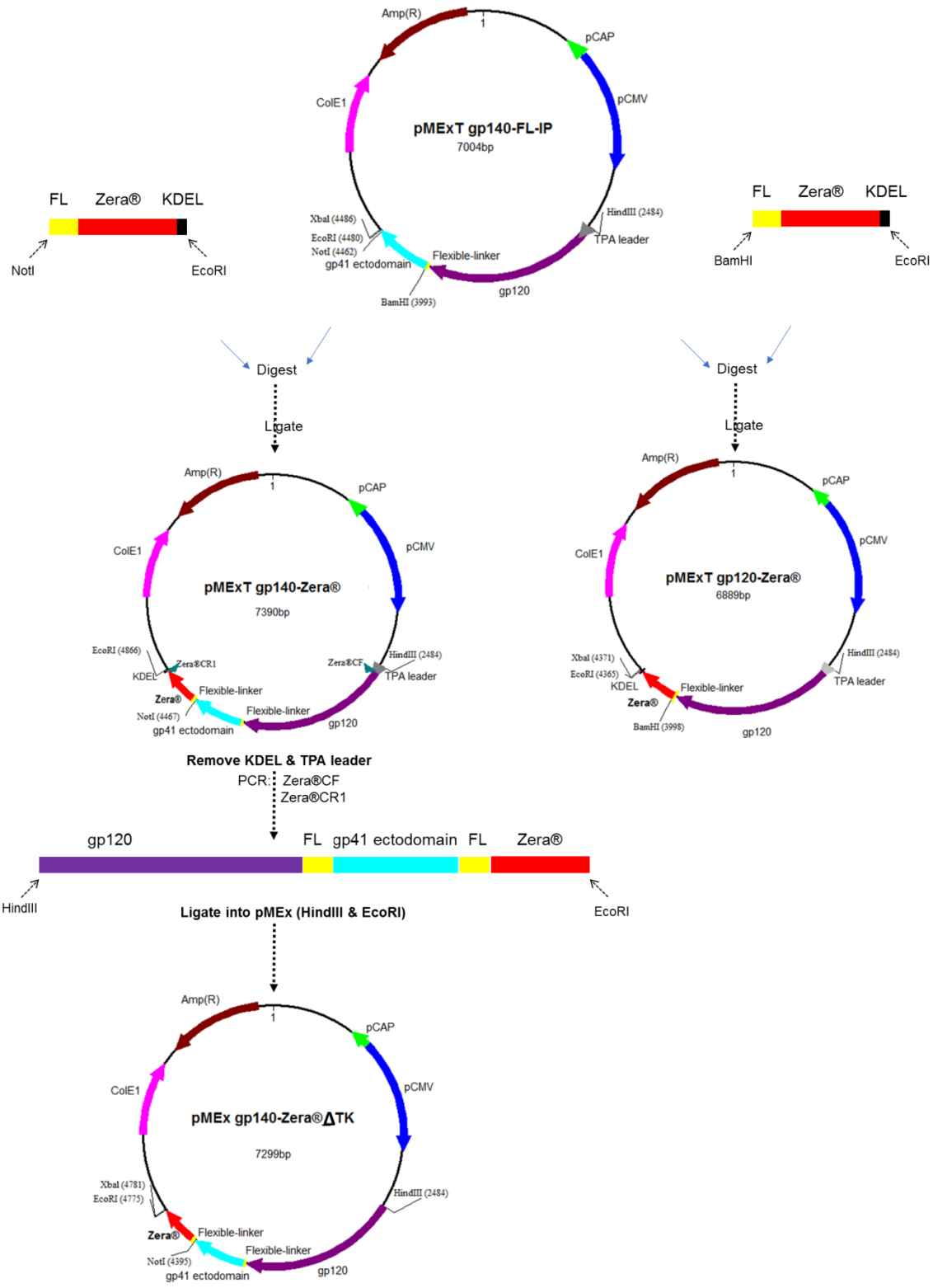

Figure 3.1: Annotated plasmid maps showing the construction of mammalian expression vectors that express gp120-Zera®, gp140-Zera® and gp140-Zera®ΔTK. pCAP = porcine circovirus enhancer element; pCMV = cytomegalovirus promoter; ColE1 = *E. coli* plasmid origin of replication; Amp(R) = ampicillin resistance; FL = flexible linker; TPA = human tissue plasminogen activator leader; KDEL = endoplasmic reticulum retention signal; ΔTK = TPA and KDEL sequences have been removed.

3.2.2 Construction of the mammalian vector encoding Zera®-gp140

pEAQ-HT: Zera®- gp140 plasmid DNA (generated in Section 2.2.2) was used as a template for PCR amplification of Zera®-gp140 using zera®NF (5' CGAAGCTTCCACCATGCGGGTGCTGC 3', HindIII site underlined) and zera®NR (5' ATGCGGCCGCATCCAGTGC 3', NotI site underlined) primers (Figure 3.2). The PCR fragment was subsequently digested with HindIII and NotI and inserted into pMExT, replacing the TPA leader to form pMEx Zera®- gp140, for expression in mammalian cells (Figure 3.2).

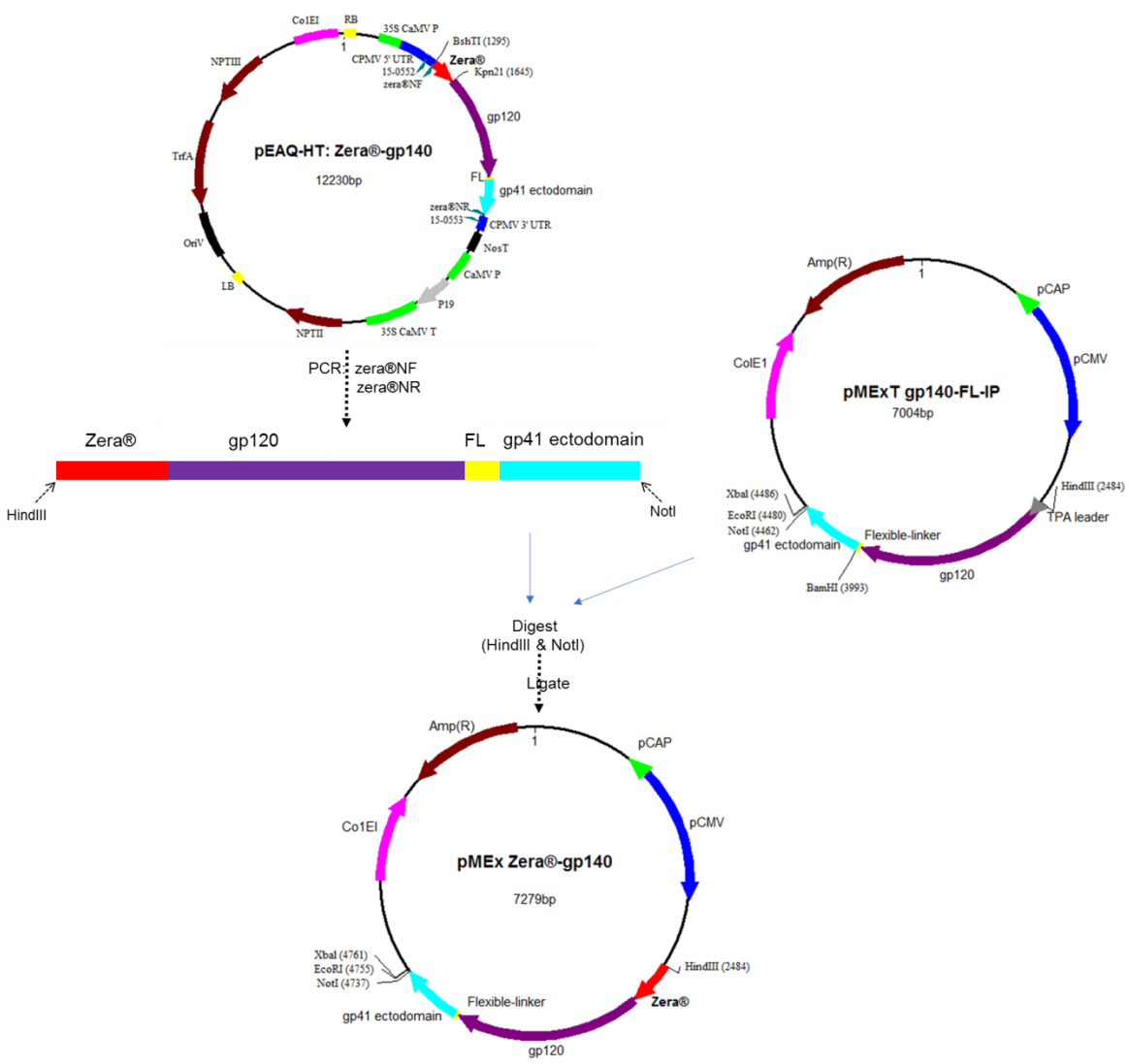

Figure 3.2: Annotated plasmid maps showing the construction of mammalian vector encoding Zera®-gp140. pMEx contained: pCAP = porcine circovirus enhancer element, pCMV = cytomegalovirus promoter, ColE1 = *E. coli* plasmid origin of replication, Amp(R) = ampicillin resistance, FL = flexible linker.

3.2.3 Construction of control mammalian vector encoding Zera®-eGFP

As a control, a plasmid that expresses Zera® fused to the 5' end of the enhanced green fluorescent protein (eGFP) was also constructed (Figure 3.3). pUC18 Zera®-eGFP was

digested with HindIII and EcoRI, and the resulting Zera®-eGFP fragment was inserted into plasmid pMExT to form pMEx Zera®-eGFP. It is important to note that all N-terminally tagged constructs, did not contain the TPA or KDEL sequences.

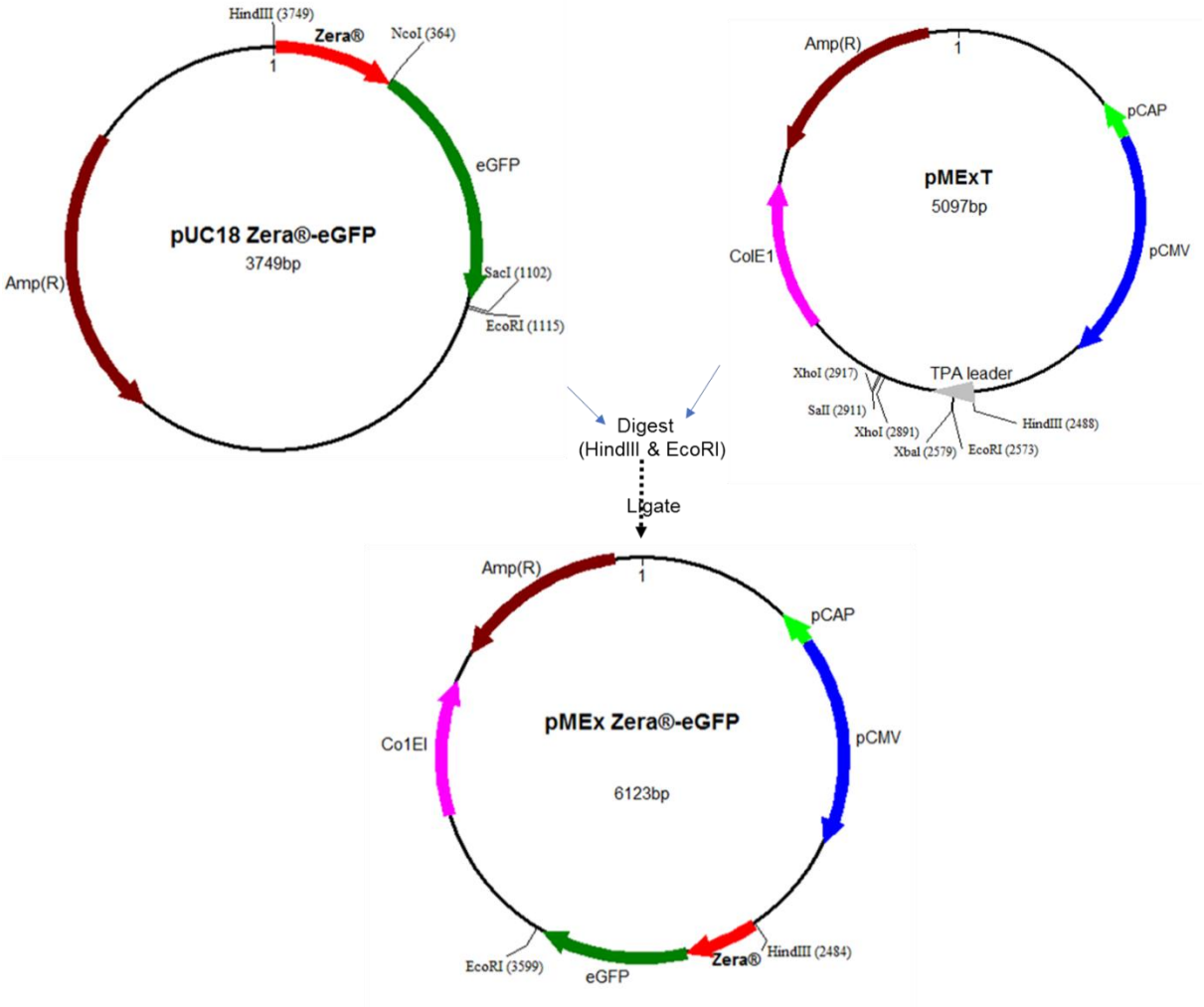

Figure 3.3: Annotated plasmid maps showing the construction of mammalian vector that expresses Zera®-eGFP. pCAP = porcine circovirus enhancer element, pCMV = cytomegalovirus promoter, ColE1 = *E. coli* plasmid origin of replication, Amp(R) = ampicillin resistance, TPA = human tissue plasminogen activator leader.

3.2.4 Seeding cells for transfections

For transient transfections of mammalian cells (refer to Appendix A, Section 3.1, for culturing and maintenance of cells), cells were seeded into 6 or 12 well plates for small-scale, T75 flasks for medium-scale and T175 flasks for large-scale transfections. Seeded cells were incubated at 37°C overnight. At 60-70% confluence, cells were transfected as per transfection reagent manufacturer's recommendations. Since the human embryonic kidney (HEK293T, ATCC® USA, CRL-3216^{TM}), and immortalised cancerous (HeLa, ATCC® USA, CCL-2^{TM}) cells are amenable to transfections using a wide range of transfection reagents, for this study, two different transfection reagents were used. These included a relatively cheap cationic polymer,

polyethylenenimine (PEI, 25kDa, branched, Sigma, St Louis) and the costly lipid-based X-tremeGENE™ HP DNA (Sigma-Aldrich) transfection reagents. The plasmid DNA and transfection reagent were generally used at 1µg DNA to 3µl transfection reagent ratios or were adjusted accordingly for economical use at improved transfection efficiencies for each construct and optimised such that the toxicity to cells was minimised. Cells were monitored regularly, and if needed, the cell medium was replaced with fresh complete medium to minimise the depletion of nutrients, which are necessary for cell growth.

3.2.5 Harvesting protein from the small-scale transfections in 12 well plates

Three to four days post-transfection, the cell medium was aspirated and transferred into labelled 1.5ml Eppendorf tubes. Cells were washed twice with sterile 1x PBS, pH7.2 (Gibco™) followed by the addition of 100µl/well Glo-lysis buffer (Promega, USA). The plate was incubated with the lysis buffer for about 5-10min at room temperature (RT), and the cell lysates were then transferred into labelled tubes. In some cases, instead of using the Glo-lysis buffer, sodium dodecyl sulphate polyacrylamide gel electrophoresis (SDS-PAGE) sample loading buffer (diluted 2x) was directly added to the cells and used to harvest the cell lysates. Harvested proteins were kept at -20°C for further analysis by SDS-PAGE.

3.2.6 Generation of stable HEK293 cell lines expressing Zera®-gp140 or gp140-Zera®

Plasmids for generating stable cell lines were constructed by using Xbal and EcoRI sites to insert an internal ribosome entry site and neomycin resistance (IRES-Neo) cassette directly downstream of Zera® and gp140 sequences in pMExT gp140-Zera® and pMEx Zera®-gp140, respectively. This formed pMExT gp140-Zera®-IRES-Neo and pMEx Zera®- gp140-IRES-Neo plasmids (maps shown, Figure 3.12). The IRES gene allows for the independent, bicistronic expression of two genes under the control of the same promoter, while the neomycin resistance gene confers resistance to geneticin or G148 antibiotics in eukaryotic cells. Instead of HEK293T cells (which are resistant to neomycin) that were commonly used in this study for transient expression, the unmodified (no T antigen) original HEK293 cells (HEK293, ATCC® USA, CRL-1573™, susceptible to neomycin) were used to generate stable cell lines. About 60-70% confluent HEK293 cells in a T75 flask were transfected with 30µg of plasmid DNA plus 90µg PEI (1mg/ml in PBS) or 60µl X-tremeGENE™ transfection reagents. Twenty-four hours post-transfection, cells were passaged using the complete medium supplemented with 600µg/ml geneticin (Gibco™, ThermoFisher scientific). Cells were monitored daily and passaged at least ten times in this medium. At passage 4, the cell medium and lysates were analysed on western blots to assess for gp140 protein expression. At passage 10, protein expression was assessed again, and stable cell lines were cryopreserved as outlined in Appendix A, Section 3.3.

3.2.7 Isolation of Zera®-gp140 or gp140-Zera® using different types of gradient-based ultracentrifugation

3.2.7.1 Extraction of Zera®-gp140 and gp140-Zera® from mammalian cells

Transiently transfected HEK293T cells expressing gp140-Zera® were used for the optimisation of a lysis method for isolation of Zera®-tagged gp140. Four to five days post-transfection, the medium was aspirated, and cells were gently washed 2x with PBS. The cell scrapers (Greiner Bio-One™, Germany) were used to scrape off the cells in the presence of Zera® buffer PBP3 (100 mM Tris pH8, 50 mM KCl, 6 mM $MgCl_2$, 10 mM EDTA, 0.4 M NaCl) supplemented with 1x cOmplete™, EDTA-free Protease Inhibitor Cocktail and 10% sucrose. Collected cells were chilled on ice followed by homogenisation through 15 up and down strokes of a Dounce glass tissue homogeniser (Kontes Glass Co., Vineland). Cell lysis was assessed under a light microscope following staining of the resultant homogenates with Trypan blue to confirm lysis. Lysates were subjected to a low-speed clarification spin (Allegra™ X-22Rcentrifugation, 1000 x *g*, 5min, 4°C). Lysates were further clarified by filtration through one layer of sterile Miracloth (Merck) to ensure the removal of residual cell debris. Cleared lysates were then transferred into ultra-Clear™ centrifuge tubes (Beckman Coulter) for ultracentrifugation.

3.2.7.2 Ultracentrifugation for the isolation of Zera®-induced protein bodies

Different ultracentrifugation methods were conducted in an attempt to purify Zera®-tagged gp140, gp140 or Zera®-eGFP from transfected mammalian cells. In a first approach: the clarified lysates were purified as per the recommended generic method described by Torrent *et al.* (2009a) for isolation of Zera® protein bodies. Briefly, the clarified lysates were loaded onto a multistep sucrose gradient (19, 27, 42, and 56%). Gradients were separated by rate-zonal ultracentrifugation (SW28, 80000 x *g*, 2 hours, 4°C) using a Beckman-Coulter L7-55 ultracentrifuge (USA). After ultracentrifugation, the supernatants were collected, and the protein pellets were resuspended in sterile 1x PBS. In a second approach, clarified lysates were loaded on a 5-35% OptiPrep™ continuous gradient prepared using a dual pump gradient maker (TRIS™, ISCO, Lincoln, USA). These gradients were separated by isopycnic ultracentrifugation (SW32Ti, 175000 x *g*, 16 hours, 4°C) using a Beckman-Coulter Optima L-100 XP ultracentrifuge. Gradients were manually fractionated by punching a hole in the bottom of the tube and slowly collecting 1ml fractions. The Brix % of each fraction was measured using an ATAGO PAL-3 refractometer (0-93%, Brix) and converted to refractive indices and densities of OptiPrep™. Band intensities (on western blots) of each fraction measured by densitometry were plotted against the densities of OptiPrep™ to determine the density

distribution of gp140-Zera® and Zera®-gp140 in comparison to gp140 and Zera®-eGFP controls. The third approach conducted was the method used to obtain sufficient protein to evaluate the immunogenicity of Zera®-gp140 and gp140-Zera® in rabbits. Briefly, Zera®-tagged proteins from the clarified lysates were concentrated by pelleting the contents by ultracentrifugation (SW28, 79000 x *g*, 2 hours, 4°C) (Figure 3.4). Protein pellets were resuspended in sterile PBS. The volume of PBS used for resuspension of protein pellets depended on the size of the pellet (approximately 3.5ml for 10 x T175 flasks). Complete pellet resuspension was achieved by gently stirring at 4°C overnight. Protein fractions from these isolation methods were all analysed on western blots as described in Section 3.5.1.1.

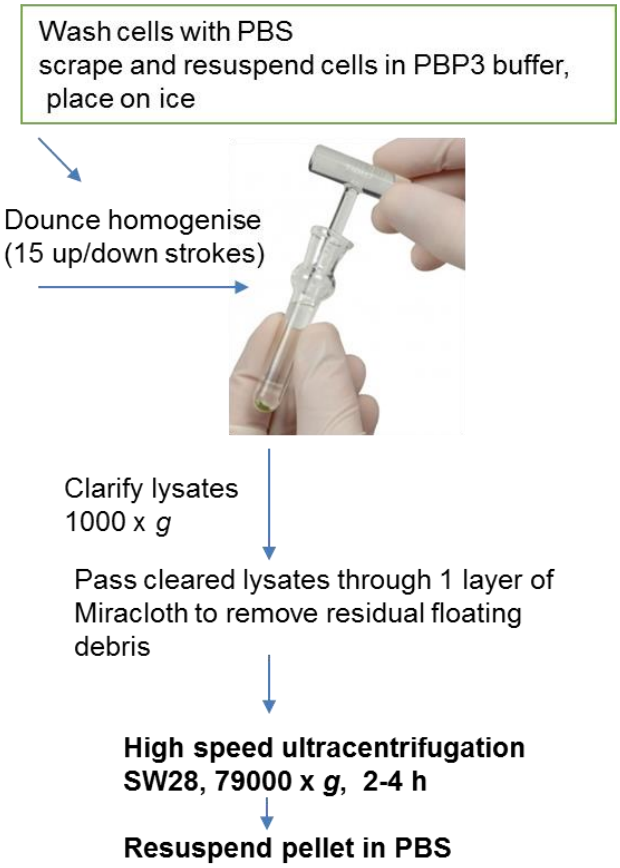

Figure 3.4 Schematic summarising the method used for isolation and concentration of Zera®-tagged proteins.

3.2.8 Lectin affinity purification of Zera®-gp140 from HEK293 stable cell lines

To evaluate if the presence of Zera® affected the trimerisation of gp140, lectin-purified Zera®-gp140 was analysed by native gel electrophoresis. Briefly, confluent T175 flasks (10x) seeded with HEK293 cells stably expressing Zera®-gp140 were washed twice with PBS before cells were scraped with PBP3 buffer supplemented with 1x cOmplete™, EDTA-free Protease Inhibitor Cocktail and 10% sucrose. Following cell homogenisation and clarification of the lysates, the volume of the clarified lysate was adjusted to 1200ml with ice-cold PBS. The lysate

was passed through a *Galanthus nivalis* lectin agarose column (Sigma, St Louis) at 4°C using a peristaltic pump at a flow rate of ~120ml/hour. The column was then washed with 100ml of 0.5M NaCl-PBS followed by 100ml of PBS only. Env protein was eluted using elution buffer (1M methyl αD-manno-pyranoside (MMP) (Sigma) in PBS). The column was filled with elution buffer, closed and allowed to incubate for 30 minutes before dripping 50ml of MMP through the column. The eluate was concentrated, and buffer exchanged to PBS using a Vivaspin Protein Concentrator with a 30kDa cut off (GE Healthcare). Collected samples were analysed under native conditions using the NativePAGE™ Novex® 3-12% Bis-Tris gel as per manufacturers (Invitrogen) instructions, and gels were stained with Bio-Safe™ Coomassie Stain (Bio-Rad-Hercules) before destaining with distilled water.

3.2.9 Quantitation of Zera®-gp140 and gp140-Zera® using densitometry

The amount of gp140 in the protein pellets containing g140-Zera® and Zera®-gp140 was estimated by densitometry analysis (Molecular Imager® Gel Doc™ XR+ imaging system software, Bio-Rad) of samples on a western blot. Gp140, purified by size exclusion chromatography and quantitated using the DC™ Protein Assay (Bio-Rad) (van Diepen *et al.* 2019), was used as a standard. All samples were treated in the same manner to reduce errors. This analysis was repeated two to three times to determine the reproducibility of the calculated protein concentrations.

3.2.10 Immunofluorescent staining and imaging of mammalian cells

Immunofluorescent staining was conducted to evaluate the formation and localisation of Zera®-induced protein bodies. Four-well chamber slides (AEC Amersham) were pre-coated with poly-L-Lysine (Sigma-Aldrich) and seeded with 30000 HeLa cells per well. Three days post-transfection with pMExT gp140-Zera®, pMEx Zera®-gp140, pMExT gp140 or pMEx Zera®-eGFP, cells were fixed with 4% paraformaldehyde for 10min, washed with 1x phosphate-buffered saline (PBS), permeabilised and blocked with 2% BSA-PBS supplemented with 0.25% Triton X-100 for 1hour at room temperature. Cells were double-stained overnight at room temperature with goat anti-HIV-1 gp120 and rabbit polyclonal antibodies to calnexin (Abcam), diluted 1:500 and 1:200, respectively in 2% BSA-PBS. Following washes with PBS, cells were incubated in the dark for 1.5 hours with the fluorophore-conjugated secondary antibodies (1:500 donkey anti-Goat-Cy3 and 1:500 donkey anti-rabbit-Alexa488/Cy3) diluted in 2% BSA-PBS. The cells were then washed with PBS and incubated for 10min with 1:5000 Hoechst nuclei stain diluted in PBS. Following washes in PBS, slides were mounted with antifade-moviol mounting media. Slides were imaged with a confocal microscope (Carl Zeiss 880 LSM confocal with Fast Airyscan technology and the Elyra S1 super-resolution microscope).

3.2.11 Electron microscopy of mammalian cells expressing PBs

Three days post-transfection, HEK293T cells (200k cells/well in a 6-well plate) transiently transfected with an empty pMExT vector or pMExT encoding gp140 or gp140-Zera® or Zera®-gp140 were scraped off in the presence of PBS pH 7.5 and pelleted for 3 minutes at 13 000 rpm (Eppendorf Centrifuge 5417C, Germany). Cell pellets were fixed with 1ml of 2.5% ice-cold glutaraldehyde (Merk, Germany) in PBS overnight at 4°C. Fixed cells were pelleted (5000 rpm, 3minutes), washed twice with 200µl PBS and resuspended in ≈20µl of 2% low melting point agarose (Lonza, Belgium) prepared in PBS and kept at 37°C in a water bath. Cells were then fixed for 1hour with 0.5% tannic acid (Sigma-Aldrich, USA) which only penetrates and enhances the electron density of cells whose membranes are damaged, enabling distinction between damaged and undamaged cells by electron microscopy. Cells were washed once in PBS prior to post-fixing with 1% osmium tetroxide (Sigma-Aldrich, USA) which stains lipids and improves the contrast of cellular structures. Samples were washed twice in PBS, twice in distilled water and subjected to a series of ethanol dehydration steps (30, 50, 70, 80, 90, 95 and 100%) for 10 minutes in each step. Dehydration in 100% ethanol for 10 minutes was repeated once more, followed by two incubations in 100% acetone for 10 minutes. Samples were then incubated in 1:1 and 1:3 acetone: agar low viscosity resin (Agar Scientific, UK) mixture overnight and for 8 h, respectively. This was followed by overnight incubation in 100% agar low viscosity resin. Identification labels for each sample were transferred into respective wells of the embedding mould holders, covered with resin, small pieces of each sample were transferred into the holders, topped with more resin, and polymerised at 60°C for 24 hours. Ultrathin sections were cut using a diamond knife. Thin sections were adsorbed onto carbon-coated copper grids, negatively stained with 2% uranyl acetate (Agar Scientific, UK) and visualised using a FEI Tecnai 20 transmission electron microscope (FEI, Netherlands). The preparation of thin sections and imaging was a service provided by the UCT Electron Microscope Unit (UCT, South Africa).

3.2.12 Immunisation of rabbits with Zera®-gp140 and gp140-Zera®

Rabbit inoculations and blood sampling were performed at the University of Stellenbosch Animal Research Facility according to the requirements, guidelines, and approval of the University of Cape Town and University of Stellenbosch Animal Ethics Committees (AEC 015-51). Two groups of five female New Zealand White rabbits were used to compare the immunogenicity of the mammalian-produced gp140-Zera® and Zera®-gp140 proteins. Forty to 50µg protein diluted in 1 x PBS to a final volume of 500µl, was administered into the quadricep muscle of the hind leg of each rabbit on day 0 and subsequently at weeks 4, 12 and 20 post initial immunisation. Blood samples were collected in VACUETTE® Z Serum Sep Clot

Activator tubes (Greiner Bio-One) at weeks 0, 4, 8, 12, 14, 16, 20 and 22 post-vaccination. At each time point, blood was allowed to coagulate at RT before it was centrifuged (U-320, BOECO Germany) at 5000rpm for 30 minutes. Serum aliquots were stored at -20°C. Rabbits were euthanised by exsanguination and terminated at week 22.

3.2.13 Quantification of gp140 binding antibodies in rabbit sera

An ELISA assay was used to quantify the gp140 antibody binding titres in rabbit sera. Briefly, 96-well Maxisorb® microtitre ELISA plates (Nunc) were coated with 10ng/well of the soluble gp140 trimers (van Diepen *et al.* 2019) and incubated at 4°C overnight. Following 3x washes in PBS, the unoccupied sites were blocked with 200µl 5% skim milk powder (Oxoid) in PBS for 1 hour at RT. Plates were washed 3x with PBST, and duplicate wells were incubated overnight at 4°C with 100µl/well of serum three-fold serially diluted from 1:10 2.5% skim milk in PBS. Following 3x washes in PBST, wells were incubated for 1 hour at RT with swine anti-rabbit IgG-HRPO conjugate (DakoCytomation) diluted 1:10 000 in 2.5% skim milk powder in PBS (100µl/well). After another 3x washes in PBST, 100µl/well of TMB ELISA substrate (high sensitivity, Abcam®) was added. The reaction was stopped after 10 minutes with 100µl of 1N H_2SO_4. The absorbance signals at 450 nm (corrected for by subtracting the background reading at 540 nm) were measured using a VersaMax ELISA Microplate Reader (Molecular Devices, Sunnyvale). Antibody end-point titres were defined as the last dilution to give a signal above the matching pre-bleed (1:10) ELISA signal. GraphPad Prism 5.0 software was used to present the end-point titres against bleed time points (weeks). The V1V2-specific antibodies in sera collected at week 0 (pre-immune) and week 22 (2 weeks after the final protein inoculation) were evaluated by an antibody binding ELISA conducted as described above except that 500ng/well of CAP256 SU V1V2 scaffolded protein was used as a capture antigen. CAP256 SU V1V2 scaffold protein was provided by Professor Penny Moore (Senior Medical Scientist, Centre for HIV and STIs, National Institute for Communicable Diseases, Johannesburg). CAP256 SU V1V2 scaffolded proteins were produced and purified by affinity chromatography using a Ni-NTA column as described previously by Gorman *et al.* (2016).

3.2.14 Neutralisation of Env-pseudotyped viruses by rabbit sera

A small panel of clade C Env-pseudotyped viruses competent for a single-cycle infection was used to evaluate the ability of anti-gp140 antibodies in serum sampled from weeks 0 and 22 to block the viral entry into susceptible TZM-bl cells. This assay was a service conducted at the National Institute for Communicable Diseases (Sandringham, Johannesburg) by Professor Lynn Morris's group. TZM-bl cell line (Montefiori. 2004), is a HeLa cell line genetically modified to stably express CD4 and CCR5 coreceptors, which are entry sites rendering maximal

susceptibility of cells to HIV-1 infection (Platt *et al.* 1998). TZM-bl cells were further modified by Wei *et al.* (2002) to stably express *E. coli* B-galactosidase and firefly luciferase reporter genes to allow for quantification of HIV-1 viral infection. The degree of neutralisation, measured in relative luminescence units (RLUs), was assayed by quantifying the reduction of Tat-regulated luciferase expression upon infection with Env-pseudotyped viruses (MW965.26, 6644 and CAP256SU). As a negative control, Env-pseudotyped virus containing Env of murine leukaemia virus (MLV) encoded in the same backbone was included. The final neutralisation titres were expressed as the reciprocal of the serum dilution resulting in a 50% reduction in relative luciferase units, or the ID_{50}.

3.3 Results

3.3.1 Analysis of expression of Zera®-eGFP as a proof of concept for the production of Zera®-induced protein bodies in mammalian cells

As a proof of concept that Zera®-induced protein bodies could be produced in HEK293T and HeLa cell lines in our laboratory, plasmid pMEx Zera®-eGFP was constructed, as Zera®-eGFP has been shown to form protein bodies by other groups (Torrent *et al.* 2009a; Saberianfar *et al.* 2016). Western blots of lysates derived from HEK293T and HeLa cells transfected with pMEx Zera®-eGFP and probed with anti-GFP (Figure 3.5 A) or anti-Zera® (Figure 3.5 B) antibodies yielded the expected ~40kDa band for Zera®-eGFP. In both these cell lines, Zera®-eGFP protein was enriched in the cell lysates (L) without significant secretion into the cell medium as observed by the lack of the 40kDa band (M). The ability of Zera® to induce ER-derived eGFP protein bodies in HeLa and HEK293T cells was confirmed by immunofluorescent staining with anti-GFP primary antibody followed by detection with anti-Cy3 labelled secondary antibody and imaging with confocal microscopy. Spherical, protein body-like fluorescent structures were observed in cells transfected with pMEx Zera®-eGFP (Figure 3.5 C & D). As expected, no PB-like structures were observed in cells transfected with a plasmid encoding eGFP alone (without the Zera® tag) (Figure 3.5 E). The advantage of using Zera® as a fusion tag is that the protein of interest can be purified easily and rapidly by virtue of high-density properties inherited from Zera®-induced PBs (Torrent *et al.* 2009a). To investigate if high-density PB-like structures were being produced in HEK293T cells transfected with pMEx Zera®-eGFP, the clarified lysates were passed through a 19-56% sucrose step gradient by rate zonal ultracentrifugation. Even though Zera®-eGFP was also found in the interfaces (IF1-IF3), the majority of Zera®-eGFP passed through the gradient and was enriched in the pellet, an indication that to some extent, these PB-like structures were particulate and dense (Figure 3.5 F).

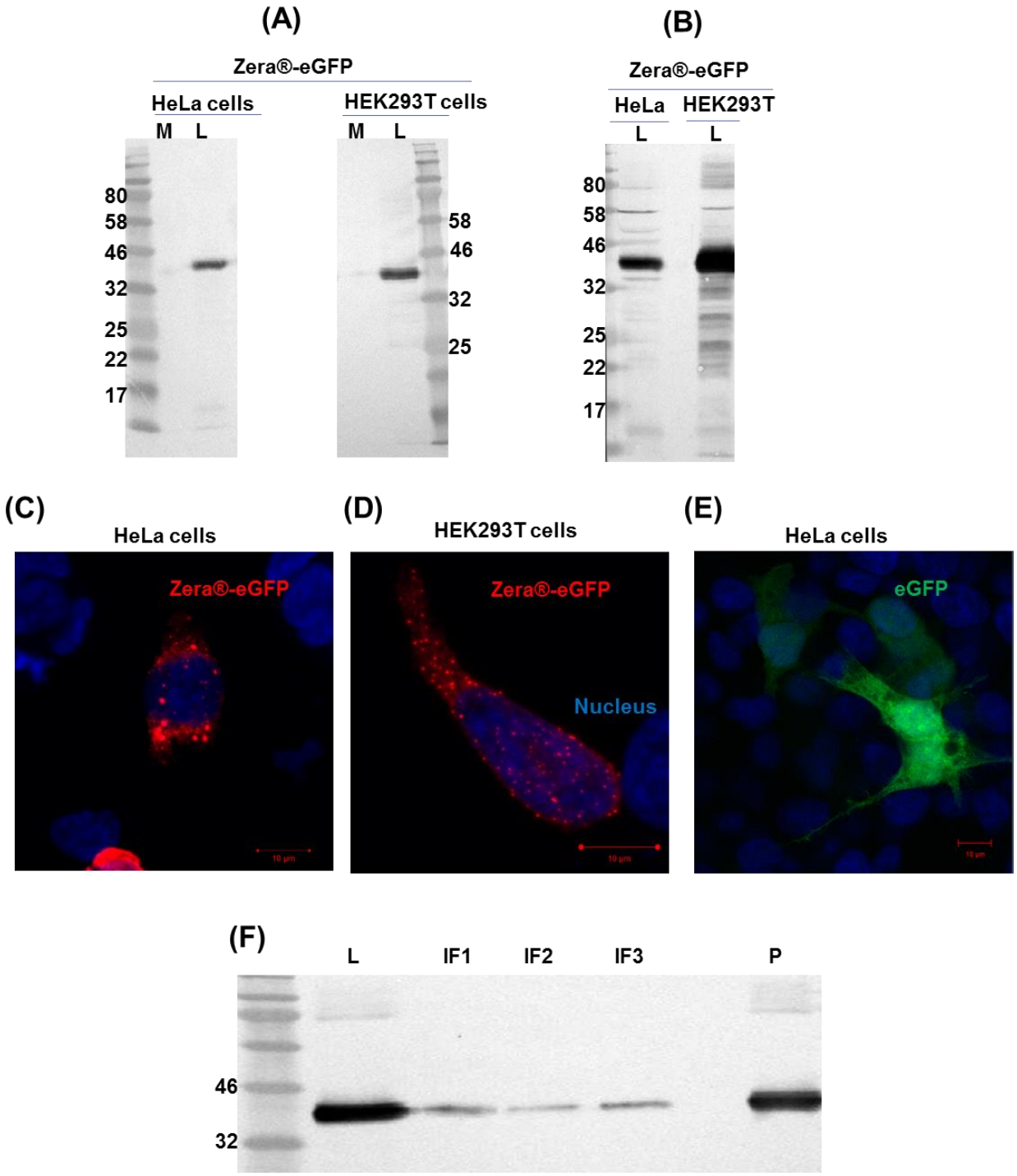

Figure 3.5: Fusion of the Zera® to the N-terminus of eGFP induced PB-like structures in mammalian cells. The cell lysates (L) and media (M) from HEK293T and HeLa cells transfected with pMEx Zera®-eGFP were analysed by western blots probed with anti-GFP **(A)** and anti-Zera® **(B)** antibodies. Immunodetection of Zera®-eGFP in protein bodies of transfected HeLa **(C)** and HEK293T cells **(D)** using anti-GFP primary antibody and anti-Cy3 labelled secondary antibody. Confocal micrographs of HeLa cells expressing eGFP **(E).** The clarified lysate (L), from HEK293T cells transfected with pMEx Zera®-eGFP, was loaded on a 19-56% sucrose gradient. After ultracentrifugation, the interphase fractions (IF) were collected from the top to the bottom (IF1, IF2 and IF3) and the final protein pellet (P) was resuspended in a phosphate buffer. Collected fractions were analysed on a western blot probed with an antibody to GFP **(F)**.

3.3.2 Confirmation of integrity of pMExT gp140-Zera®, pMExT gp120-Zera® and pMEx gp140-Zera®ΔTK plasmids

Zera®-tagged gp140 or gp120 fusions were constructed to evaluate if Zera® PBs could be induced when Zera® fused to HIV-1 Env proteins is expressed in mammalian cells. Both C- and N-terminus Zera®-tagged gp140 fusions were designed in order to evaluate which one would more efficiently form Zera®-induced PBs. Specifically, the sequence coding for Zera® was inserted into plasmid pMExT gp140-FL-IP, downstream of gp140 or gp120 to generate pMExT gp140-Zera® and pMExT gp120-Zera®, respectively. Plasmid pMExT gp120-Zera® was not designed for immunisation purposes, but rather to evaluate the effect of the smaller size of Env on the induction of PBs. Plasmid pMEx gp140-Zera®ΔTK was constructed to assess the effect of the TPA leader sequence and KDEL ER retention signal on the expression of gp140-Zera®. The integrity of these plasmids was confirmed by restriction enzyme mapping (Figure 3.6) and sequencing.

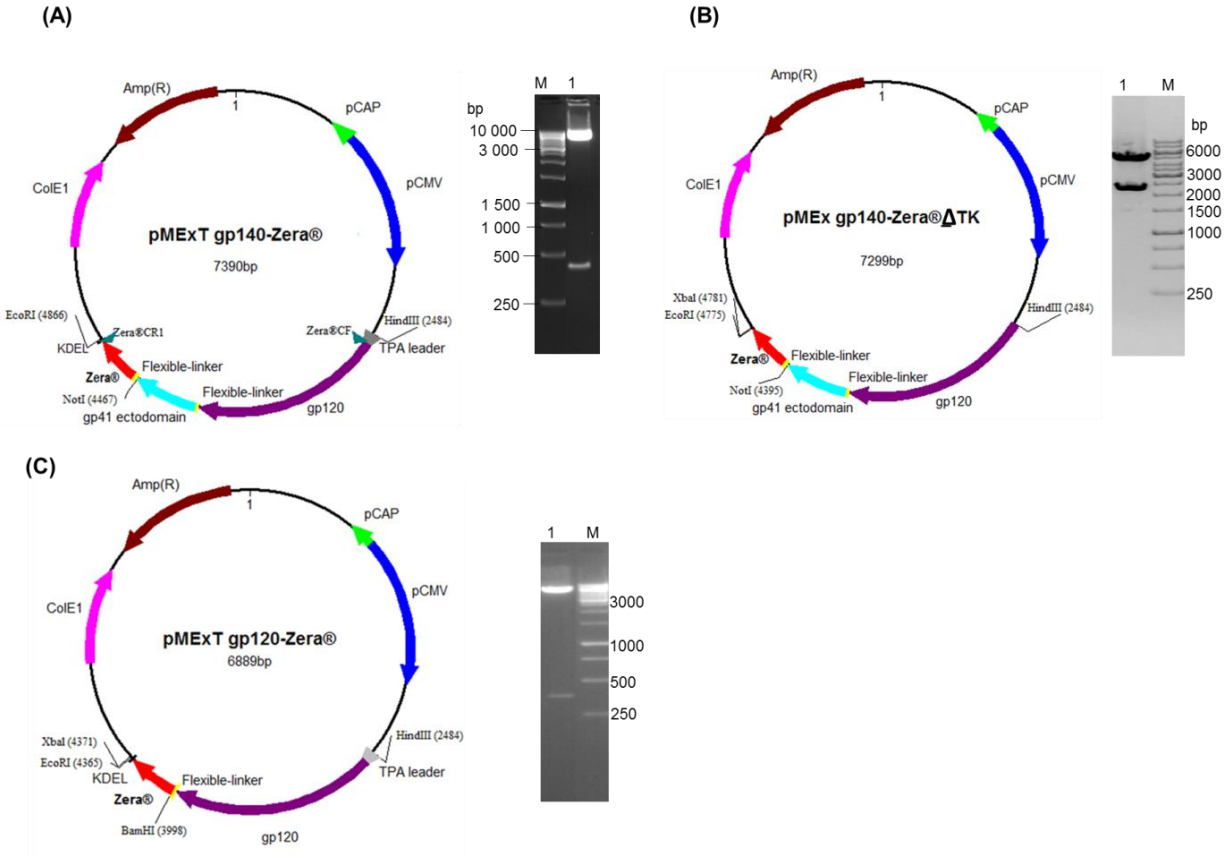

Figure 3.6: Confirmation of the integrity of mammalian expression vectors encoding Zera® fused downstream of Env. (A) Plasmid map of pMExT gp140-Zera® and restriction analysis using EcoRI and NotI enzymes**. (B)** Plasmid map of pMEx gp140-Zera®ΔTK (ΔTK, the TPA leader and KDEL sequences have been removed) and restriction analysis using HindIII and EcoRI enzymes**. (C)** Plasmid map of pMExT gp120-Zera® and restriction analysis using EcoRI and BamHI enzymes. In each case, the 1kb DNA ladder (ThermoFisher Scientific) was represented in lane M.

3.3.3 Small-scale expression of Zera®-tagged antigens in mammalian cells

The C-terminal Zera® fusions were initially used to optimise the experimental conditions for the production and processing of Zera®-tagged Env proteins in mammalian cells. HEK293T cells were transfected with plasmids that expressed gp120-Zera®, gp140-Zera®, gp120-His and gp140. Three days post-transfection, the cell media (M) and lysates (L) were harvested and analysed on a western blot probed with an antibody to Env (Figure 3.7). As expected, gp120-Zera® and gp140-Zera® accumulated in the cell lysate and very little was found in the cell media. Non-Zera®-tagged gp140 tended to accumulate in both the cell lysate and the media. The majority of Env in cells expressing gp120-His was observed in the lysate, and very little was secreted into the cell media. As expected, no Env was detected in cells transfected with an empty pMExT plasmid.

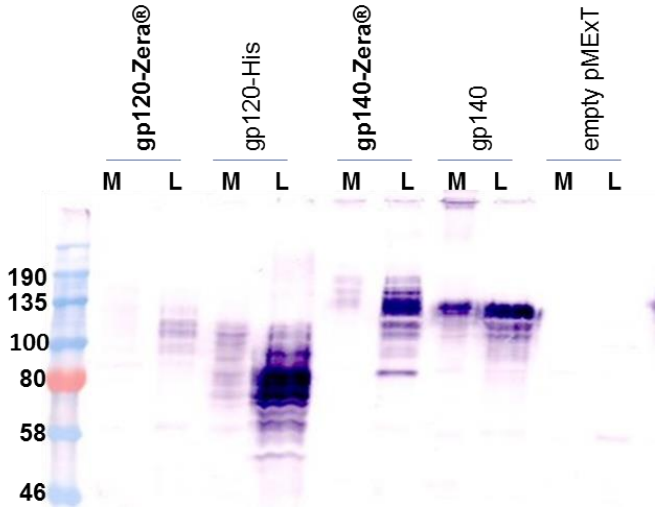

Figure 3.7: Comparison of transient expression of Zera®-tagged Env vs non-Zera®-tagged Env in HEK293T cells. HEK293T cells were transfected with plasmids that expressed gp120-Zera®, gp140-Zera®, gp120-His and gp140. Three days post-transfection, the cell media (M) and lysates (L) were harvested and analysed on a western blot probed with an antibody to Env.

Gp140-Zera® was used for further optimisations because it produced higher levels of protein than gp120-Zera®, and it was relevant for use in immunogenicity studies. The effect of the TPA leader and the KDEL ER-retention signal on the expression of gp140-Zera® was assessed in HEK293T cells transfected with pMExT gp140-Zera® and pMEx gp140-Zera®ΔTK. There were no notable differences (in the cell lysates and media prepared the same way and the same volume were loaded on a gel) in the levels of expression of gp140-Zera® with and without the TPA leader and KDEL sequences (Figure 3.8). Thus, for all the subsequent optimisation experiments, gp140-Zera® with the TPA and KDEL was used.

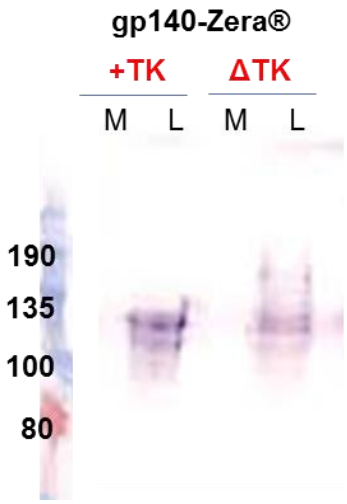

Figure 3.8: Comparison of expression of gp140-Zera® with and without the TPA leader and KDEL sequences in HEK293T cells. HEK293T cells were transfected with pMExT gp140-Zera® (+TK, contains the TPA leader and KDEL sequences) and pMEx gp140-Zera®ΔTK (ΔTK, the TPA leader and KDEL sequences have been removed). Three days post-transfection, the cell media (M) and lysates (L) were harvested and analysed on a western blot probed with an antibody to Env.

3.3.4 Medium-scale transient expression of gp140-Zera® in HEK293T cells and purification by rate-zonal ultracentrifugation

Under optimal PB-inducing conditions, Zera®-tagged proteins accumulate in electron-dense PBs, thus simplifying protein purification by ultracentrifugation-based methods (Mainieri *et al.* 2004; Torrent *et al.* 2009a; Torrent *et al.* 2009b). We evaluated if Zera®-induced PBs in cells expressing gp140-Zera® in comparison to gp140 could be isolated by low-speed ultracentrifugation. HEK293T cells were transfected with pMExT gp140-FL-IP and pMExT gp140-Zera®. The transfection efficiency of two transfection reagents, X-tremeGENE™ and PEI was compared. Three days post-transfection, cells were harvested using the recommended PBP3-10% sucrose buffer for processing of Zera®-tagged antigens and lysed by Dounce homogenisation. Cleared lysates from these cells were passed through a 19, 27, 42 and 56% step sucrose gradient by rate-zonal ultracentrifugation and the resultant fractions were analysed on a western blot probed with anti-Env antibody (Figure 3.9). Cells transfected with X-tremeGENE™ (Figure 3.9 A) resulted in higher expression levels of gp140 compared to those transfected with PEI (Figure 3.9 B). The expression level of gp140 was higher than that of gp140-Zera® (Figure 3.9 A). The distribution of gp140 in the lysates expressing gp140 and gp140-Zera® was slightly different in that both gp140-Zera® and gp140 mainly accumulated in the protein pellet but larger quantities of gp140 were also detected in the cell debris (P1) and supernatant following ultracentrifugation (S3). It was assumed that if PBs were optimally produced, the size or shape of Zera®-gp140 PBs would be larger than soluble

gp140, thus sediment faster through the gradient. Unexpectedly, gp140 pelleted to the same extent as gp140-Zera®.

Fractions from the gradients of lysates of cells transfected using X-tremeGENE™ were also analysed on SDS-PAGE stained with Coomassie blue to assess the ability of rate-zonal ultracentrifugation to purify gp140-Zera® or gp140 away from other contaminating proteins in the lysates (Figure 3.9 C). It was observed that Coomassie staining poorly detected bands that potentially corresponded to Env protein. A diffuse band (two-headed arrows, orange) at ~140kDa was thought to correspond to Env protein. The banding pattern in the lysates before gradient purification (S2) and the banding pattern in samples collected after gradient purification (P2) were similar. It was expected that the lower molecular weight proteins including soluble gp140, would be retained in the supernatant (S3) while the higher molecular weight proteins, including Env in PBs, would sediment to the bottom of the tube (P2).

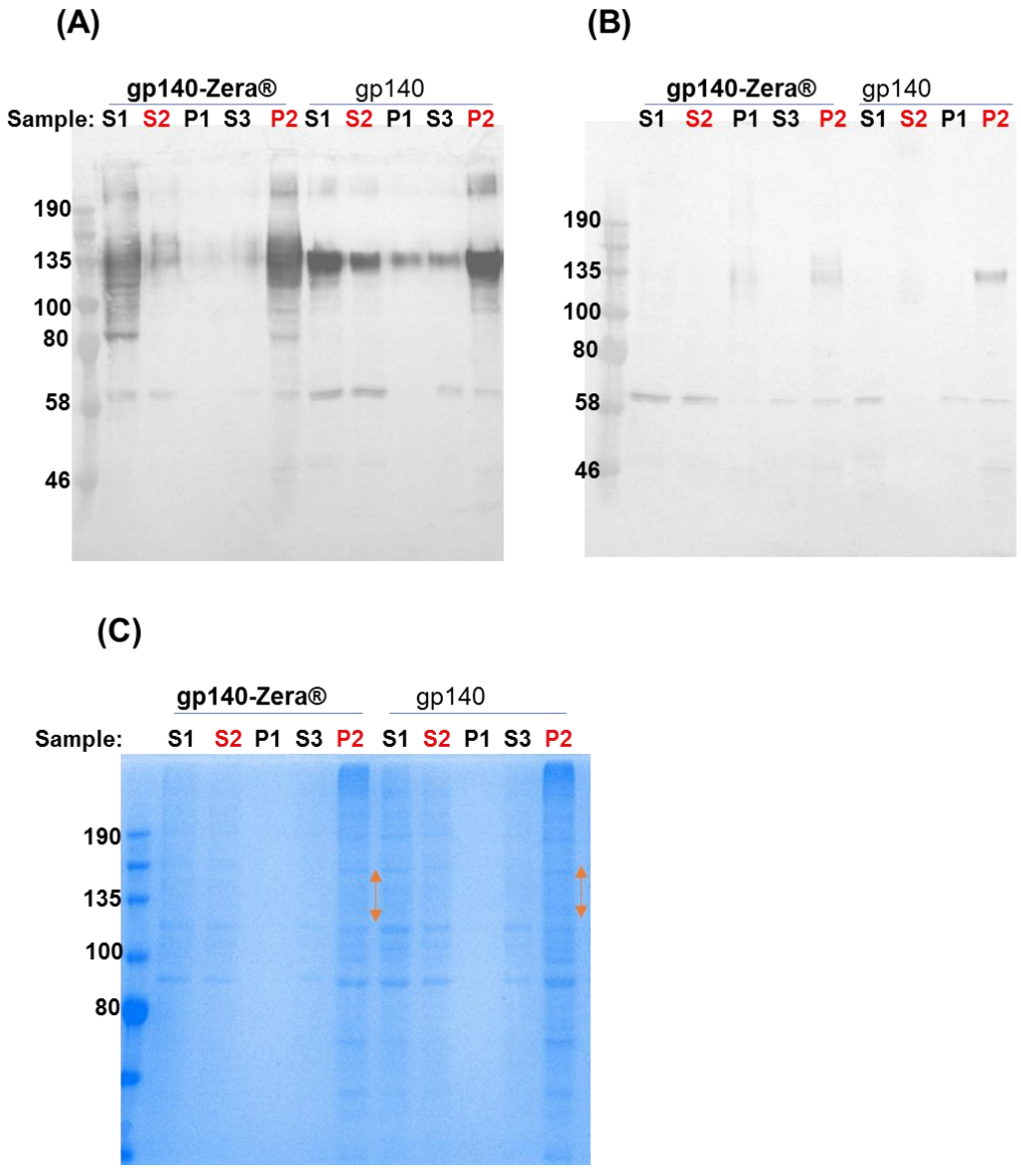

Figure 3.9: Rate zonal ultracentrifugation of lysates from cells expressing gp140-Zera® and gp140. HEK293T cells were transfected with pMExT gp140-Zera® or pMExT gp140-FL-IP in the presence of the X-tremeGENE™ **(A)** or PEI **(B)** transfection reagents. Four days post-transfection, cells were lysed (S1) and cleared (S2) from the cell debris (P1). The cleared lysates (S2) were loaded on a 19-56% step sucrose gradients. Following ultracentrifugation, the supernatant & interfaces were pooled (S3) and the protein pellet was resuspended (P2) in PBS. Fractions were analysed on western blots probed with an antibody to Env **(A & B),** and fractions from cells transfected in the presence of X-tremeGENE™ were stained with Coomassie Blue **(C)**. Red font indicates the cleared lysates (S2) as an input sample to a gradient and the protein pellet as a final output sample (P2). Two-headed arrows (orange) indicate the size range expected for gp140.

3.3.5 Confirmation of integrity of pMEx Zera®-gp140 and comparison of expression of gp140, gp140-Zera® and Zera®-gp140 in HEK293T cells

The initial optimisations of expression, processing and purification of Zera®-tagged Env in mammalian cells were performed using a fusion with Zera® on the C-terminus of CAP256 gp140 (gp140-Zera®). A plasmid expressing HIV-1 gp140 with an N-terminal Zera® tag (pMEx Zera®-gp140) was also constructed to assess whether Env expression or PB formation was more favourable when Zera® was fused to either the C- or N-terminus of gp140. The integrity of this plasmid was confirmed by restriction mapping (Figure 3.10 A) and sequencing. Transient expression of Zera®-gp140 or gp140-Zera® in comparison to gp140 in HEK293T cells was evaluated by western blot analysis of the cell media (M) and cell lysates (L) (Figure 3.10 B). Gp140 and Zera®-gp140 accumulated to similar levels in the cell lysates (n>3) whereas gp140-Zera® was barely detectable in the cell media and lysates from cells transfected with pMExT gp140-Zera®. As expected, the presence of Zera® seemed to favour the accumulation of gp140 within the cells rather than secretion into the cell media.

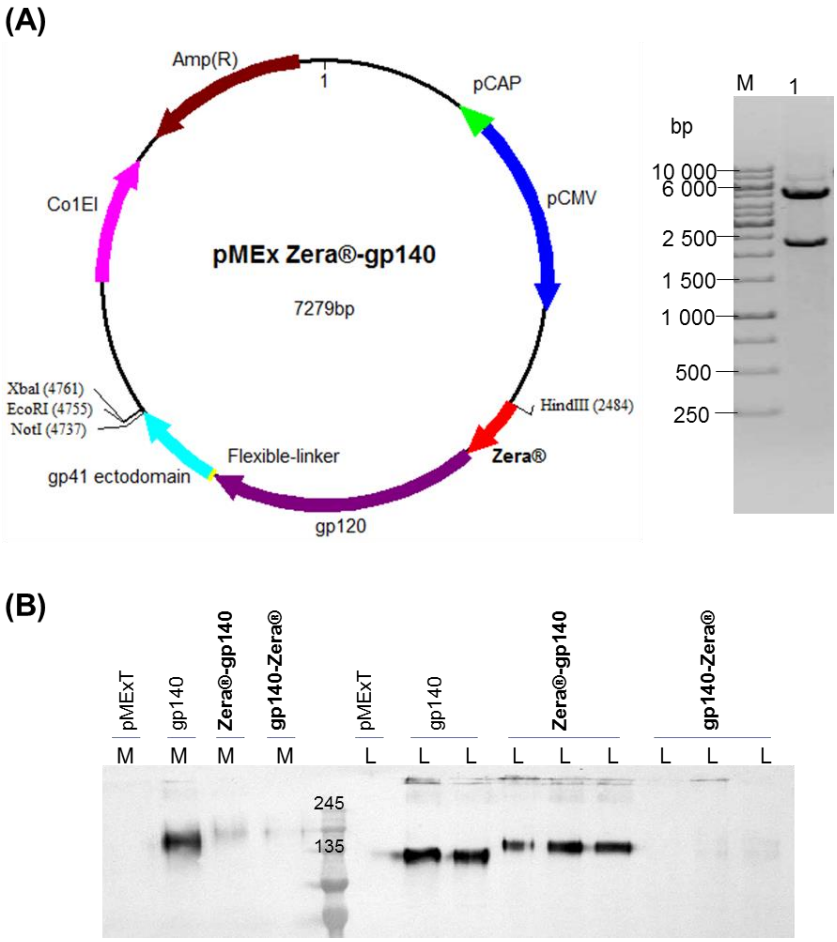

Figure 3.10: Confirmation of the integrity of pMEx Zera®-gp140 plasmid and comparison of gp140 expression in HEK293T cells transfected with pMExT, pMExT gp140-FL-IP, pMEx Zera®-gp140 and pMExT gp140-Zera®. (A) Plasmid map of pMEx Zera®-gp140 and restriction analysis using HindIII and NotI enzymes. **(B)** Anti-Env western blot of the cell lysates (L) and media (M) from HEK293T cells expressing gp140, Zera®-gp140 and gp140-Zera®.

3.3.6 Immunofluorescent staining and confocal microscopy of HeLa cells expressing gp140, gp140-Zera® and Zera®-gp140

The ability of Zera® to induce ER-derived gp140 protein bodies was evaluated by immunofluorescent staining and confocal microscopy of transfected cells (Figure 3.11). Instead of HEK293T cells, HeLa cells were used for immunostaining because they have a bigger cytoplasmic space and smaller nuclei than HEK293T cells, thus allowing for better visualisation of cellular components. HeLa cells were transiently transfected with pMExT gp140-Zera® and pMEx Zera®-gp140, stained with antibodies to HIV-1 Env and calnexin (a chaperone located in the ER) and detected with Cy3- and Alexa488-labelled secondary antibodies, respectively. Cells transfected with pMEx Zera®-eGFP or pMExT gp140-FL-IP were included as positive and negative controls, respectively. Spherical, protein body-like fluorescent structures were observed in cells expressing Zera®-eGFP and gp140-Zera®. It was noted that all the Zera®-eGFP appeared to be in protein bodies whereas gp140-Zera®

appeared to be mainly soluble protein (diffused staining of the cell) with a few relatively small possible protein bodies. Both Zera®-eGFP and gp140-Zera® partially co-localised with the calnexin ER marker. Surprisingly, cells expressing Zera®-gp140 showed very similar staining to those expressing the untagged soluble, gp140 protein and most of the gp140-Zera®. Both Zera®-gp140 and gp140 proteins also co-localised with the calnexin ER marker. This observation corresponds with the observation that gp140 accumulated both in the cell lysate (intracellularly) and media (extracellularly) as observed in western blot analysis shown in Figure 3.11 B. No fluorescence was observed in cells where the primary antibodies were omitted, an indication of the specificity of the secondary antibodies (results not shown).

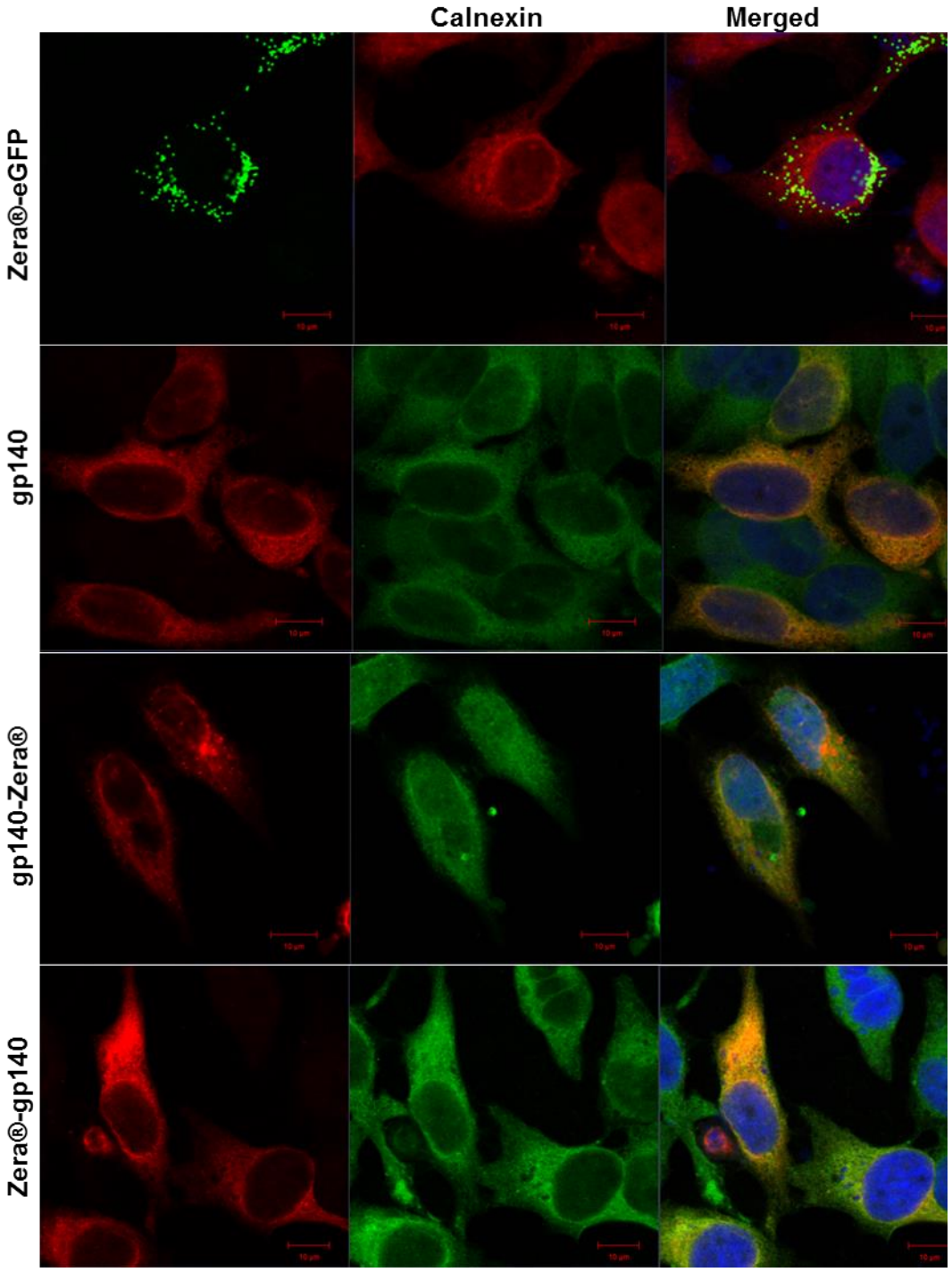

Figure 3.11: Immunofluorescent staining of HeLa cells expressing Zera®-eGFP, gp140, gp140-Zera® and Zera®-gp140. Confocal micrographs of Zera®-eGFP (green, eGFP fluorescence), gp140 (red, Cy3), calnexin (red Cy3 or green Alexa488). Cell nuclei were detected with a Hoechst stain (Blue). Scale bars represent 10µM.

3.3.7 Transmission electron microscopy of thin sections from HEK293T cells expressing gp140, Zera®-gp140 and gp140-Zera®

Transmission electron microscopy was carried out to further evaluate the formation of PBs in HEK293T cells expressing Zera®-tagged gp140. Cells transfected with empty pMExT or pMExT gp140-FL-IP were included as negative controls for the formation of PBs. Protein body-like structures were observed in cells expressing gp140-Zera® but not in those expressing gp140 or Zera®-gp140 (Figure 3.12).

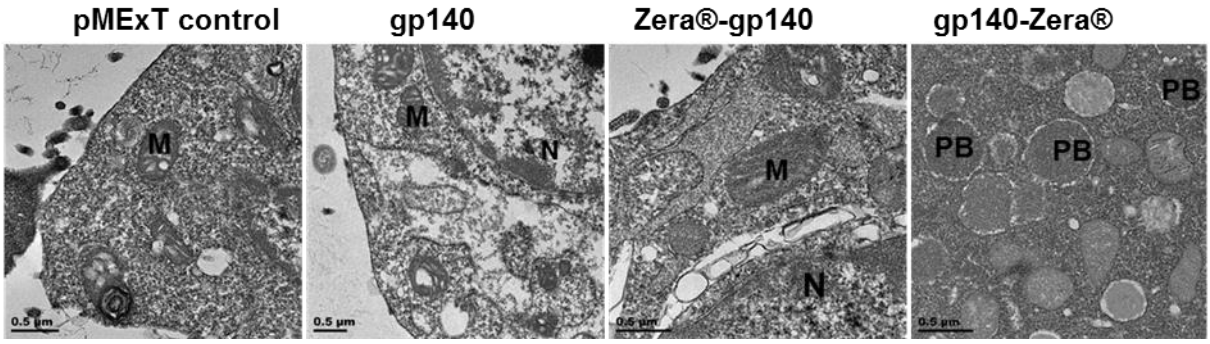

Figure 3.12: Electron micrographs to evaluate the formation of protein bodies in HEK293T cells expressing Zera®-tagged gp140. HEK293T cells were transfected with pMExT (negative control), pMExT gp140-FL-IP (negative control for PBs), pMEx Zera®-gp140 (experimental) or pMExT gp140-Zera® (experimental). Thin sections were negatively stained with uranyl acetate and viewed using the transmission electron microscope. The mitochondrion (M), nucleus (N) and protein bodies (PB) are labelled. Scale bars represent 0.5µm.

3.3.8 Construction of plasmids for the generation of stable cell lines expressing gp140-Zera® and Zera®-gp140

Although the transient expression of Zera®-gp140 and gp140-Zera® in HEK293T cells was confirmed, yields were variable using different batches of DNA for transfection. Protein expression was more consistent when an expensive transfection reagent, X-tremeGENE™, was used for transient transfection. However, it was not economical to use X-tremeGENE™ for repeated, large scale protein production. The relatively cheaper transfection reagent, polyethyleneimine (PEI), often resulted in poor yields. Thus, as a cost-effective measure, plasmids for generating stable cell lines were constructed by introducing an IRES-Neomycin (Neo) resistance cassette downstream of the Zera® and gp140 sequences in pMExT gp140-Zera® and pMEx Zera®-gp140, respectively. The integrity of pMExT-gp140-Zera®-IRES-Neo (Figure 3.13 A) and pMEx-Zera®-gp140-IRES-Neo (Figure 3.13 B) was confirmed by restriction enzyme mapping.

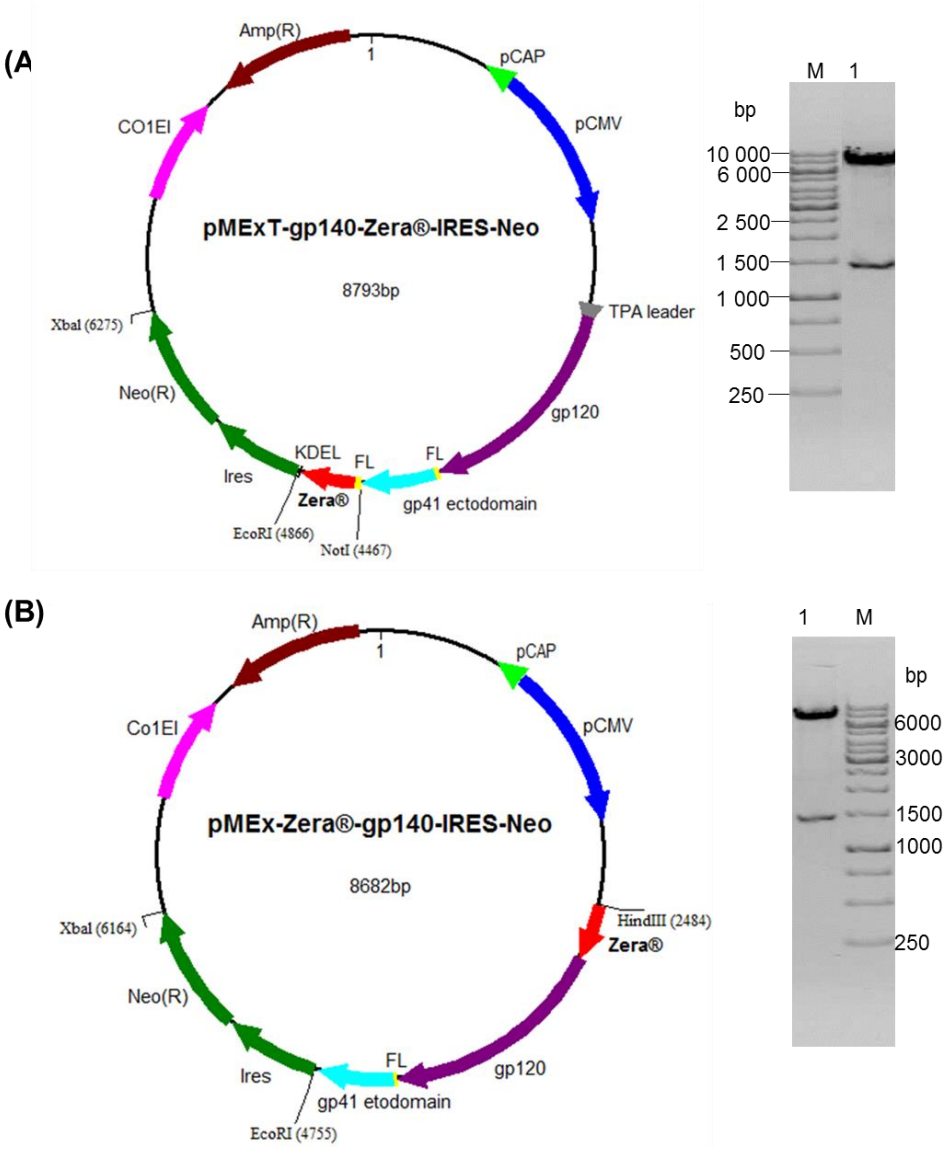

Figure 3.13: Confirmation of insertion of IRES-Neomycin (IRES-Neo) cassette downstream of the Zera® and gp140 sequences in pMExT gp140-Zera® and pMEx Zera®-gp140, respectively. (A) Plasmid map of pMExT-gp140-Zera®-IRES-Neo and restriction analysis using EcoRI and XbaI enzymes. **(B)** Plasmid map of pMEx-Zera®-gp140-IRES-Neo and restriction analysis using EcoRI and XbaI enzymes.

Stable cell lines were then generated by transfecting pMExT-gp140-Zera®-IRES-Neo or pMEx-Zera®-gp140-IRES-Neo into HEK293 cells. Transfected cells were passaged at least 10 times in complete medium supplemented with geneticin. HEK293 cells stably expressing gp140-Zera® and Zera®-gp140 were successfully generated as confirmed by anti-Env and anti-Zera® western blot analysis of the cell lysates (Figure 3.14). However, protein bodies were not visible on immunofluorescent staining of stable HEK293 cells expressing Zera®-gp140 and gp140-Zera® (results not shown).

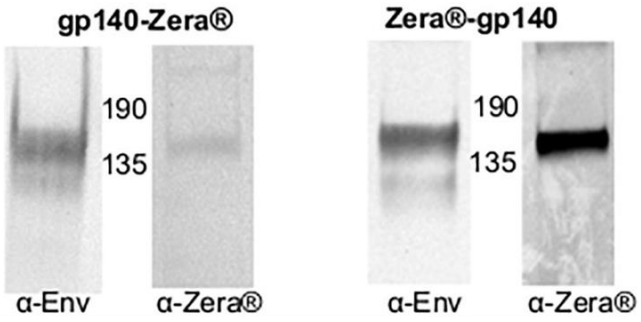

Figure 3.14: Generation of HEK293 stable cell lines expressing gp140-Zera® and Zera®-gp140. HEK293 cells were transfected with pMExT-gp140-Zera®-IRES-Neo and pMEx-Zera®-gp140-IRES-Neo. Geneticin-containing media was used for the selection of stably transfected cells. The expression of gp140-Zera® and Zera®-gp140 in stable cell lines were confirmed by anti-Env and anti-Zera® western blot analysis of the cell lysates.

3.3.9 Isopycnic ultracentrifugation of the lysates from HEK293 stable cell lines expressing Zera®-gp140 or gp140-Zera® and HEK293T transiently expressing gp140 or Zera®-eGFP

Rate-zonal ultracentrifugation was not optimal for purifying Zera®-gp140 and Zera®-gp140 PBs. The main challenge was that Zera-tagged gp140 co-pelleted with other lower and higher molecular weight proteins (as observed in Figure 3.9 C). Ultracentrifugation through a series of sequential rate zonal gradients or cushions resulted in no noticeable purification of Zera-tagged gp140 from one gradient to another. Thus, isopycnic ultracentrifugation was subsequently performed to evaluate its ability to purify Zera-induced PBs from contaminating proteins on the basis of density rather than size. Clarified lysates from cells expressing Zera®-gp140, gp140-Zera®, Zera®-eGFP and gp140 were fractionated through 5-35% OptiPrep™ gradients, and the resultant fractions were analysed by western blots probed with anti-GFP and anti-Env antibodies (Figure 3.15 A). Band intensities extrapolated from western blots were plotted against OptiPrep™ densities corresponding to each fraction (Figure 3.15 B) in order to analyse the distribution of Zera®-induced PBs in the OptiPrep™ gradient. As expected, Zera®-eGFP was distributed predominantly in fractions corresponding to a high OptiPrep™ density (1.21-1.22 g/ml). Both gp140-Zera® and Zera®-gp140 were predominantly distributed in a similar range of OptiPrep™ densities (1.11-1.13 g/ml) which was lower than that of Zera®-eGFP. Surprisingly, gp140 was predominantly distributed in fractions with relatively higher OptiPrep™ densities (1.14-1.18 g/ml) than those observed for sedimentation of Zera®-gp140 and gp140-Zera®.

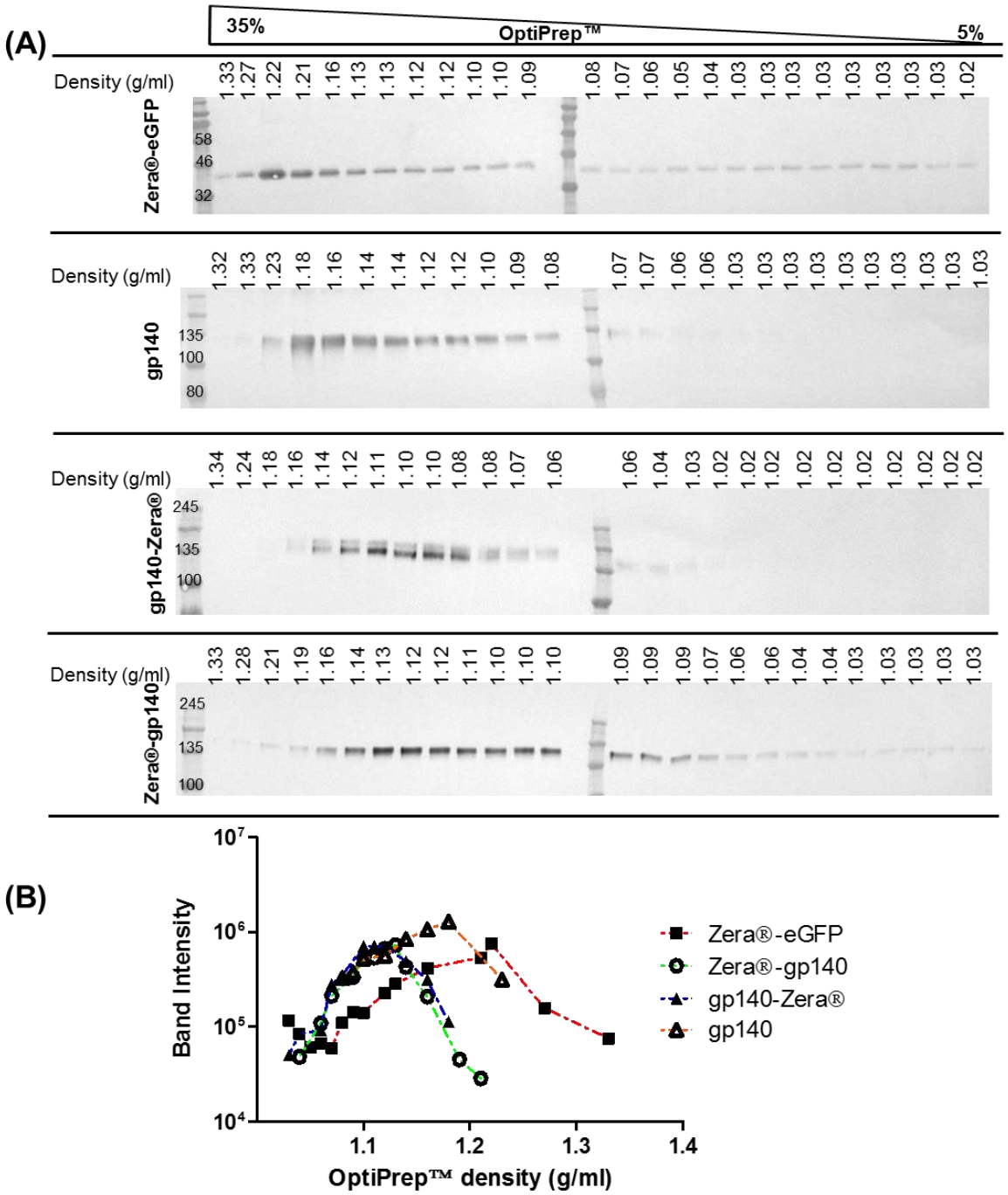

Figure 3.15: Isopycnic ultracentrifugation of the lysates from HEK293T cells transiently expressing Zera®-eGFP and gp140 as well as lysates from HEK293 stable cell lines expressing gp140-Zera® and Zera®-gp140. **(A)** Cell lysates were applied on top of a 5–35% continuous OptiPrep™ gradient followed by isopycnic ultracentrifugation. Fractions were analysed on western blots probed with antibodies to Env or GFP. Refractive indices of each fraction were converted to density (g/ml). **(B)** Band intensities from western blots were plotted against the OptiPrep™ densities.

3.3.10 Native gel electrophoresis of Zera®-tagged gp140

To increase the chances of eliciting neutralising antibodies in vaccinated animals, it is important that gp140 proteins adopt the native-like trimeric conformation. To evaluate the trimeric configuration of gp140-Zera® and Zera®-gp140 in comparison to gp140, fractions

from the OptiPrep® gradients (Figure 3.15) were analysed on a Blue Native gel electrophoresis, transferred for western blots and probed with antibodies to Env (Figure 3.16). It was observed that gp140-Zera® and Zera®-gp140 proteins predominated in the ≈720 kDa region where we would expect a trimeric molecule, as was the case for gp140.

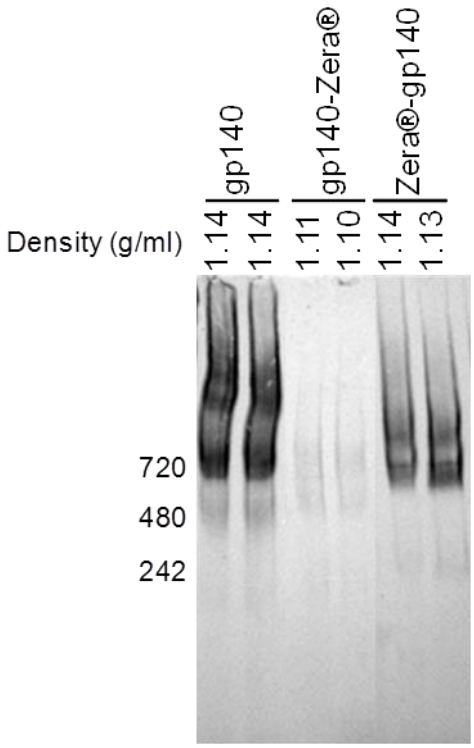

Figure 3.16: Analysis of Zera®-tagged gp140 by native gel electrophoresis. Cell lysates from HEK293 stable cell lines expressing gp140, gp140-Zera® and Zera®-gp140 were applied onto a 5-35% OptiPrep™ gradient followed by isopycnic ultracentrifugation. Two fractions containing the highest concentration of protein were separated on NativePAGE, blotted and probed with antibodies to Env. Refractive indices of each fraction were converted to density (g/ml).

gp140-Zera® was produced at lower yields than Zera®-gp140, thus; Zera®-gp140 was selected for further characterisation of the structure of Zera®-tagged gp140. Lectin (*Galanthus nivalis*) affinity column chromatography was used to purify Zera®-gp140 from clarified cell lysates (Figure 3.17). Even though putative dimeric (≈480 kDa), monomeric ≈(242 kDa) gp140 species, as well as other lower molecular weight proteins (below 242 kDa) were observed in Zera®-gp140 and gp140 (positive control), some of the Zera®-gp140 was apparently trimeric (≈720 kDa).

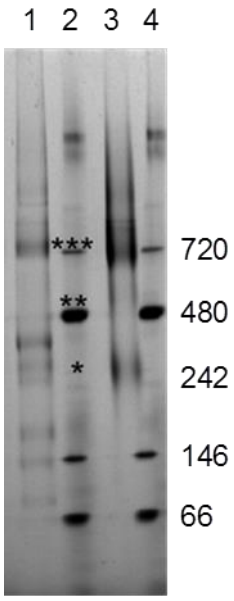

Figure 3.17: Analysis of lectin-purified Zera®-gp140 by native gel electrophoresis. Env protein in the clarified cell lysates from HEK293 stable cell lines expressing Zera®-gp140 was purified by *Galanthus nivalis* lectin affinity chromatography and analysed on Coomassie-stained NativePAGE. Lane 1 = Zera®-gp140, 2 & 4 = NativeMark Unstained Protein Standard, 3 = gp140. The expected molecular weight of trimeric gp140 (***), dimeric gp140 (**) and monomeric gp140 (*) are indicated.

3.3.11 Concentration and quantification of Zera®-gp140 and gp140-Zera® from HEK293 stable cell lines

Purification of Zera®-gp140 and gp140-Zera® by rate zonal ultracentrifugation or isopycnic ultracentrifugation was neither optimal for purification nor scalable (Figure 3.9 and 3.15) to get sufficient amounts to test immunogenicity in rabbits. Thus, a method for concentrating gp140-Zera® and Zera®-gp140 from the cell lysates was devised to get enough Env proteins to test their immunogenicity in rabbits. Instead of passing the lysates through gradients, the lysates were pelleted by ultracentrifugation. The resultant protein pellets were resuspended in PBS. The amounts of gp140 in resuspended protein pellets were estimated by densitometry analysis of gp140-Zera® and Zera®-gp140 run on western blots in parallel with gp140 as a standard (results not shown). Approximately 1.5mg of Zera®-gp140 and 0.6mg gp140-Zera® were obtained from 10x T175 flasks seeded with the respective HEK293 stable cell lines.

3.3.12 Immunogenicity of mammalian-produced gp140-Zera® and Zera®-gp140 in rabbits

The immunogenicity of gp140-Zera® and Zera®-gp140 produced in mammalian cells was evaluated by inoculating two groups of 5 rabbits with approximately 40µg Zera®-tagged gp140 protein at weeks 0, 4, 12 and 20 (Figure 3.18 A).

No adverse effects were observed in rabbits upon inoculations with Zera®-tagged Env immunogens. HIV-1 gp140 binding antibody titres from serum sampled at weeks 4, 8, 12, 14,

16, 20, and 22 were measured in an indirect binding ELISA where SEC-purified gp140 protein was used as the capture antigen (van Diepen *et al.* 2019). The accumulation of antibodies against gp140 in sera from rabbits inoculated with Zera®-gp140 and gp140-Zera® followed a similar trend, where anti-gp140 antibodies increased 2 weeks after each protein boost (weeks 14 and 22) (Figure 3.18 B). The anti-gp140 antibody titres in sera from rabbits inoculated with gp140-Zera® reached maximum titres after four protein inoculations at week 22, while rabbits inoculated with Zera®-gp140 reached maximum titres after the 3rd protein inoculation at week 14. Notably, at weeks 16-22, the anti-gp140 titres in rabbits inoculated with gp140-Zera® were 3 to 6-fold higher than titres observed in rabbits inoculated with Zera®-gp140. Interestingly, the overall anti-gp140 endpoint antibody binding titres elicited in rabbits inoculated with gp140-Zera® were significantly higher than those elicited in rabbits inoculated with Zera®-gp140 protein (* P = 0.0013, Two-Way ANOVA, Bonferroni post-tests).

Results from the RV144 trial showed that binding antibodies to V1V2 of Env correlated to protection against HIV-1 infections (Haynes *et al.* 2012). For this work, the binding antibodies to the autologous scaffolded CAP256 SU V1V2 loop were measured using rabbit sera collected at week 22 (2 weeks after the final protein boosts) (Figure 3.18 C). The anti-V1V2 tires in sera from rabbits inoculated with gp140-Zera® were higher than those observed in sera from rabbits inoculated with Zera®-gp140; however, the difference was not significant (P = 0.2747, unpaired t-test analysis).

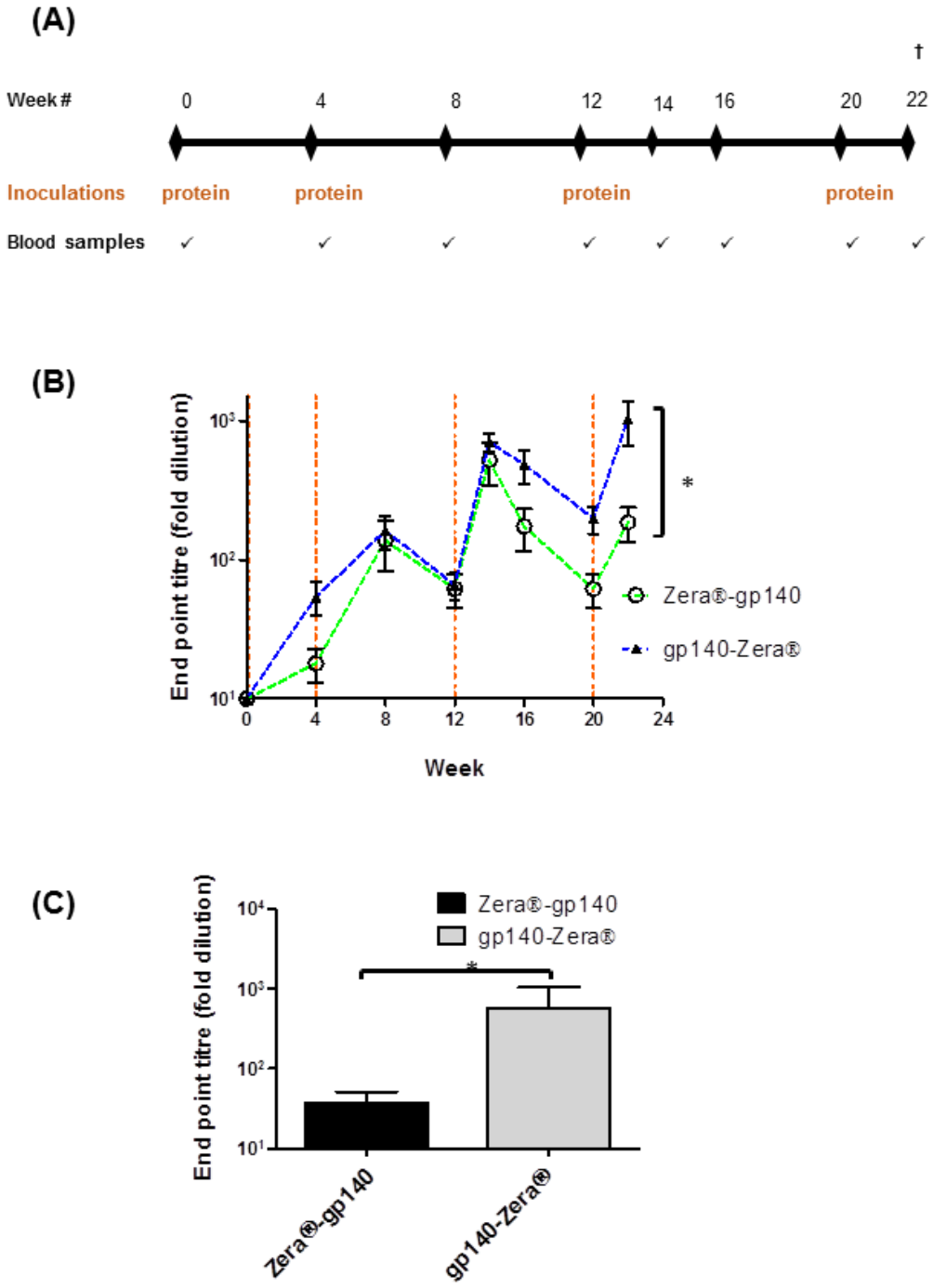

Figure 3.18: Vaccination schedule and serum characterisation. (A) Schematic showing the timing of inoculations of two groups of rabbits with Zera®-gp140 or gp140-Zera® and collection of blood samples (tick marks). **(B)** Anti-Env antibody titres in sera were quantified in an indirect ELISA where the SEC-purified gp140 trimers were used as the capture antigen. The time points for the inoculation of rabbits with proteins are indicated by vertical dotted lines (orange). Error bars indicate the standard deviation within the group at each time point. The *P*-value (* P = 0.0013) between the two groups was calculated by Two-Way ANOVA, Bonferroni post-test. **(C)** Anti-CAP256 V1V2 scaffold endpoint binding titres in sera (week 22) from rabbits inoculated with gp140-Zera® and Zera®-gp140. The P-value (P = 0.2747) was extrapolated from the unpaired t-test analysis.

3.3.13 Neutralisation assays

A TZM-bl assay was used to investigate the neutralising activity of selected sera (weeks 0 and 22) against a small panel of Env-pseudotyped clade C viruses (Figure 3.19). HIV-1 isolates demonstrate a broad spectrum of neutralisation sensitivities: thus, a panel of Env-pseudotyped viruses is categorised into four tier phenotypes (Seaman *et al.* 2010). These are Tier 1A (most sensitive), Tier 1B (second most sensitive), Tier 2 (moderately sensitive, most circulating strains) and Tier 3 (least sensitive). All the rabbits inoculated with gp140-Zera® developed neutralising antibodies against the Malawian Tier 1A pseudovirus (MW965.2) with ID50s ranging between 1:156 and 1:433, compared to only 3/5 of the rabbits vaccinated with Zera®-gp140 (ID50 1:101 to 1:135) (Figure 3.19 A). Rabbits inoculated with gp140-Zera® developed significantly higher neutralising activity against Tier 1A MW9652.2 virus than rabbits inoculated with Zera®-gp140 (Figure 3.19 B). None of the sera from either group neutralised the Tier 1B 6644 or the autologous Tier 2 CAP256SU Env-pseudotyped viruses (Figure 2.19 A).

(A)

		ID50					
		Clade C -Tier 1A		Clade C-Tier 1B		Clade C-Tier 2	
		MW965.26		6644		CAP256SU	
Vaccine	Rabbit ID	week0	week22	week0	week22	week0	week22
gp140-Zera®	RB #31	<40	165	<40	<40	<40	<40
	RB #32	<40	156	<40	<40	<40	<40
	RB #33	<40	433	<40	<40	<40	<40
	RB #34	<40	244	<40	<40	<40	<40
	RB #35	<40	305	<40	<40	<40	<40
Zera®-gp140	RB #A	<40	135	<40	<40	<40	<40
	RB #B	<40	<40	<40	<40	<40	<40
	RB #C	<40	<40	<40	<40	<40	<40
	RB #D	<40	101	<40	<40	<40	<40
	RB #E	<40	199	<40	<40	<40	<40

50% neutralisation titre
<40
40-200
200-500

(B)

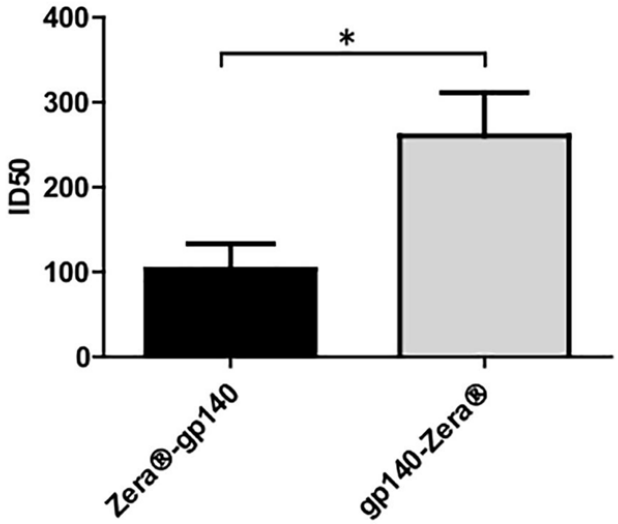

Figure 3.19: Neutralising antibody titres elicited in rabbits vaccinated with gp140-Zera® and Zera®-gp140. (A) The neutralising activity of sera collected before (week 0) and after inoculation with four doses of gp140-Zera® or Zera®-gp140 (week 22) was assayed against a small panel of Clade C pseudoviruses. Virus neutralisation was represented as the reciprocal of sera dilutions required to achieve 50% reduction of viral entry into TZM-bl cells (ID50). **(B)** Tier 1 A MW965.26 neutralisation titres in sera from rabbits inoculated with gp140-Zera® and Zera®-gp140. The P-value (P = 0.0288) was extrapolated from the unpaired t-test analysis.

3.4 Discussion

We previously compared the development of binding and neutralising antibodies in rabbits inoculated with the soluble HIV-1 CAP256 gp140 formulated in AlhydroGel® and AddaVax® adjuvants (van Diepen *et al.* 2018). This follow-up study was designed to evaluate

whether self-assembling protein nanoparticles (protein bodies) encapsulating CAP256 gp140 could improve the immunogenicity of the glycoprotein. We evaluated the production of protein bodies (PBs) by fusing the sequence encoding Zera®, a proline-rich domain derived from the γ-zein storage protein, to either the C- or N-terminus of HIV-1 CAP256 gp140. To our knowledge, this is the first time the possibility of formation of protein bodies encapsulating HIV Env has been explored in mammalian expression systems, and this is the largest glycoprotein (±140 kDa) to be fused to Zera® as it is larger than the ectodomain of influenza A virus subtype 5 HA (±75 kDa) previously fused by others (Hofbauer *et al.* 2016).

The ability of gp140-Zera® and Zera®-gp140 to form PBs in mammalian cells was compared to Zera®-eGFP, which has previously been shown to form PBs (Torrent *et al.* 2009a; Saberianfar *et al.* 2016). Immunofluorescent staining and confocal microscopy of HeLa cells expressing gp140-Zera® and Zera®-gp140 indicated that gp140-Zera® formed comparatively smaller and fewer spherical PB-like structures than Zera®-eGFP, which was solely expressed as distinct PBs. In cells expressing Zera®-gp140, Env appeared diffused in cells without any observable PB-like structures. Negative-stain electron microscopy of thin sections from transiently transfected HEK293T cells also indicated that gp140-Zera® formed PB-like structures which were not detected in cells expressing Zera®-gp140 or gp140.

Previous studies indicated that zein-derived sequences fused to either the C- or N-terminus of the protein of interest induced the formation of PBs in a wide spectrum of eukaryotic expression systems (de Virgilio *et al.* 2008; Torrent *et al.* 2009a; Joseph *et al.* 2012; Whitehead *et al.* 2014; Hofbauer *et al.* 2016). In this study, Zera® was also fused on the C-terminus of gp140 to form gp140-Zera® because it was reasoned that this would not occlude the gp120 subunits which contain important epitopes for eliciting antibodies. Even though gp140-Zera® appeared to form some small PB-like structures in transiently transfected cells, expression of gp140-Zera® was lower than Zera®-gp140 in both mammalian and plant expression systems. This pattern was also observed by de Virgilio *et al.* (2008) who showed that expression levels of zein-Nef were higher than Nef-zein, which was barely detectable, indicating that the location of Zera® can affect protein accumulation. Additionally, the complexity and large size of HIV Env may have hindered the optimal formation of Zera®-induced nanoparticles. He *et al.* (2016) showed that when gp140 was fused to the 60-meric lumazine synthase (LS), nanoparticles were not formed. They reasoned that the large size and spacing of Env antigens could limit its display on self-assembling nanoparticles (He *et al.* 2016). It is also possible that the protein bodies formed with gp140-Zera® are too labile and are broken up during extraction. To our knowledge, the largest Zera®-fusion protein that has been shown to form protein bodies is the ±75 kDa influenza H5 (Hofbauer *et al.* 2016)

The inability to detect PBs in mammalian-produced Zera®-gp140 is consistent with some of the studies from the literature that indicated that not all proteins fused to zein-derived sequences are able to assemble into PBs. For example, the HIV negative factor (Nef) protein fused to the γ-zein domain (zein-Nef) did not form PBs in plants since it was rapidly degraded in the ER. On the other hand, PBs stably encapsulating Nef were formed when Nef was fused to zeolin, a chimaeric domain composed of the γ-zein (same sequence used for zein-Nef) as well as the bean vascuolar storage protein phaseolin (Mainieri *et al.* 2004; de Virgilio *et al.* 2008). The authors reasoned that unlike the correctly folded zeolin-Nef, zein-Nef may have been recognised by the ER quality control machinery as a structurally defective protein and was thus directed to the degradation pathway in the ER before being able to assemble into PBs. This suggested that regardless of the presence of zein-derived sequences, if the fusion protein is misfolded, zein sequences do not facilitate an escape from ER-associated degradation (ERAD). Therefore, misfolded zein-Nef did not accumulate to levels sufficient for assembly into otherwise physiologically inert PBs. The misfolding of zein-Nef was thought to be due to the formation of aberrant disulphide bonds between 3 Cys residues in the Nef sequence with 6 Cys residues of zein sequence in the ER (de Virgilio *et al.* 2008). A number of different reports have shown that HIV-1 Env proteins can contain aberrant disulphide bonds which lead to the misfolding and aggregation of the protein (Klasse *et al.* 2013; Ringe *et al.* 2013; Go *et al.* 2015).

The folding of Zera®-tagged gp140 proteins was not assessed; however, the failure to form Zera®-gp140 PBs might also be due to the formation of aberrant disulphide bridges between Zera® and gp140 Cys residues. Site-directed mutagenesis of individual cysteine residues of Zera® indicated that in addition to the amphipathic $(PPPVHL)_8$ repeat of Zera®, the six cysteine residues flanking this repeat are required for disulphide cross-linking of Zera® sequences during oligomerisation into PBs (Llop-Tous *et al.* 2010). There are 18 cysteine residues in HIV-1 CAP256 gp140 which in the ER, could potentially form aberrant disulphide bonds as a result of isomerisation with the cysteine residues of Zera®, thus forming misfolded protein and inhibiting the multimerisation into PBs or trimers. Such misfolding is more likely for Zera®-gp140 than gp140-Zera® where no flexible linker was included between Zera® and gp140 sequences to allow for independent but cooperative folding. In comparison to well-folded native-like trimers, non-native gp140 trimers were reported to contain a substantial proportion of aberrant disulphide bonds (Go *et al.* 2015). Thus, we reasoned that if aberrant disulphide bond formation is a common occurrence for recombinant gp140 proteins, fusion to the Cys-rich Zera® coding sequence would probably exacerbate this phenomenon.

Ceresoli *et al.* (2016) reported another case where zein-tagged recombinant human bone morphogenetic protein 2 active dimers (zein-rhBMP2ad) accumulated at higher levels than

the native soluble protein (hBMP2nat) but failed to induce PBs. The authors did not think the failure to form PBs was due to misfolding that could be caused by the possible aberrant disulphide bridges (hBMP2ad contains 7 Cys residues). Instead, they reasoned it might have been due to *N*-glycosylation that increased the solubility of rhBMP2ad and prevented PB formation (Ceresoli *et al.* 2016). Similarly, gp140 contains ≈28 *N*-glycosylation sites which could favour solubility of the Zera®-tagged gp140, thus preventing optimal assembly into PBs.

It is also possible that in our case, the concentration of gp140 may not have been sufficient to drive the formation of PBs. Saberianfar *et al.* (2015) have reported that the fusion of GFP to other PB-inducing tags, hydrophobin-I and elastin-like polypeptides, indicated that the formation of protein bodies is a concentration-dependent mechanism where the accumulation of GFP to a minimum of 0.2% of the total soluble protein (TSP) was required for oligomerisation into PBs. The size of these PBs simultaneously increased over time with an increase in protein concentration. Interestingly, it was also observed that if GFP accumulated to a value higher than 6.5% of the TSP, PB-like structures were observed regardless of the presence or absence of the PB-inducing fusion tags (Gutierrez *et al.* 2013; Saberianfar *et al.* 2015). Unlike other proteins that have been fused to PB-inducing tags, gp140 is a complex protein that is difficult to express, and it is possible that it might not have reached the threshold concentration required for optimal assembly into PBs.

Previous studies have shown that zein-derived domains induce the formation of electron-dense PBs with a diameter of 0.5–2 μm which settle at a density of approximately 1.18–1.26 g/ml during subcellular fractionation of a density gradient, thus allowing for simple protein recovery using rate zonal or isopycnic density ultracentrifugation (Mainieri *et al.* 2004; Torrent *et al.* 2009b). In theory, if Zera®-tagged gp140 is encapsulated in PBs, it would be expected to be denser than the soluble gp140. However, Zera®-gp140 and gp140-Zera® were predominantly detected in fractions with densities ranging from 1.1 to 1.13 g/ml. These densities are lower than 1.18–1.26 g/ml reported by Torrent *et al.* (2009a). Gp140-Zera® and Zera®-gp140 fractionated at densities similar to the approximate OptiPrep™ density range for the ER, which corresponds well with the observed co-localisation of these proteins with calnexin. These results are in accordance with a previous study which showed that, unlike zeolin-Nef that formed PBs, zein-Nef did not efficiently form PBs and could not be distinguished from the ER (de Virgilio *et al.* 2008). Zein-rhBMP2ad also did not form protein bodies but was retained in the ER (Ceresoli *et al.* 2016). Our findings present another case where Zera®-tagged gp140 did not efficiently form PBs but was associated with the ER, thereby separating and settling in fractions of densities previously noted where ER membrane fragment settles. As the species of Zera®-tagged gp140 protein spanned a large range of different sizes/densities, it was not feasible to take advantage of the high-density properties

inherent to PBs for large scale protein preparations by rate zonal and isopycnic ultracentrifugation. As a result, Zera®-tagged proteins produced in stable HEK293 cell lines were concentrated by pelleting of cell lysates by ultracentrifugation to provide sufficient amounts for immunogenicity studies.

The immunogenicity of mammalian-produced Zera®-gp140 and gp140-Zera® was tested in rabbits to evaluate the adjuvant activity of Zera®. Both proteins elicited high titres of HIV-1 Env binding antibodies of similar levels after 3 immunisations but rabbits vaccinated with gp140-Zera® had significantly higher titres than those vaccinated with Zera®-gp140 after 4 immunisations. Sera from rabbits inoculated with Zera®-gp140 and gp140-Zera® showed equivalent binding titres to the CAP256 V1V2 scaffold antigen. Zera®-tagged gp140 elicited V1V2 titres similar to those observed in historical sera from rabbits inoculated with gp140 (van Diepen *et al.* 2018). This indicated that the presence of Zera® did not occlude gp140 epitopes responsible for triggering V1V2-specific responses. The V1V2 binding antibodies are of particular relevance in the context of vaccine development because they correlated with protection against HIV acquisition in the RV144 trial (Haynes *et al.* 2012). It would be interesting to evaluate the Fc-mediated effector functions such as antibody-dependent cellular cytotoxicity (ADCC) of these antibodies, the secondary correlate of protection in the RV144 trial (Haynes *et al.* 2012).

One of the goals of HIV vaccine research is to design immunogens that elicit antibodies that potently neutralise a broad range of Tier 2 circulating viruses. In a luciferase reporter gene neutralisation assay, sera from rabbits inoculated with g140-Zera® elicited significantly higher Tier 1A neutralising antibodies than sera from rabbits inoculated with Zera®-gp140. However, neither protein elicited Tier 1B or autologous Tier 2 neutralising antibodies which may be explained by limited amounts of conformationally appropriate gp140. H5-zein (Hofbauer *et al.* 2016) and the plant-produced monomeric HA fused to ELP (H5-ELP) failed to elicit neutralising antibodies, but NAbs were elicited when H5-ELP was stabilised into trimers by the addition of the GCN4-pII isoleucine-zipper trimerisation motif directly downstream of the H5 ectodomain (Harbury *et al.* 1993; Phan *et al.* 2013). Likewise, proper trimerisation of HIV Env is mandatory to yield native-like trimers that assume a conformation that optimally present epitopes for induction of Tier 2-neutralising antibodies (Sanders *et al.* 2015; de Taeye *et al.* 2016; Sanders & Moore. 2017). Additionally, the chances of eliciting good neutralisation responses could be improved by selectively using trimeric Env separated from aggregates, dimeric and monomeric Env species using size exclusion chromatography. However, during assembly into PBs, there is no way of ensuring that monomeric, dimeric and aggregated Env species are not encapsulated together with trimeric Env.

The inability to control the quality of Env or of nanoparticles can be a drawback of the use of *in vivo*-assembling protein nanoparticles. However, this can be overcome by using two-component platforms where native-like trimeric Env and nanoparticles (such as liposomes, I53 50, SpyCatcher-AP205 or SpyCatcher-mi3) are expressed and purified separately and then assembled *in vitro* (Ingale *et al.* 2016; Bale *et al.* 2017; Bruun *et al.* 2018; Brinkkemper & Sliepen. 2019; Brouwer *et al.* 2019; Brouwer & Sanders. 2019; Escolano *et al.* 2019; Cohen *et al.* 2020).

In conclusion, this was an exploratory study to assess whether we could take advantage of the beneficial properties of Zera® protein bodies for the HIV-1 envelope glycoprotein. A considerable number of assays were done to evaluate the formation of HIV Env PBs in mammalian cells and plant leaves. However, our results indicated that Zera® did not efficiently form PBs when fused to the HIV-1 gp140 protein. Despite this, this study has shown that mammalian cell-produced HIV-1 envelope proteins, tagged with Zera® at the N and C termini, elicited high titres of gp140 and V1V2 binding antibodies in rabbits. In addition, both gp140-Zera® and Zera®-gp140 elicited low levels of Tier 1 neutralising antibodies. Further studies need to be carried out to determine whether these antibodies have Fc-mediated effector functions.

CHAPTER 4: DEVELOPMENT OF A SYNTHETIC NANOPARTICLE VACCINE PRESENTING THE HIV-1 ENVELOPE GLYCOPROTEIN

4.1 Introduction

This project aimed at improving the presentation/delivery of immunogens for eliciting broadly neutralising antibodies (bNAbs) capable of neutralising Tier 2 viruses. The HIV-1 envelope is a major focus of prophylactic HIV vaccine development. However, unusually low and widely spaced incorporation of Env spikes on the virion (≈14 spikes/virion) is unfavourable for eliciting high titre, long-lasting antibody responses (Zhu *et al.* 2006; Klein & Bjorkman. 2010; Schiller & Chackerian. 2014).

The development of the soluble native-like gp140 trimers, such as those stabilised by the cleavage-dependent SOSIP.644 (Sanders *et al.* 2013) or the cleavage-independent native flexibly linked (NFL) modifications (Sharma *et al.* 2015), was a significant breakthrough in immunogen designs for induction of HIV-1 bNAbs. However, the SOSIP- or NFL-stabilised gp140 trimers formulated in strong adjuvants failed to induce substantial levels of heterologous Tier 2 bNAbs (Crooks *et al.* 2015; Sanders *et al.* 2015; Pauthner *et al.* 2017; Saunders *et al.* 2017) but were shown to elicit high titres of short-lived autologous Tier 2 neutralising antibodies in animal models (Sanders *et al.* 2015; Cheng *et al.* 2016; Feng *et al.* 2016; Klasse *et al.* 2016; Pauthner *et al.* 2017; van Diepen *et al.* 2019). Multimerisation of soluble antigens on nanoparticles, virus-like particles (VLPs) and liposomes can be used to improve immunogenicity. The large size (20-200nm) of these particulate vaccines promotes direct drainage to the lymph nodes, and the repetitive arrangements of antigens promotes the cross-linking of B-cell receptors to induce robust and durable antibody responses (Jennings & Bachmann. 2008; Bachmann & Jennings. 2010; Gomes *et al.* 2017; Schiller & Lowy. 2018). The success of the licenced VLP-based vaccines against hepatitis B virus, human papillomavirus and hepatitis E virus which induce high titre, durable neutralising antibody responses lends support to this strategy (Zhao *et al.* 2013). However, increasing the density of the HIV-1 Env glycoprotein on nanoparticles or VLPs is a challenge that needs to be overcome to elicit durable antibody responses (Schiller & Chackerian. 2014; Brinkkemper & Sliepen. 2019; Brouwer & Sanders. 2019).

HIV-1 Env trimers presented on *in vivo*-assembling ferritin nanoparticles and VLPs have been shown to increase Env display and elicit higher autologous Tier 2 neutralising antibodies compared to soluble trimers (Deml *et al.* 1997; Wang *et al.* 2007; Visciano *et al.* 2011; Sliepen *et al.* 2015; He *et al.* 2016; Vzorov *et al.* 2016; He *et al.* 2018). However, as these nanoparticles are assembled intracellularly, misfolded and non-native forms of Env have been shown to be presented on the surface of the particles (Moore *et al.* 2006; Brinkkemper & Sliepen. 2019; Brouwer & Sanders. 2019; Sliepen *et al.* 2019). Contrary to *in vivo*-assembling nanoparticles, *in vitro*-assembling nanoparticles, including liposomes (Ingale *et al.* 2016; Bale *et al.* 2017),

are ideal for the presentation of HIV-1 Env because they are a modular system that allows for quality control of both the Env trimers and the nanoparticle scaffolds as they can be produced and purified separately prior to assembly. The two components can then be combined to generate nanoparticles displaying a majority of well-folded Env trimers (Brinkkemper & Sliepen. 2019; Brouwer & Sanders. 2019). However, using conventional methods such as chemical conjugation to link the antigens to nanoparticles may impair nanoparticle assembly and affect the conformation of complex glycoproteins (Smith *et al.* 2013; Brune *et al.* 2016; Mateu. 2016). More recently, other technologies for linking antigens to nanoparticles have been developed that do not compromise the structure of the antigen (Brinkkemper & Sliepen. 2019; Brouwer *et al.* 2019; Brouwer & Sanders. 2019; Escolano *et al.* 2019; Aves *et al.* 2020).

SpyTag-SpyCatcher is one of these technologies (Brune *et al.* 2016; Aves *et al.* 2020). This is derived from the second immunoglobulin-like collagen adhesion domain (CnaB2) found in the fibronectin-binding protein of *Streptococcus pyogens* (Spy) (Kang *et al.* 2007; Hagan *et al.* 2010; Kang & Baker. 2011). Splitting the CnaB2 domain into rationally designed SpyTag peptide (13 amino acids) and SpyCatcher protein (116 amino acids), generated reactive partners that upon mixing under a wide range of physiological conditions, spontaneously form an irreversible isopeptide bond (Zakeri *et al.* 2012; Li *et al.* 2014). SpyCatcher-AP205 VLPs formed by assembly of AP205 coat proteins fused to SpyCatcher have been successfully used to display various SpyTagged antigens including malaria vaccine candidates (Brune *et al.* 2016; Thrane *et al.* 2016; Leneghan *et al.* 2017; Palladini *et al.* 2018; Yenkoidiok-Douti *et al.* 2019), complex glycoproteins such as influenza hemagglutinin (HA) trimers (Cohen *et al.* 2021b) and glycan-modified HIV-1 trimers designed to engage V3-specific bNAb precursors (Escolano *et al.* 2019).

In this study, flexibly linked HIV-1 gp140 trimers containing C-terminal SpyTags, were conjugated to SpyCatcher-AP205 VLPs to investigate the suitability of the system for displaying a high density of trimeric HIV-1 gp140.

4.2 Material and methods

4.2.1 Design, synthesis and generation of mammalian plasmids that express gp140-SpyTag or gp140-SpyCatcher

The SpyTag (ST) (GenBank accession number: KJ906520) or SpyCatcher (SC) (GenBank accession number: JQ478411) sequences with the flexible-linker (FL; GGSGGGGSGG) fused to the 5' end was human codon-optimised, synthesised by GenScript and assembled into a pUC57 vector. To generate mammalian plasmids expressing HIV gp140 with a C-terminal SpyTag or SpyCatcher, the sequence coding for the SpyTag or SpyCatcher appended with a flexible-linker (FL) on its 5' end was inserted between the NotI and EcoRI sites of pMExT

CAP256 gp140-FL-IP (van Diepen *et al.* 2018) to generate pMExT CAP256 gp140-SpyTag or pMExT CAP256 gp140-SpyCatcher, respectively (Figure 4.1). The pMExT CAP256 gp140-SpyTag plasmid was confirmed by PCR screening using CGP120-F4 (5' ATGTGGCAGGAAGTGGGC 3') and SpyTagR (5' CTTGGTGGGCTTGTAGGC 3') primers while the pMExT gp140-SpyCatcher plasmid was confirmed by PCR screening with CatcherF (5' GGCGCCATGGTGGACACC 3') and pMEx-R (5' CAAACAACAGATGGCTGG 3') primers. Restriction analysis with NotI and EcoRI and sequencing were used to verify these plasmids further.

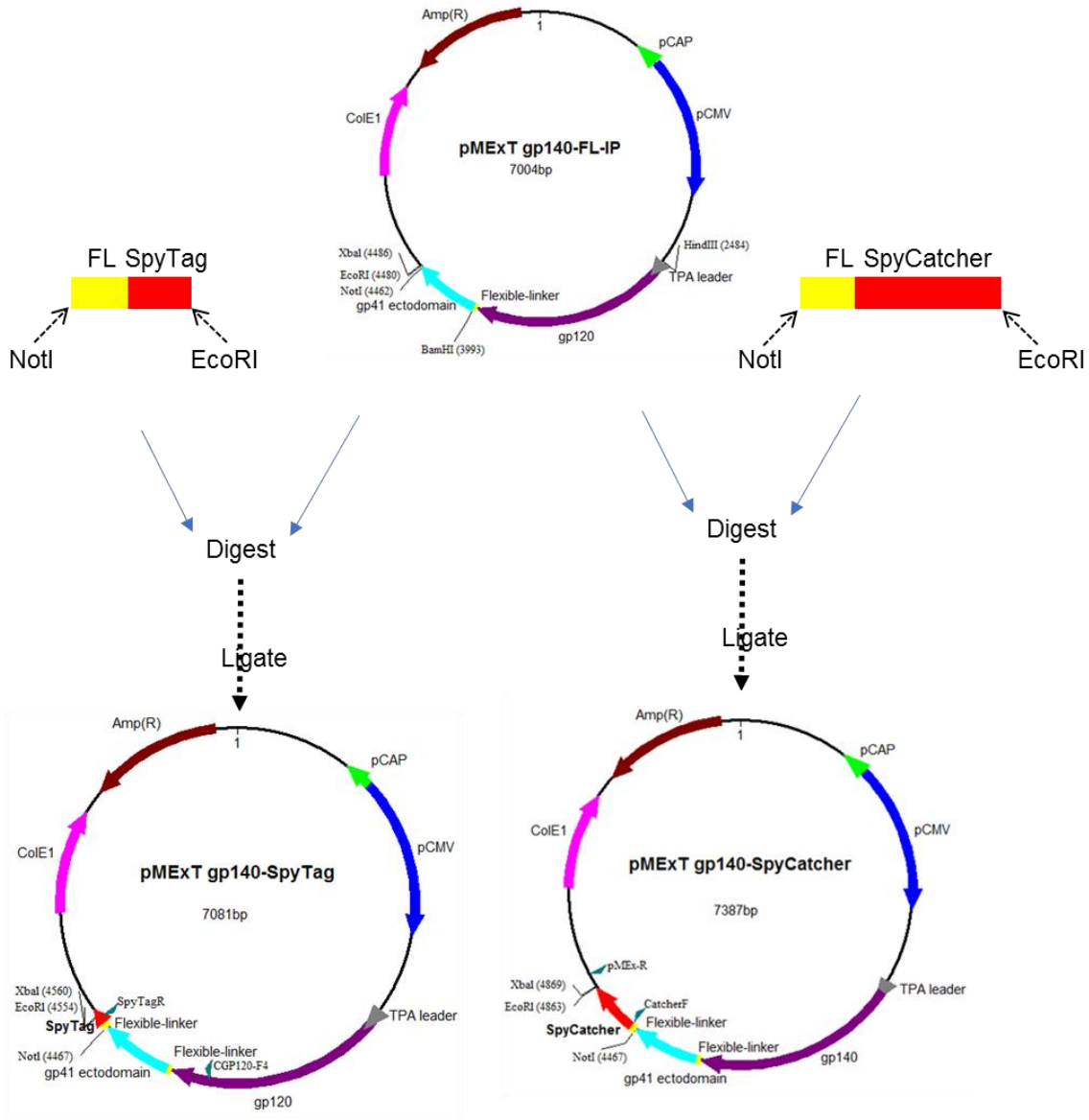

Figure 4.1: Annotated plasmid maps showing the construction of mammalian expression vectors encoding gp140-SpyTag and gp140-SpyCatcher. pCAP = porcine circovirus enhancer element; pCMV = cytomegalovirus promoter; ColE1 = *E. coli* plasmid origin of replication; Amp(R) = ampicillin resistance; FL = flexible linker and TPA = human tissue plasminogen activator leader.

4.2.2 Construction of plasmids with IRES-Neomycin cassette and generation of stable HEK293 cell lines expressing gp140-ST or gp140-SC

Plasmids for generating stable cell lines were constructed using the Xbal and EcoRI restriction sites to introduce an IRES-Neomycin (Neo) resistance cassette directly downstream of SpyTag or SpyCatcher sequences in plasmid pMExT gp140-SpyTag or pMExT CAP256 gp140-SpyCatcher, respectively. The resulting pMExT gp140-SpyTag-IRES-Neo and pMExT gp140-SpyCatcher-IRES-Neo plasmids (the maps are shown in Section 4.3.2, Figure 4.3) were transfected into HEK293 cells and passaged at least ten times in complete medium with 300µg/ml geneticin (Gibco™, ThermoFisher Scientific) selection. The expression of gp140-SpyTag (gp140-ST) or gp140-SpyCatcher (gp140-SC) in stable cell lines was confirmed by western blotting.

4.2.3 Large-scale production and purification of gp140-ST or gp140-SC proteins

Stable HEK293 cells (passage 12-15) expressing gp140-ST or gp140-SC from 12xT175 confluent flasks were transferred into 3x Hyperflasks (i.e. cells from 4xT175 flasks were seeded into a single Hyperflask). Seeded cells were grown to almost 80% confluence in the presence of DMEM-P/S supplemented with 10% FCS. At 80% confluency, the medium was switched to FCS-free DMEM-P/S to minimise contamination with alpha-2-macroglobulin (725 kDa tetrameric glycoprotein present in FCS). Three days post-medium change, the medium was harvested gently, and cells were further cultured in alternating DMEM-P/S+10% FCS and FCS-free conditions for repeat protein harvests (3-4 cycles). Harvested media were subjected to a low-speed clarification spin (Allegra™ X-22R centrifuge, 433 x *g*, 5min, 4°C). The clarified media were then pumped through a *Galanthus nivalis* lectin affinity column (Sigma, 1ml) using a steric pump. The column was washed with 0.5M NaCl-PBS followed by PBS only. Env protein was eluted by slowly passing through 50ml of 1M methyl α-D-manno-pyranoside (MMP) (Sigma) prepared in PBS. An aliquot (100µl) of the eluate was plated on antibiotic-free Luria agar and incubated at 37°C to evaluate for potential bacterial contamination. The remaining contaminant-free eluate was subsequently concentrated and buffer exchanged into ≈5.5ml PBS using Vivaspin® 20 Protein Concentrator spin columns with a 100kDa cut-off (GE Healthcare). The concentrated eluate was fractionated by size exclusion chromatography (SEC) using a Superdex 200 HiLoad 16/600 column (GE Healthcare). Native PAGE electrophoresis (NativePAGE™ Noverex® 3-12% Bis-Tris gels, Life Technologies) and Coomassie staining (Bio-Rad) of the lectin- and SEC-purified fractions were conducted to assess their oligomeric structures. The NativeMark™ unstained protein standard (20-1200 kDa) (Life Technologies) was included to estimate the molecular weights of gp140-ST or gp140-SC under native PAGE conditions. SEC fractions containing trimeric Env were either pooled, aliquoted and stored at -80°C or further concentrated using Vivaspin® 20 Protein

Concentrator spin columns with a 100kDa cut-off (GE Healthcare) before being aliquoted and stored at -80°C.

4.2.4 Quantification of SEC-purified gp140-ST or gp140-SC

The *DC*™ protein microplate assay (Bio-Rad) was used to determine the concentrations of the SEC-purified gp140-ST and gp140-SC trimers. Briefly, 5µl of 2-fold serial diluted (0.05-1.6 mg/ml) bovine serum albumin (BSA) in PBS, SEC-purified gp140-ST and gp140-SC experimental samples and the PBS-only blank were pipetted into a 96-well Maxisorb® microtitre ELISA plates (Nunc). Each standard or experimental sample was assayed in triplicate. Reagents A' (25µ/well) and B (200µ/well) were added to standards and experimental samples before incubation in the dark at RT for 15 minutes. The absorbance signals at 750 nm were measured using a VersaMax ELISA Microplate Reader (Molecular Devices, Sunnyvale). The equation extrapolated from a standard curve (absorbance vs BSA concentrations) was then used to determine gp140-ST and gp140-SC trimer concentrations.

4.2.5 Plasmid design and expression of SpyTag-AP205 and SpyCatcher-AP205 in *E. coli*

The pET15b plasmids encoding the SpyCatcher (SC) or SpyTag (ST) fused upstream of the *Acinetobacter* phage AP205 coat protein (CP3) coding sequence, SC-AP205 and ST-AP205 respectively, were a kind gift from Christoph M. Janitzek (Centre of Medical Parasitology, University of Copenhagen) (Thrane *et al.* 2016). It is important to note that pET15b-SpyTag-AP205 contained a longer flexible linker (GSGTAGGGSGS) between the SpyTag and AP205 coding sequences, while pET15b-SpyCatcher-AP205 contained a shorter flexible linker (GGSGS) between the SpyCatcher and AP205 coat protein-coding sequences.

SC-AP205 or ST-AP205 fusion proteins that assemble into icosahedral VLPs with 180 binding sites (abbreviated to SC-VLPs or ST-VLPs) were prepared as previously described (Thrane *et al.* 2016). Briefly, pET15b-SpyCatcher-AP205 or pET15b-SpyTag-AP205 plasmid was transformed into competent BL21-CodonPlus (DE3)-RIL cells (Agilent Technologies, Inc.). Transformations were plated on ampicillin (100µg/ml)-containing agar plates and incubated overnight at 37°C. Recombinant BL21 clones were inoculated into 12.5ml of 2xYT media (16g/L tryptone, 10g/L yeast extract and 5g/L NaCl in distilled water) containing 100µg/ml ampicillin and incubated overnight at 37°C with shaking. The aliquots (4ml) of the starter cultures were subcultured into 400ml of 2xYT+ ampicillin media at 37°C with shaking. When the optical density at 600nm (OD600) of the cultures reached 0.5-0.8, cultures were cooled at RT for 20 minutes before induction with 1mM Isopropylthiogalactose (IPTG, Sigma) and further incubation overnight at RT on an orbital shaker (150 rpm). The overnight cultures were

spun down (SLA-3000, 10000 *x g*, 10min, 4°C), and the bacterial pellets were frozen at -20°C or processed immediately for protein purification.

4.2.6 Preparation of lysates and purification of SC-VLPs or ST-VLPs by ultracentrifugation

The bacterial pellets in Section 4.2.5 were each resuspended in 20ml 1xPBS and lysed by sonication (80% power for 10 minutes on ice [pulse on time (2 minutes) and pulse off time (2 minutes)] using the Qsonica sonicator. The lysate was clarified by centrifugation (SS34, 40 000 *x g*, 30min, 4°C). The clarified lysates (≈2ml/centrifuge tube) were overlaid on OptiPrep™ step (1ml/sep) gradients (23, 29 and 35% in PBS) in ultra-Clear™ 13x51mm centrifuge tubes (Beckman Coulter). Gradients were subjected to rate zonal ultracentrifugation (SW55Ti, 302986 *x g*, 3.3 hours, 16°C) using a Beckman-Coulter Optima L-100 XP ultracentrifuge. Following ultracentrifugation, gradients were manually fractionated by punching a hole in the bottom of the tube and slowly collecting ≈200µl fractions. Fractions were analysed by SDS-PAGE and stained with Coomassie. VLP-containing fractions were pooled and aggregates were removed by low-speed centrifugation (16 000 x *g*, 2 min, 16°C). VLPs were stored at -80°C as 200-500µl aliquots.

4.2.7 Negative-stain electron microscopy

Carbon-coated copper grids were made hydrophilic by glow discharging at 25mA for ≈30 seconds using a Model 900 SmartSet Cold stage controller. Grids were floated on SC-VLPs or ST-VLPs (10-15µ), washed 4x in distilled water and negatively stained with 2% uranyl acetate. Grids were imaged on an FEI T20 transmission electron microscope.

4.2.8 Quantification of SC-AP205 and ST-AP205 VLPs by densitometry

The concentrations of the purified SC-AP205 and ST-AP205 VLPs were estimated by densitometric analysis of samples run on SDS-polyacrylamide gels in parallel with 2-fold serially diluted (0.025-0.1mg/ml) soy-bean trypsin inhibitor (SBTI, (Sigma-Aldrich) standards in PBS. Gels were stained with Coomassie, and the band intensities were measured using the Molecular Imager® Gel Doc™ XR and imaging system software (Bio-Rad). The concentrations of SC-VLPs and ST-VLPs were determined from the equation obtained from the standard curve (band intensity on Coomassie-stained SDS-polyacrylamide gel compared with against SBTI band intensities and corresponding concentrations).

4.2.9 Optimisation and characterisation of coupling reactions between HIV-1 gp140 and AP205 VLPs

To evaluate the coupling of gp140 to AP205 VLPs through the formation of an isopeptide bond between the SpyTag and SpyCatcher, gp140-ST was mixed with SC-AP205 VLPs in the

presence of a 1x (diluted from a 10x stock) coupling buffer (0.05M MES, 0.5M NaCl, 2.7mM KCl, 1.8mM KH2PO4, 10mM Na2HPO4, pH 6.4) overnight at 4°C. Env and VLPs were mixed at different molar ratios to optimise the coupling conditions. Coupling reactions were analysed on denaturing SDS-PAGE or 4–15% Criterion™ TGX™ (Tris-Glycine eXtended) precast gradient gels (Bio-Rad) followed by staining with Coomassie or western blotting with the anti-Env antibody. Coupling reactions were also separated on 1% SeaKem ® LE agarose (Lonza) gels prepared in a standard Tris-acetate-EDTA (TAE) buffer and stained with ethidium bromide (Sigma).

The coupled SC-AP205 VLPs were negatively stained with uranyl acetate and visualised with electron microscopy as described in Section 4.2.7.

The average VLP size (hydrodynamic diameter) distribution of the uncoupled and gp140-coupled SC-AP205 VLPs was determined by Dynamic Light Scattering (DSL) using a Zetasizer Nano-S ZEN1600 (Malvern Instruments, Worcestershire, UK) in a service conducted at the Afrigen Biologics and Vaccines (Longclaw Drive, Montague Gardens, Cape Town). Briefly, 10 µl of each VLP sample was dispersed into 990 µl of WFI (Water for Injection). The intensity distribution was measured for each sample and plotted against the average particle size diameter.

4.2.10 Immunisation of rabbits with AP205-gp140-ST VLPs

Rabbit inoculations and blood sampling were performed at the University of Cape Town Research Animal Facility according to the guidelines and approval of the University of Cape Town Animal Ethics Committee (AEC 015-51 and AEC 019-015). The SC-VLPs were mixed with gp140-ST (adjusted accordingly to ensure each rabbit received 40µg of gp140-ST) at 1:1.5 SC-VLP to gp140 molar ratios in a coupling buffer overnight at 4°C. The volume of resulting AP205-gp140-ST particles was adjusted in PBS so that each rabbit received a total volume of 500µl of vaccine during immunisations. Two groups of five female New Zealand White rabbits were used to compare the immunogenicity of AP205-gp140-ST particles in two regimens. Group one (PPPP) rabbits were injected intramuscularly in the hind leg with AP205-gp140-ST VLPs (P) at weeks 0, 4, 12 and 20. Group two (DDMMPP) was primed with DNA vaccines (D; 100µg of pTJDNA4 mixed with 100µg pMExT CAP256 gp140-FL-IP) at weeks 0 and 4, followed by rMVA Env+Gag^{M} (M; 10^{8} PFU) at weeks 8 and 12, and then boosted with AP205-gp140-ST particles at weeks 20 and 28 (van Diepen *et al.* 2019). DNA and MVA vaccines were administered intramuscularly in the hind leg of each rabbit. Blood samples were collected at week 0 (pre-immune) and then two weeks post each inoculation.

4.2.11 Quantification of gp140 binding antibodies

Antibody binding end-point titres in rabbit sera were determined as described in Section 3.2.13.

4.2.12 Quantification of neutralisation of Env-pseudotyped viruses

HIV-1 neutralisation antibody titres in sera from immunised animals were determined using a standardised pseudovirus assay as previously described in Section 3.2.14.

4.2.13 Further optimisation of coupling reactions between gp140-ST and SC-AP205 VLPs

The autologous Tier 2 neutralising antibody titres elicited by gp140 displayed on VLPs (SC-AP205 VLPs + gp140-ST) were lower than the neutralising antibody titres elicited by the soluble gp140 used in our previous experiment (van Diepen *et al.* 2019). This was not expected and indicated that displaying gp140 on AP205 VLPs did not improve the immunogenicity of gp140. The poor induction of neutralising antibodies by the SC-AP205 VLPs + gp140-ST admixture necessitated further characterisation of the coupling reactions. In an effort to determine whether the immunogenicity experiment should be repeated, further characterisation was done to 1) confirm the optimal SC-AP205 VLP to gp140-ST molar coupling ratios and also evaluate the coupling efficiency, 2) ensure that any free/excess gp140-ST protein was removed from the AP205-gp140-ST VLPs after coupling.

Considering that the native agarose gel and SDS-PAGE analyses were not sensitive enough to distinguish between gp140-ST coupled to SC-AP205 VLPs and free/excess gp140-ST in the coupling reaction, a new analysis approach was attempted to estimate the coupling efficiency. The new method included deglycosylation of the coupling reaction samples before SDS-PAGE. To achieve deglycosylation, peptide-N-glycosidase F (PNGase F) (Biolabs, New England), which removes N-linked glycans from glycoproteins, was used. After allowing different molar concentrations of gp140-ST to react with constant molar concentrations of SC-AP205 VLPs overnight at 4 °C, enzymatic deglycosylation with PNGase F under denaturing conditions was performed according to the manufacturer's (Biolabs, New England) recommendations. Glycosylated or deglycosylated samples were analysed by SDS-PAGE and stained with Coomassie or transferred to PVDF membrane for western blotting.

4.2.14 Separation of uncoupled gp140 from coupled AP205-gp140-ST VLPs

After the coupling reaction between gp140-ST and SC-AP205 VLPs, SDS-PAGE of the deglycosylated coupling reactions indicated that substantial amounts of excess or free gp140-

ST protein were present in the reaction mix. Different techniques (Section 4.2.14.1-4.2.14.4) were performed in an attempt to remove excess gp140-ST from AP205-gp140-ST VLPs.

4.2.14.1 Dialysis to remove free/excess gp140-ST from AP205-gp140-ST VLPs

To remove uncoupled/excess gp140-ST trimers (≈720 kDa) and possibly SC-AP205 (≈27 kDa) and AP205-gp140-ST (≈168 kDa) monomers from the coupled AP205-gp140-ST VLPs, the coupling reaction (SC-AP205 VLPs + gp140-ST) was dialysed (Spectra/Por® biotech grade Cellulose Ester (CE) trial kit MWCO (1000 kDa), Spectrum Laboratories, Inc.) against 1000-fold excess PBS at 4˚C. Dialysis was carried out for ≈24 hours with 3x PBS changes (after 3 hours, 12 hours and 5 hours). The DC assay (Section 4.2.8) was used to determine the total protein concentration after dialysis. Aliquots (2.1µg) from the reaction before and after dialysis were deglycosylated with PNGase F before SDS-PAGE.

4.2.14.2 PEG/NaCl precipitation of AP205-gp140-ST VLPs from free gp140-ST

PEG precipitation is a less time-consuming and convenient method for the precipitation and purification of VLPs without ultracentrifugation. The coupling reaction (SC-VLPs + gp140-ST) was combined with varying PEG8000+ NaCl concentrations to evaluate the optimal conditions that could precipitate the AP205-gp140 VLPs while retaining the free gp140-ST in the soluble fraction. PEG/NaCl precipitation was done at 4˚C without agitation. Twenty-four hours after adding PEG/NaCl, samples were centrifuged (10 000 x *g*, 30 min, 4˚C). The resulting soluble fraction (supernatant) was carefully aspirated, and the precipitated fraction (pellet) was resuspended in PBS (volume equivalent to supernatant's volume). Before SDS-PAGE and western blot analysis, both the soluble and precipitated fractions were treated with PNGase F using a method described in Section 4.2.13.

4.2.14.3 Rate zonal ultracentrifugation for separation of AP205-gp140-ST VLPs from free gp140-ST

Rate zonal ultracentrifugation of the coupling reactions was performed to remove excess or uncoupled antigen. Briefly, the coupling reaction contents (SC-AP205 VLPs + gp140-ST) were overlaid on OptiPrep™ step (1ml) gradients (15, 25, 35 and 40%) and separated by ultracentrifugation (SW55T, 132000g, 2 hours, 16°C). Uncoupled gp140-ST and uncoupled SC-VLPs were included as controls. Gradients were manually fractionated by punching a hole in the bottom of the tube and slowly collecting ≈500µl fractions. Collected fractions were resolved by SDS-PAGE and detected with Silver Stain Plus™ (Bio-Rad).

4.2.14.4 SEC separation of AP205-gp140-ST VLPs from free gp140-ST

HiPrep™ 16/60 Sephacryl® S-500 HR (Sigma), a preparative column with a 120ml bed volume, was first calibrated with a high molecular weight gel filtration calibration kit (Sigma) containing

blue dextran (2000 kDa), thyroglobulin (669 kDa), ferritin (440 kDa), aldolase (158 kDa), ovalbumin (43 kDa), carbonic anhydrase (29 kDa) and ribonuclease A (13.7 kDa). The void volume for this column was 87.5ml, a volume at which the highest molecular standard, blue dextran eluted. Gel filtration using this column was then performed in an attempted to remove excess or uncoupled gp140-ST from the coupled AP205-gp140-ST VLPs. Uncoupled SC-AP205 VLPs were also separated as a control.

4.3 Results

4.3.1 Confirmation of pMExT encoding gp140-SpyTag and gp140-SpyCatcher

Both SpyTag (ST)- and SpyCatcher (SC)-tagged gp140 fusions were designed to evaluate which fusion resulted in predominantly trimeric gp140 protein. Specifically, the sequence coding for SpyTag or SpyCatcher was inserted into plasmid pMExT gp140-FL-IP, downstream of gp140 to generate pMExT gp140-SpyTag or pMExT gp140-SpyCatcher, respectively (Figure 4.2 A and B). The integrity of pMExT gp140-SpyTag plasmid was confirmed by the expected 819 bp and 91 bp fragments following PCR with CGP120-F4 and SpyTagR primers (lane 1) and restriction analysis (lane 2), respectively (Figure 4.2 A). The integrity of pMExT gp140-SpyCatcher was confirmed by the generation of the expected 442 bp and 400 bp fragments following PCR with CatcherF and pMEx-R primers (lane 1) and restriction analysis (lane 2), respectively (Figure 4.2 B). The identity of the inserts in these plasmids was also confirmed by sequencing (results not shown).

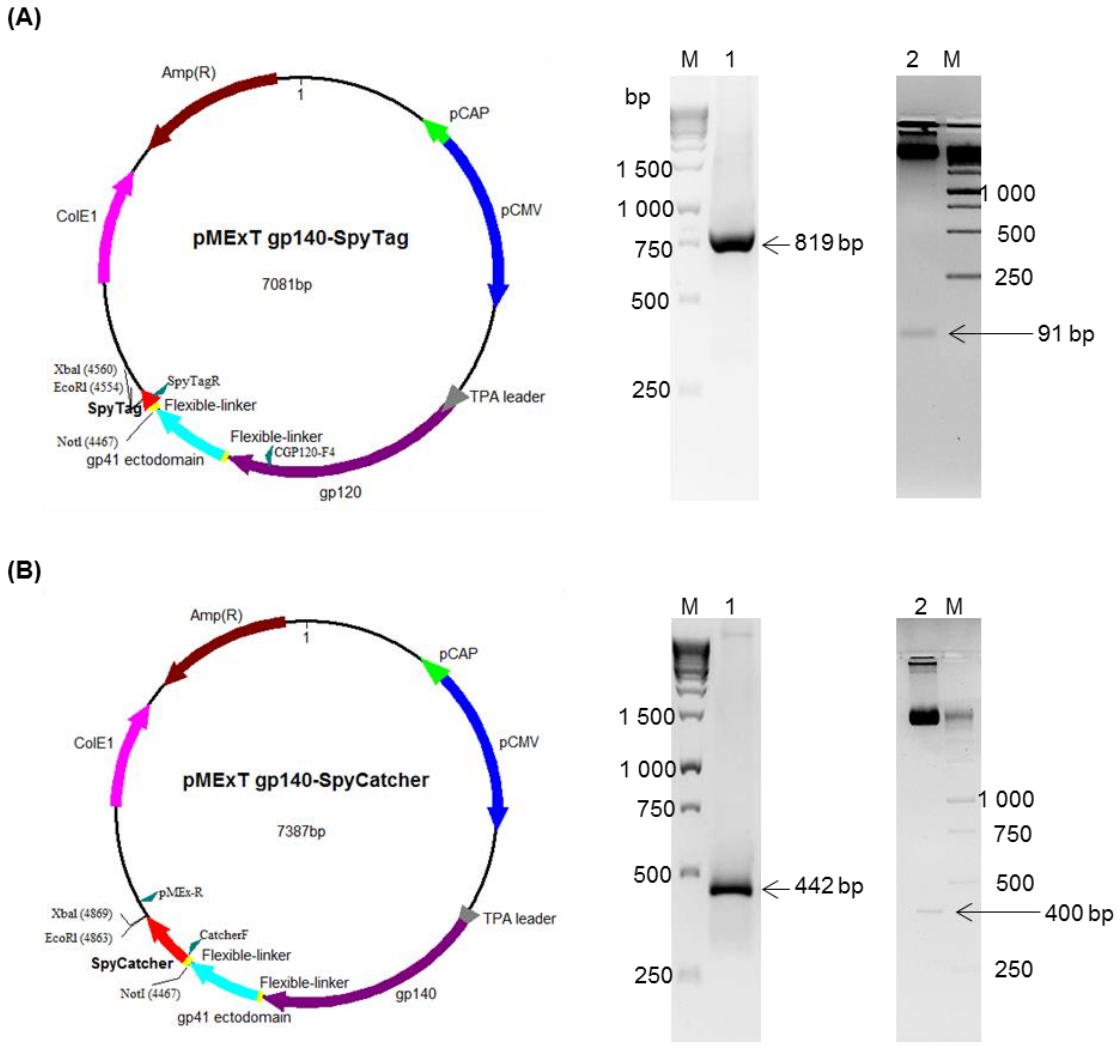

Figure 4.2: Confirmation of the integrity of mammalian expression vectors encoding SpyTag or SpyCatcher fused downstream of gp140. (A) Plasmid map of pMExT gp140-SpyTag, colony PCR screening using CGP120-F4 and SpyTag-R primers (lane 1) and restriction analysis with EcoRI and NotI enzymes (lane 2). **(B)** Plasmid map of pMExT gp140-SpyCatcher, colony PCR screening using CatcherF and pMEx-R primers (lane 1) and restriction analysis with EcoRI and NotI enzymes (lane 2). Expected fragments are indicated by the arrows. In each case, the 1kb DNA ladder (ThermoFisher Scientific) is represented in lane M.

4.3.2 Construction of plasmids for the generation of stable cell lines expressing gp140-ST and gp140-SC

For economical production of gp140-SpyTag (ST) and gp140-SpyCatcher (SC), plasmids for generating stable cell lines were constructed by introducing an IRES-Neomycin (Neo) resistance cassette downstream of the SpyTag and SpyCatcher in pMExT gp140-SpyTag and pMExT gp140-SpyCatcher, respectively. The integrity of pMExTgp140-SpyTag-IRES-Neo (Figure 4.3 A) and pMExT gp140-SpyCatcher-IRES-Neo (Figure 4.3 B) was confirmed by restriction enzyme mapping.

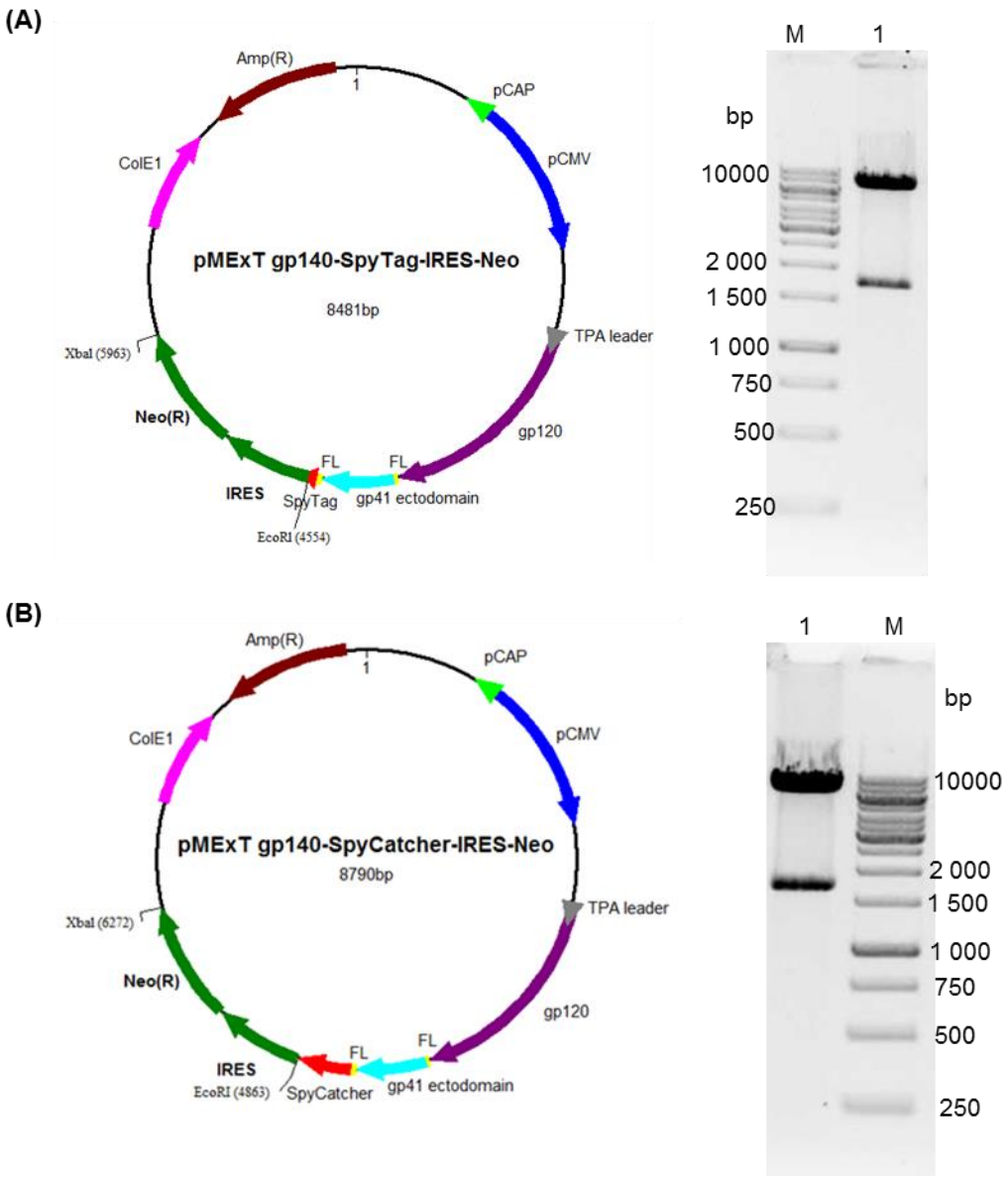

Figure 4.3: Confirmation of insertion of the IRES-Neomycin (IRES-Neo(R)) cassette downstream of the SpyTag and SpyCatcher sequences in pMExT gp140-SpyTag and pMExTgp140-SpyCatcher, respectively. (A) Plasmid map of pMExT gp140-SpyTag-IRES-Neo and restriction analysis using EcoRI and XbaI enzymes. **(B)** Plasmid map of pMExT gp140-SpyCatcher-IRES-Neo and restriction analysis using EcoRI and XbaI enzymes. In each case, the 1kb DNA ladder (ThermoFisher Scientific) is represented in lane M.

HEK293 cells stably expressing gp140-SpyTag (gp140-ST) and gp140-SpyCatcher (gp140-SC) were then generated by transfecting with pMExT gp140-SpyTag-IRES-Neo or pMExT gp140-SpyCatcher-IRES-Neo plasmids. After passaging the transfected cells at least ten times in selection media with geneticin, the expression of soluble gp140-ST or gp140-SC (≈140 kDa) in the stable HEK293 cell line was confirmed by western blotting of the cell media, which indicated a qualitative increase in the gp140 accumulation with successive passaging (P5 compared to P10) of cells in the selection media (Figure 4.4).

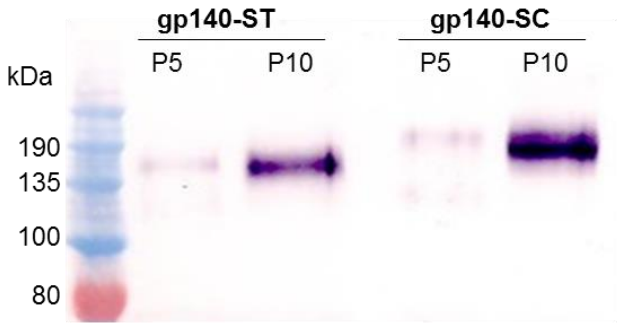

Figure 4.4: Confirmation of HEK293 stable cell lines expressing gp140-ST or gp140-SC. HEK293 cells were transfected with pMExT gp140-SpyTag-IRES-Neo or pMExT gp140-SpyCatcher-IRES-Neo. The expression of gp140-ST and gp140-SC in stable cell lines passaged 5 or 10 times (P5 and P10) in geneticin selection media was confirmed by anti-Env western blot analysis of the cell media.

4.3.3 Purification of gp140-ST and gp140-SC from the stable HEK293 cell lines

Gp140-ST or gp140-SC in the media derived from the stable HEK293 cell line was purified by *Galanthus nivalis* lectin (GNL) affinity resin followed by size exclusion chromatography (SEC). NativePAGE analyses (Figure 4.5) of gp140-ST and gp140-SC following purification by GNL affinity chromatography indicated that both these glycoproteins were predominantly trimeric as indicated by the expected 720 kDa band (***), and also contained detectable levels of higher molecular weight aggregates, monomeric species (* 242 kDa) and/or dimeric (** 480 kDa) Env species. Size exclusion chromatography effectively purified the trimeric gp140-ST (fraction 36-40) from the undesired monomeric species and protein aggregates (Figure 4.5 A and B). However, the SEC column did not effectively separate gp140-SC trimers (fraction 36-37) from the undesired dimeric and monomeric Env species. In fact, the overlaid SEC elution profiles (Figure 4.5 B) indicated that a large proportion of gp140-ST was trimeric compared to g140-SC that contained a high proportion of monomers and dimers compared to trimers.

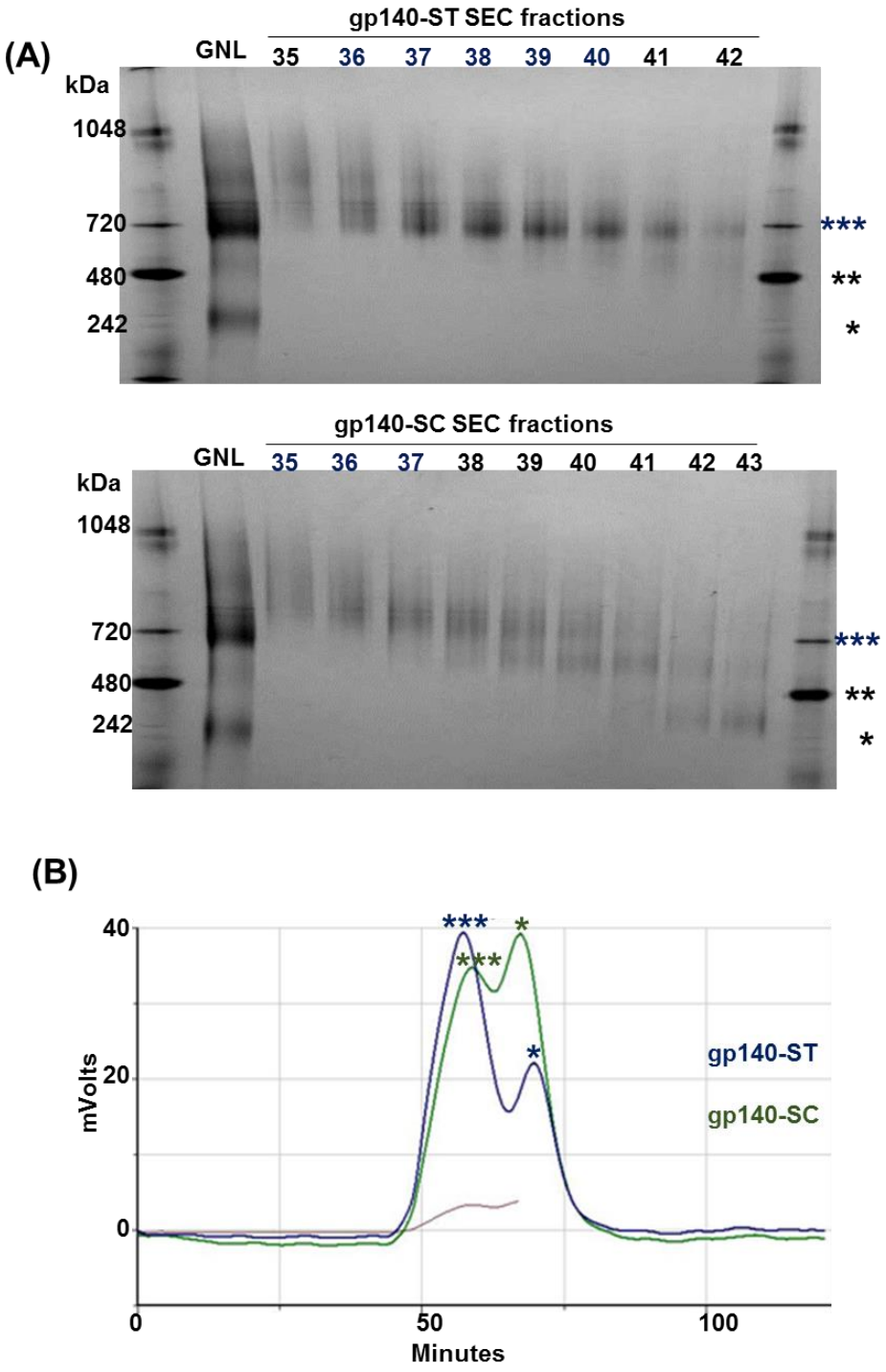

Figure 4.5: Purification of gp140-ST and gp140-SC by lectin affinity and size exclusion columns. **(A)** The *Galanthus nivalis* lectin (GNL)-purified gp140-ST or -gp140-SC from HEK293 stable cell lines was separated on a Superdex 200 (S200) size exclusion column (SEC). SEC fractions were analysed by native PAGE and stained with Coomassie. Blue font (fractions 36-40 for gp140-ST and fractions 37-37 for gp140-SC) and (***) indicate the trimeric Env species. Dimeric (**) and monomeric (*) Env species are also indicated. NativeMark Unstained Protein Standards are indicated (kDa). **(B)** Merged gp140-ST (blue) and gp140-SC (green) SEC elution profiles. Peaks representing the trimeric (***) and monomeric (*) Env species are indicated.

4.3.4 Purification and characterisation of SpyCatcher-AP205 and SpyTag-AP205 VLPs

The fusion proteins comprising the SpyCatcher (SC) or SpyTag (ST) on the N-terminus of *Acinetobacter* phage AP205 coat protein (CP3) were designed by Thrane *et al.* (2016). A 5-residue flexible linker was inserted between SC and AP205 CP3 while an 11-residue peptide linker was inserted between the ST and AP205 CP3 (Figure 4.6 A). These peptide linkers were included to ensure the extended conformation of SC or ST on the surface of VLPs. The expression of SC-AP205 or ST-AP205 fusions in *E. coli* resulted in self-assembled SC-AP205 (SC-VLPs) or ST-AP205 (ST-VLPs) VLPs respectively, capable of displaying 180 units of heterologous antigens. These VLPs were purified by density ultracentrifugation of *E. coli* lysates, and the identity of the proteins in pooled fractions after ultracentrifugation was confirmed by the presence of bands on Coomassie-stained polyacrylamide gels of the expected sizes that assemble to form SC-VLPs (27 kDa) and ST-VLPs (16 kDa) (Figure 4.6 B). Negative stain electron microscopy confirmed the assembly of SC-AP205 coat protein and ST-AP205 coat protein into non-aggregated SC-AP205 VLPs (≈32 nm, n = 62) and ST-AP205 VLPs (≈29 nm, n = 35), respectively (Figure 4.7 C).

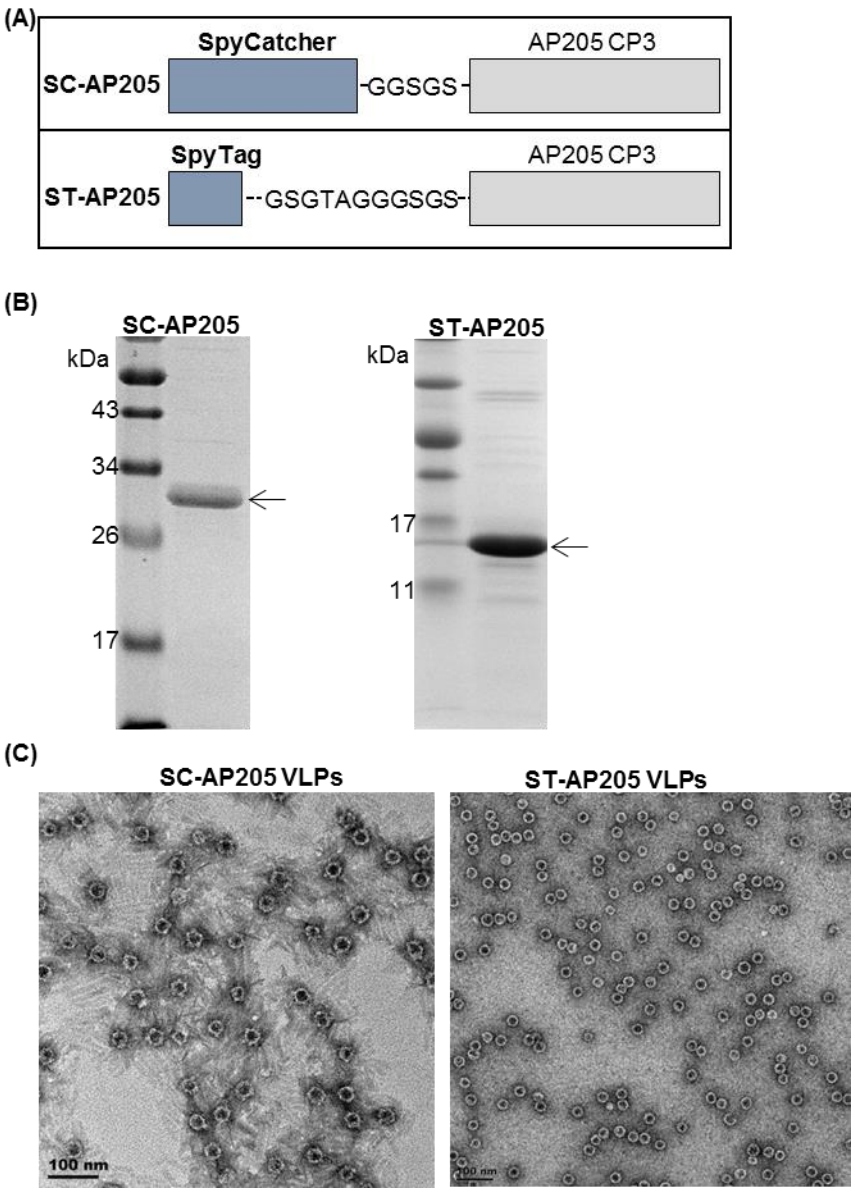

Figure 4.6: Characterisation of SpyCatcher-AP205 and SpyTag-AP205 VLPs. **(A)** Schematic representation of the SpyCatcher-AP205 (SC-AP205) and SpyTag-AP205 (ST-AP205) fusion proteins. A 5-residue (GGSGS) flexible linker between the SpyCatcher and AP205 coat protein (CP3) and an 11-residue (GSGTAGGGSGS) peptide linker between the SpyTag and AP205 CP3 are indicated. **(B)** Cell lysates from *E. coli* expressing SC-AP205 CP3 or ST-AP205 CP3 fusions were passed through an OptiPrep™ gradient by ultracentrifugation, and pooled purified fractions were analysed by SDS-PAGE stained with Coomassie. The arrows indicate the expected bands, 27 kDa and 16 kDa, corresponding to the SC-AP205 CP3 and ST-AP205 CP3 fusion proteins, respectively **(C)** Negative stain electron micrographs of purified SC-AP205 and ST-AP205 VLPs. Scale bar represents 100nm.

4.3.5 Analyses of the coupling of gp140-ST to SC-AP205 VLPs

Since gp140-ST was predominantly trimeric compared to gp140-SC, only gp140-ST was used to pursue coupling experiments to evaluate if gp140 could be displayed on AP205 VLPs using the SpyTag-SpyCatcher interaction. SpyCatcher-AP205 VLPs (SC-VLPs) were mixed with gp140-ST or gp140 at 1 SC-VLP to 1.5 Env molar ratios. Native agarose gel electrophoresis

and ethidium bromide staining were used for initial screening because it has been previously shown that during AP205 VLP assembly, nucleic acids from the expression host are encapsulated within the VLPs and they can migrate through agarose when a voltage is applied (Spohn *et al.* 2010; Freivalds *et al.* 2014). It is expected that following coupling reactions *in vitro*, if AP205 VLPs are successfully decorated with a protein of interest, there should be an increase in their surface charge and size, leading to slower migration through agarose, thereby allowing one to determine whether coupling has occurred. When compared with the migration of SC-VLPs alone, the migration of SC-VLPs which had been mixed with gp140-ST was retarded, suggesting that coupling had occurred (Figure 4.7 A). As expected, the migration of SC-VLPs was not affected when mixed with the untagged gp140 control (Figure 4.7 A). SpyCatcher-AP205 VLPs (SC-VLPs) were then mixed with increasing molar concentrations of gp140-ST to determine the optimal coupling ratios. The migration of SC-VLPs at 1:1 and 1:1.5 molar coupling ratios were similarly retarded (Figure 4.7 B). A 1:1.5 SC-VLPs to gp140-ST was chosen as a standard molar coupling ratio because it was reasoned that having excess gp140-ST in a reaction could favour high-density decoration of these VLPs.

Agarose gel electrophoresis was not a sensitive enough method for measuring the coupling efficiency or for determining if the VLPs were saturated with antigen. Thus, the coupling reactions (1 SC-VLP to 1.5 gp140-ST molar ratio) were further analysed by SDS-PAGE (Figure 4.7 C). Even though gp140-ST did not resolve well as bands were diffuse, SDS-PAGE indicated that the gp140-ST band (arrow) shifted to a slightly higher molecular weight when mixed with SC-VLPs. However, it was apparent that the intensity of the SC-VLP (asterisk) before and after coupling with gp140-ST remained similar, suggesting that not all VLP binding sites (180) were occupied/saturated with gp140-ST.

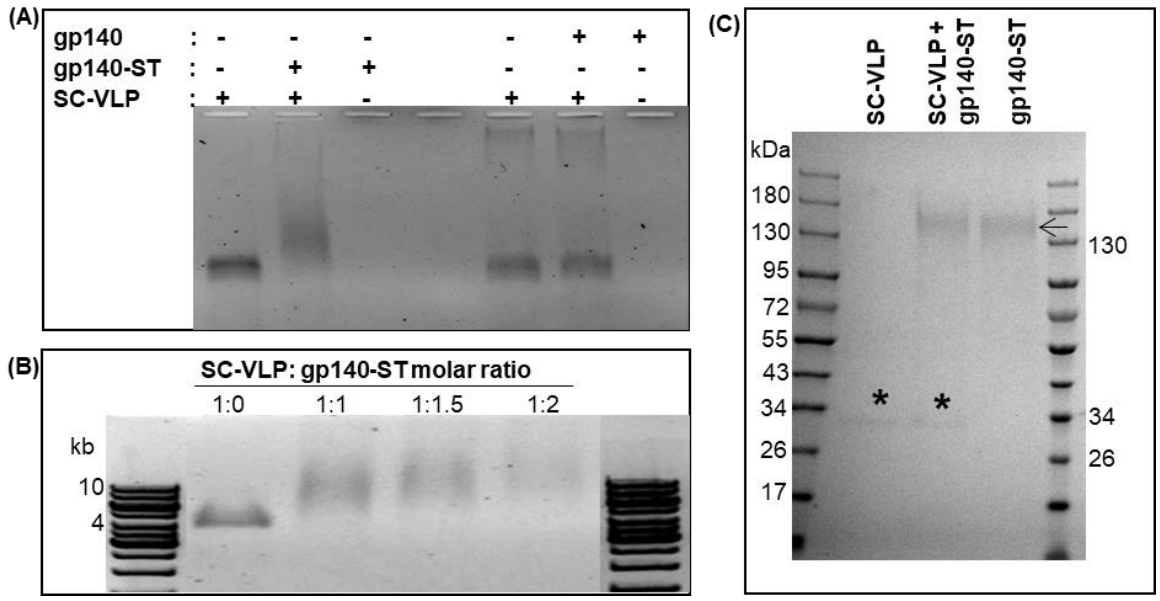

Figure 4.7: Analyses of the coupling of gp140-ST to SC-AP205 VLPs (A) Ethidium bromide-stained agarose gels after electrophoresis of SC-VLPs mixed with increasing molar concentrations of gp140-ST. **(B)** Ethidium bromide-stained agarose gels of SC-VLPs mixed with tagged gp140-ST or untaggedgp140. **(C)** Coomassie-stained reducing SDS-PAGE analysis of coupling of gp140-ST (arrows) to SC-VLPs (asterisk).

4.3.6 Negative stain electron microscope and dynamic light scattering analysis of the coupling reactions

Negative staining with uranyl acetate and imaging with a transmission electron microscope was conducted to evaluate the effect of displaying gp140-ST on the size, appearance and integrity of SC-AP205 VLPs. A slight increase in diameter of SC-AP205 VLPs from ≈32 nm (n=62) to ≈43 nm (n=35) was observed after coupling with gp140-ST (Figure 4.8). Interestingly, the surface of the uncoupled SC-AP205 VLPs appeared smooth while protruding spikes (indicated by white arrows on a zoomed-in insert) were observed when these VLPs were reacted with gp140-ST. This evidence suggested the successful display of gp140-ST on AP205 VLPs via the SpyTag-SpyCatcher interaction.

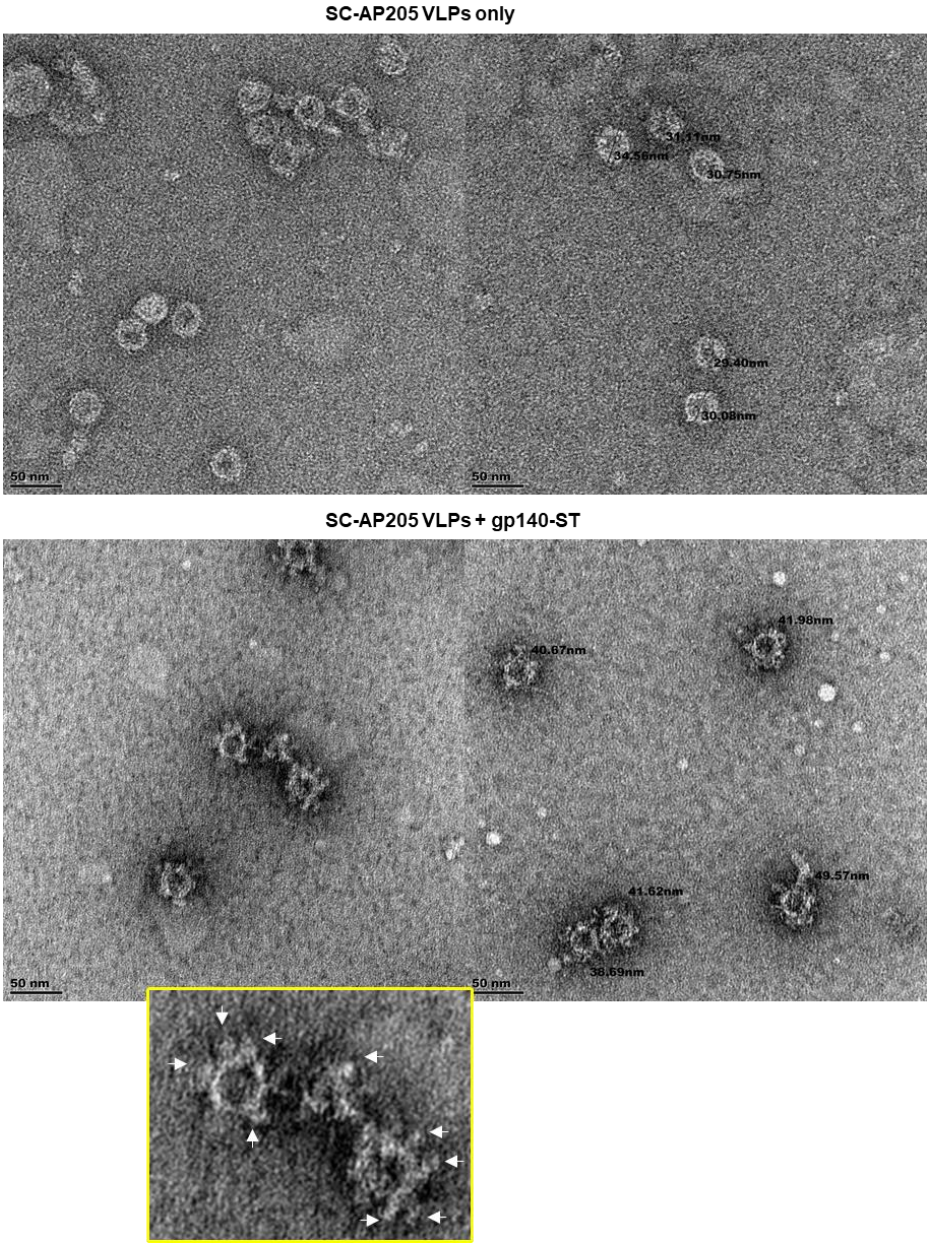

Figure 4.8: Negative-stain electron micrographs of uncoupled SC-AP205 VLPs and coupled SC-AP205+gp140-ST VLPs. Individual size measurements are shown near some VLPs. Protruding gp140-ST spikes are indicated by the white arrows in the zoomed-in image. Scale bar represents 50 nm.

Three independent measurements of purified SC-AP205 VLPs by dynamic light scattering (DSL) indicated a uniform (monodisperse) size distribution (green, blue and red peaks in Figure 4.9 A) and non-aggregated population of the uncoupled VLPs with an average particle size (hydrodynamic) diameter of 44 nm [polydispersity index (PDI) = 0.163] (Figure 4.9 A). Polydispersity index is used to estimate the average uniformity of a particle solution, and larger PDI values correspond to a larger size distribution in the particle sample. However, when SC-AP205 VLPs were coupled with gp140-ST, DSL revealed a non-uniform size distribution of VLPs with 3 independent measurements with an average diameter of 221 nm [PDI = 0.281]

(Figure 4.9 B). This heterogeneity/dispersity in the size of SC-AP205 VLPs when displaying gp140-ST suggests that each VLP particle displayed a varying number of gp140-ST, i.e. VLPs were not equally saturated with gp140-ST.

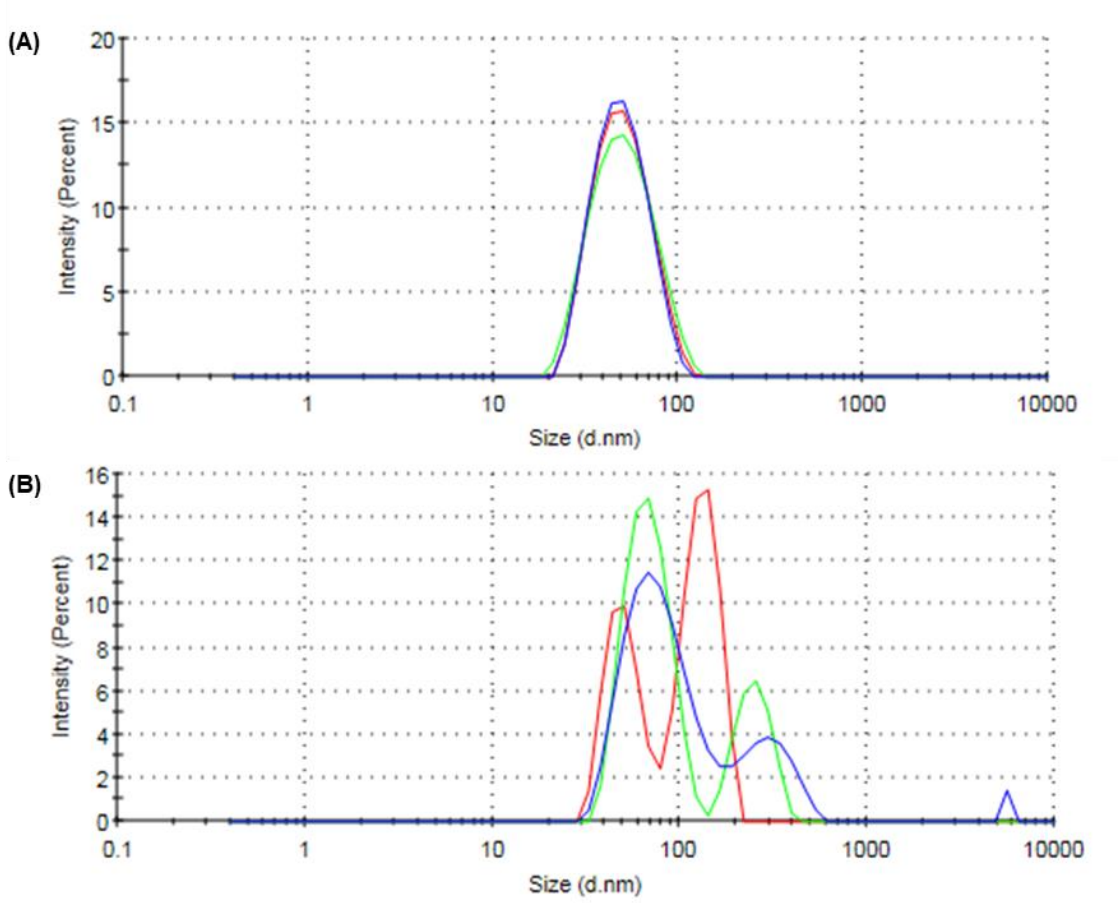

Figure 4.9: Measurement of the size of uncoupled and coupled AP205 nanoparticles using dynamic light scattering. Three independent measurements (represented by blue, red and green profiles) were recorded for the uncoupled SC-AP205 VLPs **(A)** and SC-AP205 VLP + gp140-ST coupling reaction **(B)**.

4.3.7 Rabbit immunisation and characterisation of anti-Env binding titres

The immunogenicity of AP205-gp140-ST VLPs was evaluated by inoculating two groups of 5 rabbits with two regimens (Figure 4.10 A). Group 1 (PPPP) rabbits were injected with AP205-gp140-ST VLPs (1:1.5 SC-AP205 VLPs to gp140-ST molar ratios) (P) at weeks 0, 4, 12 and 20. Group 2 (DDMMPP) rabbits were inoculated with DNA (D) vaccines expressing HIV Env and Gag^{M} at weeks 0 and 4, followed by MVA (M) expressing the same antigens (van Diepen *et al.* 2019) at weeks 8 and 12 and finally boosted at weeks 20 and 28 with AP205-gp140-ST particles (P). Anti-gp140 binding antibody titres from sera sampled at weeks 0, 6, 14, and 22 for Group 1 and weeks 0, 6, 10, 14, 22 and 30 for Group 2 were measured in an indirect binding ELISA (Figure 4.10 B). Group 1 rabbits had lower anti-gp140 antibody titres than Group 2 at all time-points except week 6. For Group 1 rabbits, the antibody binding titres were

3-fold higher after the third AP205-gp140-ST VLP boost compared to the second AP205-gp140-ST VLP boost; and the fourth AP205-gp140-ST VLP boost increased antibody titres by only 1-fold compared to titres observed after the third boost. For Group 2 rabbits, the binding antibody titres were 18-fold higher after the first MVA inoculation as compared to titres observed after priming with the second DNA vaccine. After the second MVA inoculation, the binding antibody titres were 15-fold higher than those observed after the first MVA inoculation. The first AP205-gp140-ST VLP particle inoculation increased binding antibody titres of the Group 2 rabbits by 2-fold; however, the second inoculation did not boost titres any further.

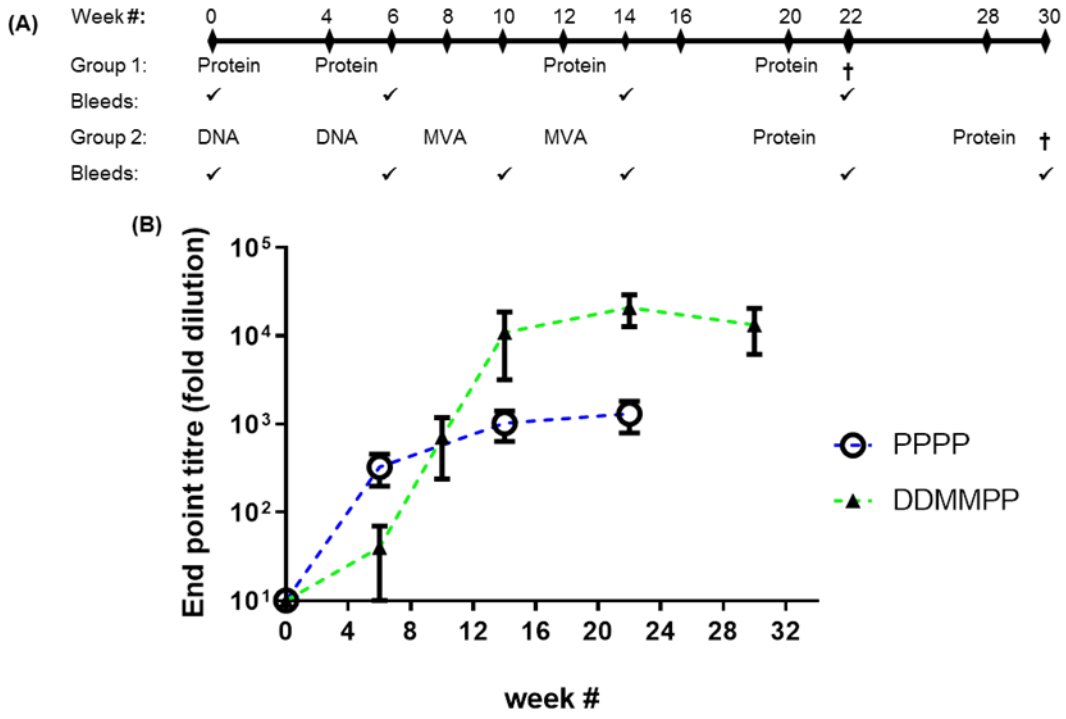

Figure 4.10: Vaccination schedule and serum binding antibody titres. **(A)** Schematic showing regimens received by the two groups of rabbits and the collection of blood samples (tick marks) over the indicated time course. Protein (P) refers to AP205-gp140-ST VLPs while DNA (D) and MVA (M) vaccines both expressed Env+Gag^{M}. **(B)** Anti-Env antibody titres in sera from the two groups were quantified in an indirect ELISA. Error bars indicate the standard deviation within the group at each time point.

4.3.8 Neutralisation assays with Env-pseudotyped viruses

A standard TZM-bl assay was used to evaluate the neutralising activity of sera from selected time points against a small panel of Env-pseudotyped clade C viruses (Table 1). In accordance with the trend observed for anti-gp140 binding titres, Group 2 rabbits generally showed higher neutralisation titres against Tier 1A, Tier 1B and Tier 2 representative viruses. Group 1 rabbits failed to elicit neutralising antibodies (NAbs) against the Tier 1B 6644 or the autologous Tier 2 CAP256SU pseudovirions. However, 2/5 rabbits from Group 2 developed NAbs against 6644 after the second MVA inoculation (M2 ID50 1:138 to 1:152), which were maintained after

the first VLP inoculation (P1 ID50 1:46 to 1:57) but were not detected after the second VLP inoculation (P2). Interestingly, the same rabbits in Group 2 that developed Tier 1B neutralisation titres, developed autologous Tier 2 neutralising titres (ID50 1:55 to 1:120) after the first AP205-gp140-ST VLP boost. Both these rabbits retained Tier 2 virus CAP256SU neutralisation after the second AP205-gp140-ST VLP boost.

Comparing these results (autologous Tier 2 neutralising antibody titres) to those of a previous experiment carried out by our group using soluble gp140 formulated in AlhydroGel® (van Diepen *et al.* 2019) indicated there was no improvement in immunogenicity when gp140 was coupled to the AP205 particles. This was not expected and hence it was decided that further characterisations of the coupling reactions were needed to decide whether repetition of the animal studies using more refinely purified AP205-gp140-ST VLPs (excess gp140-ST removed from the coupled VLPs) and a suitable adjuvant should be considered.

Table 1: TZM-bl assays to determine neutralising antibody titres in serum[a].

		Clade C - Tier 1A - MW965.26			Clade C - Tier 1B - 6644			Clade C - Tier 2 - CAP256SU		
		ID50 after:								
Regimen	Rabbit ID	P3	P4	N/A	P3	P4	N/A	P3	P4	N/A
PPPP	1	244	245	N/A	<20	<20	N/A	<20	<20	N/A
	2	1291	147	N/A	<20	<20	N/A	<20	<20	N/A
	3	479	791	N/A	<20	24	N/A	<20	<20	N/A
	4	225	300	N/A	<20	<20	N/A	<20	<20	N/A
	5	73	48	N/A	<20	<20	N/A	<20	<20	N/A
		M2	P1	P2	M2	P1	P2	M2	P1	P2
DDMMPP	a	195	584	1771	<20	<20	<20	<20	<20	<20
	b	822	496	407	<20	<20	<20	<20	<20	<20
	c	1042	916	573	152	57	30	<20	120	137
	d	4186	3437	2352	138	46	38	<20	55	35
	e	75	207	245	<20	<20	<20	<20	<20	<20

50% nuetralisation titre
1 000 -10 000
100 - 1 000
20 - 100
<20
N/A not applicable

[a]The serum was taken two weeks post each protein boost (P3 and P4) for rabbits that received the PPPP regimen. The serum was taken two weeks after the second MVA boost (M2) and two weeks post each protein boost (P1 and P2) for rabbits that received the DDMMPP regimen. Titres below 20 were considered non-neutralising and were shaded in grey while neutralising titres were colour-coded and categorised according to their potency.

4.3.9 Further characterisation of the coupling reactions

4.3.9.1 Optimisation of reactions to maximise coupling efficiency

The poor resolution (diffuse bands) of gp140-ST glycoprotein (before and after coupling) on SDS-polyacrylamide gels made it difficult to visualise the extent of SpyTag-SpyCatcher-mediated coupling when SC-VLPs and gp140-ST were coupled at different molar ratios. In

addition, densitometric analyses on these diffuse bands to determine the optimal molar coupling ratios or estimate the coupling efficiency lent itself to more inaccurate calculations. In an effort to improve the resolution of gp140-ST on the gels, coupling reactions were treated with PNGase F (to remove Env glycans) prior to SDS-polyacrylamide gel analysis (Figure 4.11). After treatment with PNGase F, the uncoupled and deglycosylated gp140-ST bands resolved as a much more discrete ≈95 kDa band (white arrow) instead of a diffuse ≈140 kDa band (black arrow) when no PNGase F was added. Interestingly, after deglycosylation, samples from the gp140-ST+SC-VLP coupling reaction separated into two discrete Env bands at ≈120 kDa (white asterisk) and ≈95 kDa (white arrow). The ≈120 kDa corresponded to the gp140-ST attached to the SC-AP205 CP3 while the ≈95 kDa is most likely attributed to the uncoupled/excess/free gp140-ST that was present in the coupling reaction. The presence of a ≈95 kDa band in the coupling reaction indicated that not all gp140-ST added to the coupling reaction was displayed on the SC-AP205 VLPs. SC-AP205 CP3 resolved as a distinct ≈27 kDa band (black arrow) before and after treatment with PNGase F, suggesting that these VLPs were not N-glycosylated, as expected. As expected, a 36 kDa band (black asterisk) corresponding to PNGase F was observed in samples treated with PNGase F.

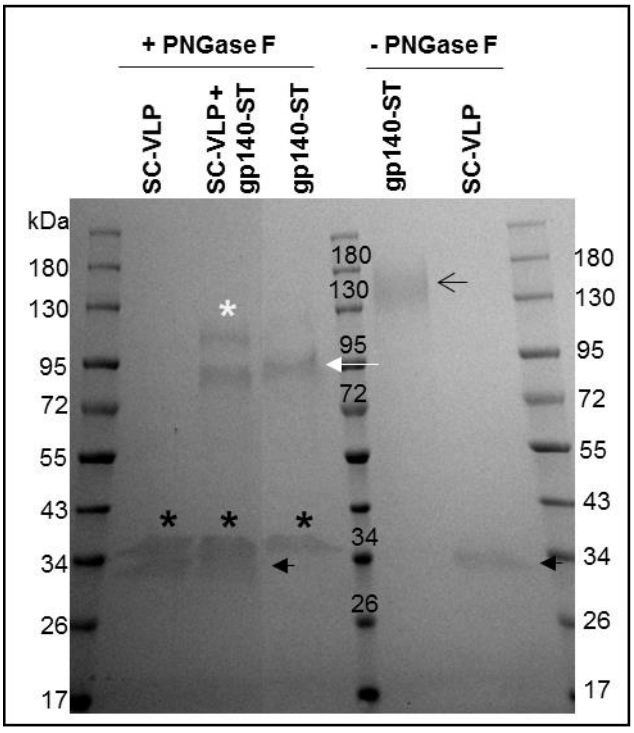

Figure 4.11: SDS-PAGE of the coupling reactions after deglycosylation with PNGase F. SC-AP205 VLPs were coupled with gp140-ST (1:1.5 VLP to gp140-ST molar ratio). Uncoupled SC-AP205 VLPs and gp140-ST only were included as controls. Aliquots from each reaction were treated with PNGase F (+PNGase F), or the deglycosylation enzyme was omitted (-PNGase F) before analysis on a pre-cast 4-15% gradient gel and detection with Coomassie. The coupled AP205-gp140-ST (≈ 120 kDa, deglycosylated, white asterisk), free/excess gp140-ST (≈ 95 kDa, deglycosylated, white arrow),

gp140-ST only (≈ 140 kDa, glycosylated, black arrow), PNGase F (36 kDa, black asterisk) and SC-AP205 VLPs (27 kDa, thick, black arrow) are indicated.

To determine the optimal coupling ratios between SC-AP205 VLPs and gp140-ST, these VLPs were reacted with increasing (1:2, 1:2.5, 1:3, 1:4, 1:5 and 1:6) molar ratios of g140-ST. After allowing these components to react, samples were treated with PNGase F before SDS-PAGE and Coomassie staining (Figure 4.12). It appeared that the band corresponding to the coupled AP205-gp140-ST protein (≈120 kDa) was more intense for the 1:3 SC-VLP to gp140-ST molar coupling ratio (blue asterisk). The corresponding band when using increased molar ratios of gp140-ST (1:4-1:6) did not seem to change from this. Instead, the intensity of the band corresponding to excess/free gp140-ST (blue arrow) appeared stronger, suggesting that the maximum capacity (without saturating the VLPs) for displaying trimeric gp140 on these VLPs had probably been attained, and more gp140-ST could not be displayed on the particles. Due to the proximity of the PNGase F protein band to that of SC-AP205 CP3, a densitometric analysis comparing the intensity of the SC-AP205 CP3 band before and after coupling with gp140-ST could not be done using this gel.

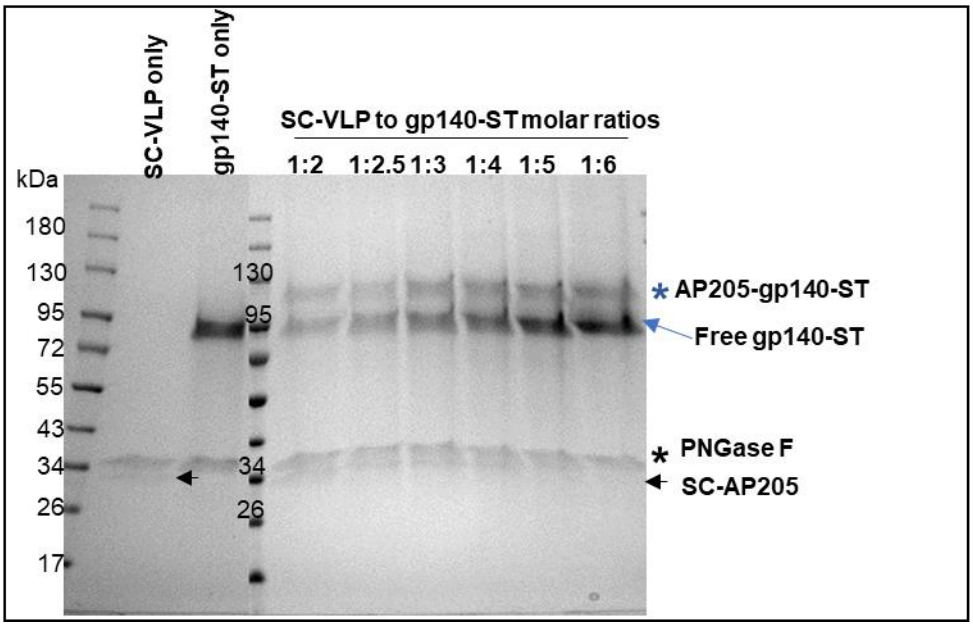

Figure 4.12: Optimisation of SC-VLP to gp140-ST molar coupling ratios. SC-AP205 VLPs were reacted with increasing molar concentrations of gp140-ST (1:2-1:6). Uncoupled SC-VLPs and gp140-ST were included as controls. Reactions were treated with PNGase F before analysis on a pre-cast 4-15% gradient gel and detection with Coomassie. Coupled AP205-gp140-ST (≈ 120 kDa, deglycosylated, blue asterisk), free/excess gp140-ST (≈ 95 kDa, deglycosylated, blue arrow), PNGase F (= 36 kDa, black asterisk), and SC-AP205 capsid (= 27 kDa, deglycosylated, black arrow) are indicated.

In order to more accurately measure the band intensities of AP205-gp140-ST protein (120 kDa) to determine which molar coupling ratio was the most optimal, the coupling reactions

were repeated and treated with PNGase F as done in Figure 4.13. Samples were analysed on SDS-PAGE and blotted with an antibody to Env (Figure 4.13 A). Densitometric analysis of the 120 kDa western blot bands (Figure 4.13 B) indicated that a 1:3 SC-AP205 VLP to gp140-ST molar ratio gave a slightly higher amount of the coupled AP205-gp140-ST protein, which agreed with the observations previously made in Figure 4.11. However, comparing the AP205-gp140-ST bands intensities at 1:1.5 and 1:3 SC-AP205 VLP to gp140-ST molar coupling ratios indicated that the coupling efficiency was not too different between the two ratios, suggesting that both ratios could be used for the coupling reactions. This also suggested that the 1:1.5 SC-AP205 VLP to gp140-ST molar coupling ratios were appropriately used to immunise rabbits in Section 4.3.7. At 1:4 VLP:gp140-ST ratio, the intensity of the AP205-gp140-ST unexpectedly decreased such that it was lower than the intensities observed when the lower amount of gp140-ST was used (1:1, 1:1.5 and 1:3). These results also indicated that regardless of the molar coupling ratio used, the uncoupled gp140-ST was always higher than the coupled AP205-gp140-ST VLPs.

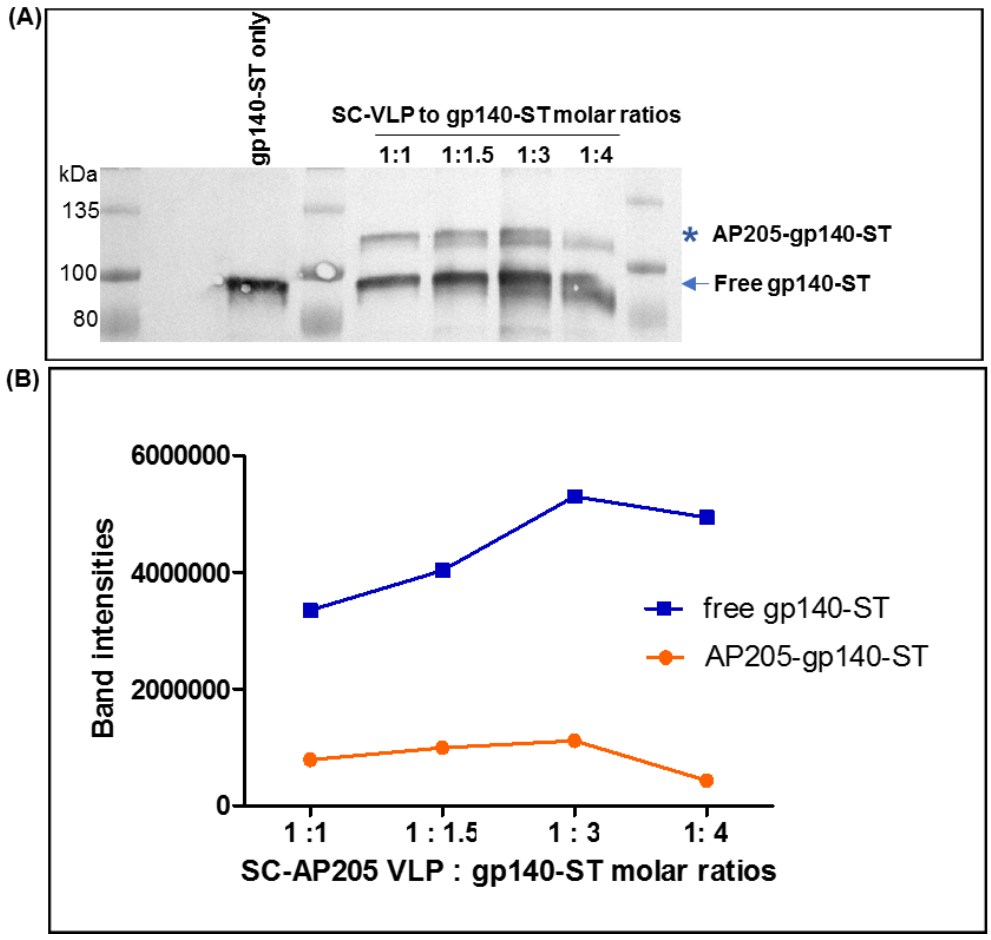

Figure 4.13: Optimisation of SC-VLP to gp140-ST molar coupling ratios. SC-AP205 VLPs were reacted with increasing molar concentrations of gp140-ST (1:1-1:4). Uncoupled gp140-ST was included

as uncoupled control. (A) Reactions were treated with PNGase F before analysis on 8% SDS-PAGE and western blotting with an antibody to Env. Coupled AP205-gp140-ST (≈ 120 kDa, deglycosylated, blue asterisk), free/excess gp140-ST (≈ 95 kDa, deglycosylated, blue arrow) are indicated. (B) Densitometric analysis was used to measure band intensities (coupled AP205-gp140-ST VLP and gp140-ST) on the western blot.

In addition to determining the optimal molar coupling ratios, coupling reactions were repeated in an attempt to determine the coupling efficiency or % occupancy of AP205 VLP binding sites after reaction with gp140-ST (Figure 4.14 A). Upon a successful reaction between the SC-AP205 VLP with a SpyTagged antigen, the free SC-AP205 CP3 protein should decrease with a corresponding decrease in protein band intensity on a SDS-polyacrylamide gel. Hence, the coupling efficiency is often estimated by comparing the band intensity of the SC-AP205 CP3 before and after coupling with the antigen of interest and then calculating the percentage difference (Thrane *et al.* 2016). This method has been used successfully by others to estimate the coupling efficiency when VLPs were reacted with small and monomeric proteins. However, in this study, this method of estimating the coupling efficiency did not seem appropriate for estimating the coupling efficiency because 1) it was not clear if each trimer used 1 or 2 or 3 of its SpyTags to bind to the SpyCatchers on AP205 VLP, and 2) the coupling was limited by steric hindrances hence VLPs were possibly not uniformly decorated with gp140-ST. For these reasons, we could not estimate the coupling efficiency and the average number of gp140-ST trimers displayed per VLP. Instead, the band intensities of the SC-AP205 before and after coupling with varying molar ratios of gp140-ST were plotted against the molar coupling ratios to indicate the optimal molar coupling ratio (Figure 4.14 B). These results also indicated that the coupling was higher at 1:3 molar coupling ratios.

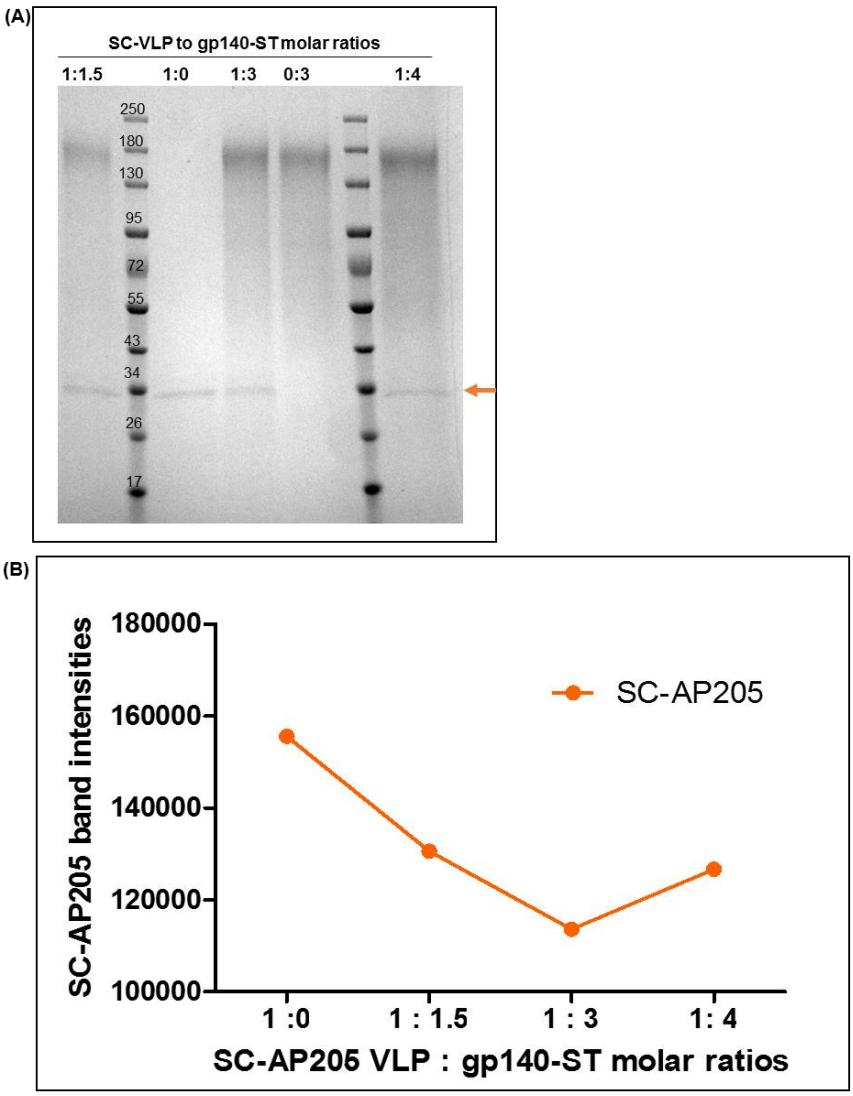

Figure 4.14: Densitometric analysis of the coupling reactions to estimate the coupling efficiency between SC-VLP and gp140-ST reacted at different molar coupling ratios. SC-AP205 VLPs were reacted with increasing molar concentrations of gp140-ST (1:1.5 to 1:4). Uncoupled SC-AP205 VLPs were included as a control. **(A)** Reactions were analysed on a 4-15% Tris-glycine gel and stained with Coomassie. The SC-AP205 band is indicated (orange arrow). **(B)** Densitometric analysis was used to measure SC-AP205 band intensities before and after coupling with gp140-ST.

4.3.9.2 Removal of excess/free gp140-ST from coupled AP205-gp140-ST VLPs

It is possible that the limited immunogenicity response measured by autologous Tier 2 antibody titres may have been a result of the free gp140-ST present in the vaccine after coupling. In order to address this, we looked at different methods to remove free/excess gp140-ST from coupled AP205-gp140-ST VLPs after coupling.

Dialysis using a 1000 kDa molecular weight cut-off membrane was first used in an attempt to remove free/excess gp140-ST (≈720 kDa in its trimeric/ non-denatured state) from coupled AP205-gp140-ST VLPs [SC-AP205 VLP = 27 kDa SC-AP205 monomers x 180 subunits =

4860 kDa (>4 MDa); even bigger when displaying gp140-ST]. To evaluate if the dialysis was effective in removing excess gp140-ST, equal amounts of the reaction mix before and after dialysis were treated with PNGase F before analysis by SDS-PAGE. It was thought that a noticeable reduction of the intensity of the band corresponding to free gp140-ST (≈95 kDa when gp140-ST is deglycosylated under denaturing conditions) would indicate that dialysis was successful. However, the intensity of the ≈95 kDa band (excess gp140-ST) remained visibly similar before and after dialysis (Figure 4.15).

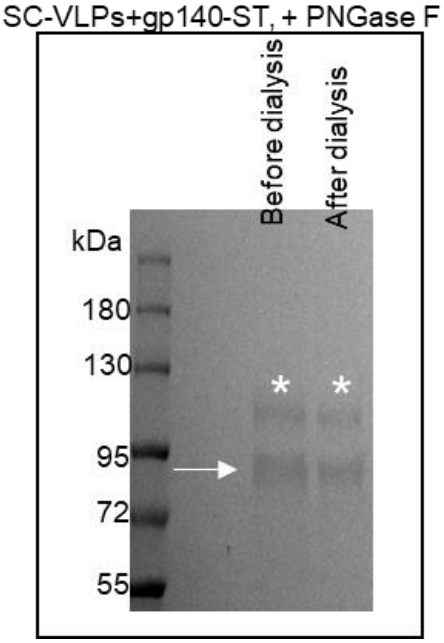

Figure 4.15: SDS-PAGE analysis of the coupling reaction (SC-VLPs + gp140-ST) before and after dialysis. After the coupling reaction between SC-AP205 VLPs and gp140-ST, an aliquot was kept (before dialysis) while the rest of the reaction was dialysed using a 1000 kDa membrane. Equal amounts of the reaction before and after dialysis were treated with PNGase F before SDS-PAGE and Coomassie staining. Coupled AP205-gp140-ST (deglycosylated) ≈ 120 kDa (white asterisk), free/excess gp140-ST (deglycosylated) ≈ 95 kDa (white arrow) are indicated.

PEG/NaCl precipitation was a second method that was assessed in an effort to remove free/excess gp140-ST from coupled AP205-gp140-ST VLPs. In theory, it was expected that the optimal concentration of PEG+NaCl would precipitate (pellet) out the relatively higher molecular weight AP205-gp140-ST VLP while retaining the lower molecular weight gp140-ST in the soluble fraction (supernatant). In the presence of 1M NaCl and a range of PEG8000 concentrations, SDS-PAGE analysis indicated that the uncoupled SC-AP205 VLPs precipitated completely over a wide range (8-14%) of PEG8000 concentrations (Figure 4.16 A). The lowest optimal concentration of PEG8000, 8%, with increasing concentrations of NaCl (0.4-1M), was then used to evaluate if it was possible to separate the coupled AP205-gp140-ST (≈120 kDa, deglycosylated) from free/excess gp140-ST (≈95 kDa, deglycosylated). Anti-Env western blot analysis of the supernatants and pellet resuspensions (treated with PNGase

F) after precipitation indicated that none of the PEG+NaCl conditions tested was able to completely separate the coupled AP205-gp140-ST particles from the uncoupled gp140-ST (Figure 4.16 B). Lowering the concentration of PEG8000 did not improve the separation of AP205-gp140-ST particles from the uncoupled gp140-ST (Figure 4.16 C). Instead, the lower % of PEG8000 shifted the coupled AP205-gp140-ST particles towards the soluble fraction with gp140-ST. Thus, PEG/NaCl precipitation was not optimal for removing free gp140-ST from coupled AP205-gp140-ST VLPs.

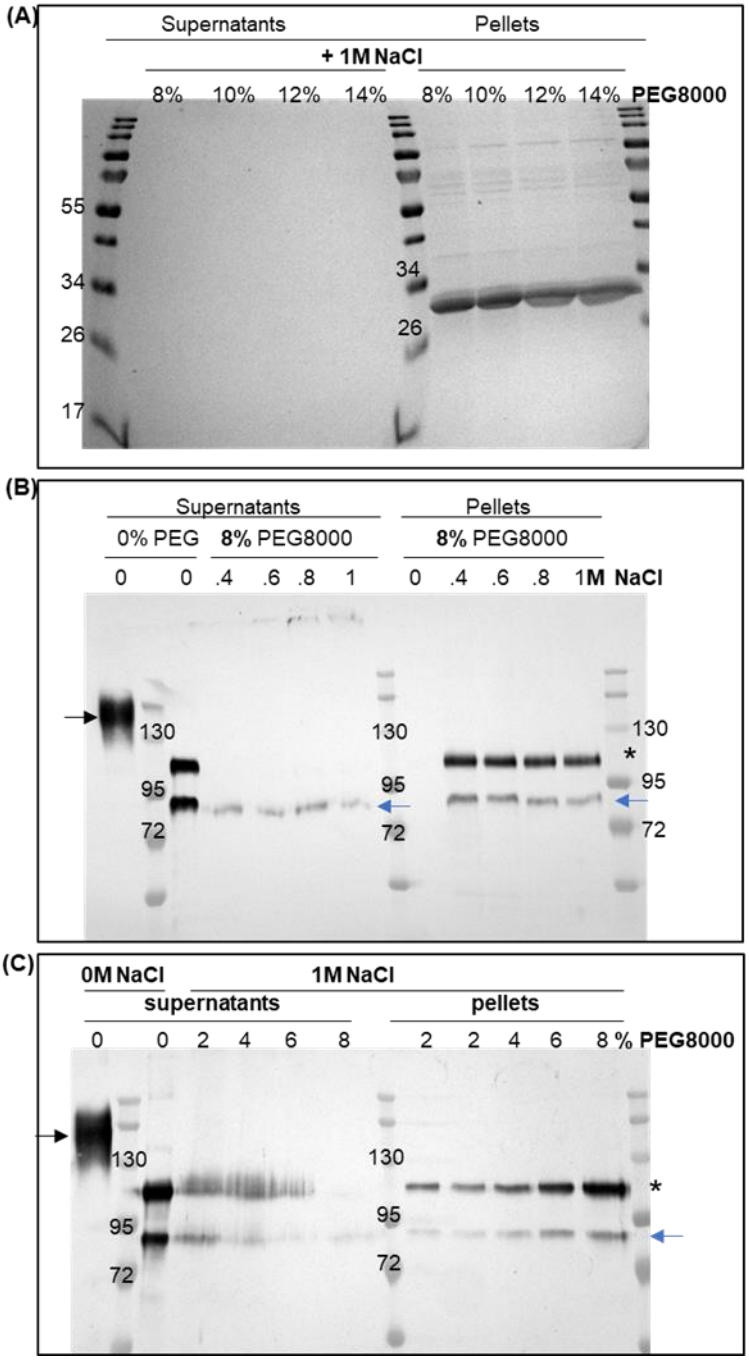

Figure 4.16: PEG/NaCl precipitation of coupled AP205-gp140-ST VLPs from free gp140-ST. (A) Uncoupled SC-AP205 VLPs were first precipitated with 8-14% PEG8000 + 1M NaCl to optimise PEG

concentrations. Collected fractions (supernatants and pellets) were analysed on SDS-PAGE and stained with Coomassie. **(B)** Aliquots from SC-AP205 VLPs + gp140-ST coupling reaction were mixed with 0.4-1M NaCl in the presence of 8% PEG8000. PEG/NaCl-precipitated samples were centrifuged, and the resulting supernatants and pellets (resuspended in the same volume as the supernatants) were deglycosylated with PNGase F. Deglycosylated samples were analysed on a western blot probed with an antibody to Env. Negative controls included samples that were not subjected to PEG/NaCl precipitation and deglycosylation. **(C)** Aliquots from SC-AP205 VLPs + gp140-ST coupling reaction were mixed with 2-8% PEG8000 in the presence of 1M NaCl, and samples were processed as in **(B)**. Coupled AP205-gp140-ST (≈ 140 kDa, glycosylated, black arrow), coupled AP205-gp140-ST (≈ 120 kDa, deglycosylated, asterisk) and free/excess gp140-ST (≈ 95 kDa, deglycosylated, blue arrow) are indicated.

Rate zonal ultracentrifugation of the coupling reaction was a third method that was conducted to evaluate its suitability for removing excess gp140-ST from coupled AP205-gp140-ST VLPs. The SC-VLP + gp140-ST coupling reaction was fractionated through an OptiPrep™ gradient, and the resultant fractions were separated by SDS-PAGE and silver-stained (Figure 4.17). Uncoupled gp140-ST was included as a control (Figure 4.17 A). Uncoupled gp140-ST predominantly fractionated at 0-15% with a small amount in the 25% OptiPrep™ fraction (Figure 4.17 A lane 6). The coupled SC-AP205 VLP + gp140-ST (AP205-gp140-ST VLPs) was predominantly in the at 25-35% fraction (Figure 4.17 B lanes 4 & 5, these possibly represent the coupled AP205-gp140-ST), with some in the 0-15% fraction (Figure 4.17 B lanes 7 & 8, these possibly correspond to the uncoupled/excess gp140-ST). The protein band for the coupled AP205-gp140-ST CP3 protein sample in lanes 4 and 5 appeared to be of slightly higher molecular weight compared to the protein band seen in lanes 7-9, further verifying that the coupling reaction occurred (Figure 4.17 B).

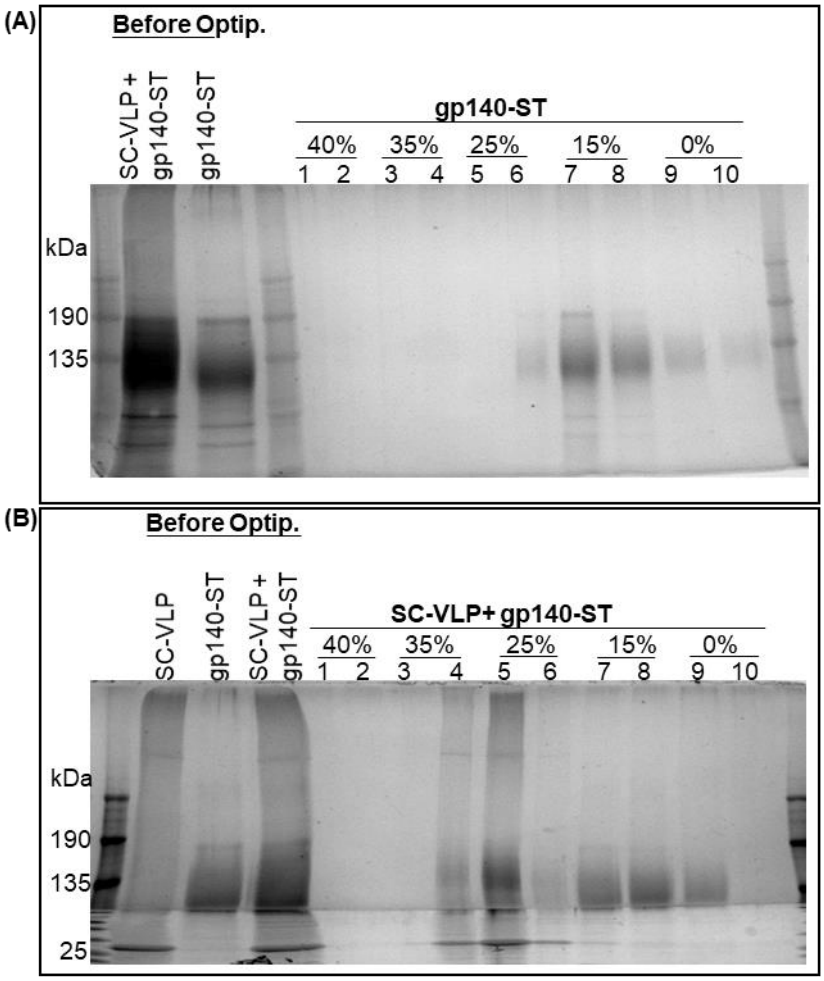

Figure 4.17: Separation of uncoupled gp140-ST from coupled AP205-gp140-ST VLPs by rate zonal centrifugation. (A) Uncoupled gp140-ST control and **(B)** SC-VLPs + gp140-ST coupled particles were applied on top of a 15-40% step OptiPrep™ gradient followed by rate zonal ultracentrifugation. Fractions before and after OptiPrep™ were analysed by SDS-PAGE and silver stained.

Lastly, the separation of uncoupled or excess gp140-ST from the coupled AP205-gp140-ST VLPs using the HiPrep™ 16/60 Sephacryl® S-500 HR size exclusion chromatography was attempted. However, this technique was not economically feasible because this 120ml preparative column required a high quantity of the coupled AP205-gp140-ST VLPs for them to be detectable after gel filtration. This proved difficult as the coupling efficiency was low, and it did not help that the sample got diluted during the SEC run. For example, coupled AP205-gp140-ST VLPs were not detected (on SEC elution profile (absorbance at 280 nm) and western blots) after the separation of a coupling reaction containing ≈100µg SC-AP205 VLPs + ≈500µg gp140-ST (results not shown). If higher molar concentrations of SC-AP205 VLPs than gp140-ST molar concentrations were to be used for the coupling reactions, this would have compromised the chances of increasing Env density, the sole objective of this project. Hence, gel filtration using a 120ml HiPrep™ 16/60 Sephacryl® S-500 HR column was not

pursued further in an attempt to remove excess gp140-ST from coupled AP205-gp140-ST VLPs. It was reasoned that a smaller preparative column, such as a Superose 6 10/300 GL column with a 24ml bed volume that is most suitable for separation of a small 25-500µl sample, would be ideal for this experiment to be economically feasible for small-scale preparations.

4.4 Discussion

One of the major aims of an HIV-1 envelope-based vaccine is to elicit broadly cross-neutralising antibodies against the circulating Tier 2 HIV-1 strains (Haynes & Burton. 2017; Sanders & Moore. 2017). However, the immune responses to HIV-1 Env are short-lived due to the slow spike density and wide spacing on a virion surface, among other atypical features of HIV-1 Env (Schiller & Chackerian. 2014; Klasse *et al.* 2020). In an attempt to enhance the immunogenicity of HIV-1 Env, in this Chapter, the high-density display/decoration of the flexibly linked HIV-1 gp140 trimers on *Acinetobacter* phage AP205 VLPs was evaluated using the in vitro two-component SpyTag/SpyCatcher technology.

Two C-terminally tagged soluble HIV-1 Env fusion proteins, gp140-SpyTag (gp140-ST) and gp140-SpyCatcher (gp140-SC), were produced in stably transfected HEK293 cells. Separation of the proteins on a native polyacrylamide gel showed that gp140-ST protein purified using size-exclusion chromatography (SEC) was predominantly trimeric compared to gp140-SC protein, which was mainly dimeric and monomeric. The inability of gp140-SC to efficiently form trimers could have been due to the extended length of the SpyCatcher protein (116 amino acids) that interfered with Env trimerisation as compared to the shorter SpyTag peptide (13 amino acids) that had no noticeable effect on the trimerisation of gp140-ST. Since gp140 trimers have been shown to elicit superior neutralising antibodies compared to their monomeric or dimeric counterparts (Medina-Ramírez *et al.* 2017), only the gp140-ST trimers were chosen for further experimentation and coupling to AP205 VLPs. A homogenous/monodisperse population of ≈32nm SpyCatcher-AP205 VLPs were successfully produced in high yields in *E. coli*, as confirmed by electron microscopy and dynamic light scattering. Each icosahedral AP205 VLP particle should theoretically be assembled from 180 units of the AP205 coat protein (CP3), and hence there are 180 potential SpyCatcher binding sites for the attachment of gp140-ST trimers.

Other groups that have explored using two-component nanoparticles to present HIV-1 Env trimers have used particles with valencies of up to 20, apart from Escolano *et al.* (2019), who also used the AP205 nanoparticle (Brouwer & Sanders. 2019; Antanasijevic *et al.* 2020; Brouwer *et al.* 2021a). While a high-density display of monomeric and small proteins is often attainable, the presentation of multimeric glycoproteins is not always efficient, and one cannot

reliably predict the approximate antigen valency after a conjugation reaction (Ueda *et al.* 2020; Rahikainen *et al.* 2021). In this study, we anticipated that the SpyTag-SpyCatcher-mediated assembly would be highly efficient, leading to a higher Env density on the AP205 VLPs (180-meric, hence expected >20 trimers per VLP) as compared to 24-meric (about 8 trimers displayed per nanoparticle) or 60-meric (about 20 trimers displayed per nanoparticle) nanoparticles commonly used for the presentation of HIV-1 trimers (Brinkkemper & Sliepen. 2019; Brouwer *et al.* 2019; Antanasijevic *et al.* 2020). Native agarose gel electrophoresis analysis showed in our experiments that the SpyTag/SpyCatcher-mediated isopeptide bond successfully coupled gp140 to the pre-assembled SC-AP205 VLPs. However, densitometric analysis of the SC-AP205 band intensity before and after the coupling reaction SDS-PAGE analysis suggested that the VLP binding sites were not saturated with gp140-ST trimers. In addition, the heterogeneity in diameter of coupled AP205-gp140-ST VLPs, as evaluated by dynamic light scattering, suggested that the VLPs were not uniformly saturated with coupled gp140 trimers. Considering that gp140 is a large (>720 kDa) trimeric and heavily glycosylated protein, the low coupling efficiency/capacity could be due to steric hindrance presented by the large size of gp140 trimers; this might have led to under-saturation of the VLPs even though gp140-ST was used in molar excess. The effect of steric hindrance on coupling efficiency is not unexpected because it has been reported previously that the increase in the size of an antigen was associated with a decrease in the number of coupled antigens per VLP (Thrane *et al.* 2016). For example, Thrane *et al.* (2016) calculated an 88% coupling efficiency for a 15 kDa protein to Spy-tagged AP205 VLPs, while a 34% coupling efficiency was calculated for a non-oligomeric 118 kDa protein (Thrane *et al.* 2016).

The unanticipated low incorporation of trimeric gp140 on phage particles was also observed previously in a study that evaluated the use of lambda phage particles as a scaffold for presentation of Env trimers in an enhanced immunological context (Mattiacio *et al.* 2011). In that study, the display of Env was achieved by mixing varying molar ratios of gp140-gpD fusion with the complementing gpD-deficient lambda phage capsid particles. In general, each lambda phage particle (±50 nm in diameter) contains 405 gpD binding sites. Unexpectedly, only 30 copies of gp140 trimers were incorporated per lambda phage particle, which translated to only 90 (i.e. approximately 25%) gpD binding sites that were likely used. Our results, together with those of Mattiacio *et al.* (2011), suggest that the high valency of nanoparticle scaffolds does not always translate to a high-density display of the protein of interest, especially for oligomeric proteins. On the contrary, the successful use of AP205 VLPs for a high-density display of different epitopes covering the alpha-helical region of HIV gp41, which were considerably smaller (2-9 kDa) than the gp140 trimers (720 kDa) investigated in this study, has been reported (Pastori *et al.* 2012); this supports the idea that the size and oligomeric nature of an

antigen can affect the displaying capacity on these VLPs. Although the stability of AP205-gp140-ST was not investigated in this study, it was noted that the steric interference of HIV-1 trimers has not only been previously associated with the incomplete decoration of the icosahedral 60-meric I53_dn5 nanoparticles but the overcrowding also affected the stability of these nanoparticles (Antanasijevic *et al.* 2020). These results suggested that the valency of nanoparticle scaffolds for the presentation of HIV-1 Env trimers does not necessarily need to be high, as the improvement in immunogenicity of ConM-SOSIP trimers displayed on low valency T33_dn2 (4 trimers per particle) was similar to that observed for trimers presented on 60-meric I53-50 nanoparticles where autologous Tier 1 ConM virus neutralising antibodies were detected (Brouwer *et al.* 2019; Antanasijevic *et al.* 2020).

In another study that investigated the display of different antigens with variable sizes and symmetries (monomers, cyclic dimers, trimers and tetramers) on mi3 nanoparticles that are immunologically similar to AP205 VLPs (Bruun *et al.* 2018), it was evident that in addition to the size of the antigen, the orientation (symmetry of antigen in relation to the nanoparticle's symmetry) of the antigens' subunits can impact the coupling efficiency (Rahikainen *et al.* 2021). These observations highlight the need to critically evaluate the geometry of nanoparticles in relation to the antigen that needs to be presented.

The immunogenicity of the coupled SC-AP205 VLPs + gp140-ST reaction preparation (called AP205-gp140-ST VLPs for simplicity) was evaluated in a pilot rabbit study. Two groups of rabbits received different regimens: Group 1 was inoculated four times with unadjuvanted AP205-gp140-ST VLPs (PPPP) while Group 2 was primed with two DNA, two rMVA (both encoding Env+Gag) and boosted with two unadjuvanted AP205-gp140-ST VLPs (DDMMPP). When evaluated in an autologous Env binding ELISA, both these regimens elicited anti-Env binding titres in rabbits, with the DDMMPP regimen showing overall higher binding titres than the PPPP regimen. The DDMMPP regimen elicited anti-Env binding titres after the second DNA prime, and they reached a peak after the 2nd MVA boost. Further boosting with AP205-gp140-ST VLPs did not increase the binding titres. Comparing the binding titres of rabbits that received the PPPP regimen versus titres in rabbits that received the DDMMPP regimen, our results further justify the narrative that heterologous prime-boost regimens improve the immune responses (Goepfert *et al.* 2014; Shen *et al.* 2017; Excler & Kim. 2019; van Diepen *et al.* 2019).

Neutralisation assays indicated that the PPPP regimen did not elicit antibodies with neutralising activities against Tier 1B and autologous Tier 2 viruses. This suggested that AP205-gp140-ST VLPs alone are not a suitable vaccine regimen. However, the DDMMPP regimen elicited Tier 1B neutralising antibodies after the 2nd MVA boost and after the first and

second boost with AP205-gp140-ST VLPs. Interestingly, autologous Tier 2 neutralising antibodies in the DDMMPP regimen were not detected after boosting with recombinant MVA but were observed after the 1st boost with AP205-gp140-ST VLPs, suggesting that these VLPs were an effective boost in this heterologous prime-boost regimen. The usefulness of phage-displayed gp140 as a boost in a heterologous prime-boost regimen as compared to when used as a sole regimen has been reported previously (Mattiacio *et al.* 2011).

When comparing the immunogenicity (autologous Tier 2 neutralising antibodies) of VLP-displayed gp140-ST to the results from our previous study that evaluated the immunogenicity of the soluble CAP256 gp140 (formulated in AlhydroGel® adjuvant) in the same prime-boost regimen used here (van Diepen *et al.* 2019) the autologous Tier 2 titres were lower when gp140 was displayed on AP205 VLPs. A notable difference between the soluble CAP256 gp140 vaccine and those tested here is that the AP205-gp140 VLPs were not formulated in any adjuvant. The modest immunological benefits of presenting HIV-1 gp140 trimers on AP205 VLPs echoes the ongoing hurdles of HIV Env nanoparticle vaccines that were reviewed in a meta-analysis study that indicated that the display of the relatively complex gp140 trimers on diverse scaffolds has not yet achieved significant enhancement in immunogenicity as compared to other viral immunogens (Kanekiyo *et al.* 2013; Darricarrère *et al.* 2018; Brinkkemper & Sliepen. 2019; Marcandalli *et al.* 2019). In addition, there is some evidence to suggest that the composition of the vaccine candidate tested may have been sub-standard: it is possible that the density of the gp140 trimers displayed on the AP205 VLPs were insufficiently dense, and there may have been an excess of uncoupled gp140-ST in the preparation due to a low coupling efficiency which has little potential for contributing to immunogenicity.

To address this, we looked at maximising coupling efficiency by varying coupling ratios as well as trying to remove excess gp140-ST from coupled VLP preparations. Densitometric analysis of coupled AP205-gp140-ST or SC-AP205 CP3 bands on SDS-PAGE suggested that increasing the gp140-ST to VLP molar coupling ratio in an attempt to saturate the VLPs did not significantly improve the coupling efficiency. Several different techniques were evaluated to remove excess gp140-ST from conjugated AP205-gp140-ST VLPs. Although dialysis using a MW cut-off membrane to allow for retention of the coupled VLPs only, as well as PEG/NaCl precipitation of the VLPs were unsuccessful in removing uncoupled gp140-ST, rate zonal centrifugation was successful. However, after this, the yield of coupled VLPs was extremely low, making the preparation of sufficient amounts of coupled VLPs for vaccine doses impractical. This evidence also confirmed that the coupling efficiency of gp140-ST to SC-AP205 VLPs was very low.

In conclusion, although the SpyTag/SpyCatcher technology used in this work is generally considered an effective technique for generating particle display vaccine candidates, its applicability was limited in this study by the complex nature and size of HIV-1 gp140 trimers. The steric hindrance from gp140 trimers made it difficult to display these trimers in a high-density manner on the surface of the AP205 VLPs. Due to the poor coupling efficiency of gp140-ST to SC-AP205 VLPs and subsequent low yields of coupled particles, we concluded that the AP205 VLPs are not the most suitable scaffolds for achieving high-density display of the trimeric gp140. It is possible that the optimal presentation of gp140 trimers could be achieved by using larger display nanoparticles (in diameter) with optimal spacing to reduce steric clashes or computationally designed scaffolds such as I53-50 and a recently established library consisting of nanoparticles with tetrahedral (T33_dn2; present four HIV-1 Env trimers per nanoparticle) or icosahedral (I53_dn5, present 20 trimers per nanoparticle) symmetries (Bale *et al.* 2016; Brouwer *et al.* 2019; Antanasijevic *et al.* 2020; Ueda *et al.* 2020). These nanoparticles are designed to take into consideration two critical parameters: 1) the geometric compatibility between the chosen scaffold and the trimeric gp140 trimers, and 2) optimal spacing between displayed trimers to obtain nanoparticles that present the neutralisation epitopes located at the trimer apex or the trimer base (Antanasijevic *et al.* 2020; Ueda *et al.* 2020).

CHAPTER 5: GENERAL CONCLUSION

An effective HIV-1 vaccine is expected to elicit broadly cross-neutralising antibodies against the circulating clinically relevant Tier 2 HIV-1 strains (Haynes & Burton. 2017; Sanders & Moore. 2017; Pauthner & Hangartner. 2020). The HIV-1 envelope glycoprotein (Env) is the sole viral antigen that can be used in a vaccine to elicit neutralising antibodies. However, several structural features of HIV-1 Env, including metastability of the trimer, dense arrays of glycans that occlude the conserved Env epitopes and the low spike density per virion surface, render Env poorly immunogenic and an atypical immunogen for induction of durable bNAbs (Schiller & Chackerian. 2014; Kong *et al.* 2016; Crispin *et al.* 2018; del Moral-Sánchez & Sliepen. 2019; Klasse *et al.* 2020; Watanabe *et al.* 2020). The generation of soluble HIV-1 Env trimers, such as SOSIP- and NFL-stabilised trimers that closely mimic the native conformation of the Env spike, has enabled the induction of autologous Tier-2 neutralising antibody responses in animal models (Sanders *et al.* 2015; Sanders & Moore. 2017). However, none of these soluble trimers has been able to elicit consistent and adequate levels of Tier 2 bNAbs required for a broadly effective vaccine (Martinez-Murillo *et al.* 2017; Torrents *et al.* 2018; Dubrovskaya *et al.* 2019; Kong *et al.* 2019; Brouwer *et al.* 2021a). This suggests that strategies beyond the stabilisation of the trimers need to be investigated to improve the immunogenicity of soluble Env trimers.

Presentation of otherwise soluble immunogens on self-assembling nanoparticles and virus-like particles (VLPs) is a novel approach for enhancing their immunogenicity (Bachmann & Jennings. 2010; López-Sagaseta *et al.* 2016; Moyer *et al.* 2016; Gause *et al.* 2017; Irvine & Read. 2020). Initial efforts focused on using recombinant HIV-1 Gag VLPs as a scaffold for the presentation of Env trimers. However, the same limitations (low spike density, wide spacing and incorporation of non-native trimers) observed on a native virion were encountered for recombinant Gag-Env VLPs (Moore *et al.* 2006; Crooks *et al.* 2007). Even though these issues were somewhat addressed by introducing sequence modifications to stabilise Env trimers, removal of the gp41 cytoplasmic tail and proteolytic digestion to remove non-native trimers (Crooks *et al.* 2011; Crooks *et al.* 2015; Stano *et al.* 2017), the yields of recombinant Gag-Env VLPs were still low, limiting investigation of their efficacy in animal models (Brouwer & Sanders. 2019).

Although the investigation of various different HIV-1 Env nanoparticle vaccine platforms has been initiated in recent years, many studies are still exploratory and highlight both the potential of nanoparticle vaccines and the amount of optimisation still required to improve the outcomes in this field. This thesis details the investigation of two different nanoparticle presentation approaches in an effort to improve the immunogenicity of HIV-1 Env antigens.

The first approach investigated the impact of genetically fusing the protein body-forming Zera® peptide to either the N- or C-terminus of CAP256 gp140 to generate Zera®-gp140 and gp140-Zera® fusions, respectively. Fusion of Zera® to a protein of interest usually results in the formation of dense endoplasmic reticulum-derived protein bodies (PBs) which comprise many copies of the protein of interest which are also protected from degradation; this encourages much higher yields of the recombinant protein and facilitates efficient purification using gradient ultracentrifugation (Llop *et al.* 2006; Torrent *et al.* 2009a; Llompart *et al.* 2010; Schwestka & Stoger. 2021). Even though Zera® is derived from the plant storage protein zein, the formation of Zera®-induced PBs is not only limited to plant expression hosts. A wide range of eukaryotic expression hosts, including mammalian cells, insect cells and filamentous fungi, have been reported to support the production of Zera® PBs (Torrent *et al.* 2009a; Smith *et al.* 2014). In this work, the potential production of Zera®-gp140 and gp140-Zera® protein bodies was initially evaluated in *N. benthamiana* plants. This was motivated by results reported by Medicago Inc on the rapid production of influenza vaccine candidates in plants and their subsequent safety profiles in human clinical trials (D'Aoust *et al.* 2008; Landry *et al.* 2010; Cummings *et al.* 2014; Rybicki. 2014). Molecular farming is fast becoming an accepted method for the production of recombinant proteins and vaccines as it has advantages of ease of scalability and cost-effectiveness (Fischer & Buyel. 2020; Tsekoa *et al.* 2020; Schillberg & Finnern. 2021). In addition, our laboratory had recently established and optimised a transient expression system in *N. benthamiana* using *Agrobacterium*-mediated infiltration for producing soluble CAP256 gp140 (Margolin *et al.* 2019).

Analysis of homogenised plant leaf extracts collected post infiltration indicated successful expression of the Zera®-gp140 protein. However, no expression of the gp140-Zera® protein was observed despite further optimisation of the extraction buffers and harvesting at different times post-infiltration. Whole-mount immunofluorescent staining of protoplasts prepared from leaves infiltrated with Zera®-gp140 indicated the presence of unexpectedly small PB-like structures, but none were detected in protoplasts prepared from leaves expressing the untagged gp140, suggesting that the fusion of Zera® had an influence on the protein. Considering that to our knowledge, gp140 (140 kDa) is the second-largest protein that has been fused to Zera® after the ±75 kDa influenza H5 (Hofbauer *et al.* 2016), it is possible the complexity, extensive size, as well as low accumulation of HIV Env may have prevented larger-sized PBs to be formed.

Unlike our soluble gp140 secreted to the cell media (Margolin *et al.* 2019), Zera®-gp140 was largely targeted to the leaf plant's intracellular compartments (ER). It is worth noting that the plasmid encoding Zera®-gp140 did not have the LPH secretion signal sequence, which drives the translocation of the soluble gp140 protein through the plant secretory pathway. The

retention of Zera® in the ER is thought to be facilitated by its unique sequence properties regardless of the presence of the native zein signal peptide and the absence of an obvious ER-retention signal (Geli *et al.* 1994; Kogan *et al.* 2001; Llop-Tous *et al.* 2010). Tissue disruption or homogenisation of the infiltrated leafy biomass is a must to recover the target protein, and this generally leads to the accumulation of plant debris that can be detrimental to the quality of the upstream purification processes (Buyel *et al.* 2015).

Unfortunately, we were faced with this challenging bottleneck as well. Zera®-gp140 PBs were unsatisfactorily separated from plant debris despite trying a variety of methods, including aqueous chloroform precipitation and pH shift/heat precipitation of the plant leaf homogenates before ultracentrifugation. As an alternative to using ultracentrifugation for purification of Zera® PBs from plants, Schwestka *et al.* (2020) recently developed a sequential tangential flow filtration (TFF) method for downstream purification of PBs, and this also enabled the use of flow cytometry to separate PBs on the basis of their size (Schwestka *et al.* 2020). The TFF method incorporates non-ionic Triton-X100 (2%) in the extraction buffers to aid the solubilisation of ER membranes (which potentially causes the association of PBs with residual leaf material remaining after the initial clarification steps) and separation of host proteins from the target protein. The extracted homogenate for TFF is first clarified by low-speed centrifugation, as done for ultracentrifugation. However, instead of using the supernatant that is typically used for ultracentrifugation, in the TFF method, the protein pellet is washed several times using the same extraction buffer and then applied to a sequential TFF system with differently sized nylon filters. The first filtration step removes cell debris, while the second filtration step concentrates PBs (Schwestka *et al.* 2020). The TFF system seems to simplify the downstream processing of PBs without solubilising them as the buffer used does not include reducing agents like dithiothreitol, and we will consider it in future for purification of Zera® PBs from plants.

Taken together, the inability to achieve acceptable quality and purity of the plant-derived Zera®-gp140 protein for evaluating the immunogenicity of PBs containing HIV-1 gp140 in rabbits is testament to the ongoing challenge of downstream processing (extraction and purification from plant-specific particulates) of proteins from leafy biomass – and especially for intracellular accumulating proteins like Zera®-tagged fusions (Buyel & Fischer. 2014; Sabalza *et al.* 2014; Buyel *et al.* 2015).

In efforts to generate better-purified samples, the generation of Zera®-induced gp140 protein bodies was subsequently evaluated in a mammalian expression system. Despite the high cost of this production platform, the mammalian expression system affords proper folding and glycosylation of glycoproteins compared to plant expression systems where complex

glycosylation is limited and may influence immune responses if used as vaccine candidates (Margolin *et al.* 2018; Margolin *et al.* 2020). In this study, stable HEK293 cell lines that successfully expressed Zera®-gp140 or gp140-Zera® were generated. Both Zera®-gp140 and gp140-Zera® proteins accumulated intracellularly rather than being secreted into the cell media, a common phenomenon for Zera® fusions as they are retained in the ER. Unlike what was observed in the plant expression system, gp140-Zera® was expressed in mammalian cells, albeit at lower levels than Zera®-gp140. It is not clear why gp140-Zera® was not expressed in plants. The low expression of a C- compared to N-terminal Zera® fusion has also been reported previously - the yields of Nef-zein were lower than zein-Nef, suggesting that the position of Zera®/zein can influence protein expression de Virgilio *et al.* (2008). Immunofluorescent staining, electron microscopy and ultracentrifugation confirmed the presence of small PB-like structures in cells expressing gp140-Zera®. However, no PB-like structures were observed in mammalian cells expressing Zera®-gp140. The discrepancy in the detection of Zera®-gp140 PB-like structures in plants but not in mammalian cells is a reflection that several factors, including intrinsic properties of the expression host, can impact the PB-inducing capacity of Zera®. This indicates that the success of Zera® technology can only be determined empirically. Properties of the protein fused to Zera® matter and the suitable recombinant expression host for expression of a particular fusion requires optimisation. In addition, considering that it has been reported that PB formation is a concentration-dependent mechanism (Saberianfar *et al.* 2015): thus, the relatively inefficient formation of Zera® PBs, in our case, could suggest that yields were too low.

Additionally, the cysteine residues in the Zera® domain are essential for oligomerisation into PBs (Llop-Tous *et al.* 2010). The gp140 sequence is cysteine-rich (18 cysteine residues) and contains N glycosylation sites. Hence, it is possible that the mispairing of the cysteine residues could have led to the formation of aberrant disulphide bridges as a result of isomerisation with the six cysteine residues of Zera®, thus forming misfolded protein that is targeted to the ERAD for degradation before reaching PBs; this could potentially reduce the total protein accumulation, meaning a threshold protein concentration optimal for assembly into PBs was not reached. The highly N-glycosylated nature (≈28 *N*-glycosylation sites) of HIV-1 Env could have favoured the solubilisation of the translated protein. Both these features likely contributed to the inadequate formation of Zera®-induced Env PBs. Rate zonal and isopycnic ultracentrifugation was not optimal for purification of Zera®-tagged gp140 protein because of the variable sizes/densities of gp140-Zera® or Zera®-gp140-specific proteins that separated across a wide range of gradient concentration. The variability in size or density of PBs could indicate that they were harvested at different developmental stages of the PBs. PB induction is initiated by hydrophobic interaction between Zera® molecules followed by the formation of

the intermolecular disulphide bridges to stabilise PBs and subsequent growth in the size of PB as the protein concentration increases over time, and newly formed proteins get deposited into pre-formed PBs (Llop-Tous *et al.* 2010). Thus, gp140-Zera® and Zera®-gp140 protein expressed from stable HEK293 cell lines were concentrated by pelleting cell lysates by ultracentrifugation and resuspension of the protein pellet to provide sufficient amounts for immunogenicity studies. The immunogenicity of Zera®-gp140 and gp140-Zera® was evaluated by injecting two groups of 5 rabbits four times and measuring the binding and neutralising antibody titres. Anti-Env binding antibody titres and Tier 1A neutralising serum titres were higher for gp140-Zera® than for Zera®-gp140. Neither gp140-Zera® nor Zera®-gp140-specific sera neutralised a Tier 1B pseudovirus or the autologous Tier 2 CAP256SU pseudovirus, suggesting that Zera® might have compromised the structure of the Zera®-tagged gp140 proteins.

Overall, it is apparent that Zera® technology is a novel concept that may be suitable for protein body formation for monomeric and small proteins only, possibly where conformation is not critical. However, in this study, the relatively large size, oligomeric, amino acid composition (cysteine-rich and N-glycosylation sites) and the low accumulation of gp140 could have all contributed to the inefficient production of Zera®-induced Env protein bodies. In addition, retaining the native-like conformation of gp140 is essential to increase the likelihood of eliciting neutralising antibody titres. Hence it became clear that fusing Zera® to gp140 was not a good fit for HIV Env immunogens designed to elicit neutralising responses. As an alternative to genetically fusing Zera® to gp40 sequence, one can independently purify Env trimers to an acceptable quality and also independently express and purify PBs. The purified trimers can then be formulated with the PBs for immunisations. The adjuvant properties of pre-formed PBs have been previously reported by Whitehead *et al.* (2014). They observed that the formulation of empty Zera® PBs with the human papillomavirus 16E7SH immunogen provided adjuvant effects that could not be further enhanced by adding the commercial adjuvant (Whitehead *et al.* 2014). The inability of gp140-Zera® and Zera®-gp140 immunogens to elicit autologous Tier 2 neutralising antibodies reiterated the limitations of using in vivo assembling nanoparticle approaches for HIV-1 Env (Brinkkemper & Sliepen. 2019; Brouwer & Sanders. 2019).

The second nanoparticle approach used was to *in vitro*-assemble two-component virus-like particles to display multiple copies of the soluble HIV-1 CAP256 gp140 trimers. Unlike PB assembly, in vitro-assembling nanoparticles permit the independent expression and purification of Env trimers and the nanoparticle scaffolds. The SpyTag/SpyCatcher-mediated isopeptide bond (Brune *et al.* 2016; Aves *et al.* 2020) was used for coupling CAP256 gp140

to the surface of *Acinetobacter* phage AP205 VLPs. AP205 VLPs are 180-meric VLPs; hence we expected a high-density display of gp140 trimers on the particles.

HIV-1 CAP256 gp140-SpyTag (gp140-ST) was expressed in HEK293 stable cell lines, and trimers (≈720 kDa) were separated from other Env species using lectin affinity and size exclusion chromatography (SEC). SpyCatcher (SC)-AP205 VLPs (35 nm) were produced in *E. coli* and purified by ultracentrifugation. These VLPs were mixed in varying molar ratios with HIV gp140-ST trimers, and coupling was confirmed by SDS-PAGE, native agarose gel electrophoresis and dynamic light scattering. These analyses suggested that the VLPs were not saturated with gp140, i.e. not all SpyCatcher tags on the particles were bound to a SpyTagged gp140 molecule, indicating a low coupling efficiency. It was theorised that the low coupling efficiency could be due to the steric hindrance caused by the large size of gp140 trimers. The immunogenicity of coupled VLPs (SC-AP205 VLPs + gp140-ST) was evaluated in a pilot study in rabbits using two different immunisation regimens. One group was injected four times with coupled VLPs, and the second group with DNA vaccines expressing Env and mosaic Gag, followed by modified vaccinia Ankara (MVA) expressing the same antigens then boosted twice with coupled VLPs. None of these immunogens was formulated with an adjuvant. The binding and neutralising antibody responses were measured. Modest Tier 1B and autologous Tier 2 neutralising antibody titres were observed in 2/5 rabbits primed with DNA and MVA, but not in rabbits injected only with coupled VLPs. These results suggested that although the coupled VLPs were not immunogenic (i.e. did not elicit autologous Tier 2 neutralising antibody titres) on their own, they could potentially be useful as a boost in heterologously primed animals. However, the neutralising antibody titres elicited were similar to those using soluble gp140 (unpublished results). The modest antibody titres were probably due to the low density of the gp140 trimers displayed on a proportion of the AP205 VLPs.

Further experimentation – for example, optimising the molar coupling ratios - to increase the density of gp140 on AP205 VLPs did not significantly improve the coupling efficiency. The rate zonal ultracentrifugation successfully removed excess gp140-ST from the coupled AP205-gp140-ST VLPs. However, the yield of coupled VLPs was low, making the preparation of sufficient amounts of coupled VLPs for vaccine doses impractical. This evidence also confirmed that the coupling efficiency of gp140-ST to SC-AP205 VLPs was very low.

In conclusion, the SpyTag-SpyCatcher technology is a novel coupling strategy. However, to achieve an ordered and dense display of the complex Env trimers, it is essential to identify or design optimally-sized nanoparticles with trimeric threefold symmetries, for example, the I53-50 nanoparticles (Bale *et al.* 2016; Bale *et al.* 2017; Brouwer *et al.* 2021a). These computationally designed scaffolds may be more suitable for displaying HIV-1 Env trimers at

a defined valency and spacing (Nguyen & Tolia. 2021). In future, we hope to explore different nanoparticle scaffolds, including the rationally designed dodecahedral 60-meric mi3 nanoparticles derived from the aldolase of the hyperthermophilic bacterium *Thermotoga maritima* (Bruun *et al.* 2018).

I acknowledge that there were shortcomings in this study that could be addressed in future studies. The antigenicity of gp140 arrayed on AP205 VLPs remains to be determined. The antigenic features of Env displayed on these VLPs are set to be determined using two assays: 1) antibody capture of the purified AP205-gp140-ST VLPs followed by detection with native/non-native Env-specific monoclonal antibodies and 2) Octet assay based on bio-layer interferometry. Cryo-electron microscopy and 3D reconstruction could be a valuable technique for determining the number of gp140-ST displayed per VLP and the spacing between the coupled trimers. Another interesting prospect is that instead of displaying the structurally complex full-length gp140 trimers, one could decorate these VLPs with conformation-specific Env peptides.

APPENDIX

1. General molecular biology protocols

1.1 Small-scale plasmid DNA isolation

A single recombinant colony from a freshly streaked/plated selective plate was inoculated into 3ml LB medium containing the appropriate antibiotic/s and incubated overnight at 37°C with shaking. Bacterial (*E. coli*) cells from 2 ml of the overnight culture were harvested by centrifugation at maximum speed in a table-top microcentrifuge for 15 seconds. The rest of the overnight culture was stored at 4°C for downstream usage. The supernatant was discarded while the bacterial pellet was gently resuspended with 250µl of the resuspension solution (P1 solution). Cells were lysed by adding 250µl of the lysis solution (P2 solution) and gently inverting the tube 4-6 times. The neutralising solution (P3 solution), 350µl, was added before mixing by inverting the tube several times. After centrifugation at a maximum speed for 10min, 700µl of the clear supernatant was transferred to a new 1.5 ml Eppendorf tube. To precipitate DNA, 700µl of ice-cold isopropanol was added to the collected supernatant and incubated at -20°C for 1 hour. Precipitated DNA was harvested by centrifugation at maximum speed for 20mins. The supernatant was carefully removed without disturbing the pellet, and the DNA pellet was washed by adding 180µl of 70% of ice-cold ethanol. The ethanol wash was removed by centrifugation at high speed for 1 min. The supernatant was discarded, and the DNA pellet was airdried for ≈5 min while ensuring that the pellet was not overdried. The DNA pellet was resuspended with 50µl of sterile distilled water.

1.2 Large-scale plasmid DNA isolation

Large scale plasmid DNA isolations were carried out using the ZymoPURE ™ II Plasmid Maxiprep Kit (Zymo Research). A single recombinant colony from a freshly streaked plate was inoculated into 100ml LB medium containing the appropriate antibiotic/s and incubated overnight at 37°C with shaking. From the overnight culture, glycerol (15%) stocks were made by mixing 700µl of the culture with 300µl sterile 50% glycerol and stored at -80°C. The remaining overnight culture was transferred into 2x50ml falcon tubes, and the bacterial cells were harvested by centrifugation (BOECO u-320, 4000 rpm, 10 minutes). The supernatant was discarded while the pellets (pellets from both falcon tubes were pooled) were resuspended by pipetting up and down with 14ml of ZymoPURE™ P1 (Red) buffer. ZymoPURE™ P2 (Green) buffer (14ml) was added to the resuspension and mixed in immediately by inverting the tubes 6 times. After adding 14ml of ZymoPURE™ P3 (yellow) buffer, tubes were gently inverted several times to mix. The lysate was filtred using a ZymoPURE™ Syringe Filter into a clean 50ml falcon tube. ZymoPURE™ Binding buffer

(14ml) was added to the clarified lysate and mixed by inverting the tube 10 times. The mixture was passed through a Zymo-Spin™ V-P Column assembly by applying a vacuum. The Zymo-Spin™ V-P Column was washed by passing through 5ml of ZymoPURE™ Wash 1 using a vacuum. The Zymo-Spin™ V-P Column was washed twice more with 2x5ml of ZymoPURE™ Wash 2. At each step, the vacuum was applied until the entire liquid passed through the column. The Zymo-Spin™ V-P Column was removed from the vacuum manifold, transferred into a clean 1.5ml Eppendorf tube and spun at ≈10 000 x *g* for 1 min to remove residual wash buffer. The Zymo-Spin™ V-P Column was transferred into another clean 1.5ml Eppendorf tube, and 400µl of ZymoPURE™ Elution buffer was added directly to the column matrix. After incubation for 2 minutes at room temperature, pure plasmid DNA was harvested by centrifugation at 10 000 x *g* for 1 minute. The plasmid DNA concentration was measured using a NanoDrop (Thermo Fisher Scientific).

1.3 Restriction digestion of plasmid DNA

All enzymatic digestion of the plasmid DNA was achieved using the FastDigest Restriction Enzymes (Thermo Scientific) in a single universal buffer (10X FasDigest Green Buffer). For a double digest of a plasmid DNA, 1.5µl of 10X FasDigest Green Buffer, 1µl of each of the two restriction enzymes and 1µg of the plasmid were added to distilled water to get a 25µl reaction. Fast digest reactions were incubated at 37°C for 30-60minutes before analysis on an agarose gel.

1.4 Agarose gel electrophoresis

Plasmid DNA preparations were analysed by agarose gel electrophoresis. Agarose gels (0.8%) were prepared by dissolving SeaKem® LE Agarose (Lonza) in Tris/Borate/EDTA (TBE) buffer. Before pouring the agarose solution into a gel casting tray, the agarose solution was supplemented with 0.5µg/ml ethidium bromide (EtBr) (Sigma-Aldrich). The experimental DNA samples and the 1kb DNA ladder (ThermoFisher Scientific) were loaded on a gel before electrophoresis at 80-100 V for 90 minutes. The gels' digital images were captured using the UV-light Molecular Imager® Gel Doc™ XR+ Imaging System (Bio-Rad). If DNA fragments were needed for cloning, the agarose gel was visualised using a blue light BLooK LED transilluminator (GeneDireX).

1.5 Extraction of DNA fragments from agarose gels

The Zymoclean™ Gen DNA Recovery Kit (Zymo Research) was used to recover DNA from agarose gels. Agarose gels were visualised using a blue-light illuminator BLooK LED transilluminator (GeneDireX), and a razor blade was used to excise a fragment of interest.

The excised DNA-containing agarose gel was transferred into a clean 1.5ml Eppendorf tube and weighed on a scale that had been pre-blanked with the same but empty 1.5ml Eppendorf tube. Three volumes of the Agarose Dissolving Buffer (ADB) was added to one volume of the excised agarose gel. The tube was inserted into a heat block set at 50°C and incubated until the agarose was completely dissolved (≈5-10 minutes). The melted agarose solution was transferred into a Zymo-Spin™ Column in a Collection Tube. After centrifugation (15 000 x *g*, 1 min), the flow-through was discarded, and the Zymo-Spin™ Column was washed with 200µl of DNA Wash buffer. After centrifugation for 30 seconds, the wash step was repeated. The Zymo-Spin™ Column was transferred into a clean 1.5ml Eppendorf before adding 30µl of pre-warmed (50°C) DNA Elution Buffer. After incubation for 1 minute at room temperature, DNA was eluted from the Zymo-Spin™ Column into the 1.5ml tube by spinning for 1 min.

1.6 DNA ligation

DNA fragments were ligated into respective plasmid vectors using the T4 DNA ligase (Thermo Fisher Scientific). A typical ligation reaction contained 2µl of T4 DNA ligase buffer, 1µl of digested plasmid vector (1µg) that had been recovered from an agarose gel, 3µl DNA insert that had also been recovered from agarose gel and 1µl T4 DNA ligase. Plasmid only (no insert but with T4 DNA ligase) and no ligase (plasmid only without T4 DNA ligase and the insert) reactions were included as controls. Reactions were incubated for 1 hour at room temperature before transformation into competent *E. coli* cells.

1.7 Transformation of plasmid DNA into competent bacterial cells

The ligation reactions or purified plasmid vectors were transformed into *E.* cloni 10G chemically competent cells (Lucigen). Briefly, 15µl of competent cells were transferred into 1.5ml Eppendorf tubes in ice, 1µl of ligation reaction or 1ng of plasmid DNA was added and incubated on ice for 30 minutes. Transformed cells were heat-shocked for 30 seconds in a 37°C heat block and placed back in ice for 2 minutes. To each transformation tube, 400µl of the recovering media was added, and the mixture was incubated at 37°C for 1hour with gently shaking. An aliquot, 140µl, from each transformation reaction, were plated onto LB agar plates containing an appropriate antibiotic. Plates were incubated overnight at 37°C.

2 General methods for protein analysis

2.1 SDS-PAGE analysis

Protein samples, as well as the Color Prestained Protein standards (BioLabs, New England), were analysed by sodium dodecyl sulfate-polyacrylamide gel electrophoresis (SDS-PAGE) using a method modified from Laemmli (1970). A discontinuous buffer system was used

comprising a 8% resolving gel [5.3ml distilled H_2O; 2.5ml of 1.5 M Tris-HCl pH 8.8; 2ml Acrylamide-bis ready to use solution 40%, 29.1:0.9 (Merck, Germany); 0.1ml 10% SDS; 0.1ml of 10% ammonium persulphate (APS, Amresco®, Solon, Ohio) and 6µl tetramethyl ethylenediamine (TEMED)] and a 4% stacking gel [3.8ml distilled H_2O; 0.63ml 1.5M Tris-HCl pH 6.8; 0.5ml Acrylamide-bis ready to use solution 40% (29.1:0.9), 50µl of 10% SDS; 50µl of 10% APS and 5µl TEMED]. Protein samples were combined with 4x sample analysis/loading buffer (SAB) (4ml of 100% glycerol, 1.6ml of 1.5M Tris-HCl pH 6.8, 0.8g SDS, 4mg bromophenol blue, 0.5ml 2-beta mercaptoethanol and 3.9ml dH_2O) and boiled for 5min. Following loading of samples into SDS-polyacrylamide gel wells, electrophoresis was conducted at 200V for ≈1 hour using the Mini-PROTEAN® Tetra System (Bio-Rad) in the presence of 1x running buffer (10x: 10g SDS, 30.3g Tris, 29g glycine, to 1L dH_2O). Depending on the sensitivity required for the experiment, after electrophoresis, gels were either stained with commercially available Bio-Safe™ Coomassie Stain (Bio-Rad-Hercules) or Silver Stain Plus kit (Bio-Rad-Hercules) as per supplier's recommendations or transferred for western blotting (Appendix A, Section 2.2).

2.2 Western blot analysis

Western blot analysis of proteins was conducted according to the protocol described by Towbin *et al.* (1979). Following separation by SDS-PAGE (Appendix A, Section 2.2), proteins were transferred from the gel onto a PVDF membrane (Bio-Rad-Hercules) that was briefly pre-activated in 100% methanol followed by further soaking in a transfer buffer (0.37g SDS, 5.8g tris, 14.4g glycine, 800ml dH_2O, and 200ml methanol). Protein transfer was achieved using the Trans-Blot® SD Semi-Dry Transfer Cell (Bio-Rad, Hercules) at 20V for 1 hour. Upon completion of protein transfer onto the PVDF membrane, the unoccupied sites on the membrane were blocked in 2% Bovine Serum Albumin Fraction V (BSA, Roche) dissolved in PBST [1x PBS (Lonza), 0.1% Tween-20 (VWR AMRESCO, LIFE SCIENCE)] for 1 hour at RT. The membrane was then incubated at RT overnight with the primary antibody (1:1000 dilution of goat anti-HIV-1 gp120 antibody (Bio-Rad)) or 1:4000 mouse anti-GFP antibody (Sigma-Aldrich) or 1:5000 rabbit anti-Zera® serum (generously provided by the Biopharming Research Unit lab, Molecular and Cellular Biology, University of Cape Town)). Rabbit anti-Zera® serum was pre-adsorbed with lysates from un-transfected HEK293T cells to minimise non-specific background. Membranes were washed (3x10 min) with PBST and incubated with the appropriate secondary antibody conjugates [1:10 000 anti-goat/sheep-alkaline phosphatase (Sigma-Aldrich) or goat anti-mouse alkaline phosphatase (Sigma-Aldrich) or anti-rabbit alkaline phosphatase (Sigma-Aldrich), respectively] diluted in 2% BSA-PBST. Following washes in PBST, the membranes were developed with 5ml of BCIP/NBT Phosphatase Substrate (KPL). The reaction was stopped by several washes in distilled water.

2.3 Coomassie staining

After SDS-PAGE or BN-PAGE electrophoresis, gels were incubated for 1 hour with Bio-Safe™ Coomassie stain (Bio-Rad) at room temperature with gentle agitation. Gels were briefly washed 2-3 times with water and imaged using a Molecular Imager® Gel Doc™ XR+ Imaging System (Bio-Rad). Alternatively, gels were incubated for 1 hour with Coomassie Blue [0.125% (w/v) Coomassie brilliant Blue G-250 (Bio-Rad), 50% (v/v) methanol, 10% (v/v) acetic acid, 40% (v/v) distilled water] whilst gentle shaking. After staining with Coomassie Blue, gels were incubated with the destaining solution [50% (v/v) methanol, 10% (v/v) acetic acid, 40% (v/v) distilled water] overnight at room temperature whilst shaking. If necessary, the destaining was repeated before another detaining with water until the gel expanded to its original size. Gels were imaged using a Molecular Imager® Gel Doc™ XR+ Imaging System (Bio-Rad).

2.4 Silver staining

In order to visualise very low amounts of protein on SDS-PAGE gels, a 30-50-fold more sensitive (than Coomassie Blue stain) Silver Stain Plus™ Kit (Bio-Rad) was used. After electrophoresis, gels were incubated with the fixative enhancer solution [50% (v/v) methanol, 10% (v/v) acetic acid, 10% (v/v) fixative enhancer concentrate, 30% (v/v) distilled water] for 20 minutes at room temperature with gentle shaking. Gels were washed for 2x10min with distilled water. Proteins were detected by incubation for ≈15min in a freshly prepared developing solution [2.5g Development Accelerator reagent dissolved in 50ml distilled water + Staining solution (35ml distilled water, 5ml Silver Complex Solution, 5ml Reduction Moderator Solution, 5ml Image Development Solution)]. The staining reaction was stopped by incubating gels with 5% (v/v) acetic acid for 15 min with gentle agitation. Gels were rinsed several times with distilled water before imaging using a Molecular Imager® Gel Doc™ XR+ Imaging System (Bio-Rad).

2.5 BN-PAGE

NativePAGE™ Novex® 3–12% Bis-Tris Gels (Thermo Fisher Scientific) were used to separate proteins under native (non-denaturing) electrophoresis conditions. Briefly, samples were prepared in a 4x NativePAGE™ Sample Buffer (Thermo Fisher Scientific). After rinsing the wells of the NativePAGE™ Novex® 3–12% Bis-Tris gel 3x with 1x NativePAGE™ Light Blue Cathode Buffer [diluted 50ml of 20x NativePAGE™ Running Buffer and 5ml of 20x NativePAGE™ Cathode Additive (Thermo Fisher Scientific) in 945ml distilled water], gels were placed in a Mini Gel Tank (ThermoFisher Scientific). The inner gel chamber was filled with the 1x NativePAGE™ Light Blue Cathode Buffer, while the outer chamber was filled with the 1x

NativePAGE™ Anode Buffer. Samples were loaded in parallel with the NativeMark™ Unstained Protein Standard (ThermoFisher Scientific). Gels were run at 150V for 2 hours.

3 Standard tissue culture protocol

3.1 Thawing and culturing of cells

For this study, adherent human embryonic kidney (HEK293T (ATCC® USA, CRL-3216™), HEK293 (ATCC® USA, CRL-1573™) and immortalised cancerous (HeLa, ATCC® USA, CCL-2™) cell lines were used for transient expression. HEK293T cells were derived by modifying the original HEK293 cells to express the simian virus 40 large T antigen (SV40), which enhances the transient expression of SV40-bearing plasmid vectors (Rio et al, 1985). Cells cryopreserved in liquid nitrogen or -80°C were revived by rapid thawing in a 37°C water bath, and transferred into pre-warmed complete medium [Dulbecco's Modified Eagle's Medium (DMEM, Lonza, Basel) supplemented with 10% heat-inactivated fetal calf serum (FCS, Gibco™, ThermoFisher Scientific, Waltham, US) and 5000 U/ml Penicillin-Streptomycin (Gibco™, ThermoFisher Scientific, Waltham, US)]. The volume of the medium and the size of the tissue culture vessel used for plating cells depended on the approximate cell density at which the cells were originally frozen down per cryotube. The viability of cells was monitored by staining with Trypan Blue Stain (0.4% Gibco™, US). Cells were grown at 37°C in a 5% humidified CO_2 incubator. One day after reviving cryopreserved cells, cells were viewed using the light microscope (Olympus, CK2, Japan), the medium was replaced with fresh complete medium and incubated at 37°C until 60-80% confluence was reached.

3.2 Trypsinizing, splitting and seeding of cells

At the desired confluence, cells were passaged as follows. The cell medium was removed from the confluent T75 flask, washed with 10ml PBS, trypsinised with 2ml of 0.25 % Trypsin-EDTA (Gibco™, Paisley, UK) and incubated for a few minutes to allow cells to detach. Cell detachment was enhanced by gently tapping the sides of the flask. Trypsin was diluted by adding 10ml of complete medium followed by pipetting up and down to avoid cell clumping. Depending on how confluent the cells were when split and when the cells were intended to be used, cells were seeded into a new flask(s) at appropriate dilutions and incubated at 37°C. Cells were maintained by passaging them every second day during the week or third day after a weekend.

3.3 Freezing cells

For cryopreservation of cells, the confluent flasks were split as above, counted and subjected to a short centrifugation (413 x *g*, 5min, 4°C) using the Allegra™ X-22R centrifuge (Beckman,

Coulter). The cell pellet was gently resuspended in a complete medium supplemented with 10% DMSO. The volume used for resuspending the cell pellets was adjusted to allow for freezing of about 2 million cells/ml per vial. A steady rate of cooling of cells was achieved by placing cryovials in chilled “Mr Frosty” freezing containers (Cryo 1°C freezing container, Nalgene™) or Styrofoam boxes, and stored at -80°C for about a day. The following day, cryovials were transferred into normal freezer boxes for further short storage (less than six months) at -80°C. For long-term storage, cells that tested mycoplasma-free as per manufactures protocol (MycoProbe®, R& D systems, USA) were further stored in liquid nitrogen.

REFERENCES

Ackerman ME, Mikhailova A, Brown EP, Dowell KG, Walker BD, Bailey-Kellogg C, Suscovich TJ and Alter G (2016) Polyfunctional HIV-specific antibody responses are associated with spontaneous HIV control. *PLoS pathogens* **12:** e1005315

Alam SM, Morelli M, Dennison SM, Liao H-X, Zhang R, Xia S-M, Rits-Volloch S, Sun L, Harrison SC and Haynes BF (2009) Role of HIV membrane in neutralization by two broadly neutralizing antibodies. *Proceedings of the National Academy of Sciences* **106:** 20234-20239

Alfsen A and Bomsel M (2002) HIV-1 gp41 envelope residues 650–685 exposed on native virus act as a lectin to bind epithelial cell galactosyl ceramide. *Journal of Biological Chemistry* **277:** 25649-25659

Allan J, Coligan J, Barin F, McLane M, Sodroski J, Rosen C, Haseltine WA, Lee T and Essex M (1985) Major glycoprotein antigens that induce antibodies in AIDS patients are encoded by HTLV-III. *Science* **228:** 1091-1094

Alter G and Barouch D (2018) Immune correlate-guided HIV vaccine design. *Cell host & microbe* **24:** 25-33

Alvarez ML, Topal E, Martin F and Cardineau GA (2010) Higher accumulation of F1-V fusion recombinant protein in plants after induction of protein body formation. *Plant molecular biology* **72:** 75-89

Andrabi R, Su C-Y, Liang C-H, Shivatare SS, Briney B, Voss JE, Nawazi SK, Wu C-Y, Wong C-H and Burton DR (2017) Glycans function as anchors for antibodies and help drive HIV broadly neutralizing antibody development. *Immunity* **47:** 524-537. e523

Andrabi R, Voss JE, Liang C-H, Briney B, McCoy LE, Wu C-Y, Wong C-H, Poignard P and Burton DR (2015) Identification of common features in prototype broadly neutralizing antibodies to HIV envelope V2 apex to facilitate vaccine design. *Immunity* **43:** 959-973

Antanasijevic A, Ueda G, Brouwer PJM, Copps J, Huang D, Allen JD, Cottrell CA, Yasmeen A, Sewall LM, Bontjer I, Ketas TJ, Turner HL, Berndsen ZT, Montefiori DC, Klasse PJ, Crispin M, Nemazee D, Moore JP, Sanders RW, King NP, Baker D and Ward AB (2020) Structural and functional evaluation of de novo-designed, two-component nanoparticle carriers for HIV Env trimer immunogens. *PLoS Pathog* **16:** e1008665

Anuar INK, Banerjee A, Keeble AH, Carella A, Nikov GI and Howarth M (2019) Spy&Go purification of SpyTag-proteins using pseudo-SpyCatcher to access an oligomerization toolbox. *Nature communications* **10:** 1-13

Arendrup M, Nielsen C, Hansen J-E, Pedersen C, Mathiesen L and Nielsen JO (1992) Autologous HIV-1 neutralizing antibodies: emergence of neutralization-resistant escape virus and subsequent development of escape virus neutralizing antibodies. *Journal of acquired immune deficiency syndromes* **5:** 303-307

Aves K-L, Goksøyr L and Sander AF (2020) Advantages and Prospects of Tag/Catcher Mediated Antigen Display on Capsid-Like Particle-Based Vaccines. *Viruses* **12:** 185

Bachmann MF and Jennings GT (2010) Vaccine delivery: a matter of size, geometry, kinetics and molecular patterns. *Nature Reviews Immunology* **10:** 787-796

Bachmann MF and Zinkernagel RM (1996) The influence of virus structure on antibody responses and virus serotype formation. *Immunology today* **17:** 553-558

Baden LR, Karita E, Mutua G, Bekker L-G, Gray G, Page-Shipp L, Walsh SR, Nyombayire J, Anzala O and Roux S (2016) Assessment of the safety and immunogenicity of 2 novel vaccine platforms for HIV-1 prevention: a randomized trial. *Annals of internal medicine* **164:** 313-322

Bale JB, Gonen S, Liu Y, Sheffler W, Ellis D, Thomas C, Cascio D, Yeates TO, Gonen T and King NP (2016) Accurate design of megadalton-scale two-component icosahedral protein complexes. *Science* **353:** 389-394

Bale S, Goebrecht G, Stano A, Wilson R, Ota T, Tran K, Ingale J, Zwick MB and Wyatt RT (2017) Covalent linkage of HIV-1 trimers to synthetic liposomes elicits improved B cell and antibody responses. *Journal of virology* **91:** e00443-00417

Bárcena J and Blanco E (2013) Design of novel vaccines based on virus-like particles or chimeric virions. In *Structure and Physics of Viruses*. Springer, pp. 631-665

Barouch DH, Alter G, Broge T, Linde C, Ackerman ME, Brown EP, Borducchi EN, Smith KM, Nkolola JP and Liu J (2015) Protective efficacy of adenovirus/protein vaccines against SIV challenges in rhesus monkeys. *Science* **349:** 320-324

Barré-Sinoussi F, Chermann J-C, Rey F, Nugeyre MT, Chamaret S, Gruest J, Dauguet C, Axler-Blin C, Vézinet-Brun F and Rouzioux C (1983) Isolation of a T-lymphotropic retrovirus from a patient at risk for acquired immune deficiency syndrome (AIDS). *Science* **220:** 868-871

Bbosa N, Kaleebu P and Ssemwanga D (2019) HIV subtype diversity worldwide. *Current Opinion in HIV and AIDS* **14:** 153-160

Beitari S, Wang Y, Liu S-L and Liang C (2019) HIV-1 envelope glycoprotein at the interface of host restriction and virus evasion. *Viruses* **11:** 311

Bekker L-G, Moodie Z, Grunenberg N, Laher F, Tomaras GD, Cohen KW, Allen M, Malahleha M, Mngadi K and Daniels B (2018) Subtype C ALVAC-HIV and bivalent subtype C gp120/MF59 HIV-1 vaccine in low-risk, HIV-uninfected, South African adults: a phase 1/2 trial. *The Lancet HIV* **5:** e366-e378

Berger BW and Sallada ND (2019) Hydrophobins: multifunctional biosurfactants for interface engineering. *Journal of biological engineering* **13:** 10

Bhiman JN, Anthony C, Doria-Rose NA, Karimanzira O, Schramm CA, Khoza T, Kitchin D, Botha G, Gorman J and Garrett NJ (2015) Viral variants that initiate and drive maturation of V1V2-directed HIV-1 broadly neutralizing antibodies. *Nature medicine* **21:** 1332

Binley JM, Ban Y-EA, Crooks ET, Eggink D, Osawa K, Schief WR and Sanders RW (2010) Role of complex carbohydrates in human immunodeficiency virus type 1 infection and resistance to antibody neutralization. *Journal of virology* **84:** 5637-5655

Binley JM, Sanders RW, Clas B, Schuelke N, Master A, Guo Y, Kajumo F, Anselma DJ, Maddon PJ and Olson WC (2000) A recombinant human immunodeficiency virus type 1 envelope glycoprotein complex stabilized by an intermolecular disulfide bond between the gp120 and gp41 subunits is an antigenic mimic of the trimeric virion-associated structure. *Journal of virology* **74:** 627-643

Binley JM, Sanders RW, Master A, Cayanan CS, Wiley CL, Schiffner L, Travis B, Kuhmann S, Burton DR and Hu S-L (2002) Enhancing the proteolytic maturation of human immunodeficiency virus type 1 envelope glycoproteins. *Journal of virology* **76:** 2606-2616

Blattner C, Lee JH, Sliepen K, Derking R, Falkowska E, de la Peña AT, Cupo A, Julien J-P, van Gils M and Lee PS (2014) Structural delineation of a quaternary, cleavage-dependent epitope at the gp41-gp120 interface on intact HIV-1 Env trimers. *Immunity* **40:** 669-680

Bomsel M, Tudor D, Drillet A-S, Alfsen A, Ganor Y, Roger M-G, Mouz N, Amacker M, Chalifour A and Diomede L (2011) Immunization with HIV-1 gp41 subunit virosomes induces mucosal antibodies protecting nonhuman primates against vaginal SHIV challenges. *Immunity* **34:** 269-280

Bonsignori M, Pollara J, Moody MA, Alpert MD, Chen X, Hwang K-K, Gilbert PB, Huang Y, Gurley TC and Kozink DM (2012) Antibody-dependent cellular cytotoxicity-mediating antibodies from an HIV-1 vaccine efficacy trial target multiple epitopes and preferentially use the VH1 gene family. *Journal of virology* **86:** 11521-11532

Brinkkemper M and Sliepen K (2019) Nanoparticle vaccines for inducing HIV-1 neutralizing antibodies. *Vaccines* **7:** 76

Brouwer PJ, Antanasijevic A, Berndsen Z, Yasmeen A, Fiala B, Bijl TP, Bontjer I, Bale JB, Sheffler W and Allen JD (2019) Enhancing and shaping the immunogenicity of native-like HIV-1 envelope trimers with a two-component protein nanoparticle. *Nature communications* **10:** 1-17

Brouwer PJ, Antanasijevic A, de Gast M, Allen JD, Bijl TP, Yasmeen A, Ravichandran R, Burger JA, Ozorowski G and Torres JL (2021a) Immunofocusing and enhancing autologous Tier-2 HIV-1 neutralization by displaying Env trimers on two-component protein nanoparticles. *NPJ vaccines* **6:** 1-14

Brouwer PJ, Brinkkemper M, Maisonnasse P, Dereuddre-Bosquet N, Grobben M, Claireaux M, de Gast M, Marlin R, Chesnais V and Diry S (2021b) Two-component spike nanoparticle vaccine protects macaques from SARS-CoV-2 infection. *Cell* **184:** 1188-1200. e1119

Brouwer PJ and Sanders RW (2019) Presentation of HIV-1 envelope glycoprotein trimers on diverse nanoparticle platforms. *Current Opinion in HIV and AIDS* **14:** 302-308

Brune KD, Buldun CM, Li Y, Taylor IJ, Brod F, Biswas S and Howarth M (2017) Dual plug-and-display synthetic assembly using orthogonal reactive proteins for twin antigen immunization. *Bioconjugate chemistry* **28:** 1544-1551

Brune KD and Howarth M (2018) New routes and opportunities for modular construction of particulate vaccines: Stick, click, and glue. *Frontiers in immunology* **9:** 1432

Brune KD, Leneghan DB, Brian IJ, Ishizuka AS, Bachmann MF, Draper SJ, Biswas S and Howarth M (2016) Plug-and-Display: decoration of Virus-Like Particles via isopeptide bonds for modular immunization. *Scientific reports* **6:** 19234

Bruun TU, Andersson A-MC, Draper SJ and Howarth M (2018) Engineering a rugged nanoscaffold to enhance plug-and-display vaccination. *ACS nano* **12:** 8855-8866

Buchbinder SP, Mehrotra DV, Duerr A, Fitzgerald DW, Mogg R, Li D, Gilbert PB, Lama JR, Marmor M and del Rio C (2008) Efficacy assessment of a cell-mediated immunity HIV-1 vaccine (the Step Study): a double-blind, randomised, placebo-controlled, test-of-concept trial. *The Lancet* **372:** 1881-1893

Bui T, Dykers T, Hu S-L, Faltynek CR and Ho R (1994) Effect of MTP-PE liposomes and interleukin-7 on induction of antibody and cell-mediated immune responses to a recombinant HIV-envelope protein. *Journal of acquired immune deficiency syndromes* **7:** 799-806

Buldun CM, Jean JX, Bedford MR and Howarth M (2018) SnoopLigase Catalyzes peptide–peptide locking and enables solid-phase conjugate isolation. *Journal of the American Chemical Society* **140:** 3008-3018

Bültmann A, Muranyi W, Seed B and Haas J (2001) Identification of two sequences in the cytoplasmic tail of the human immunodeficiency virus type 1 envelope glycoprotein that inhibit cell surface expression. *Journal of virology* **75:** 5263-5276

Burton DR and Hangartner L (2016) Broadly neutralizing antibodies to HIV and their role in vaccine design. *Annual review of immunology* **34:** 635-659

Burton DR, Pyati J, Koduri R, Sharp SJ, Thornton GB, Parren P, Sawyer LS, Hendry RM, Dunlop N and Nara PL (1994) Efficient neutralization of primary isolates of HIV-1 by a recombinant human monoclonal antibody. *Science* **266:** 1024-1027

Buyel J, Twyman R and Fischer R (2015) Extraction and downstream processing of plant-derived recombinant proteins. *Biotechnology advances* **33:** 902-913

Buyel JF and Fischer R (2014) Downstream processing of biopharmaceutical proteins produced in plants: the pros and cons of flocculants. *Bioengineered* **5:** 138-142

Cai L, Gochin M and Liu K (2011) Biochemistry and biophysics of HIV-1 gp41-membrane interactions and implications for HIV-1 envelope protein mediated viral-cell fusion and fusion inhibitor design. *Current topics in medicinal chemistry* **11:** 2959-2984

Caillat C, Guilligay D, Sulbaran G and Weissenhorn W (2020) Neutralizing Antibodies Targeting HIV-1 gp41. *Viruses* **12:** 1210

Calarese DA, Scanlan CN, Zwick MB, Deechongkit S, Mimura Y, Kunert R, Zhu P, Wormald MR, Stanfield RL and Roux KH (2003) Antibody domain exchange is an immunological solution to carbohydrate cluster recognition. *Science* **300:** 2065-2071

Cale EM, Gorman J, Radakovich NA, Crooks ET, Osawa K, Tong T, Li J, Nagarajan R, Ozorowski G and Ambrozak DR (2017) Virus-like particles identify an HIV V1V2 apex-binding neutralizing antibody that lacks a protruding loop. *Immunity* **46:** 777-791. e710

Capucci S, Wee EG, Schiffner T, LaBranche CC, Borthwick N, Cupo A, Dodd J, Dean H, Sattentau Q and Montefiori D (2017) HIV-1-neutralizing antibody induced by simian adenovirus-and poxvirus MVA-vectored BG505 native-like envelope trimers. *PloS one* **12**

Ceresoli V, Mainieri D, Del Fabbro M, Weinstein R and Pedrazzini E (2016) A Fusion between Domains of the Human Bone Morphogenetic Protein-2 and Maize 27 kD gamma-Zein Accumulates to High Levels in the Endoplasmic Reticulum without Forming Protein Bodies in Transgenic Tobacco. *Front Plant Sci* **7:** 358

Chapman BS, Thayer RM, Vincent KA and Haigwood NL (1991) Effect of intron A from human cytomegalovirus (Towne) immediate-early gene on heterologous expression in mammalian cells. *Nucleic acids research* **19:** 3979-3986

Chapman R, van Diepen M, Galant S, Kruse E, Margolin E, Ximba P, Hermanus T, Moore P, Douglass N and Williamson A-L (2020) Immunogenicity of HIV-1 Vaccines Expressing Chimeric Envelope Glycoproteins on the Surface of Pr55 Gag Virus-Like Particles. *Vaccines* **8:** 54

Checkley MA, Luttge BG and Freed EO (2011) HIV-1 envelope glycoprotein biosynthesis, trafficking, and incorporation. *Journal of molecular biology* **410:** 582-608

Chen B (2019) Molecular mechanism of HIV-1 entry. *Trends in microbiology* **27:** 878-891

Chen Q and Davis KR (2016) The potential of plants as a system for the development and production of human biologics. *F1000Research* **5**

Chen X, Lin M, Qian S, Zhang Z, Fu Y, Xu J, Han X, Ding H, Dong T and Shang H (2018) The early antibody-dependent cell-mediated cytotoxicity response is associated with lower viral set point in individuals with primary HIV infection. *Frontiers in immunology* **9:** 2322

Cheng C, Pancera M, Bossert A, Schmidt SD, Chen RE, Chen X, Druz A, Narpala S, Doria-Rose NA and McDermott AB (2016) Immunogenicity of a prefusion HIV-1 envelope trimer in complex with a quaternary-structure-specific antibody. *Journal of virology* **90:** 2740-2755

Cho KJ, Shin HJ, Lee J-H, Kim K-J, Park SS, Lee Y, Lee C, Park SS and Kim KH (2009) The crystal structure of ferritin from Helicobacter pylori reveals unusual conformational changes for iron uptake. *Journal of molecular biology* **390:** 83-98

Chrispeels MJ and Herman EM (2000) Endoplasmic reticulum-derived compartments function in storage and as mediators of vacuolar remodeling via a new type of organelle, precursor protease vesicles. *Plant Physiology* **123:** 1227-1234

Chung AW, Navis M, Isitman G, Centre R, Finlayson R, Bloch M, Gelgor L, Kelleher A, Kent SJ and Stratov I (2011) Activation of NK cells by ADCC responses during early HIV infection. *Viral immunology* **24:** 171-175

Cohen AA, Gnanapragasam PN, Lee YE, Hoffman PR, Ou S, Kakutani LM, Keeffe JR, Wu H-J, Howarth M and West AP (2021a) Mosaic nanoparticles elicit cross-reactive immune responses to zoonotic coronaviruses in mice. *Science* **371:** 735-741

Cohen AA, Yang Z, Gnanapragasam P, Ou S, Dam K-M, Wang H and Bjorkman PJ (2020) Construction, characterization, and immunization of nanoparticles that display a diverse array of influenza HA trimers. *bioXiv doi: 101101/20200118911388*

Cohen AA, Yang Z, Gnanapragasam PN, Ou S, Dam K-MA, Wang H and Bjorkman PJ (2021b) Construction, characterization, and immunization of nanoparticles that display a diverse array of influenza HA trimers. *PloS one* **16:** e0247963

Cohen J. (2020) Combo of two HIV vaccines fails its big test. American Association for the Advancement of Science.

Cohen MS, Chen YQ, McCauley M, Gamble T, Hosseinipour MC, Kumarasamy N, Hakim JG, Kumwenda J, Grinsztejn B and Pilotto JH (2011) Prevention of HIV-1 infection with early antiretroviral therapy. *New England journal of medicine* **365:** 493-505

Conley AJ, Joensuu JJ, Menassa R and Brandle JE (2009) Induction of protein body formation in plant leaves by elastin-like polypeptide fusions. *BMC biology* **7:** 48

Conley AJ, Joensuu JJ, Richman A and Menassa R (2011) Protein body-inducing fusions for high-level production and purification of recombinant proteins in plants. *Plant biotechnology journal* **9:** 419-433

Corey L, Gilbert PB, Tomaras GD, Haynes BF, Pantaleo G and Fauci AS (2015) Immune correlates of vaccine protection against HIV-1 acquisition. *Science translational medicine* **7:** 310rv317-310rv317

Cortez V, Odem-Davis K, McClelland RS, Jaoko W and Overbaugh J (2012) HIV-1 superinfection in women broadens and strengthens the neutralizing antibody response. *PLoS pathogens* **8:** e1002611

Crispin M, Ward AB and Wilson IA (2018) Structure and immune recognition of the HIV glycan shield. *Annual review of biophysics* **47:** 499-523

Crooks ET, Moore PL, Franti M, Cayanan CS, Zhu P, Jiang P, de Vries RP, Wiley C, Zharkikh I and Schülke N (2007) A comparative immunogenicity study of HIV-1 virus-like particles bearing various forms of envelope proteins, particles bearing no envelope and soluble monomeric gp120. *Virology* **366:** 245-262

Crooks ET, Osawa K, Tong T, Grimley SL, Dai YD, Whalen RG, Kulp DW, Menis S, Schief WR and Binley JM (2017) Effects of partially dismantling the CD4 binding site glycan fence of HIV-1 Envelope glycoprotein trimers on neutralizing antibody induction. *Virology* **505:** 193-209

Crooks ET, Tong T, Chakrabarti B, Narayan K, Georgiev IS, Menis S, Huang X, Kulp D, Osawa K and Muranaka J (2015) Vaccine-elicited tier 2 HIV-1 neutralizing antibodies bind to quaternary epitopes involving glycan-deficient patches proximal to the CD4 binding site. *PLoS pathogens* **11**

Crooks ET, Tong T, Osawa K and Binley JM (2011) Enzyme digests eliminate nonfunctional Env from HIV-1 particle surfaces, leaving native Env trimers intact and viral infectivity unaffected. *Journal of virology* **85:** 5825-5839

Cummings JF, Guerrero ML, Moon JE, Waterman P, Nielsen RK, Jefferson S, Gross FL, Hancock K, Katz JM and Yusibov V (2014) Safety and immunogenicity of a plant-produced recombinant monomer hemagglutinin-based influenza vaccine derived from influenza A (H1N1) pdm09 virus: a Phase 1 dose-escalation study in healthy adults. *Vaccine* **32:** 2251-2259

Curlin ME, Zioni R, Hawes SE, Liu Y, Deng W, Gottlieb GS, Zhu T and Mullins JI (2010) HIV-1 envelope subregion length variation during disease progression. *PLoS pathogens* **6**

D'Aoust MA, Lavoie PO, Couture MMJ, Trépanier S, Guay JM, Dargis M, Mongrand S, Landry N, Ward BJ and Vézina LP (2008) Influenza virus-like particles produced by transient expression in Nicotiana benthamiana induce a protective immune response against a lethal viral challenge in mice. *Plant biotechnology journal* **6:** 930-940

D'arc M, Ayouba A, Esteban A, Learn GH, Boué V, Liegeois F, Etienne L, Tagg N, Leendertz FH and Boesch C (2015) Origin of the HIV-1 group O epidemic in western lowland gorillas. *Proceedings of the National Academy of Sciences* **112:** E1343-E1352

Dalton AK, Ako-Adjei D, Murray PS, Murray D and Vogt VM (2007) Electrostatic interactions drive membrane association of the human immunodeficiency virus type 1 Gag MA domain. *Journal of virology* **81:** 6434-6445

Darricarrère N, Pougatcheva S, Duan X, Rudicell RS, Chou T-H, DiNapoli J, Ross TM, Alefantis T, Vogel TU and Kleanthous H (2018) Development of a Pan-H1 influenza vaccine. *Journal of Virology* **92:** e01349-01318

Das S, Kumar R, Ahmed S, Parray HA and Samal S (2020) Efficiently cleaved HIV-1 envelopes: can they be important for vaccine immunogen development? *Therapeutic Advances in Vaccines and Immunotherapy* **8:** 2515135520957763

de Taeye SW, Moore JP and Sanders RW (2016) HIV-1 Envelope Trimer Design and Immunization Strategies To Induce Broadly Neutralizing Antibodies. *Trends Immunol* **37:** 221-232

de Taeye SW, Ozorowski G, de la Peña AT, Guttman M, Julien J-P, van den Kerkhof TL, Burger JA, Pritchard LK, Pugach P and Yasmeen A (2015) Immunogenicity of stabilized HIV-1 envelope trimers with reduced exposure of non-neutralizing epitopes. *Cell* **163:** 1702-1715

de Virgilio M, De Marchis F, Bellucci M, Mainieri D, Rossi M, Benvenuto E, Arcioni S and Vitale A (2008) The human immunodeficiency virus antigen Nef forms protein bodies in leaves of transgenic tobacco when fused to zeolin. *J Exp Bot* **59:** 2815-2829

del Moral-Sánchez I and Sliepen K (2019) Strategies for inducing effective neutralizing antibody responses against HIV-1. *Expert review of vaccines* **18:** 1127-1143

Deml L, Schirmbeck R, Reimann J, Wolf H and Wagner R (1997) Recombinant Human Immunodeficiency Pr55gagVirus-like Particles Presenting Chimeric Envelope Glycoproteins Induce Cytotoxic T-Cells and Neutralizing Antibodies. *Virology* **235:** 26-39

Derdeyn CA, Moore PL and Morris L (2014) Development of broadly neutralizing antibodies from autologous neutralizing antibody responses. *Current opinion in HIV and AIDS* **9:** 210

Desrosiers RC (2017) Protection against HIV Acquisition in the RV144 Trial. *Journal of virology*

Ding X, Cao K, Wang J, Wan Y, Chen Q, Ren Y, Zheng Y, Zhu M, Tian R and Wang W (2021) Exploration of a Sequential Gp140-Gp145 Immunization Regimen with Heterologous Envs to Induce a Protective Cross-Reactive HIV Neutralizing Antibody Response In Non-human Primates. *Virologica Sinica***:** 1-12

Domingo GJ and Perham RN (2001) Multiple display of peptides and proteins on a macromolecular scaffold derived from a multienzyme complex. *Journal of Molecular Biology* **305:** 259-267

Doria-Rose NA, Bhiman JN, Roark RS, Schramm CA, Gorman J, Chuang G-Y, Pancera M, Cale EM, Ernandes MJ and Louder MK (2016) New member of the V1V2-directed CAP256-VRC26 lineage that shows increased breadth and exceptional potency. *Journal of virology* **90:** 76-91

Doria-Rose NA, Klein RM, Manion MM, O'Dell S, Phogat A, Chakrabarti B, Hallahan CW, Migueles SA, Wrammert J and Ahmed R (2009) Frequency and phenotype of human immunodeficiency virus envelope-specific B cells from patients with broadly cross-neutralizing antibodies. *Journal of virology* **83:** 188-199

Doria-Rose NA, Schramm CA, Gorman J, Moore PL, Bhiman JN, DeKosky BJ, Ernandes MJ, Georgiev IS, Kim HJ and Pancera M (2014) Developmental pathway for potent V1V2-directed HIV-neutralizing antibodies. *Nature* **509:** 55-62

Du SX, Idiart RJ, Mariano EB, Chen H, Jiang P, Xu L, Ostrow KM, Wrin T, Phung P and Binley JM (2009) Effect of trimerization motifs on quaternary structure, antigenicity, and immunogenicity of a noncleavable HIV-1 gp140 envelope glycoprotein. *Virology* **395:** 33-44

Dubrovskaya V, Tran K, Ozorowski G, Guenaga J, Wilson R, Bale S, Cottrell CA, Turner HL, Seabright G and O'Dell S (2019) Vaccination with glycan-modified HIV NFL envelope trimer-liposomes elicits broadly neutralizing antibodies to multiple sites of vulnerability. *Immunity* **51:** 915-929. e917

Duerr A, Huang Y, Buchbinder S, Coombs RW, Sanchez J, del Rio C, Casapia M, Santiago S, Gilbert P and Corey L (2012) Extended follow-up confirms early vaccine-enhanced risk of HIV

acquisition and demonstrates waning effect over time among participants in a randomized trial of recombinant adenovirus HIV vaccine (Step Study). *The Journal of infectious diseases* **206:** 258-266

Earl PL, Koenig S and Moss B (1991) Biological and immunological properties of human immunodeficiency virus type 1 envelope glycoprotein: analysis of proteins with truncations and deletions expressed by recombinant vaccinia viruses. *Journal of virology* **65:** 31-41

Easterhoff D, Moody MA, Fera D, Cheng H, Ackerman M, Wiehe K, Saunders KO, Pollara J, Vandergrift N and Parks R (2017) Boosting of HIV envelope CD4 binding site antibodies with long variable heavy third complementarity determining region in the randomized double blind RV305 HIV-1 vaccine trial. *PLoS pathogens* **13:** e1006182

Easterhoff D, Pollara J, Luo K, Janus B, Gohain N, Williams LD, Tay MZ, Monroe A, Peachman K and Choe M (2020) HIV vaccine delayed boosting increases Env variable region 2–specific antibody effector functions. *JCI insight* **5**

Engelman A and Cherepanov P (2012) The structural biology of HIV-1: mechanistic and therapeutic insights. *Nature Reviews Microbiology* **10:** 279-290

Escolano A, Gristick HB, Abernathy ME, Merkenschlager J, Gautam R, Oliveira TY, Pai J, West AP, Barnes CO and Cohen AA (2019) Immunization expands B cells specific to HIV-1 V3 glycan in mice and macaques. *Nature* **570:** 468-473

Excler J-L and Kim JH (2019) Novel prime-boost vaccine strategies against HIV-1. *Expert review of vaccines* **18:** 765-779

Falkowska E, Le KM, Ramos A, Doores KJ, Lee JH, Blattner C, Ramirez A, Derking R, van Gils MJ and Liang C-H (2014) Broadly neutralizing HIV antibodies define a glycan-dependent epitope on the prefusion conformation of gp41 on cleaved envelope trimers. *Immunity* **40:** 657-668

Fauci AS (2017) An HIV vaccine is essential for ending the HIV/AIDS pandemic. *Jama* **318:** 1535-1536

Fauci AS and Marston HD (2014) Ending AIDS—is an HIV vaccine necessary? *New England Journal of Medicine* **370:** 495-498

Felber BK, Lu Z, Hu X, Valentin A, Rosati M, Remmel CA, Weiner JA, Carpenter MC, Faircloth K and Stanfield-Oakley S (2020) Co-immunization of DNA and Protein in the Same Anatomical Sites Induces Superior Protective Immune Responses against SHIV Challenge. *Cell Reports* **31:** 107624

Feng Y, Tran K, Bale S, Kumar S, Guenaga J, Wilson R, de Val N, Arendt H, DeStefano J and Ward AB (2016) Thermostability of well-ordered HIV spikes correlates with the elicitation of autologous tier 2 neutralizing antibodies. *PLoS pathogens* **12**

Fierer JO, Veggiani G and Howarth M (2014) SpyLigase peptide–peptide ligation polymerizes affibodies to enhance magnetic cancer cell capture. *Proceedings of the National Academy of Sciences* **111:** E1176-E1181

Fischer R and Buyel JF (2020) Molecular farming–the slope of enlightenment. *Biotechnology advances* **40:** 107519

Flynn NM, Forthal DN, Harro CD, Judson FN, Mayer KH and Para MF (2005) Placebo-controlled phase 3 trial of a recombinant glycoprotein 120 vaccine to prevent HIV-1 infection. *J Infect Dis* **191:** 654-665

Fong Y, Shen X, Ashley VC, Deal A, Seaton KE, Yu C, Grant SP, Ferrari G, deCamp AC and Bailer RT (2018) Modification of the association between T-cell immune responses and human immunodeficiency virus type 1 infection risk by vaccine-induced antibody responses in the HVTN 505 trial. *The Journal of infectious diseases* **217:** 1280-1288

Forthal DN, Gilbert PB, Landucci G and Phan T (2007) Recombinant gp120 vaccine-induced antibodies inhibit clinical strains of HIV-1 in the presence of Fc receptor-bearing effector cells and correlate inversely with HIV infection rate. *The Journal of Immunology* **178:** 6596-6603

Freed EO (2015) HIV-1 assembly, release and maturation. *Nature Reviews Microbiology* **13:** 484-496

Freivalds J, Kotelovica S, Voronkova T, Ose V, Tars K and Kazaks A (2014) Yeast-expressed bacteriophage-like particles for the packaging of nanomaterials. *Molecular biotechnology* **56:** 102-110

Frey G, Peng H, Rits-Volloch S, Morelli M, Cheng Y and Chen B (2008) A fusion-intermediate state of HIV-1 gp41 targeted by broadly neutralizing antibodies. *Proceedings of the National Academy of Sciences* **105:** 3739-3744

Frost SD, Wrin T, Smith DM, Pond SLK, Liu Y, Paxinos E, Chappey C, Galovich J, Beauchaine J and Petropoulos CJ (2005) Neutralizing antibody responses drive the evolution of human

immunodeficiency virus type 1 envelope during recent HIV infection. *Proceedings of the National Academy of Sciences* **102:** 18514-18519

Galili G. (2004) ER-derived compartments are formed by highly regulated processes and have special functions in plants. Am Soc Plant Biol.

Gallo SA, Finnegan CM, Viard M, Raviv Y, Dimitrov A, Rawat SS, Puri A, Durell S and Blumenthal R (2003) The HIV Env-mediated fusion reaction. *Biochimica et Biophysica Acta (BBA)-Biomembranes* **1614:** 36-50

Ganser-Pornillos BK, Yeager M and Pornillos O (2012) Assembly and architecture of HIV. In *Viral molecular machines*. Springer, pp. 441-465

Gao F, Bailes E, Robertson DL, Chen Y, Rodenburg CM, Michael SF, Cummins LB, Arthur LO, Peeters M and Shaw GM (1999) Origin of HIV-1 in the chimpanzee Pan troglodytes troglodytes. *Nature* **397:** 436-441

Gao F, Yue L, White AT, Pappas PG, Barchue J, Hanson AP, Greene BM, Sharp PM, Shaw GM and Hahn BH (1992) Human infection by genetically diverse SIV SM-related HIV-2 in West Africa. *Nature* **358:** 495-499

Garber DA, Adams DR, Guenthner P, Mitchell J, Kelley K, Schoofs T, Gazumyan A, Nason M, Seaman MS and McNicholl J (2020) Durable protection against repeated penile exposures to simian-human immunodeficiency virus by broadly neutralizing antibodies. *Nature communications* **11:** 1-9

Gause KT, Wheatley AK, Cui J, Yan Y, Kent SJ and Caruso F (2017) Immunological principles guiding the rational design of particles for vaccine delivery. *ACS nano* **11:** 54-68

Gautam R, Nishimura Y, Gaughan N, Gazumyan A, Schoofs T, Buckler-White A, Seaman MS, Swihart BJ, Follmann DA and Nussenzweig MC (2018) A single injection of crystallizable fragment domain–modified antibodies elicits durable protection from SHIV infection. *Nature medicine* **24:** 610-616

Gautam R, Nishimura Y, Pegu A, Nason MC, Klein F, Gazumyan A, Golijanin J, Buckler-White A, Sadjadpour R and Wang K (2016) A single injection of anti-HIV-1 antibodies protects against repeated SHIV challenges. *Nature* **533:** 105-109

Geiß Y and Dietrich U (2015) Catch me if you can—The race between HIV and neutralizing antibodies. *AIDS Rev* **17:** 107-113

Geli MI, Torrent M and Ludevid D (1994) Two structural domains mediate two sequential events in [gamma]-zein targeting: protein endoplasmic reticulum retention and protein body formation. *The Plant Cell* **6:** 1911-1922

Georgiev IS, Joyce MG, Chen RE, Leung K, McKee K, Druz A, Van Galen JG, Kanekiyo M, Tsybovsky Y and Yang ES (2018) Two-component ferritin nanoparticles for multimerization of diverse trimeric antigens. *ACS infectious diseases* **4:** 788-796

Georgiev IS, Joyce MG, Yang Y, Sastry M, Zhang B, Baxa U, Chen RE, Druz A, Lees CR and Narpala S (2015) Single-chain soluble BG505. SOSIP gp140 trimers as structural and antigenic mimics of mature closed HIV-1 Env. *Journal of virology* **89:** 5318-5329

Gheysen D, Jacobs E, de Foresta F, Thiriart C, Francotte M, Thines D and De Wilde M (1989) Assembly and release of HIV-1 precursor Pr55gag virus-like particles from recombinant baculovirus-infected insect cells. *Cell* **59:** 103-112

Gilbert P, Wang M, Wrin T, Petropoulos C, Gurwith M, Sinangil F, D'Souza P, Rodriguez-Chavez IR, DeCamp A and Giganti M (2010) Magnitude and breadth of a nonprotective neutralizing antibody response in an efficacy trial of a candidate HIV-1 gp120 vaccine. *The Journal of infectious diseases* **202:** 595-605

Gilbert PB, Peterson ML, Follmann D, Hudgens MG, Francis DP, Gurwith M, Heyward WL, Jobes DV, Popovic V and Self SG (2005) Correlation between immunologic responses to a recombinant glycoprotein 120 vaccine and incidence of HIV-1 infection in a phase 3 HIV-1 preventive vaccine trial. *The Journal of infectious diseases* **191:** 666-677

Go EP, Cupo A, Ringe R, Pugach P, Moore JP and Desaire H (2015) Native Conformation and Canonical Disulfide Bond Formation Are Interlinked Properties of HIV-1 Env Glycoproteins. *J Virol* **90:** 2884-2894

Goepfert PA, Elizaga ML, Seaton K, Tomaras GD, Montefiori DC, Sato A, Hural J, DeRosa SC, Kalams SA and McElrath MJ (2014) Specificity and 6-month durability of immune responses induced by DNA and recombinant modified vaccinia Ankara vaccines expressing HIV-1 virus-like particles. *The Journal of infectious diseases* **210:** 99-110

Gomes AC, Mohsen M and Bachmann MF (2017) Harnessing nanoparticles for immunomodulation and vaccines. *Vaccines* **5:** 6

Goo L, Chohan V, Nduati R and Overbaugh J (2014) Early development of broadly neutralizing antibodies in HIV-1–infected infants. *Nature medicine* **20:** 655-658

Gorman J, Soto C, Yang MM, Davenport TM, Guttman M, Bailer RT, Chambers M, Chuang G-Y, DeKosky BJ and Doria-Rose NA (2016) Structures of HIV-1 Env V1V2 with broadly neutralizing antibodies reveal commonalities that enable vaccine design. *Nature structural & molecular biology* **23:** 81

Gottlieb MS, Schroff R, Schanker HM, Weisman JD, Fan PT, Wolf RA and Saxon A (1981) Pneumocystis carinii pneumonia and mucosal candidiasis in previously healthy homosexual men: evidence of a new acquired cellular immunodeficiency. *New England Journal of Medicine* **305:** 1425-1431

Göttlinger HG (2001) HIV-1 Gag: a molecular machine driving viral particle assembly and release. *HIV sequence Compendium***:** 2-28

Göttlinger HG, Sodroski JG and Haseltine WA (1989) Role of capsid precursor processing and myristoylation in morphogenesis and infectivity of human immunodeficiency virus type 1. *Proceedings of the National Academy of Sciences* **86:** 5781-5785

Govasli ML, Diaz Y and Puntervoll P (2019) Virus-like particle-display of the enterotoxigenic Escherichia coli heat-stable toxoid STh-A14T elicits neutralizing antibodies in mice. *Vaccine* **37:** 6405-6414

Gray E, Moore P, Choge I, Decker J, Bibollet-Ruche F, Li H, Leseka N, Treurnicht F, Mlisana K and Shaw G (2007) Neutralizing antibody responses in acute human immunodeficiency virus type 1 subtype C infection. *Journal of virology* **81:** 6187-6196

Gray ES, Madiga MC, Hermanus T, Moore PL, Wibmer CK, Tumba NL, Werner L, Mlisana K, Sibeko S and Williamson C (2011a) The neutralization breadth of HIV-1 develops incrementally over four years and is associated with CD4+ T cell decline and high viral load during acute infection. *Journal of virology* **85:** 4828-4840

Gray G, Allen M, Moodie Z, Churchyard G, Bekker L, Nchabeleng M, Mlisana K, Metch B, de Bruyn G and Latka M (2011b) Safety and efficacy assessment of the HVTN 503/Phambili Study: A double-blind randomized placebo-controlled test-of-concept study of a Clade B-based HIV-1 vaccine in South Africa. *The Lancet infectious diseases* **11:** 507

Gray GE, Moodie Z, Metch B, Gilbert PB, Bekker L-G, Churchyard G, Nchabeleng M, Mlisana K, Laher F and Roux S (2014) The phase 2b HVTN 503/Phambili study test-of-concept HIV vaccine study, investigating a recombinant adenovirus type 5 HIV gag/pol/nef vaccine in South Africa: unblinded, long-term follow-up. *The Lancet Infectious diseases* **14:** 388

Gruell H and Klein F (2018) Antibody-mediated prevention and treatment of HIV-1 infection. *Retrovirology* **15:** 1-11

Güthe S, Kapinos L, Möglich A, Meier S, Grzesiek S and Kiefhaber T (2004) Very fast folding and association of a trimerization domain from bacteriophage T4 fibritin. *Journal of molecular biology* **337:** 905-915

Gutierrez SP, Saberianfar R, Kohalmi SE and Menassa R (2013) Protein body formation in stable transgenic tobacco expressing elastin-like polypeptide and hydrophobin fusion proteins. *BMC Biotechnol* **13:** 40

Guttman M, Cupo A, Julien J-P, Sanders RW, Wilson IA, Moore JP and Lee KK (2015) Antibody potency relates to the ability to recognize the closed, pre-fusion form of HIV Env. *Nature communications* **6:** 1-11

Hagan RM, Björnsson R, McMahon SA, Schomburg B, Braithwaite V, Bühl M, Naismith JH and Schwarz-Linek U (2010) NMR spectroscopic and theoretical analysis of a spontaneously formed Lys–Asp isopeptide bond. *Angewandte Chemie International Edition* **49:** 8421-8425

Hamburger AE, West Jr AP, Hamburger ZA, Hamburger P and Bjorkman PJ (2005) Crystal structure of a secreted insect ferritin reveals a symmetrical arrangement of heavy and light chains. *Journal of molecular biology* **349:** 558-569

Hammer SM, Sobieszczyk ME, Janes H, Karuna ST, Mulligan MJ, Grove D, Koblin BA, Buchbinder SP, Keefer MC and Tomaras GD (2013) Efficacy trial of a DNA/rAd5 HIV-1 preventive vaccine. *New England Journal of Medicine* **369:** 2083-2092

Harbury PB, Kim PS and Alber T (1994) Crystal structure of an isoleucine-zipper trimer. *Nature* **371:** 80-83

Harbury PB, Zhang T, Kim PS and Alber T (1993) A switch between two-, three-, and four-stranded coiled coils in GCN4 leucine zipper mutants. *Science* **262:** 1401-1407

Hartzell EJ, Lieser RM, Sullivan MO and Chen W (2020) Modular Hepatitis B Virus-like Particle Platform for Biosensing and Drug Delivery. *ACS nano* **14:** 12642-12651

Hatlem D, Trunk T, Linke D and Leo JC (2019) Catching a SPY: using the SpyCatcher-SpyTag and related systems for labeling and localizing bacterial proteins. *International journal of molecular sciences* **20:** 2129

Hayes PJ, Cox JH, Coleman AR, Fernandez N, Bergin PJ, Kopycinski JT, Nitayaphan S, Pitisuttihum P, De Souza M and Duerr A (2016) Adenovirus-based HIV-1 vaccine candidates tested in efficacy trials elicit CD8+ T cells with limited breadth of HIV-1 inhibition. *Aids* **30:** 1703-1712

Haynes BF and Burton DR (2017) Developing an HIV vaccine. *Science* **355:** 1129-1130

Haynes BF, Fleming J, Clair EWS, Katinger H, Stiegler G, Kunert R, Robinson J, Scearce RM, Plonk K and Staats HF (2005) Cardiolipin polyspecific autoreactivity in two broadly neutralizing HIV-1 antibodies. *Science* **308:** 1906-1908

Haynes BF, Gilbert PB, McElrath MJ, Zolla-Pazner S, Tomaras GD, Alam SM, Evans DT, Montefiori DC, Karnasuta C and Sutthent R (2012) Immune-correlates analysis of an HIV-1 vaccine efficacy trial. *New England Journal of Medicine* **366:** 1275-1286

Haynes BF and Shattock RJ (2008) Critical issues in mucosal immunity for HIV-1 vaccine development. *Journal of Allergy and Clinical Immunology* **122:** 3-9

He L, De Val N, Morris CD, Vora N, Thinnes TC, Kong L, Azadnia P, Sok D, Zhou B and Burton DR (2016) Presenting native-like trimeric HIV-1 antigens with self-assembling nanoparticles. *Nature communications* **7:** 1-15

He L, Kumar S, Allen JD, Huang D, Lin X, Mann CJ, Saye-Francisco KL, Copps J, Sarkar A and Blizard GS (2018) HIV-1 vaccine design through minimizing envelope metastability. *Science advances* **4:** eaau6769

He L, Lin X, Wang Y, Abraham C, Sou C, Ngo T, Zhang Y, Wilson IA and Zhu J (2021) Single-component, self-assembling, protein nanoparticles presenting the receptor binding domain and stabilized spike as SARS-CoV-2 vaccine candidates. *Science Advances* **7:** eabf1591

Hefferon KL (2012) Plant virus expression vectors set the stage as production platforms for biopharmaceutical proteins. *Virology* **433:** 1-6

Hemelaar J (2012) The origin and diversity of the HIV-1 pandemic. *Trends in molecular medicine* **18:** 182-192

Hemelaar J, Gouws E, Ghys PD and Osmanov S (2006) Global and regional distribution of HIV-1 genetic subtypes and recombinants in 2004. *Aids* **20:** W13-W23

Herman EM and Larkins BA (1999) Protein storage bodies and vacuoles. *The Plant Cell* **11:** 601-613

Herschhorn A, Ma X, Gu C, Ventura JD, Castillo-Menendez L, Melillo B, Terry DS, Smith AB, Blanchard SC and Munro JB (2016) Release of gp120 restraints leads to an entry-competent intermediate state of the HIV-1 envelope glycoproteins. *MBio* **7:** e01598-01516

Herzog C, Hartmann K, Künzi V, Kürsteiner O, Mischler R, Lazar H and Glück R (2009) Eleven years of Inflexal® V—a virosomal adjuvanted influenza vaccine. *Vaccine* **27:** 4381-4387

Hessell AJ, Poignard P, Hunter M, Hangartner L, Tehrani DM, Bleeker WK, Parren PW, Marx PA and Burton DR (2009) Effective, low-titer antibody protection against low-dose repeated mucosal SHIV challenge in macaques. *Nature medicine* **15:** 951-954

Hirsch VM, Olmsted RA, Murphey-Corb M, Purcell RH and Johnson PR (1989) An African primate lentivirus (SIV sm closely related to HIV-2. *Nature* **339:** 389-392

Hofbauer A, Melnik S, Tschofen M, Arcalis E, Phan HT, Gresch U, Lampel J, Conrad U and Stoger E (2016) The encapsulation of hemagglutinin in protein bodies achieves a stronger immune response in mice than the soluble antigen. *Frontiers in plant science* **7:** 142

Hofbauer A, Peters J, Arcalis E, Rademacher T, Lampel J, Eudes F, Vitale A and Stoger E (2014) The induction of recombinant protein bodies in different subcellular compartments reveals a cryptic plastid-targeting signal in the 27-kDa γ-zein sequence. *Frontiers in bioengineering and biotechnology* **2:** 67

Hraber P, Seaman MS, Bailer RT, Mascola JR, Montefiori DC and Korber BT (2014) Prevalence of broadly neutralizing antibody responses during chronic HIV-1 infection. *AIDS (London, England)* **28:** 163

Hsia Y, Bale JB, Gonen S, Shi D, Sheffler W, Fong KK, Nattermann U, Xu C, Huang P-S and Ravichandran R (2016) Correction: Corrigendum: Design of a hyperstable 60-subunit protein icosahedron. *Nature* **540:** 150-150

Hu JK, Crampton JC, Cupo A, Ketas T, van Gils MJ, Sliepen K, de Taeye SW, Sok D, Ozorowski G and Deresa I (2015) Murine antibody responses to cleaved soluble HIV-1 envelope trimers are highly restricted in specificity. *Journal of virology* **89:** 10383-10398

Huang J, Kang BH, Ishida E, Zhou T, Griesman T, Sheng Z, Wu F, Doria-Rose NA, Zhang B and McKee K (2016) Identification of a CD4-binding-site antibody to HIV that evolved near-pan neutralization breadth. *Immunity* **45:** 1108-1121

Huang J, Kang BH, Pancera M, Lee JH, Tong T, Feng Y, Imamichi H, Georgiev IS, Chuang G-Y and Druz A (2014) Broad and potent HIV-1 neutralization by a human antibody that binds the gp41–gp120 interface. *Nature* **515:** 138-142

Huang J, Ofek G, Laub L, Louder MK, Doria-Rose NA, Longo NS, Imamichi H, Bailer RT, Chakrabarti B and Sharma SK (2012) Broad and potent neutralization of HIV-1 by a gp41-specific human antibody. *Nature* **491:** 406-412

Ingale J, Stano A, Guenaga J, Sharma SK, Nemazee D, Zwick MB and Wyatt RT (2016) High-density array of well-ordered HIV-1 spikes on synthetic liposomal nanoparticles efficiently activate B cells. *Cell reports* **15:** 1986-1999

Irimia A, Sarkar A, Stanfield RL and Wilson IA (2016) Crystallographic identification of lipid as an integral component of the epitope of HIV broadly neutralizing antibody 4E10. *Immunity* **44:** 21-31

Irvine DJ and Read BJ (2020) Shaping humoral immunity to vaccines through antigen-displaying nanoparticles. *Current opinion in immunology* **65:** 1-6

Izard T, Ævarsson A, Allen MD, Westphal AH, Perham RN, de Kok A and Hol WG (1999) Principles of quasi-equivalence and Euclidean geometry govern the assembly of cubic and dodecahedral cores of pyruvate dehydrogenase complexes. *Proceedings of the National Academy of Sciences* **96:** 1240-1245

Izoré T, Contreras-Martel C, El Mortaji L, Manzano C, Terrasse R, Vernet T, Di Guilmi AM and Dessen A (2010) Structural basis of host cell recognition by the pilus adhesin from Streptococcus pneumoniae. *Structure* **18:** 106-115

Jacquet N, Navarre C, Desmecht D and Boutry M (2014) Hydrophobin fusion of an influenza virus hemagglutinin allows high transient expression in Nicotiana benthamiana, easy purification and immune response with neutralizing activity. *PloS one* **9**

Janitzek CM, Matondo S, Thrane S, Nielsen MA, Kavishe R, Mwakalinga SB, Theander TG, Salanti A and Sander AF (2016) Bacterial superglue generates a full-length circumsporozoite protein virus-like particle vaccine capable of inducing high and durable antibody responses. *Malaria journal* **15:** 545

Jardine J, Julien J-P, Menis S, Ota T, Kalyuzhniy O, McGuire A, Sok D, Huang P-S, MacPherson S and Jones M (2013) Rational HIV immunogen design to target specific germline B cell receptors. *Science* **340:** 711-716

Jardine JG, Ota T, Sok D, Pauthner M, Kulp DW, Kalyuzhniy O, Skog PD, Thinnes TC, Bhullar D and Briney B (2015) Priming a broadly neutralizing antibody response to HIV-1 using a germline-targeting immunogen. *Science* **349:** 156-161

Jeffs S, Goriup S, Kebble B, Crane D, Bolgiano B, Sattentau Q, Jones S and Holmes H (2004) Expression and characterisation of recombinant oligomeric envelope glycoproteins derived from primary isolates of HIV-1. *Vaccine* **22:** 1032-1046

Jeffs S, McKeating J, Lewis S, Craft H, Biram D, Stephens P and Brady R (1996) Antigenicity of truncated forms of the human immunodeficiency virus type 1 envelope glycoprotein. *Journal of general virology* **77:** 1403-1410

Jennings GT and Bachmann MF (2008) The coming of age of virus-like particle vaccines. *Biological chemistry* **389:** 521-536

Joensuu JJ, Conley AJ, Lienemann M, Brandle JE, Linder MB and Menassa R (2010) Hydrophobin fusions for high-level transient protein expression and purification in Nicotiana benthamiana. *Plant physiology* **152:** 622-633

Joseph M, Ludevid MD, Torrent M, Rofidal V, Tauzin M, Rossignol M and Peltier J-B (2012) Proteomic characterisation of endoplasmic reticulum-derived protein bodies in tobacco leaves. *BMC plant biology* **12:** 36

Julg B, Liu P-T, Wagh K, Fischer WM, Abbink P, Mercado NB, Whitney JB, Nkolola JP, McMahan K and Tartaglia LJ (2017) Protection against a mixed SHIV challenge by a broadly neutralizing antibody cocktail. *Science translational medicine* **9**

Julien J-P, Cupo A, Sok D, Stanfield RL, Lyumkis D, Deller MC, Klasse P-J, Burton DR, Sanders RW and Moore JP (2013) Crystal structure of a soluble cleaved HIV-1 envelope trimer. *Science* **342:** 1477-1483

Julien J-P, Lee JH, Ozorowski G, Hua Y, de la Peña AT, de Taeye SW, Nieusma T, Cupo A, Yasmeen A and Golabek M (2015) Design and structure of two HIV-1 clade C SOSIP. 664

trimers that increase the arsenal of native-like Env immunogens. *Proceedings of the National Academy of Sciences* **112:** 11947-11952

Kalia V, Sarkar S, Gupta P and Montelaro RC (2003) Rational site-directed mutations of the LLP-1 and LLP-2 lentivirus lytic peptide domains in the intracytoplasmic tail of human immunodeficiency virus type 1 gp41 indicate common functions in cell-cell fusion but distinct roles in virion envelope incorporation. *Journal of virology* **77:** 3634-3646

Kanekiyo M, Bu W, Joyce MG, Meng G, Whittle JR, Baxa U, Yamamoto T, Narpala S, Todd J-P and Rao SS (2015) Rational design of an Epstein-Barr virus vaccine targeting the receptor-binding site. *Cell* **162:** 1090-1100

Kanekiyo M, Wei C-J, Yassine HM, McTamney PM, Boyington JC, Whittle JR, Rao SS, Kong W-P, Wang L and Nabel GJ (2013) Self-assembling influenza nanoparticle vaccines elicit broadly neutralizing H1N1 antibodies. *Nature* **499:** 102-106

Kang HJ and Baker EN (2011) Intramolecular isopeptide bonds: protein crosslinks built for stress? *Trends in biochemical sciences* **36:** 229-237

Kang HJ, Coulibaly F, Clow F, Proft T and Baker EN (2007) Stabilizing isopeptide bonds revealed in gram-positive bacterial pilus structure. *Science* **318:** 1625-1628

Kang Y-F, Sun C, Zhuang Z, Yuan R-Y, Zheng Q, Li J-P, Zhou P-P, Chen X-C, Liu Z and Zhang X (2021) Rapid development of SARS-CoV-2 spike protein receptor-binding domain self-assembled nanoparticle vaccine candidates. *ACS nano* **15:** 2738-2752

Karacostas V, Nagashima K, Gonda MA and Moss B (1989) Human immunodeficiency virus-like particles produced by a vaccinia virus expression vector. *Proceedings of the National Academy of Sciences* **86:** 8964-8967

Karch CP and Burkhard P (2016) Vaccine technologies: from whole organisms to rationally designed protein assemblies. *Biochemical pharmacology* **120:** 1-14

Karch CP, Burkhard P, Matyas GR and Beck Z (2021) The diversity of HIV-1 fights against vaccine efficacy: how self-assembling protein nanoparticle technology may fight back. *Nanomedicine* **16:** 673-680

Keeble AH, Banerjee A, Ferla MP, Reddington SC, Anuar INK and Howarth M (2017) Evolving accelerated amidation by SpyTag/SpyCatcher to analyze membrane dynamics. *Angewandte Chemie International Edition* **56:** 16521-16525

Keeble AH and Howarth M (2020) Power to the protein: enhancing and combining activities using the Spy toolbox. *Chemical Science* **11:** 7281-7291

Keeble AH, Turkki P, Stokes S, Anuar INK, Rahikainen R, Hytönen VP and Howarth M (2019) Approaching infinite affinity through engineering of peptide–protein interaction. *Proceedings of the National Academy of Sciences* **116:** 26523-26533

Kersten GF and Crommelin DJ (1995) Liposomes and ISCOMS as vaccine formulations. *Biochimica et Biophysica Acta (BBA)-Reviews on Biomembranes* **1241:** 117-138

Khan I, Twyman RM, Arcalis E and Stoger E (2012) Using storage organelles for the accumulation and encapsulation of recombinant proteins. *Biotechnology journal* **7:** 1099-1108

Kim JH, Excler J-L and Michael NL (2015) Lessons from the RV144 Thai phase III HIV-1 vaccine trial and the search for correlates of protection. *Annual review of medicine* **66:** 423-437

Kim M, Qiao Z-S, Montefiori DC, Haynes BF, Reinherz EL and Liao H-X (2005) Comparison of HIV Type 1 ADA gp120 monomers versus gp140 trimers as immunogens for the induction of neutralizing antibodies. *AIDS Research & Human Retroviruses* **21:** 58-67

King NP and Lai Y-T (2013) Practical approaches to designing novel protein assemblies. *Current opinion in structural biology* **23:** 632-638

Klasse P, LaBranche CC, Ketas TJ, Ozorowski G, Cupo A, Pugach P, Ringe RP, Golabek M, van Gils MJ and Guttman M (2016) Sequential and simultaneous immunization of rabbits with HIV-1 envelope glycoprotein SOSIP. 664 trimers from clades A, B and C. *PLoS pathogens* **12**

Klasse P, Ozorowski G, Sanders RW and Moore JP (2020) Env Exceptionalism: Why Are HIV-1 Env Glycoproteins Atypical Immunogens? *Cell Host & Microbe* **27:** 507-518

Klasse PJ, Depetris RS, Pejchal R, Julien J-P, Khayat R, Lee JH, Marozsan AJ, Cupo A, Cocco N and Korzun J (2013) Influences on trimerization and aggregation of soluble, cleaved HIV-1 SOSIP envelope glycoprotein. *Journal of virology* **87:** 9873-9885

Klein F, Diskin R, Scheid JF, Gaebler C, Mouquet H, Georgiev IS, Pancera M, Zhou T, Incesu R-B and Fu BZ (2013) Somatic mutations of the immunoglobulin framework are generally required for broad and potent HIV-1 neutralization. *Cell* **153:** 126-138

Klein JS and Bjorkman PJ (2010) Few and far between: how HIV may be evading antibody avidity. *PLoS pathogens* **6**

Kleinpeter AB and Freed EO (2020) HIV-1 maturation: lessons learned from inhibitors. *Viruses* **12:** 940

Klovins J, Overbeek G, Van den Worm S, Ackermann H and Van Duin J (2002) Nucleotide sequence of a ssRNA phage from Acinetobacter: kinship to coliphages. *Journal of general Virology* **83:** 1523-1533

Kogan MJ, Dalcol I, Gorostiza P, López-Iglesias C, Pons M, Sanz F, Ludevid D and Giralt E (2001) Self-assembly of the amphipathic helix (VHLPPP) 8. A mechanism for zein protein body formation. *Journal of molecular biology* **312:** 907-913

Kondo N, Miyauchi K, Meng F, Iwamoto A and Matsuda Z (2010) Conformational changes of the HIV-1 envelope protein during membrane fusion are inhibited by the replacement of its membrane-spanning domain. *Journal of Biological Chemistry* **285:** 14681-14688

Kong L, He L, De Val N, Vora N, Morris CD, Azadnia P, Sok D, Zhou B, Burton DR and Ward AB (2016) Uncleaved prefusion-optimized gp140 trimers derived from analysis of HIV-1 envelope metastability. *Nature communications* **7:** 1-15

Kong L, Lee JH, Doores KJ, Murin CD, Julien J-P, McBride R, Liu Y, Marozsan A, Cupo A and Klasse P-J (2013) Supersite of immune vulnerability on the glycosylated face of HIV-1 envelope glycoprotein gp120. *Nature structural & molecular biology* **20:** 796

Kong R, Duan H, Sheng Z, Xu K, Acharya P, Chen X, Cheng C, Dingens AS, Gorman J and Sastry M (2019) Antibody lineages with vaccine-induced antigen-binding hotspots develop broad HIV neutralization. *Cell* **178:** 567-584. e519

Konvalinka J, Kräusslich H-G and Müller B (2015) Retroviral proteases and their roles in virion maturation. *Virology* **479:** 403-417

Kovacs JM, Nkolola JP, Peng H, Cheung A, Perry J, Miller CA, Seaman MS, Barouch DH and Chen B (2012) HIV-1 envelope trimer elicits more potent neutralizing antibody responses than monomeric gp120. *Proceedings of the National Academy of Sciences* **109:** 12111-12116

Kovacs JM, Noeldeke E, Ha HJ, Peng H, Rits-Volloch S, Harrison SC and Chen B (2014) Stable, uncleaved HIV-1 envelope glycoprotein gp140 forms a tightly folded trimer with a native-like structure. *Proceedings of the National Academy of Sciences* **111:** 18542-18547

Kratochvil S, McKay PF, Kopycinski JT, Bishop C, Hayes PJ, Muir L, Pinder CL, Cizmeci D, King D and Aldon Y (2017) A phase 1 human immunodeficiency virus vaccine trial for cross-profiling the kinetics of serum and mucosal antibody responses to CN54gp140 modulated by two homologous prime-boost vaccine regimens. *Frontiers in immunology* **8:** 595

Krebs SJ, Kwon YD, Schramm CA, Law WH, Donofrio G, Zhou KH, Gift S, Dussupt V, Georgiev IS and Schätzle S (2019) Longitudinal analysis reveals early development of three MPER-directed neutralizing antibody lineages from an HIV-1-infected individual. *Immunity* **50:** 677-691. e613

Kumar R, Tuen M, Li H, Doris BT and Hioe CE (2011) Improving immunogenicity of HIV-1 envelope gp120 by glycan removal and immune complex formation. *Vaccine* **29:** 9064-9074

Kwong PD, Doyle ML, Casper DJ, Cicala C, Leavitt SA, Majeed S, Steenbeke TD, Venturi M, Chaiken I and Fung M (2002) HIV-1 evades antibody-mediated neutralization through conformational masking of receptor-binding sites. *Nature* **420:** 678-682

Kwong PD and Mascola JR (2012) Human antibodies that neutralize HIV-1: identification, structures, and B cell ontogenies. *Immunity* **37:** 412-425

Kwong PD, Wyatt R, Robinson J, Sweet RW, Sodroski J and Hendrickson WA (1998) Structure of an HIV gp120 envelope glycoprotein in complex with the CD4 receptor and a neutralizing human antibody. *Nature* **393:** 648-659

Labrijn AF, Poignard P, Raja A, Zwick MB, Delgado K, Franti M, Binley J, Vivona V, Grundner C and Huang C-C (2003) Access of antibody molecules to the conserved coreceptor binding site on glycoprotein gp120 is sterically restricted on primary human immunodeficiency virus type 1. *Journal of virology* **77:** 10557-10565

Laemmli UK (1970) Cleavage of structural proteins during the assembly of the head of bacteriophage T4. *nature* **227:** 680-685

Laher F, Bekker L-G, Garrett N, Lazarus EM and Gray GE (2020a) Review of preventative HIV vaccine clinical trials in South Africa. *Archives of virology***:** 1-14

Laher F, Moodie Z, Cohen KW, Grunenberg N, Bekker L-G, Allen M, Frahm N, Yates NL, Morris L and Malahleha M (2020b) Safety and immune responses after a 12-month booster in healthy HIV-uninfected adults in HVTN 100 in South Africa: A randomized double-blind placebo-controlled trial of ALVAC-HIV (vCP2438) and bivalent subtype C gp120/MF59 vaccines. *PLoS medicine* **17:** e1003038

Lampinen V, Heinimäki S, Laitinen OH, Pesu M, Hankaniemi MM, Blazevic V and Hytönen VP (2021) Modular vaccine platform based on the norovirus-like particle. *Journal of nanobiotechnology* **19:** 1-14

Landais E and Moore PL (2018) Development of broadly neutralizing antibodies in HIV-1 infected elite neutralizers. *Retrovirology* **15:** 61

Landry N, Ward BJ, Trépanier S, Montomoli E, Dargis M, Lapini G and Vézina L-P (2010) Preclinical and clinical development of plant-made virus-like particle vaccine against avian H5N1 influenza. *PloS one* **5:** e15559

Lawson DM, Artymiuk PJ, Yewdall SJ, Smith JM, Livingstone JC, Treffry A, Luzzago A, Levi S, Arosio P and Cesareni G (1991) Solving the structure of human H ferritin by genetically engineering intermolecular crystal contacts. *Nature* **349:** 541-544

Lee JH, Andrabi R, Su C-Y, Yasmeen A, Julien J-P, Kong L, Wu NC, McBride R, Sok D and Pauthner M (2017) A broadly neutralizing antibody targets the dynamic HIV envelope trimer apex via a long, rigidified, and anionic β-hairpin structure. *Immunity* **46:** 690-702

Lee S-F, Ko C-Y, Wang C-T and Chen SS-L (2002) Effect of point mutations in the N terminus of the lentivirus lytic peptide-1 sequence of human immunodeficiency virus type 1 transmembrane protein gp41 on Env stability. *Journal of Biological Chemistry* **277:** 15363-15375

Lee SF, Wang CT, Liang JY, Hong SL, Huang CC and Chen SS (2000) Multimerization potential of the cytoplasmic domain of the human immunodeficiency virus type 1 transmembrane glycoprotein gp41. *The Journal of biological chemistry* **275:** 15809-15819

Lema D, Garcia A and De Sanctis JB (2014) HIV vaccines: a brief overview. *Scandinavian journal of immunology* **80:** 1-11

Lending CR and Larkins BA (1989) Changes in the zein composition of protein bodies during maize endosperm development. *The Plant Cell* **1:** 1011-1023

Leneghan DB, Miura K, Taylor IJ, Li Y, Jin J, Brune KD, Bachmann MF, Howarth M, Long CA and Biswas S (2017) Nanoassembly routes stimulate conflicting antibody quantity and quality for transmission-blocking malaria vaccines. *Scientific reports* **7:** 1-14

Leonard CK, Spellman MW, Riddle L, Harris RJ, Thomas JN and Gregory T (1990) Assignment of intrachain disulfide bonds and characterization of potential glycosylation sites of the type 1 recombinant human immunodeficiency virus envelope glycoprotein (gp120) expressed in Chinese hamster ovary cells. *Journal of Biological Chemistry* **265:** 10373-10382

Lewis GK (2014) Role of F c-mediated antibody function in protective immunity against HIV-1. *Immunology* **142:** 46-57

Li B, Decker JM, Johnson RW, Bibollet-Ruche F, Wei X, Mulenga J, Allen S, Hunter E, Hahn BH and Shaw GM (2006) Evidence for potent autologous neutralizing antibody titers and compact envelopes in early infection with subtype C human immunodeficiency virus type 1. *Journal of virology* **80:** 5211-5218

Li H, Chien PC, Tuen M, Visciano ML, Cohen S, Blais S, Xu C-F, Zhang H-T and Hioe CE (2008) Identification of an N-linked glycosylation in the C4 region of HIV-1 envelope gp120 that is critical for recognition of neighboring CD4 T cell epitopes. *The Journal of Immunology* **180:** 4011-4021

Li L, Fierer JO, Rapoport TA and Howarth M (2014) Structural analysis and optimization of the covalent association between SpyCatcher and a peptide Tag. *Journal of molecular biology* **426:** 309-317

Liao H-X, Lynch R, Zhou T, Gao F, Alam SM, Boyd SD, Fire AZ, Roskin KM, Schramm CA and Zhang Z (2013) Co-evolution of a broadly neutralizing HIV-1 antibody and founder virus. *Nature* **496:** 469-476

Lippincott-Schwartz J, Freed E and Van Engelenburg S (2017) A consensus view of ESCRT-mediated human immunodeficiency virus type 1 abscission. *Annual review of virology* **4:** 309-325

Liu Y, Cao W, Sun M and Li T (2020) Broadly neutralizing antibodies for HIV-1: efficacies, challenges and opportunities. *Emerging Microbes & Infections* **9:** 194-206

Llompart B, Llop-Tous I, Marzabal P, Torrent M, Pallissé R, Bastida M, Ludevid MD and Walas F (2010) Protein production from recombinant protein bodies. *Process Biochemistry* **45:** 1816-1820

Llop-Tous I, Madurga S, Giralt E, Marzabal P, Torrent M and Ludevid MD (2010) Relevant elements of a maize γ-zein domain involved in protein body biogenesis. *Journal of Biological Chemistry* **285:** 35633-35644

Llop-Tous I, Ortiz M, Torrent M and Ludevid MD (2011) The expression of a xylanase targeted to ER-protein bodies provides a simple strategy to produce active insoluble enzyme polymers in tobacco plants. *PLoS One* **6:** e19474

Llop I, Torrent M, Marzabal P, Bastida M, Llompart B and Ludevid D (2006) Zera®, a novel technology for stable accumulation and easy recovery of recombinant proteins in eukaryotic protein-production hosts. *Microbial Cell Factories* **5:** S42

López-Sagaseta J, Malito E, Rappuoli R and Bottomley MJ (2016) Self-assembling protein nanoparticles in the design of vaccines. *Computational and structural biotechnology journal* **14:** 58-68

Ludevid MMD, Torrent QM and Lasserre-Ramassamy S. (2005) Production of peptides and proteins by accumulation in plant endoplasmic reticulum-derived protein bodies. Google Patents.

Lynch RM, Tran L, Louder MK, Schmidt SD, Cohen M, DerSimonian R, Euler Z, Gray ES, Karim SA and Kirchherr J (2012) The development of CD4 binding site antibodies during HIV-1 infection. *Journal of virology* **86:** 7588-7595

Ma X, Zou F, Yu F, Li R, Yuan Y, Zhang Y, Zhang X, Deng J, Chen T and Song Z (2020) Nanoparticle vaccines based on the receptor binding domain (RBD) and heptad repeat (HR) of SARS-CoV-2 elicit robust protective immune responses. *Immunity* **53:** 1315-1330. e1319

Maclean J, Koekemoer M, Olivier A, Stewart D, Hitzeroth I, Rademacher T, Fischer R, Williamson A-L and Rybicki E (2007) Optimization of human papillomavirus type 16 (HPV-16) L1 expression in plants: comparison of the suitability of different HPV-16 L1 gene variants and different cell-compartment localization. *Journal of General Virology* **88:** 1460-1469

Madhavi V, Wines BD, Amin J, Emery S, Lopez E, Kelleher A, Center RJ, Hogarth PM, Chung AW and Kent SJ (2017) HIV-1 Env-and Vpu-specific antibody-dependent cellular cytotoxicity responses associated with elite control of HIV. *Journal of virology* **91**

Mailler E, Bernacchi S, Marquet R, Paillart J-C, Vivet-Boudou V and Smyth RP (2016) The life-cycle of the HIV-1 Gag–RNA complex. *Viruses* **8:** 248

Mainieri D, Morandini F, Maîtrejean M, Saccani A, Pedrazzini E and Vitale A (2014) Protein body formation in the endoplasmic reticulum as an evolution of storage protein sorting to vacuoles: insights from maize γ-zein. *Frontiers in plant science* **5:** 1-11

Mainieri D, Rossi M, Archinti M, Bellucci M, De Marchis F, Vavassori S, Pompa A, Arcioni S and Vitale A (2004) Zeolin. A new recombinant storage protein constructed using maize gamma-zein and bean phaseolin. *Plant Physiol* **136:** 3447-3456

Marcandalli J, Fiala B, Ols S, Perotti M, de van der Schueren W, Snijder J, Hodge E, Benhaim M, Ravichandran R and Carter L (2019) Induction of potent neutralizing antibody responses by a designed protein nanoparticle vaccine for respiratory syncytial virus. *Cell* **176:** 1420-1431. e1417

Margolin E, Chapman R, Meyers A, van Diepen M, Ximba P, Hermanus T, Crowther C, Weber B, Morris L and Williamson A-L (2019) Production and immunogenicity of soluble plant-produced HIV-1 subtype C envelope gp140 immunogens. *Frontiers in plant science* **10:** 1378

Margolin E, Chapman R, Williamson AL, Rybicki EP and Meyers AE (2018) Production of complex viral glycoproteins in plants as vaccine immunogens. *Plant biotechnology journal* **16:** 1531-1545

Margolin E, Crispin M, Meyers A, Chapman R and Rybicki EP (2020) A roadmap for the molecular farming of viral glycoprotein vaccines: Engineering glycosylation and glycosylation-directed folding. *Frontiers in Plant Science* **11:** 1901

Marini A, Zhou Y, Li Y, Taylor IJ, Leneghan DB, Jin J, Zaric M, Mekhaiel D, Long CA and Miura K (2019) A universal plug-and-display vaccine carrier based on HBsAg VLP to maximize effective antibody response. *Frontiers in immunology* **10:** 2931

Martinez-Murillo P, Tran K, Guenaga J, Lindgren G, Àdori M, Feng Y, Phad GE, Bernat NV, Bale S and Ingale J (2017) Particulate array of well-ordered HIV clade C Env trimers elicits neutralizing antibodies that display a unique V2 cap approach. *Immunity* **46:** 804-817. e807

Mascola JR, D'Souza P, Gilbert P, Hahn BH, Haigwood NL, Morris L, Petropoulos CJ, Polonis VR, Sarzotti M and Montefiori DC (2005) Recommendations for the design and use of standard virus panels to assess neutralizing antibody responses elicited by candidate human immunodeficiency virus type 1 vaccines. *Journal of virology* **79:** 10103-10107

Mateu MG (2016) Assembly, engineering and applications of virus-based protein nanoparticles. In *Protein-based engineered nanostructures*. Springer, pp. 83-120

Mattei S, Anders M, Konvalinka J, Kräusslich H-G, Briggs JA and Müller B (2014) Induced maturation of human immunodeficiency virus. *Journal of virology* **88:** 13722-13731

Mattiacio J, Walter S, Brewer M, Domm W, Friedman AE and Dewhurst S (2011) Dense display of HIV-1 envelope spikes on the lambda phage scaffold does not result in the generation of improved antibody responses to HIV-1 Env. *Vaccine* **29:** 2637-2647

Mbewana S, Mortimer E, Pêra FF, Hitzeroth II and Rybicki EP (2015) Production of H5N1 influenza virus matrix protein 2 ectodomain protein bodies in tobacco plants and in insect cells as a candidate universal influenza vaccine. *Frontiers in bioengineering and biotechnology* **3:** 197

McChesney MB and Miller CJ (2013) New directions for HIV vaccine development from animal models. *Current opinion in HIV and AIDS* **8:** 376

McCoy LE (2018) The expanding array of HIV broadly neutralizing antibodies. *Retrovirology* **15:** 70

McCoy LE and Weiss RA (2013) Neutralizing antibodies to HIV-1 induced by immunization. *Journal of Experimental Medicine* **210:** 209-223

McElrath MJ, De Rosa SC, Moodie Z, Dubey S, Kierstead L, Janes H, Defawe OD, Carter DK, Hural J and Akondy R (2008) HIV-1 vaccine-induced immunity in the test-of-concept Step Study: a case–cohort analysis. *The Lancet* **372:** 1894-1905

McLellan JS, Pancera M, Carrico C, Gorman J, Julien J-P, Khayat R, Louder R, Pejchal R, Sastry M and Dai K (2011) Structure of HIV-1 gp120 V1/V2 domain with broadly neutralizing antibody PG9. *Nature* **480:** 336-343

Medina-Ramírez M, Sanders RW and Sattentau QJ (2017) Stabilized HIV-1 envelope glycoprotein trimers for vaccine use. *Current Opinion in HIV and AIDS* **12:** 241

Melikyan GB, Markosyan RM, Hemmati H, Delmedico MK, Lambert DM and Cohen FS (2000) Evidence that the transition of HIV-1 gp41 into a six-helix bundle, not the bundle configuration, induces membrane fusion. *The Journal of cell biology* **151:** 413-424

Meyer DE and Chilkoti A (1999) Purification of recombinant proteins by fusion with thermally-responsive polypeptides. *Nature biotechnology* **17:** 1112-1115

Moldt B, Khoa L, Carnathan DG, Whitney JB, Schultz N, Lewis MG, Borducchi E, Smith K, Mackel JJ and Sweat SL (2016) Neutralizing antibody affords comparable protection against vaginal and rectal SHIV challenge in macaques. *AIDS (London, England)* **30:** 1543

Moldt B, Rakasz EG, Schultz N, Chan-Hui P-Y, Swiderek K, Weisgrau KL, Piaskowski SM, Bergman Z, Watkins DI and Poignard P (2012) Highly potent HIV-specific antibody neutralization in vitro translates into effective protection against mucosal SHIV challenge in vivo. *Proceedings of the National Academy of Sciences* **109:** 18921-18925

Montefiori DC (2004) Evaluating neutralizing antibodies against HIV, SIV, and SHIV in luciferase reporter gene assays. *Current protocols in immunology* **64:** 12.11. 11-12.11. 17

Montefiori DC, Karnasuta C, Huang Y, Ahmed H, Gilbert P, de Souza MS, McLinden R, Tovanabutra S, Laurence-Chenine A and Sanders-Buell E (2012) Magnitude and breadth of the neutralizing antibody response in the RV144 and Vax003 HIV-1 vaccine efficacy trials. *The Journal of infectious diseases* **206:** 431-441

Montefiori DC, Robinson WE, Jr. and Mitchell WM (1988) Role of protein N-glycosylation in pathogenesis of human immunodeficiency virus type 1. *Proceedings of the National Academy of Sciences of the United States of America* **85:** 9248-9252

Montefiori DC, Roederer M, Morris L and Seaman MS (2018) Neutralization tiers of HIV-1. *Current Opinion in HIV and AIDS* **13:** 128

Moodie Z, Walsh SR, Laher F, Maganga L, Herce ME, Naidoo S, Hosseinipour MC, Innes C, Bekker L-G and Grunenberg N (2020) Antibody and cellular responses to HIV vaccine regimens with DNA plasmid as compared with ALVAC priming: An analysis of two randomized controlled trials. *PLoS Medicine* **17:** e1003117

Moore PL, Crooks ET, Porter L, Zhu P, Cayanan CS, Grise H, Corcoran P, Zwick MB, Franti M and Morris L (2006) Nature of nonfunctional envelope proteins on the surface of human immunodeficiency virus type 1. *Journal of virology* **80:** 2515-2528

Moore PL, Sheward D, Nonyane M, Ranchobe N, Hermanus T, Gray ES, Karim SSA, Williamson C and Morris L (2013) Multiple pathways of escape from HIV broadly cross-neutralizing V2-dependent antibodies. *Journal of virology* **87:** 4882-4894

Morgan C, Marthas M, Miller C, Duerr A, Cheng-Mayer C, Desrosiers R, Flores J, Haigwood N, Hu S-L and Johnson RP (2008) The use of nonhuman primate models in HIV vaccine development. *PLoS Med* **5:** e173

Moris A, Pereira M and Chakrabarti L (2019) A role for antibodies in natural HIV control. *Current Opinion in HIV and AIDS* **14:** 265-272

Moser C, Amacker M, Kammer AR, Rasi S, Westerfeld N and Zurbriggen R (2007) Influenza virosomes as a combined vaccine carrier and adjuvant system for prophylactic and therapeutic immunizations. *Expert review of vaccines* **6:** 711-721

Mouquet H (2014) Antibody B cell responses in HIV-1 infection. *Trends in immunology* **35:** 549-561

Moyer TJ, Zmolek AC and Irvine DJ (2016) Beyond antigens and adjuvants: formulating future vaccines. *The Journal of clinical investigation* **126:** 799-808

Munro JB, Gorman J, Ma X, Zhou Z, Arthos J, Burton DR, Koff WC, Courter JR, Smith AB and Kwong PD (2014) Conformational dynamics of single HIV-1 envelope trimers on the surface of native virions. *Science* **346:** 759-763

Murakami T (2008) Roles of the interactions between Env and Gag proteins in the HIV-1 replication cycle. *Microbiology and immunology* **52:** 287-295

Murakami T (2012) Retroviral env glycoprotein trafficking and incorporation into virions. *Molecular biology international* **2012**

Murphy RE and Saad JS (2020) The Interplay between HIV-1 Gag Binding to the Plasma Membrane and Env Incorporation. *Viruses* **12:** 548

Mushahwar IK (2006) Human immunodeficiency viruses: molecular virology, pathogenesis, diagnosis and treatment. *Perspectives in Medical Virology* **13:** 75-87

Muster T, Steindl F, Purtscher M, Trkola A, Klima A, Himmler G, Rüker F and Katinger H (1993) A conserved neutralizing epitope on gp41 of human immunodeficiency virus type 1. *Journal of virology* **67:** 6642-6647

Musumeci D, Riccardi C and Montesarchio D (2015) G-quadruplex forming oligonucleotides as anti-HIV agents. *Molecules* **20:** 17511-17532

Nelson JD, Brunel FM, Jensen R, Crooks ET, Cardoso RM, Wang M, Hessell A, Wilson IA, Binley JM and Dawson PE (2007) An affinity-enhanced neutralizing antibody against the membrane-proximal external region of human immunodeficiency virus type 1 gp41 recognizes an epitope between those of 2F5 and 4E10. *Journal of virology* **81:** 4033-4043

Nguyen B and Tolia NH (2021) Protein-based antigen presentation platforms for nanoparticle vaccines. *npj Vaccines* **6:** 1-11

Nikolov ZL and Woodard SL (2004) Downstream processing of recombinant proteins from transgenic feedstock. *Current opinion in biotechnology* **15:** 479-486

Nitayaphan S, Pitisuttithum P, Karnasuta C, Eamsila C, De Souza M, Morgan P, Polonis V, Benenson M, VanCott T and Ratto-Kim S (2004) Safety and immunogenicity of an HIV subtype B and E prime-boost vaccine combination in HIV-negative Thai adults. *Journal of Infectious Diseases* **190:** 702-706

Nkolola JP, Peng H, Settembre EC, Freeman M, Grandpre LE, Devoy C, Lynch DM, La Porte A, Simmons NL and Bradley R (2010) Breadth of neutralizing antibodies elicited by stable, homogeneous clade A and clade C HIV-1 gp140 envelope trimers in guinea pigs. *Journal of virology* **84:** 3270-3279

Nyamweya S, Hegedus A, Jaye A, Rowland-Jones S, Flanagan KL and Macallan DC (2013) Comparing HIV-1 and HIV-2 infection: Lessons for viral immunopathogenesis. *Reviews in medical virology* **23:** 221-240

Okba NM, Widjaja I, van Dieren B, Aebischer A, van Amerongen G, de Waal L, Stittelaar KJ, Schipper D, Martina B and van den Brand JM (2020) Particulate multivalent presentation of the receptor binding domain induces protective immune responses against MERS-CoV. *Emerging microbes & infections* **9:** 1080-1091

Olshevsky U, Helseth E, Furman C, Li J, Haseltine W and Sodroski J (1990) Identification of individual human immunodeficiency virus type 1 gp120 amino acids important for CD4 receptor binding. *Journal of virology* **64:** 5701-5707

Palladini A, Thrane S, Janitzek CM, Pihl J, Clemmensen SB, de Jongh WA, Clausen TM, Nicoletti G, Landuzzi L and Penichet ML (2018) Virus-like particle display of HER2 induces potent anti-cancer responses. *Oncoimmunology* **7:** e1408749

Pancera M, Shahzad-ul-Hussan S, Doria-Rose NA, McLellan JS, Bailer RT, Dai K, Loesgen S, Louder MK, Staupe RP and Yang Y (2013) Structural basis for diverse N-glycan recognition by HIV-1–neutralizing V1–V2–directed antibody PG16. *Nature structural & molecular biology* **20:** 804

Pancera M, Zhou T, Druz A, Georgiev IS, Soto C, Gorman J, Huang J, Acharya P, Chuang G-Y and Ofek G (2014) Structure and immune recognition of trimeric pre-fusion HIV-1 Env. *Nature* **514:** 455-461

Pantaleo G, Janes H, Karuna S, Grant S, Ouedraogo GL, Allen M, Tomaras GD, Frahm N, Montefiori DC and Ferrari G (2019) Safety and immunogenicity of a multivalent HIV vaccine comprising envelope protein with either DNA or NYVAC vectors (HVTN 096): a phase 1b, double-blind, placebo-controlled trial. *The Lancet HIV* **6:** e737-e749

Pasternak T, Tietz O, Rapp K, Begheldo M, Nitschke R, Ruperti B and Palme K (2015) Protocol: an improved and universal procedure for whole-mount immunolocalization in plants. *Plant Methods* **11:** 50

Pastori C, Tudor D, Diomede L, Drillet A, Jegerlehner A, Röhn T, Bomsel M and Lopalco L (2012) Virus like particle based strategy to elicit HIV-protective antibodies to the alpha-helic regions of gp41. *Virology* **431:** 1-11

Pauthner M, Havenar-Daughton C, Sok D, Nkolola JP, Bastidas R, Boopathy AV, Carnathan DG, Chandrashekar A, Cirelli KM and Cottrell CA (2017) Elicitation of robust tier 2 neutralizing antibody responses in nonhuman primates by HIV envelope trimer immunization using optimized approaches. *Immunity* **46:** 1073-1088. e1076

Pauthner MG and Hangartner L (2020) Broadly neutralizing antibodies to highly antigenically variable viruses as templates for vaccine design. *Vaccination Strategies Against Highly Variable Pathogens***:** 31-87

Pegu A, Yang Z-y, Boyington JC, Wu L, Ko S-Y, Schmidt SD, McKee K, Kong W-P, Shi W and Chen X (2014) Neutralizing antibodies to HIV-1 envelope protect more effectively in vivo than those to the CD4 receptor. *Science translational medicine* **6:** 243ra288-243ra288

Pejawar-Gaddy S, Kovacs JM, Barouch DH, Chen B and Irvine DJ (2014) Design of lipid nanocapsule delivery vehicles for multivalent display of recombinant Env trimers in HIV vaccination. *Bioconjugate chemistry* **25:** 1470-1478

Pejchal R, Doores KJ, Walker LM, Khayat R, Huang P-S, Wang S-K, Stanfield RL, Julien J-P, Ramos A and Crispin M (2011) A potent and broad neutralizing antibody recognizes and penetrates the HIV glycan shield. *Science* **334:** 1097-1103

Phan HT and Conrad U (2011) Membrane-based inverse transition cycling: an improved means for purifying plant-derived recombinant protein-elastin-like polypeptide fusions. *International journal of molecular sciences* **12:** 2808-2821

Phan HT, Hause B, Hause G, Arcalis E, Stoger E, Maresch D, Altmann F, Joensuu J and Conrad U (2014) Influence of elastin-like polypeptide and hydrophobin on recombinant hemagglutinin accumulations in transgenic tobacco plants. *PLoS One* **9**

Phan HT, Pohl J, Floss DM, Rabenstein F, Veits J, Le BT, Chu HH, Hause G, Mettenleiter T and Conrad U (2013) ELP ylated haemagglutinins produced in tobacco plants induce potentially neutralizing antibodies against H5N 1 viruses in mice. *Plant biotechnology journal* **11:** 582-593

Piller SC, Dubay JW, Derdeyn CA and Hunter E (2000) Mutational analysis of conserved domains within the cytoplasmic tail of gp41 from human immunodeficiency virus type 1: effects on glycoprotein incorporation and infectivity. *J Virol* **74:** 11717-11723

Pinto D, Fenwick C, Caillat C, Silacci C, Guseva S, Dehez F, Chipot C, Barbieri S, Minola A and Jarrossay D (2019) Structural basis for broad HIV-1 neutralization by the MPER-specific human broadly neutralizing antibody LN01. *Cell host & microbe* **26:** 623-637. e628

Pitisuttithum P, Gilbert P, Gurwith M, Heyward W, Martin M, van Griensven F, Hu D, Tappero JW and Group BVE (2006) Randomized, double-blind, placebo-controlled efficacy trial of a bivalent recombinant glycoprotein 120 HIV-1 vaccine among injection drug users in Bangkok, Thailand. *The Journal of infectious diseases* **194:** 1661-1671

Pitisuttithum P and Marovich MA (2020) Prophylactic HIV vaccine: vaccine regimens in clinical trials and potential challenges. *Expert Review of Vaccines* **19:** 133-142

Plantier J-C, Leoz M, Dickerson JE, De Oliveira F, Cordonnier F, Lemée V, Damond F, Robertson DL and Simon F (2009) A new human immunodeficiency virus derived from gorillas. *Nature medicine* **15:** 871

Platt EJ, Wehrly K, Kuhmann SE, Chesebro B and Kabat D (1998) Effects of CCR5 and CD4 cell surface concentrations on infections by macrophagetropic isolates of human immunodeficiency virus type 1. *Journal of virology* **72:** 2855-2864

Poignard P, Moulard M, Golez E, Vivona V, Franti M, Venturini S, Wang M, Parren PW and Burton DR (2003) Heterogeneity of envelope molecules expressed on primary human immunodeficiency virus type 1 particles as probed by the binding of neutralizing and nonneutralizing antibodies. *Journal of virology* **77:** 353-365

Pollard SR, Rosa MD, Rosa JJ and Wiley D (1992) Truncated variants of gp120 bind CD4 with high affinity and suggest a minimum CD4 binding region. *The EMBO journal* **11:** 585-591

Pornillos O and Ganser-Pornillos BK (2019) Maturation of retroviruses. *Current opinion in virology* **36:** 47-55

Powell RL, Kinge T and Nyambi PN (2010) Infection by discordant strains of HIV-1 markedly enhances the neutralizing antibody response against heterologous virus. *Journal of virology* **84:** 9415-9426

Priddy FH, Brown D, Kublin J, Monahan K, Wright DP, Lalezari J, Santiago S, Marmor M, Lally M and Novak RM (2008) Safety and immunogenicity of a replication-incompetent adenovirus type 5 HIV-1 clade B gag/pol/nef vaccine in healthy adults. *Clinical infectious diseases* **46:** 1769-1781

Rahikainen R, Rijal P, Tan TK, Wu HJ, Andersson AMC, Barrett JR, Bowden TA, Draper SJ, Townsend AR and Howarth M (2021) Overcoming Symmetry Mismatch in Vaccine Nanoassembly through Spontaneous Amidation. *Angewandte Chemie* **133:** 325-334

Rahman MA and Robert-Guroff M (2019) Accelerating HIV vaccine development using non-human primate models. *Expert Review of Vaccines* **18:** 61-73

Rajarapu G (2013) Genes and Genome of HIV-1. *Journal of Phylogenetics & Evolutionary Biology***:** 1-7

Raska M and Novak J (2010) Involvement of envelope-glycoprotein glycans in HIV-1 biology and infection. *Archivum immunologiae et therapiae experimentalis* **58:** 191-208

Reddington SC and Howarth M (2015) Secrets of a covalent interaction for biomaterials and biotechnology: SpyTag and SpyCatcher. *Current opinion in chemical biology* **29:** 94-99

Rerks-Ngarm S, Pitisuttithum P, Nitayaphan S, Kaewkungwal J, Chiu J, Paris R, Premsri N, Namwat C, de Souza M and Adams E (2009) Vaccination with ALVAC and AIDSVAX to prevent HIV-1 infection in Thailand. *New England Journal of Medicine* **361:** 2209-2220

Richman DD, Wrin T, Little SJ and Petropoulos CJ (2003) Rapid evolution of the neutralizing antibody response to HIV type 1 infection. *Proceedings of the National Academy of Sciences* **100:** 4144-4149

Ringe RP, Sanders RW, Yasmeen A, Kim HJ, Lee JH, Cupo A, Korzun J, Derking R, van Montfort T and Julien J-P (2013) Cleavage strongly influences whether soluble HIV-1 envelope glycoprotein trimers adopt a native-like conformation. *Proceedings of the National Academy of Sciences* **110:** 18256-18261

Rolland M, Edlefsen PT, Larsen BB, Tovanabutra S, Sanders-Buell E, Hertz T, Decamp AC, Carrico C, Menis S and Magaret CA (2012) Increased HIV-1 vaccine efficacy against viruses with genetic signatures in Env V2. *Nature* **490:** 417-420

Rybicki EP (2014) Plant-based vaccines against viruses. *Virology journal* **11:** 205

Saad JS, Miller J, Tai J, Kim A, Ghanam RH and Summers MF (2006) Structural basis for targeting HIV-1 Gag proteins to the plasma membrane for virus assembly. *Proceedings of the National Academy of Sciences* **103:** 11364-11369

Sabalza M, Christou P and Capell T (2014) Recombinant plant-derived pharmaceutical proteins: current technical and economic bottlenecks. *Biotechnology letters* **36:** 2367-2379

Saberianfar R, Joensuu JJ, Conley AJ and Menassa R (2015) Protein body formation in leaves of Nicotiana benthamiana: a concentration-dependent mechanism influenced by the presence of fusion tags. *Plant Biotechnol J* **13:** 927-937

Saberianfar R and Menassa R (2017) Protein bodies: how the ER deals with high accumulation of recombinant proteins. *Plant biotechnology journal* **15:** 671

Saberianfar R, Sattarzadeh A, Joensuu JJ, Kohalmi SE and Menassa R (2016) Protein bodies in leaves exchange contents through the endoplasmic reticulum. *Frontiers in plant science* **7:** 693

Sainsbury F, Sack M, Stadlmann J, Quendler H, Fischer R and Lomonossoff GP (2010) Rapid transient production in plants by replicating and non-replicating vectors yields high quality functional anti-HIV antibody. *PLoS One* **5:** e13976

Sainsbury F, Thuenemann EC and Lomonossoff GP (2009) pEAQ: versatile expression vectors for easy and quick transient expression of heterologous proteins in plants. *Plant biotechnology journal* **7:** 682-693

Sajadi MM, Dashti A, Tehrani ZR, Tolbert WD, Seaman MS, Ouyang X, Gohain N, Pazgier M, Kim D and Cavet G (2018) Identification of near-pan-neutralizing antibodies against HIV-1 by deconvolution of plasma humoral responses. *Cell* **173:** 1783-1795. e1714

Sanders RW, Derking R, Cupo A, Julien J-P, Yasmeen A, de Val N, Kim HJ, Blattner C, de la Peña AT and Korzun J (2013) A next-generation cleaved, soluble HIV-1 Env trimer, BG505 SOSIP. 664 gp140, expresses multiple epitopes for broadly neutralizing but not non-neutralizing antibodies. *PLoS pathogens* **9**

Sanders RW and Moore JP (2017) Native-like Env trimers as a platform for HIV-1 vaccine design. *Immunological reviews* **275:** 161-182

Sanders RW, van Gils MJ, Derking R, Sok D, Ketas TJ, Burger JA, Ozorowski G, Cupo A, Simonich C and Goo L (2015) HIV-1 neutralizing antibodies induced by native-like envelope trimers. *Science* **349:** aac4223

Sanders RW, Vesanen M, Schuelke N, Master A, Schiffner L, Kalyanaraman R, Paluch M, Berkhout B, Maddon PJ and Olson WC (2002) Stabilization of the soluble, cleaved, trimeric form of the envelope glycoprotein complex of human immunodeficiency virus type 1. *Journal of virology* **76:** 8875-8889

Saunders KO, Verkoczy LK, Jiang C, Zhang J, Parks R, Chen H, Housman M, Bouton-Verville H, Shen X and Trama AM (2017) Vaccine induction of heterologous tier 2 HIV-1 neutralizing antibodies in animal models. *Cell reports* **21:** 3681-3690

Scharf L, Scheid JF, Lee JH, West Jr AP, Chen C, Gao H, Gnanapragasam PN, Mares R, Seaman MS and Ward AB (2014) Antibody 8ANC195 reveals a site of broad vulnerability on the HIV-1 envelope spike. *Cell reports* **7:** 785-795

Scheid JF, Mouquet H, Ueberheide B, Diskin R, Klein F, Oliveira TY, Pietzsch J, Fenyo D, Abadir A and Velinzon K (2011) Sequence and structural convergence of broad and potent HIV antibodies that mimic CD4 binding. *Science* **333:** 1633-1637

Schillberg S and Finnern R (2021) Plant molecular farming for the production of valuable proteins–Critical evaluation of achievements and future challenges. *Journal of plant physiology* **258:** 153359

Schiller J and Chackerian B (2014) Why HIV virions have low numbers of envelope spikes: implications for vaccine development. *PLoS pathogens* **10**

Schiller J and Lowy D (2018) Explanations for the high potency of HPV prophylactic vaccines. *Vaccine* **36:** 4768-4773

Schmidt SR (2013) Protein bodies in nature and biotechnology. *Molecular biotechnology* **54:** 257-268

Schoberer J and Strasser R (2018) Plant glyco-biotechnology. In *Seminars in Cell & Developmental Biology*, Vol. 80, pp 133-141.

Schülke N, Vesanen MS, Sanders RW, Zhu P, Lu M, Anselma DJ, Villa AR, Parren PW, Binley JM and Roux KH (2002) Oligomeric and conformational properties of a proteolytically mature, disulfide-stabilized human immunodeficiency virus type 1 gp140 envelope glycoprotein. *Journal of virology* **76:** 7760-7776

Schwestka J and Stoger E (2021) Microparticles and Nanoparticles from Plants—The Benefits of Bioencapsulation. *Vaccines* **9:** 369

Schwestka J, Tschofen M, Vogt S, Marcel S, Grillari J, Raith M, Swoboda I and Stoger E (2020) Plant-derived protein bodies as delivery vehicles for recombinant proteins into mammalian cells. *Biotechnology and bioengineering* **117:** 1037-1047

Seaman MS, Janes H, Hawkins N, Grandpre LE, Devoy C, Giri A, Coffey RT, Harris L, Wood B and Daniels MG (2010) Tiered categorization of a diverse panel of HIV-1 Env pseudoviruses for assessment of neutralizing antibodies. *Journal of virology* **84:** 1439-1452

Seelamgari A, Maddukuri A, Berro R, de la Fuente C, Kehn K, Deng L, Dadgar S, Bottazzi ME, Ghedin E and Pumfery A (2004) Role of viral regulatory and accessory proteins in HIV-1 replication. *Front Biosci* **9:** 2388-2413

Shaik MM, Peng H, Lu J, Rits-Volloch S, Xu C, Liao M and Chen B (2019) Structural basis of coreceptor recognition by HIV-1 envelope spike. *Nature* **565:** 318-323

Shang L, Yue L and Hunter E (2008) Role of the membrane-spanning domain of human immunodeficiency virus type 1 envelope glycoprotein in cell-cell fusion and virus infection. *Journal of virology* **82:** 5417-5428

Sharma A and Sharma US (1997) Liposomes in drug delivery: progress and limitations. *International journal of pharmaceutics* **154:** 123-140

Sharma SK, de Val N, Bale S, Guenaga J, Tran K, Feng Y, Dubrovskaya V, Ward AB and Wyatt RT (2015) Cleavage-independent HIV-1 Env trimers engineered as soluble native spike mimetics for vaccine design. *Cell reports* **11:** 539-550

Sharp PM (2002) Origins of human virus diversity. *Cell* **108:** 305-312

Sharp PM and Hahn BH (2011) Origins of HIV and the AIDS pandemic. *Cold Spring Harbor perspectives in medicine* **1:** a006841

Sheets RL, Zhou T and Knezevic I (2016) Review of efficacy trials of HIV-1/AIDS vaccines and regulatory lessons learned: A review from a regulatory perspective. *Biologicals* **44:** 73-89

Shen W-J and Forde BG (1989) Efficient transformation of Agrobacterium spp. by high voltage electroporation. *Nucleic acids research* **17:** 8385

Shen X, Basu R, Sawant S, Beaumont D, Kwa SF, LaBranche C, Seaton KE, Yates NL, Montefiori DC and Ferrari G (2017) HIV-1 gp120 and modified vaccinia virus Ankara (MVA) gp140 boost immunogens increase immunogenicity of a DNA/MVA HIV-1 vaccine. *Journal of virology* **91**

Sheward DJ, Marais J, Bekker V, Murrell B, Eren K, Bhiman JN, Nonyane M, Garrett N, Woodman ZL and Karim QA (2018) HIV superinfection drives de novo antibody responses and not neutralization breadth. *Cell host & microbe* **24:** 593-599. e593

Shewry PR and Halford NG (2002) Cereal seed storage proteins: structures, properties and role in grain utilization. *Journal of experimental botany* **53:** 947-958

Shingai M, Donau OK, Plishka RJ, Buckler-White A, Mascola JR, Nabel GJ, Nason MC, Montefiori D, Moldt B and Poignard P (2014) Passive transfer of modest titers of potent and broadly neutralizing anti-HIV monoclonal antibodies block SHIV infection in macaques. *Journal of Experimental Medicine* **211:** 2061-2074

Simek MD, Rida W, Priddy FH, Pung P, Carrow E, Laufer DS, Lehrman JK, Boaz M, Tarragona-Fiol T and Miiro G (2009) Human immunodeficiency virus type 1 elite neutralizers: individuals with broad and potent neutralizing activity identified by using a high-throughput neutralization assay together with an analytical selection algorithm. *Journal of virology* **83:** 7337-7348

Simon F, Mauclère P, Roques P, Loussert-Ajaka I, Müller-Trutwin MC, Saragosti S, Georges-Courbot MC, Barré-Sinoussi F and Brun-Vézinet F (1998) Identification of a new human immunodeficiency virus type 1 distinct from group M and group O. *Nature medicine* **4:** 1032-1037

Sliepen K, Han BW, Bontjer I, Mooij P, Garces F, Behrens AJ, Rantalainen K, Kumar S, Sarkar A, Brouwer PJM, Hua Y, Tolazzi M, Schermer E, Torres JL, Ozorowski G, van der Woude P, de la Pena AT, van Breemen MJ, Camacho-Sanchez JM, Burger JA, Medina-Ramirez M, Gonzalez N, Alcami J, LaBranche C, Scarlatti G, van Gils MJ, Crispin M, Montefiori DC, Ward AB, Koopman G, Moore JP, Shattock RJ, Bogers WM, Wilson IA and Sanders RW (2019) Structure and immunogenicity of a stabilized HIV-1 envelope trimer based on a group-M consensus sequence. *Nat Commun* **10:** 2355

Sliepen K, Ozorowski G, Burger JA, van Montfort T, Stunnenberg M, LaBranche C, Montefiori DC, Moore JP, Ward AB and Sanders RW (2015) Presenting native-like HIV-1 envelope trimers on ferritin nanoparticles improves their immunogenicity. *Retrovirology* **12:** 82

Slomski A (2020) Leading HIV Vaccine Trial Stopped for Ineffectiveness. *Jama* **323:** 1124-1124

Smith MT, Hawes AK and Bundy BC (2013) Reengineering viruses and virus-like particles through chemical functionalization strategies. *Current opinion in biotechnology* **24:** 620-626

Smith W, Jäntti J, Oja M and Saloheimo M (2014) Comparison of intracellular and secretion-based strategies for production of human α-galactosidase A in the filamentous fungus Trichoderma reesei. *BMC biotechnology* **14:** 1-12

Speck RF, Wehrly K, Platt EJ, Atchison RE, Charo IF, Kabat D, Chesebro B and Goldsmith MA (1997) Selective employment of chemokine receptors as human immunodeficiency virus type 1 coreceptors determined by individual amino acids within the envelope V3 loop. *Journal of virology* **71:** 7136-7139

Spohn G, Jennings GT, Martina BE, Keller I, Beck M, Pumpens P, Osterhaus AD and Bachmann MF (2010) A VLP-based vaccine targeting domain III of the West Nile virus E protein protects from lethal infection in mice. *Virology journal* **7:** 146

Stamatatos L, Morris L, Burton DR and Mascola JR (2009) Neutralizing antibodies generated during natural HIV-1 infection: good news for an HIV-1 vaccine? *Nature medicine* **15:** 866

Stano A, Leaman DP, Kim AS, Zhang L, Autin L, Ingale J, Gift SK, Truong J, Wyatt RT and Olson AJ (2017) Dense array of spikes on HIV-1 virion particles. *Journal of virology* **91:** e00415-00417

Starcich BR, Hahn BH, Shaw GM, McNeely PD, Modrow S, Wolf H, Parks ES, Parks WP, Josephs SF and Gallo RC (1986) Identification and characterization of conserved and variable regions in the envelope gene of HTLV-III/LAV, the retrovirus of AIDS. *Cell* **45:** 637-648

Strasser R, Stadlmann J, Schähs M, Stiegler G, Quendler H, Mach L, Glössl J, Weterings K, Pabst M and Steinkellner H (2008) Generation of glyco-engineered Nicotiana benthamiana for the production of monoclonal antibodies with a homogeneous human-like N-glycan structure. *Plant biotechnology journal* **6:** 392-402

Su B, Dispinseri S, Iannone V, Zhang T, Wu H, Carapito R, Bahram S, Scarlatti G and Moog C (2019) Update on Fc-Mediated Antibody Functions Against HIV-1 Beyond Neutralization. *Frontiers in Immunology* **10:** 2968

Sunde M, Kwan AH, Templeton MD, Beever RE and Mackay JP (2008) Structural analysis of hydrophobins. *Micron* **39:** 773-784

Sundquist WI and Kräusslich H-G (2012) HIV-1 assembly, budding, and maturation. *Cold Spring Harbor perspectives in medicine* **2:** a006924

Tamamis P and Floudas CA (2014) Molecular recognition of CCR5 by an HIV-1 gp120 V3 loop. *PloS one* **9**

Tan TK, Rijal P, Rahikainen R, Keeble A, Schimanski L, Hussain S, Harvey R, Hayes J, Edwards J and McLean R (2020) A COVID-19 vaccine candidate using SpyCatcher multimerization of the SARS-CoV-2 spike protein receptor-binding domain induces potent neutralising antibody responses. *bioRxiv*

Tanzer FL, Shephard EG, Palmer KE, Burger M, Williamson A-L and Rybicki EP (2011) The porcine circovirus type 1 capsid gene promoter improves antigen expression and immunogenicity in a HIV-1 plasmid vaccine. *Virology journal* **8:** 51

Tay MZ, Liu P, Williams LD, McRaven MD, Sawant S, Gurley TC, Xu TT, Dennison SM, Liao H-X and Chenine A-L (2016) Antibody-mediated internalization of infectious HIV-1 virions differs among antibody isotypes and subclasses. *PLoS pathogens* **12:** e1005817

Tedbury PR and Freed EO (2015) The cytoplasmic tail of retroviral envelope glycoproteins. In *Progress in molecular biology and translational science* Vol. 129. Elsevier, pp. 253-284

Thrane S, Janitzek CM, Matondo S, Resende M, Gustavsson T, De Jongh WA, Clemmensen S, Roeffen W, van de Vegte-Bolmer M and Van Gemert GJ (2016) Bacterial superglue enables easy development of efficient virus-like particle based vaccines. *Journal of nanobiotechnology* **14:** 30

Tissot AC, Renhofa R, Schmitz N, Cielens I, Meijerink E, Ose V, Jennings GT, Saudan P, Pumpens P and Bachmann MF (2010) Versatile virus-like particle carrier for epitope based vaccines. *PloS one* **5**

Tomaras GD, Ferrari G, Shen X, Alam SM, Liao H-X, Pollara J, Bonsignori M, Moody MA, Fong Y and Chen X (2013) Vaccine-induced plasma IgA specific for the C1 region of the HIV-1 envelope blocks binding and effector function of IgG. *Proceedings of the National Academy of Sciences* **110:** 9019-9024

Tomaras GD and Plotkin SA (2017) Complex immune correlates of protection in HIV-1 vaccine efficacy trials. *Immunological reviews* **275:** 245-261

Tong T, Crooks ET, Osawa K and Binley JM (2012) HIV-1 virus-like particles bearing pure env trimers expose neutralizing epitopes but occlude nonneutralizing epitopes. *Journal of virology* **86:** 3574-3587

Torrent M, Llompart B, Lasserre-Ramassamy S, Llop-Tous I, Bastida M, Marzabal P, Westerholm-Parvinen A, Saloheimo M, Heifetz PB and Ludevid MD (2009a) Eukaryotic protein production in designed storage organelles. *BMC biology* **7:** 5

Torrent M, Llop-Tous I and Ludevid MD (2009b) Protein body induction: a new tool to produce and recover recombinant proteins in plants. In *Recombinant Proteins from Plants*. Springer, pp. 193-208

Torrents dlPA, de Taeye SW, Sliepen K, LaBranche CC, Burger JA, Schermer EE, Montefiori DC, Moore JP, Klasse PJ and Sanders RW (2018) Immunogenicity in Rabbits of HIV-1 SOSIP Trimers from Clades A, B, and C, Given Individually, Sequentially, or in Combination. *Journal of virology* **92**

Towbin H, Staehelin T and Gordon J (1979) Electrophoretic transfer of proteins from polyacrylamide gels to nitrocellulose sheets: Procedure and some applications *Proceedings of the National Academy of Sciences of the United States of America* **76:** 4350-4354

Tsekoa TL, Singh AA and Buthelezi SG (2020) Molecular farming for therapies and vaccines in Africa. *Current opinion in biotechnology* **61:** 89-95

Ueda G, Antanasijevic A, Fallas JA, Sheffler W, Copps J, Ellis D, Hutchinson G, Moyer A, Yasmeen A and Tsybovsky Y (2020) Tailored Design of Protein Nanoparticle Scaffolds for Multivalent Presentation of Viral Glycoprotein Antigens. *BioRXiv*

Umotoy J, Bagaya BS, Joyce C, Schiffner T, Menis S, Saye-Francisco KL, Biddle T, Mohan S, Vollbrecht T and Kalyuzhniy O (2019) Rapid and focused maturation of a VRC01-Class HIV broadly neutralizing antibody lineage involves both binding and accommodation of the N276-Glycan. *Immunity* **51:** 141-154. e146

Urry DW (1988) Entropic elastic processes in protein mechanisms. I. Elastic structure due to an inverse temperature transition and elasticity due to internal chain dynamics. *Journal of protein chemistry* **7:** 1-34

Urry DW. (1997) Physical chemistry of biological free energy transduction as demonstrated by elastic protein-based polymers. ACS Publications.

Vaccari M, Poonam P and Franchini G (2010) Phase III HIV vaccine trial in Thailand: a step toward a protective vaccine for HIV. *Expert review of vaccines* **9:** 997-1005

Vallari A, Holzmayer V, Harris B, Yamaguchi J, Ngansop C, Makamche F, Mbanya D, Kaptué L, Ndembi N and Gürtler L (2011) Confirmation of putative HIV-1 group P in Cameroon. *Journal of virology* **85:** 1403-1407

van den Worm SH, Koning RI, Warmenhoven HJ, Koerten HK and van Duin J (2006) Cryo electron microscopy reconstructions of the Leviviridae unveil the densest icosahedral RNA packing possible. *Journal of molecular biology* **363:** 858-865

van Diepen MT, Chapman R, Douglass N, Galant S, Moore PL, Margolin E, Ximba P, Morris L, Rybicki EP and Williamson A-L (2019) Prime-boost immunizations with DNA, modified vaccinia virus Ankara, and protein-based vaccines elicit robust HIV-1 tier 2 neutralizing antibodies against the CAP256 superinfecting virus. *Journal of virology* **93:** e02155-02118

van Diepen MT, Chapman R, Moore PL, Margolin E, Hermanus T, Morris L, Ximba P, Rybicki EP and Williamson A-L (2018) The adjuvant AlhydroGel elicits higher antibody titres than AddaVax when combined with HIV-1 subtype C gp140 from CAP256. *PloS one* **13**

van Loggerenberg F, Mlisana K, Williamson C, Auld SC, Morris L, Gray CM, Karim QA, Grobler A, Barnabas N and Iriogbe I (2008) Establishing a cohort at high risk of HIV infection in South Africa: challenges and experiences of the CAPRISA 002 acute infection study. *PloS one* **3:** e1954

van Zyl AR, Meyers AE and Rybicki EP (2017) Development of plant-produced protein body vaccine candidates for bluetongue virus. *BMC biotechnology* **17:** 47

VanCott TC, Bethke F, Burke D, Redfield R and Birx D (1995a) Lack of induction of antibodies specific for conserved, discontinuous epitopes of HIV-1 envelope glycoprotein by candidate AIDS vaccines. *The Journal of Immunology* **155:** 4100-4110

VanCott TC, Veit S, Kalyanaraman V, Earl P and Birx D (1995b) Characterization of a soluble, oligomeric HIV-1 gp160 protein as a potential immunogen. *Journal of immunological methods* **183:** 103-117

Veazey RS, Klasse PJ, Schader SM, Hu Q, Ketas TJ, Lu M, Marx PA, Dufour J, Colonno RJ and Shattock RJ (2005) Protection of macaques from vaginal SHIV challenge by vaginally delivered inhibitors of virus–cell fusion. *Nature* **438:** 99-102

Veggiani G, Nakamura T, Brenner MD, Gayet RV, Yan J, Robinson CV and Howarth M (2016) Programmable polyproteams built using twin peptide superglues. *Proceedings of the National Academy of Sciences* **113:** 1202-1207

Visciano M, Diomede L, Tagliamonte M, Tornesello M, Asti V, Bomsel M, Buonaguro F, Lopalco L and Buonaguro L (2011) Generation of HIV-1 Virus-Like Particles expressing different HIV-1 glycoproteins. *Vaccine* **29:** 4903-4912

Votteler J and Sundquist WI (2013) Virus budding and the ESCRT pathway. *Cell host & microbe* **14:** 232-241

Vzorov AN, Wang L, Chen J, Wang B-Z and Compans RW (2016) Effects of modification of the HIV-1 Env cytoplasmic tail on immunogenicity of VLP vaccines. *Virology* **489:** 141-150

Walker LM, Huber M, Doores KJ, Falkowska E, Pejchal R, Julien J-P, Wang S-K, Ramos A, Chan-Hui P-Y and Moyle M (2011) Broad neutralization coverage of HIV by multiple highly potent antibodies. *Nature* **477:** 466-470

Walker LM, Phogat SK, Chan-Hui P-Y, Wagner D, Phung P, Goss JL, Wrin T, Simek MD, Fling S and Mitcham JL (2009) Broad and potent neutralizing antibodies from an African donor reveal a new HIV-1 vaccine target. *Science* **326:** 285-289

Walls AC, Fiala B, Schäfer A, Wrenn S, Pham MN, Murphy M, Longping VT, Shehata L, O'Connor MA and Chen C (2020) Elicitation of potent neutralizing antibody responses by designed protein nanoparticle vaccines for SARS-CoV-2. *Cell* **183:** 1367-1382. e1317

Wang B-Z, Liu W, Kang S-M, Alam M, Huang C, Ye L, Sun Y, Li Y, Kothe DL and Pushko P (2007) Incorporation of high levels of chimeric human immunodeficiency virus envelope glycoproteins into virus-like particles. *Journal of virology* **81:** 10869-10878

Wang H, Gristick HB, Scharf L, West Jr AP, Galimidi RP, Seaman MS, Freund NT, Nussenzweig MC and Bjorkman PJ (2017) Asymmetric recognition of HIV-1 Envelope trimer by V1V2 loop-targeting antibodies. *Elife* **6:** e27389

Watanabe Y, Berndsen ZT, Raghwani J, Seabright GE, Allen JD, Pybus OG, McLellan JS, Wilson IA, Bowden TA and Ward AB (2020) Vulnerabilities in coronavirus glycan shields despite extensive glycosylation. *Nature communications* **11:** 1-10

Watkins DI, Burton DR, Kallas EG, Moore JP and Koff WC (2008) Nonhuman primate models and the failure of the Merck HIV-1 vaccine in humans. *Nature medicine* **14:** 617-621

Watts JM, Dang KK, Gorelick RJ, Leonard CW, Bess Jr JW, Swanstrom R, Burch CL and Weeks KM (2009) Architecture and secondary structure of an entire HIV-1 RNA genome. *Nature* **460:** 711-716

Wei X, Decker JM, Liu H, Zhang Z, Arani RB, Kilby JM, Saag MS, Wu X, Shaw GM and Kappes JC (2002) Emergence of resistant human immunodeficiency virus type 1 in patients receiving fusion inhibitor (T-20) monotherapy. *Antimicrobial agents and chemotherapy* **46:** 1896-1905

Wei X, Decker JM, Wang S, Hui H, Kappes JC, Wu X, Salazar-Gonzalez JF, Salazar MG, Kilby JM and Saag MS (2003) Antibody neutralization and escape by HIV-1. *Nature* **422:** 307-312

Weissenhorn W, Dessen A, Harrison S, Skehel J and Wiley D (1997) Atomic structure of the ectodomain from HIV-1 gp41. *Nature* **387:** 426-430

West AP, Diskin R, Nussenzweig MC and Bjorkman PJ (2012) Structural basis for germ-line gene usage of a potent class of antibodies targeting the CD4-binding site of HIV-1 gp120. *Proceedings of the National Academy of Sciences* **109:** E2083-E2090

Whitehead M, Öhlschläger P, Almajhdi FN, Alloza L, Marzábal P, Meyers AE, Hitzeroth II and Rybicki EP (2014) Human papillomavirus (HPV) type 16 E7 protein bodies cause tumour regression in mice. *BMC cancer* **14:** 367

Wibmer CK, Moore PL and Morris L (2015) HIV broadly neutralizing antibody targets. *Current opinion in HIV and AIDS* **10:** 135

Wilken LR and Nikolov ZL (2012) Recovery and purification of plant-made recombinant proteins. *Biotechnology advances* **30:** 419-433

Williams LD, Ofek G, Schätzle S, McDaniel JR, Lu X, Nicely NI, Wu L, Lougheed CS, Bradley T and Louder MK (2017) Potent and broad HIV-neutralizing antibodies in memory B cells and plasma. *Science immunology* **2**

Wu X, Parast AB, Richardson BA, Nduati R, John-Stewart G, Mbori-Ngacha D, Rainwater SM and Overbaugh J (2006) Neutralization escape variants of human immunodeficiency virus type 1 are transmitted from mother to infant. *Journal of virology* **80:** 835-844

Wu X, Yang Z-Y, Li Y, Hogerkorp C-M, Schief WR, Seaman MS, Zhou T, Schmidt SD, Wu L and Xu L (2010) Rational design of envelope identifies broadly neutralizing human monoclonal antibodies to HIV-1. *Science* **329:** 856-861

Wu X, Zhang Z, Schramm CA, Joyce MG, Do Kwon Y, Zhou T, Sheng Z, Zhang B, O'Dell S and McKee K (2015) Maturation and diversity of the VRC01-antibody lineage over 15 years of chronic HIV-1 infection. *Cell* **161:** 470-485

Wyatt R, Sullivan N, Thali M, Repke H, Ho D, Robinson J, Posner M and Sodroski J (1993) Functional and immunologic characterization of human immunodeficiency virus type 1 envelope glycoproteins containing deletions of the major variable regions. *Journal of virology* **67:** 4557-4565

Xu L, Pegu A, Rao E, Doria-Rose N, Beninga J, McKee K, Lord DM, Wei RR, Deng G and Louder M (2017) Trispecific broadly neutralizing HIV antibodies mediate potent SHIV protection in macaques. *Science* **358:** 85-90

Yamaguchi M, Danev R, Nishiyama K, Sugawara K and Nagayama K (2008) Zernike phase contrast electron microscopy of ice-embedded influenza A virus. *Journal of structural biology* **162:** 271-276

Yamamoto T, Hoshikawa K, Ezura K, Okazawa R, Fujita S, Takaoka M, Mason HS, Ezura H and Miura K (2018) Improvement of the transient expression system for production of recombinant proteins in plants. *Scientific reports* **8:** 1-10

Yan Y, Wang X, Lou P, Hu Z, Qu P, Li D, Li Q, Xu Y, Niu J and He Y (2020) A nanoparticle-based hepatitis C virus vaccine with enhanced potency. *The Journal of Infectious Diseases* **221:** 1304-1314

Yang X, Farzan M, Wyatt R and Sodroski J (2000a) Characterization of stable, soluble trimers containing complete ectodomains of human immunodeficiency virus type 1 envelope glycoproteins. *Journal of virology* **74:** 5716-5725

Yang X, Florin L, Farzan M, Kolchinsky P, Kwong PD, Sodroski J and Wyatt R (2000b) Modifications that stabilize human immunodeficiency virus envelope glycoprotein trimers in solution. *Journal of virology* **74:** 4746-4754

Yang X, Lee J, Mahony EM, Kwong PD, Wyatt R and Sodroski J (2002) Highly stable trimers formed by human immunodeficiency virus type 1 envelope glycoproteins fused with the trimeric motif of T4 bacteriophage fibritin. *Journal of virology* **76:** 4634-4642

Yang X, Wyatt R and Sodroski J (2001) Improved elicitation of neutralizing antibodies against primary human immunodeficiency viruses by soluble stabilized envelope glycoprotein trimers. *Journal of virology* **75:** 1165-1171

Yates NL, Liao H-X, Fong Y, DeCamp A, Vandergrift NA, Williams WT, Alam SM, Ferrari G, Yang Z-y and Seaton KE (2014) Vaccine-induced Env V1-V2 IgG3 correlates with lower HIV-1 infection risk and declines soon after vaccination. *Science translational medicine* **6:** 228ra239-228ra239

Yenkoidiok-Douti L, Williams AE, Canepa GE, Molina-Cruz A and Barillas-Mury C (2019) engineering a Virus-Like particle as an Antigenic Platform for a Pfs47-targeted Malaria transmission-Blocking Vaccine. *Scientific reports* **9:** 1-9

Yuan T, Li J and Zhang M-Y (2013) HIV-1 envelope glycoprotein variable loops are indispensable for envelope structural integrity and virus entry. *PLoS One* **8**

Yuste E, Reeves JD, Doms RW and Desrosiers RC (2004) Modulation of Env content in virions of simian immunodeficiency virus: correlation with cell surface expression and virion infectivity. *Journal of virology* **78:** 6775-6785

Zabel F, Kündig TM and Bachmann MF (2013) Virus-induced humoral immunity: on how B cell responses are initiated. *Current opinion in virology* **3:** 357-362

Zakeri B, Fierer JO, Celik E, Chittock EC, Schwarz-Linek U, Moy VT and Howarth M (2012) Peptide tag forming a rapid covalent bond to a protein, through engineering a bacterial adhesin. *Proceedings of the National Academy of Sciences* **109:** E690-E697

Zhang B, Chao CW, Tsybovsky Y, Abiona OM, Hutchinson GB, Moliva JI, Olia AS, Pegu A, Phung E and Stewart-Jones G (2020) A Platform Incorporating Trimeric Antigens into Self-Assembling Nanoparticles Reveals SARS-CoV-2-Spike Nanoparticles to Elicit Substantially Higher Neutralizing Responses than Spike Alone. *BioRxiv*

Zhang L, Irimia A, He L, Landais E, Rantalainen K, Leaman DP, Vollbrecht T, Stano A, Sands DI and Kim AS (2019) An MPER antibody neutralizes HIV-1 using germline features shared among donors. *Nature communications* **10:** 1-16

Zhang LF, Zhou J, Chen S, Cai LL, Bao QY, Zheng FY, Lu JQ, Padmanabha J, Hengst K and Malcolm K (2000) HPV6b virus like particles are potent immunogens without adjuvant in man. *Vaccine* **18:** 1051-1058

Zhang X, Konarev PV, Petoukhov MV, Svergun DI, Xing L, Cheng RH, Haase I, Fischer M, Bacher A and Ladenstein R (2006) Multiple assembly states of lumazine synthase: a model relating catalytic function and molecular assembly. *Journal of molecular biology* **362:** 753-770

Zhang X, Meining W, Fischer M, Bacher A and Ladenstein R (2001) X-ray structure analysis and crystallographic refinement of lumazine synthase from the hyperthermophile Aquifex aeolicus at 1.6 Å resolution: determinants of thermostability revealed from structural comparisons. *Journal of molecular biology* **306:** 1099-1114

Zhao Q, Li S, Yu H, Xia N and Modis Y (2013) Virus-like particle-based human vaccines: quality assessment based on structural and functional properties. *Trends in biotechnology* **31:** 654-663

Zhao S, Schuurman N, Tieke M, Quist B, Zwinkels S, van Kuppeveld FJ, de Haan CA and Egberink H (2020) Serological screening of influenza A virus antibodies in cats and dogs indicates frequent infection with different subtypes. *Journal of clinical microbiology* **58**

Zhou T, Lynch RM, Chen L, Acharya P, Wu X, Doria-Rose NA, Joyce MG, Lingwood D, Soto C and Bailer RT (2015) Structural repertoire of HIV-1-neutralizing antibodies targeting the CD4 supersite in 14 donors. *Cell* **161:** 1280-1292

Zhu P, Liu J, Bess J, Chertova E, Lifson JD, Grisé H, Ofek GA, Taylor KA and Roux KH (2006) Distribution and three-dimensional structure of AIDS virus envelope spikes. *Nature* **441:** 847-852

Zolla-Pazner S and Cardozo T (2010) Structure–function relationships of HIV-1 envelope sequence-variable regions refocus vaccine design. *Nature reviews Immunology* **10:** 527-535

Zotova A, Atemasova A, Pichugin A, Filatov A and Mazurov D (2019) Distinct Requirements for HIV-1 Accessory Proteins during Cell Coculture and Cell-Free Infection. *Viruses* **11:** 390

Zwick MB, Labrijn AF, Wang M, Spenlehauer C, Saphire EO, Binley JM, Moore JP, Stiegler G, Katinger H and Burton DR (2001) Broadly neutralizing antibodies targeted to the membrane-

proximal external region of human immunodeficiency virus type 1 glycoprotein gp41. *Journal of virology* **75:** 10892-10905